Theory and applications of a novel formulation of the space of perceived colors

Nicoletta Prencipe

THÈSE DE DOCTORAT

PRÉSENTÉE À

L'UNIVERSITÉ DE BORDEAUX

ÉCOLE DOCTORALE DE MATHÉMATIQUES ET D'INFORMATIQUE

PAR **Nicoletta PRENCIPE**

SOUS LA DIRECTION DE **Edoardo PROVENZI**

POUR OBTENIR LE GRADE DE **DOCTEUR**

SPÉCIALITÉ : Mathématiques Appliquées et Calcul Scientifique

Théorie et applications d'une nouvelle formulation de l'espace des couleurs perçues

---

Soutenue le 28 novembre 2022 à l'Institut de Mathématiques de Bordeaux
devant le jury composé de :

Rémi Cozot	Professeur, Université du Littoral Côte d'Opale	Président
Ivar Farup	Professeur, Norwegian University of Science and Technology	Rapporteur
Nir Sochen	Professeur, Tel Aviv University	Rapporteur
Emmanuel Chevallier	Maître de Conferences, Aix-Marseille Université	Examinateur
Paola Iacomussi	Chargée de recherche, Istituto Nazionale di Ricerca Metrologica	Examinatrice
Toinon Vigier	Maîtresse de Conferences, Nantes Université	Examinatrice
Michel Berthier	Professeur, Université de La Rochelle	Invité
Joseph Meehan	Ingénieur, PhD, Huawei Technologies France	Co-encadrant
Edoardo Provenzi	Professeur, Université de Bordeaux	Directeur

Théorie et applications d'une nouvelle formulation de l'espace des couleurs perçues

Résumé : Cette thèse porte sur une nouvelle approche mathématique de la perception des couleurs et ses premières applications au traitement d'images. Alors que la littérature existante suggère à la fois la nature hyperbolique des espaces couleurs et l'importance du mécanisme d'opposition de Hering dans le processus de la vision, il n'existe aucun modèle mathématique intégrant naturellement ces caractéristiques.
L'approche présentée dans cette thèse, partant de l'axiomatisation de Newton, Grassmann, Helmholtz, Schrödinger et Resnikoff, conduit à une structure algébrique qui est le pendant réel de celle utilisée en mécanique quantique, qui présente des caractéristiques hyperboliques et encode l'opposition de Hering dans les matrices de Pauli réelles.
Ces similitudes avec les théories modernes de la physique peuvent être expliquées à un niveau intuitif par le fait que la perception des couleurs est un processus basé sur la dualité entre le contexte de mesure et l'appareil d'observation, dans la mesure où cela n'a aucun sens de parler d'une couleur perçue sans spécifier les conditions dans lesquelles elle a été mesurée. Les couleurs perçues ne sont en effet pas absolues, mais relatives aux conditions d'observation.
Ce manuscrit donne une vue d'ensemble de cette nouvelle théorie en mettant l'accent sur ses aspects relativistes. De plus, des définitions rigoureuses des attributs colorimétriques classiques (dont la teinte, la saturation, la luminosité...) sont fournies dans ce cadre.
D'autre part, cette thèse comprend également des applications de ce nouveau formalisme, à travers des algorithmes de traitement d'images en couleur. Ces derniers sont destinés à faire en sorte que l'appareil photo numérique imite le comportement du système visuel humain. Deux premières applications sont présentées : un boost de Lorentz normalisé utilisé comme transformée d'adaptation chromatique pour la balance des blancs, c'est-à-dire l'algorithme qui émule l'adaptation aux conditions d'illumination, et quelques premières applications de constructions classiques provenant de la géométrie hyperbolique au tone mapping.

Mots-clés : *Perception de la couleur, Géométrie de l'espace des couleurs, Relativité spéciale, Information quantique.*

Unité de Recherche: Université de Bordeaux, CNRS, Bordeaux INP, Institut de Mathématiques de Bordeaux (IMB), UMR 5251, 351 Cours de la Libération, 33405 Talence, France.

Theory and applications of a novel formulation of the space of perceived colors

Abstract: This thesis is about a novel mathematical approach to color perception and its first applications to color image processing. While the literature suggests both the hyperbolic nature of color spaces and the importance of Hering's opponent mechanism in the vision pipeline, no mathematical model exists naturally incorporating these features.
This new approach, starting by the axiomatization of Newton, Grassmann, Helmholtz, Schrödinger, and Resnikoff, leads to an algebraic structure that is the real case of the one used in quantum mechanics, which has hyperbolic features and encodes Hering's opponent mechanism in the real Pauli matrices.
Color perception is a process based on the duality between context of measure and observing apparatus. This recalls the duality in quantum mechanics, in the sense that it makes no sense to talk about a perceived color without specifying the conditions in which it has been measured. Perceived colors are indeed not absolute, but relative to the viewing conditions.
The previous considerations show, at an intuitive level, that the mathematical tools developed for modern theories in physics are suitable to model color perception.
The present manuscript provides an overview of this novel theory with a particular focus on its relativistic aspects. Furthermore rigorous definitions of the classic color attributes (hue, saturation, brightness...) are provided within the formalism of this framework. On the other hand this thesis includes as well some first applications of this new formalism to color image processing algorithms. These latter are meant to make the digital camera mimic the human visual system's behavior. Two first applications are shown: a normalized Lorentz boost used as a chromatic adaptation transform for white balance, i.e. the algorithm that emulates adaptation to the illumination condition, and some first applications of classic constructions of hyperbolic geometry to tone mapping.

Keywords: *Color perception, Geometry of color spaces, Special relativity, Quantum information*

Contents

Introduction et aperçu de la thèse

La perception des couleurs est un sujet placé au carrefour de nombreux domaines scientifiques. Les questions relatives à la couleur ont occupé nombre de grands penseurs de l'histoire, dont Platon lui-même, et interpellent encore aujourd'hui n'importe lequel d'entre nous, comme le prouve le récent débat à propos de *The Dress*[*]. L'étude de ces questions relève à la fois de la philosophie (dans la tradition de Goethe, Schopenhauer, Russell ou Wittgenstein), de la neurophysiologie de la vision (dans la tradition de Hubel ou de Valois), ou encore de la physique mathématique (dans la tradition de Newton, Maxwell, von Helmholtz, Schrödinger, Yilmaz ou Resnikoff).

Dans cette thèse, nous abordons le problème de la perception des couleurs d'un point de vue mathématique.

Les couleurs physiques, c'est-à-dire les lumières réfléchies ou émises qui pénètrent dans les yeux à partir d'un environnement visuel, sont converties en couleurs perçues par l'homme grâce à des mécanismes neurophysiologiques. Mathématiquement, une couleur physique est un spectre, c'est-à-dire une fonction définie sur l'intervalle des longueurs d'onde visibles, donc un élément d'un espace de dimension infinie, alors qu'il est connu que pour modéliser les couleurs perçues, il faut un espace de dimension 3. Malgré sa plus petite dimension, l'espace des couleurs perçues est beaucoup moins compris et beaucoup plus controversé pour être modélisé mathématiquement.

Cela tient à la complexité des processus neurophysiologiques conduisant à notre perception des couleurs. En effet, cette dernière fait intervenir dans un premier temps trois types de photorécepteurs, les cônes LMS, chacun d'entre eux étant plus sensible à une partie différente du spectre du visible. Les lettres L, M et S sont utilisées pour représenter les longueurs d'onde *Long*, *Middle* et *Short* correspondant aux différents pics de sensibilité des cônes. Dans un second temps, le mécanisme dit d'opposition des champs réceptifs de la rétine se met en place. Ce dernier est induit par l'entrelacement des connexions entre cônes et cellules ganglionnaires.

Il existe essentiellement deux façons de modéliser l'espace des couleurs perçues : la première inspirée par la présence de trois types de cônes ayant des sensibilités différentes (approche dite trichromatique), et la seconde inspirée par le mechanisme d'opposition (proposé initialement par Hering à la fin du XIX siècle et analysé empiriquement par Hurvich et Jameson seulement vers la moitié du XX siècle). Ce dernier est basé sur le fait que certaines couleurs sont opposées, c'est-à-dire qu'elles ne peuvent pas être mélangées sans obtenir une couleur dite achromatique. Le rouge et le vert (également le jaune et le bleu) sont opposés car nous ne pouvons pas percevoir un vert rougeâtre ou un rouge verdâtre. Dans un système construit de cette manière, une couleur perçue est caractérisée par deux degrés d'opposition (rouge-vert et jaune-bleu) et une valeur achromatique (un niveau de gris entre le noir et le blanc). Bien que cette seconde approche soit plus fidèle à la façon dont les humains distinguent et représentent les couleurs, les espaces colorimétriques les plus utilisés dans la littérature pour la reproduction des couleurs ont été construits selon la première approche trichromatique. Cependant, ces modèles sont plus orientés vers l'informatique et ne fournissent pas un formalisme mathématique capable

[*]Voir https://en.wikipedia.org/wiki/The_dress.

de décrire les effets perceptuels connus, ce qui a conduit à de nombreux travaux consistant en des ajustements de paramètres a posteriori, pour combler les lacunes de ces modèles. Ceci souligne le besoin d'un modèle mathématique plus avancé, qui serait plus à même de décrire la complexité de notre vision des couleurs.

L'idée c'est de établir un ensemble d'axiomes que l'espace des couleurs perçues $\mathcal{C}$ doit satisfaire, afin de discerner les structures mathématiques qui sont compatibles avec ces axiomes.

Historiquement, le premier à établir un système d'axiomes pour l'espace des couleurs perçues fut Schrödinger en 1920 [138]. Il reprend et complète les propriétés des couleurs perçues identifiées par ses prédécesseurs Newton, Grassmann et von Helmholtz, obtenant que $\mathcal{C}$ doit être un cône convexe et régulier de dimension 3. En 1974 Resnikoff, dans [135], complète les travaux de Schrödinger en ajoutant un axiome supplémentaire d'homogénéité (c'est-à-dire l'existence d'un groupe de transformations agissant transitivement sur $\mathcal{C}$).

Un théorème de Koecher et Vinberg décrit l'origine algébrique des cônes satisfaisant tous les axiomes décrits jusqu'ici et un axiome supplémentaire d'auto-dualité, ajouté par Berthier dans [12]. En particulier, il stipule que $\mathcal{C}$ peut être identifié avec le cône des éléments positifs d'une algèbre de Jordan formellement réelle (FRJA) $\mathcal{A}$ de dimension 3.
D'après la classification des FRJA de Jordan, von Neumann et Wigner, il n'existe que deux choix possibles (non isomorphes en tant que FRJA) pour $\mathcal{A}$. Appelons-les $\mathcal{A}_1$ et $\mathcal{A}_2$.

La première FRJA admissible est $\mathcal{A}_1 = \mathbb{R} \oplus \mathbb{R} \oplus \mathbb{R}$, dont le cône positif est $\mathcal{C}_1 = \mathbb{R}^+ \times \mathbb{R}^+ \times \mathbb{R}^+$. La seconde possède deux représentations, isomorphes en tant que FRJA, $\mathcal{A}_2 = \mathbb{R} \oplus \mathbb{R}^2 \cong \mathcal{H}(2, \mathbb{R})$. La première représentation est appelée *spin factor*, tandis que la seconde est l'ensemble des matrices symétriques réelles 2×2. Le cône de leurs éléments positifs est $\mathcal{C}_2 = \mathbb{R}^+ \times \mathbb{H}$, où $\mathbb{H}$ est un espace hyperbolique de dimension 2. Dans la représentation du spin factor, $\mathcal{C}_2$ correspond au cône de lumière du futur de la théorie de la relativité restreinte en trois dimensions, tandis que dans la représentation utilisant des matrices symétriques, $\mathcal{C}_2 = \mathcal{H}^+(2, \mathbb{R})$ est l'ensemble des matrices symétriques réelles définies positives 2×2.

Il est remarquable que cette approche axiomatique conduise à deux modèles, $\mathcal{C}_1$ et $\mathcal{C}_2$, qui correspondent exactement aux deux approches (trichromie et opposition) décrites ci-dessus. En fait, les espaces couleurs classiques, construits selon l'approche de la trichromatique, comme RGB, XYZ etc., peuvent être assimilés au modèle $\mathcal{C}_1$, car ils sont construits à partir d'un ensemble de trois primaires. Nous nous concentrons sur l'étude du second modèle $\mathcal{C}_2$, car il possède une structure mathématique plus riche et nouvelle par rapport à l'état de l'art. Plus précisément, sa structure est représentable en adaptant le qubit de la mécanique quantique (cas complexe) au cas réel, voir [12], et correspond également au cône de lumière du futur dans la théorie de la relativité restreinte, voir [13, 165]. Il faut souligner que ce second modèle contient le mécanisme d'opposition de Hering naturellement encodé dans les deux matrices de Pauli réelles. Dans la formulation algébrique de la mécanique quantique la propriété d'auto-dualité du cône des éléments positifs de la FRJA est d'importance fondamentale, car elle permet de représenter intrinsèquement la dualité état-observable.

Comme il sera détaillé dans le Chapitre 5, les opérations de Lüders ont été introduites dans la théorie moderne de l'information quantique pour modéliser le *changement d'état quantique après une procédure de mesure*. En particulier, elles sont paramétrées par des éléments du dual de $\mathcal{C}_2$, qui coïncide avec $\mathcal{C}_2$ par auto-dualité, et sont stables sur $\mathcal{C}_2$.

Une première application de ce point de vue, qui sera détaillée dans le Chapitre 7, est l'utilisation des boost de Lorentz normalisés, liés aux opération de Lüders comme expliqué dans le Chapitre 5, comme transformations d'adaptation chromatique (CATs) pour effectuer la balance des blancs d'images numériques. La balance des blancs est un algorithme qui émule la capacité du système visuel humain à s'adapter à une illumination colorée dans une scène

visuelle (jaunâtre dans la première image de la Figure 1) en voyant la scène comme si elle était éclairée par une lumière blanche. Elle se compose de deux étapes : la première consiste en la détection de l'information sur la chromaticité de l'illuminant contenue dans un vecteur $\vec{L}$, et la seconde est la correction de l'image à l'aide d'une CAT paramétrée par $\vec{L}$. La Figure 1 montre, respectivement, une image d'entrée non corrigée, la même image corrigée avec un algorithme de correction classique (CAT de von Kries), et la même image corrigée à l'aide de la CAT que nous proposons.

Figure 1: *Gauche* : image d'entrée. *Centre* : image de sortie après la balance des blancs en utilisant la CAT de von Kries. *Droite* : image de sortie après balance des blancs effectuée en utilisant la CAT que l'on propose. Les images de sortie ont été obtenues en utilisant la même estimation de l'illuminant.

La structure de $\mathcal{C}_2$ est particulièrement riche grâce aux concepts qui peuvent être adaptés de leurs analogues en mécanique quantique. En particulier, dans ce cadre, une couleur n'est plus décrite en termes de coordonnées, mais elle est le résultat d'une procédure de mesure qui peut être décrite mathématiquement, voir les Chapitres 5 et 6.
Cela nous a permis de fournir des définitions rigoureuses des attributs colorimétriques connus dans la littérature. La présence d'un ensemble de bonnes définitions est essentielle, par exemple pour modéliser des phénomènes connus qui influencent directement la façon dont nous percevons les couleurs (par exemple l'effet de Hunt ou la *lightness constancy*, détaillé dans le Chapitre 6). Il faut souligner qu'il n'existe actuellement aucune justification rigoureuse de ces phénomènes qui puisse permettre, par exemple, de les intégrer dans des algorithmes de traitement d'images en couleur.

En outre, le modèle suggère certaines distances basées sur la théorie, comme la métrique de Hilbert-Klein, invariante sous l'adaptation chromatique, ou l'entropie relative symétrisée, augmentant avec l'adaptation chromatique, qui pourraient être utilisées pour mesurer les différences de couleur, très utiles dans les applications, par exemple comme fonctions de perte en Machine Learning.

Le présent manuscrit est organisé de la manière suivante : après un premier chapitre consacré à l'état de l'art en colorimétrie, les chapitres 2, 3, 4, 5 et 6 fournissent une description de plusieurs aspects du modèle théorique, tandis que les chapitres 7 et 8 sont destinés à montrer la potentialité de cette nouvelle approche à travers des applications au traitement d'images en couleur. Le plan de la thèse est détaillé ci-dessous.

Dans le **Chapitre 1** nous fournissons un bref aperçu de la colorimétrie classique. L'idée est de motiver la présence de notre approche dictée par certaines nécessités et indices présents dans la littérature. En particulier, nous commençons par décrire brièvement la physiologie de la vision des couleurs en nous concentrant sur le mécanisme d'opposition de Hering, puis nous présentons la construction mathématique des espaces de couleurs basés sur la trichromie, en soulignant le fait que l'opposition de Hering n'est pas intégrée dans les espaces obtenus de cette manière. Nous donnons un aperçu de l'utilisation des structures hyperboliques dans la littérature sur la couleur et une brève description de la phénoménologie de la perception des couleurs, en mentionnant notamment les effets perceptuels, les phénomènes de color constancy et lightness constancy, dans le but de souligner les difficultés de modélisation de la perception des couleurs.

Le **Chapitre 2** porte sur le modèle relativiste de perception des couleurs de Yilmaz. En 1962, Yilmaz [166, 165] a été le premier à souligner les analogies formelles entre la théorie de la relativité restreinte et la perception des couleurs. Partant de trois résultats provenant d'expériences, il a déduit que le changement de condition d'adaptation à un illuminant peut être modélisé à l'aide des transformations classiques de la théorie de la relativité restreinte : les boosts de Lorentz. Comme dans [124], nous fournissons dans ce chapitre une interprétation et une analyse de la faisabilité de ses expériences et, en supposant que les résultats expérimentaux soient vrais, nous refondons dans un cadre plus rigoureux la procédure mathématique qui a conduit à l'obtention des boosts de Lorentz pour modéliser l'adaptation chromatique.

Dans le **Chapitre 3** nous commençons par décrire l'approche mathématique de Resnikoff [135] à la perception des couleurs. En particulier, il a complété la formulation algébrique de ses prédécesseurs (initiée par Grassmann et axiomatisée par Schrödinger). Nous présentons ensuite une vue d'ensemble et les définitions de base d'une nouvelle approche mathématique basée sur la réinterprétation quantique des travaux de Resnikoff [15, 129, 12, 16, 18]. Ce nouveau cadre mathématique réconcilie la trichromie et l'opposition des couleurs mentionnées dans le Chapitre 1 et permettra, dans le chapitre suivant, de justifier, sur une base purement théorique, les spéculations de Yilmaz sur les aspects relativistes de la perception des couleurs, en surmontant les problèmes soulignés dans le Chapitre 2.

Dans le **Chapitre 4**, comme dans l'article [13], nous fournissons une preuve théorique des résultats expérimentaux de Yilmaz dans le cadre du cadre de type quantique introduit dans le chapitre précédent. De nouvelles définitions sont introduites afin d'incorporer également les phénomènes relativistes. En particulier, le concept de vecteur chromatique est d'une importance fondamentale, puisque les expériences de Yilmaz peuvent être expliquées en termes de loi d'addition d'Einstein-Poincaré entre les vecteurs chromatiques. De plus, ces résultats théoriques s'avèrent cohérents avec des données expérimentales existantes. Dans ce chapitre, nous présentons la métrique hyperbolique de Hilbert fondée sur la théorie, dont la pertinence est due au fait qu'elle exprime une propriété de constance chromatique par rapport aux changements d'observateurs.

Dans le **Chapitre 5** nous étendons la théorie présentée dans le Chapitre 3 en introduisant certains concepts issus de la théorie de l'information quantique, parmi lesquels : les effets quantiques, les états généralisés post-mesure, les opérations de Lüders et l'entropie relative. Dans ce contexte, une couleur n'est plus décrite par un ensemble de trois coordonnées, mais elle est conçue comme le résultat d'un acte de mesure : il s'agit en fait de l'état généralisé post-mesure obtenu par l'interaction d'un effet et d'un état généralisé. Les concepts introduits ici sont utilisés au Chapitre 6 pour établir les définitions des attributs de colorimétriques dans le cadre du modèle quantique.

Dans le **Chapitre 6**, comme dans [14], les concepts d'information quantique introduits dans le chapitre précédent sont utilisés pour élaborer des définitions mathématiques des attributs colorimétriques (brightness, luminosité, colorfulness, chroma, saturation et teinte). La compréhension de l'expression mathématique de ces attributs est une question fondamentale, notamment parce qu'ils sont impliqués dans les phénomènes d'apparence de la couleur et en raison de leur impact important sur les applications. Nous soulignons que les problèmes de recherche des coordonnées à associer aux attributs colorimétriques ainsi que la description mathématique des phénomènes d'apparence de la couleur sont encore des sujets non résolus et débattus dans la littérature. Pour illustrer le potentiel de ce nouveau système de définitions, nous présentons une justification rigoureuse du phénomène de lightness constancy, introduit dans le Chapitre 1.

Le **Chapitre 7** porte sur une première application du modèle théorique au problème de la balance des blancs en traitement d'images. Plus précisément, nous montrons dans quelles conditions particulières il est possible d'utiliser un boost de Lorentz normalisé, correspondant à l'action d'une opération de Lüders représentée comme agissant sur $\overline{\mathcal{C}}(\mathbb{R} \oplus \mathbb{R}^2)$, comme transformée d'adaptation chromatique. Les premiers tests ont été effectués dans le domaine conique HCV de l'état de l'art, mais les évaluations qualitatives ont montré que le rendu des teintes rouges n'était pas optimal, en particulier qu'elles devenaient rosées. Nous proposons donc deux modifications simples de HCV, intégrant de manière heuristique l'opposition de Hering dans le cercle des teintes. Ces modifications produisent qualitativement des meilleurs résultats. Nous procédons ensuite à une première évaluation quantitative de l'algorithme dans l'espace HCV et de ses modifications en comparaison avec à la CAT classique de von Kries.

Le **Chapitre 8** est consacré aux applications au problème du tone mapping, c'est-à-dire la compression d'une image high dynamic range. Dans une première partie, comme dans [125], nous traitons un opérateur classique de tone mapping, l'équation dite de Naka-Rushton, en l'analysant d'un point de vue géométrique en utilisant les transformations de Möbius. Dans une seconde partie, nous proposons un opérateur de tone mapping en cours de développement, KTMO, inspiré de la construction du disque de Klein.

Dans le **Chapitre 9**, nous concluons le manuscrit en mentionnant des perspectives de recherche futures.

Introduction and thesis outline

In any serious question uncertainty
extends to the very roots of the problem.
– Wittgenstein, *Remarks on colour*.

Color is placed at the crossroads of many scientific paths. Questions about color kept occupied many of the history great thinkers, including Plato himself, and arrive to interpell anyone of us, as proven by the recent debate on *The Dress*[†]. Color is involved in issues related to philosophy (in the tradition of Goethe, Schopenhauer, Russell or Wittgenstein), to the neurophysiology of vision (in the tradition of Hubel or de Valois), or to models of mathematical physics (in the tradition of Newton, Maxwell, von Helmholtz, Schrödinger, Yilmaz or Resnikoff).

In this thesis we deal with the problem of treating color perception from a mathematical point of view.

Physical colors, i.e. reflected or emitted lights entering the eyes from a visual environment, are converted into perceived colors sensed by humans through neurophysiological mechanisms. Mathematically, a physical color is a spectrum, i.e. a function defined on the interval of visible wavelengths, thus an element of a space of infinite dimension, while it is known that to model perceived colors one needs a space of dimension 3. Despite of the smaller dimension, the space of perceived colors is far way less understood and much more controversial to be modeled mathematically.

This is due to the complexity of the neurophysiological processes leading to color perception. Indeed, color perception involves at first three types of photoreceptors, the LMS cones, each one of them is more sensible to a different part of the visible spectrum, in fact the letters L, M, S are used to represent the *Long*, *Middle* and *Short* wavelengths corresponding to the different sensitivity peaks of the cones. Then, in a second moment, the so-called mechanism of opponency of the receptive fields of the retina, induced by the intertwining of connections between cones and ganglion cells, takes place.

There are basically two ways of modeling the space of perceived colors: the first inspired by the presence of three types of cones having different sensitivities, and the second inspired by opponent process or opponency (initially proposed by Hering at the end of the 19^{th} century and experimentally analyzed by Hurvich and Jameson only towards the half of the 20^{th} century). The latter is based on the fact that some colors are opponent, i.e. they cannot be mixed without obtaining a color called achromatic. Red and green (also yellow and blue) are opponent because we can not perceive a reddish green or a greenish red. In a system built in this way, a perceived color is characterized by two opponency degrees (red-green and yellow-blue) and an achromatic value (a gray level between black and white). Despite the fact that this second approach is more faithful to the way humans distinguish and represent colors, the most commonly used color spaces in literature for color reproduction were built following the first trichromatic

[†]See https://en.wikipedia.org/wiki/The_dress.

approach. However, these models are more computer-science oriented and do not provide a mathematical formalism able to describe known perceptual effects, which led to many works consisting of adjustments of parameters a posteriori, to fill the gaps of these models. This underlines the need for a more advanced mathematical model, which would be better able to describe the complexity of our color vision.

The idea is to establish a set of axioms that the space of perceived colors $\mathcal{C}$ must satisfy, in order to discern the mathematical structures that are compatible with these axioms. Historically, the first one to establish an system of axioms for the space of perceived colors was Schrödinger in 1920 [138]. He resumed and completed the properties of perceived colors identified by his predecessors Newton, Grassmann and von Helmholtz, obtaining that $\mathcal{C}$ must be a convex, regular cone of dimension 3. In 1974 Resnikoff, in [135], completed the work of Schrödinger adding a further axiom of homogeneity (i.e. the existence of a group of transformations acting transitively on $\mathcal{C}$).

A theorem by Koecher and Vinberg describes the algebraic origin of the cones satisfying all the axioms described up to now and a further axiom of self-duality, added by Berthier in [12]. In particular it states that $\mathcal{C}$ can be identified with the cone of positive elements of a formally real Jordan algebra $\mathcal{A}$ (FRJA) of dimension 3.
From the classification of FRJAs by Jordan, von Neumann, and Wigner there are only two possible (non isomorphic as FRJAs) choices for $\mathcal{A}$. Let us call them $\mathcal{A}_1$ and $\mathcal{A}_2$.

The first case is $\mathcal{A}_1 = \mathbb{R} \oplus \mathbb{R} \oplus \mathbb{R}$, whose positive cone is $\mathcal{C}_1 = \mathbb{R}^+ \times \mathbb{R}^+ \times \mathbb{R}^+$. The second one has two representations, isomorphic as FRJAs, $\mathcal{A}_2 = \mathbb{R} \oplus \mathbb{R}^2 \cong \mathcal{H}(2, \mathbb{R})$, the first representation is called *spin factor*, while the second one is the set of the real symmetric matrices 2×2. The cone of their positive elements is $\mathcal{C}_2 = \mathbb{R}^+ \times \mathbb{H}$, where $\mathbb{H}$ is a hyperbolic space of dimension 2. In the spin-factor representation $\mathcal{C}_2$ corresponds to the future light-cone of special relativity theory in three dimensions, while in the representation, using symmetric matrices, $\mathcal{C}_2 = \mathcal{H}^+(2, \mathbb{R})$ is the set of real positive definite symmetric matrices 2×2.

It is remarkable that this axiomatic approach leads to two models, $\mathcal{C}_1$ and $\mathcal{C}_2$, that correspond exactly to the two approaches (trichromacy and opponency) described above. In fact classic color spaces, built following the trichromacy approach, like RGB, XYZ etc., can be assimilated to the model $\mathcal{C}_1$, because they are constructed starting from a set of three primaries. We focus on the study of the second model $\mathcal{C}_2$, because it has a mathematically more interesting and novel structure compared to the state of the art. More precisely, its structure is representable by adapting the qubit of quantum mechanics (complex case) to the real case, see [12], and also corresponds to the future light cone in special relativity theory, see [13, 165]. We must stress that this second model contains Hering's opponency mechanism naturally encoded in the two real Pauli matrices. In the algebraic formulation of quantum mechanics the property of self-duality of the cone of positive elements of the FRJA is of fundamental importance, because it permits to intrinsically represent the duality state-observable.

Lüders operations, as it will be detailed in Chapter 5, were introduced in modern quantum information theory to model the *quantum state change after a measurement procedure*. In particular they are parametrized by elements of the dual of $\mathcal{C}_2$, which coincides with $\mathcal{C}_2$ by self-duality, and are stable on $\mathcal{C}_2$.

A first application of this novel approach, as it will be detailed in Chapter 7, is the use normalized Lorentz boosts, related to Lüders operations as explained in Chapter 5, as Chromatic Adaptation Transforms (CATs) to perform white balance of a digital images. White balance is an algorithm that emulates the ability of the human visual system to adapt to a colored illumination in a visual scene (yellowish in the first picture in Figure 2) by seeing the scene as if it was illuminated by white light. It is composed of two steps: the first consist of the detection

of a vector $\vec{L}$ encoding the illuminant's chromaticity, and the second is the correction of the image using a CAT parametrized by $\vec{L}$. Figure 2 shows, respectively, a non-white balanced image, the same image corrected with a classical correction algorithm (von Kries CAT), and the same image corrected using the CAT that we propose.

Figure 2: *Left*: input image. *Center*: output image after white balance using the von Kries CAT. *Right*: output image after white balance using the CAT that we propose. The white balanced images have been obtained using the same illuminant estimation.

The structure of $\mathcal{C}_2$ is particularly rich thanks to the concepts that can be adapted from their analogues in quantum mechanics. In particular, within this framework, a color is not described anymore in terms of coordinates, but it is the outcome of a measurement procedure that can be described mathematically, see Chapters 5 and 6.
This allowed us to provide rigorous definitions of the color attributes known in literature. The presence of a set of good definitions in essential e.g. to model known phenomena directly influencing the way we perceive colors (e.g. Hunt's effect or the *lightness constancy* phenomenon detailed in Chapter 6). We must stress that there is currently no rigorous justification of these phenomena that can allow, for example, to integrate them into color image processing algorithms.

Furthermore the model suggests some theoretically-based distances like the Hilbert-Klein metric, invariant under chromatic adaptation, or the symmetrized relative entropy, increasing with chromatic adaptation, that could be used to measure color differences, very useful in applications, e.g. as loss functions for Machine Learning.

The present manuscript is organized in the following way: after a first chapter about state-of-the art colorimetry, chapters 2,3,4,5,6 provide a description of several aspects of the theoretical model, while chapters 7 and 8 are meant to show the potentiality of this novel approach through applications to color image processing. The thesis outline is detailed below.

In **Chapter 1** we provide a short overview of standard colorimetry. The idea is to motivate the presence of our approach dictated by certain necessities and hints present in the literature. In particular we start by briefly describing the physiology of color vision with a focus on Hering's opponent mechanism, then we present the mathematical construction of trichromacy-based color solids, underlining the fact that Hering's opponent mechanism is not integrated in

color solids obtained in this way. We provide an overview of the use of hyperbolic structures in the color science literature and a brief description of the phenomenology of color perception, in particular mentioning perceptual effects, lightness constancy and color constancy, with the aim of stressing the difficulties of modeling color perception.

Chapter 2 is about Yilmaz's relativistic model of color perception. In 1962 Yilmaz [166, 165] was the first to underline the formal analogies between special relativity theory and color perception. Starting from three results that he claimed to be coming from experiments, he deduced that the change of adaptation condition to an illuminant can be modeled using the classic transformations of special relativity theory: Lorentz boosts. As in [124], in this chapter we provide an interpretation and analysis of the feasibility of his experiments and, assuming the experimental outcome to be true, we recast in a more rigorous framework the mathematical procedure that lead to obtain Lorentz boosts to model chromatic adaptation.

In **Chapter 3** we start by describing Resnikoff's [135] mathematical approach to color perception. In particular he completed the algebraic formulation of his predecessors (started by Grassmann and axiomatized by Schrödinger). Then an overview and the basic definitions of a novel mathematical approach based on the quantum reinterpretation of Resnikoff's work [15, 129, 12, 16, 18] is presented. This new mathematical framework reconciles trichromacy and color opponency mentioned in Chapter 1 and will permit, in the following chapter, to justify on a purely theoretical basis Yilmaz's speculations about the relativistic aspects of color perception, overcoming the issues underlined in Chapter 2.

In **Chapter 4**, as in [13], we provide a theoretical proof of the experimental outcomes claimed by Yilmaz in the setting of the quantum-like framework introduced in the previous chapter. Novel definitions are introduced in order to incorporate also relativistic phenomena. In particular the concept of chromatic vector is of fundamental importance, since Yilmaz's experiments can be explained in terms of Einstein-Poincaré's addition law between chromatic vectors. Moreover these theoretical results are shown to be coherent with existing experimental data. In this chapter we introduce the theoretically-based Hilbert hyperbolic metric, whose relevance is due to the fact that it expresses a chromatic constancy property with respect to observer changes.

In **Chapter 5** we extend the theory presented in Chapter 3 introducing some concepts coming from quantum information theory, among them: quantum effects, post-measurement generalized states, Lüders operations and relative quantum entropy. In this setting a color is not described anymore by a set of three coordinates, but it intended as the outcome of a measurement procedure: in fact it is the post-measurement generalized state obtained from the interaction of an effect and a generalized state. The concepts introduced here are used in Chapter 6 to establish definitions of color attributes within the quantum-like model.

In **Chapter 6**, as in [14], the quantum-information concepts introduced in the previous chapter are used to elaborate mathematical definitions of color appearance attributes (brightness, lightness, colorfulness, chroma, saturation and hue). Understanding the mathematical expression of color attributes is a fundamental question also because they are involved in the so called color appearance phenomena and because of their high impact on applications. We stress that both problems of finding coordinates to associate to color appearance attributes and a mathematical description of color appearance phenomena are still unsolved and debated topics in the literature. To illustrate the potential of these new system of definitions, a rigorous derivation of the lightness constancy phenomenon, introduced in 1, is provided.

Chapter 7 is about a first application of the theoretical model to the problem of white balance in image processing. More specifically we show under which particular conditions it is possible to use a normalized Lorentz boost, corresponding to the action of a Lüders operation represented as acting on $\overline{\mathcal{C}}(\mathbb{R} \oplus \mathbb{R}^2)$, as a chromatic adaptation transform. The first tests were performed in the conic-shaped state-of-the art HCV color domain, but qualitative evaluations showed that the rendering of red hues was not optimal, in particular they were turning pinkish. Hence we propose two simple modifications of the HCV color domain, heuristically integrating Hering's opponency in the hue circle, that give better results. Finally a first quantitative evaluation of the algorithm in HCV and its modifications is provided and compared with respect to the classic von Kries CAT.

Chapter 8 is dedicated to applications to the problem of tone mapping, i.e. the compression of a high dynamic range image. In a first part, as in [125], we treat a classic tone mapping operator, the so-called Naka-Rushton equation, analyzing it from a geometrical point of view using Möbius transformations. In a second part we propose a work-in-progress tone mapping operator, KTMO, inspired by Klein's disk construction.

In **Chapter 9** we conclude the manuscript mentioning some possible future research directions.

Contributions

This thesis is based upon the following publications, listed chronologically:

Journals

[124] N. Prencipe, V. Garcin, and E. Provenzi. Origins of hyperbolicity in color perception. *Journal of Imaging*, 42(6):1-19, 2020.

[13] M. Berthier, V. Garcin, N. Prencipe, and E. Provenzi. The relativity of color perception. *Journal of Mathematical Psychology*, 103:102562, 2021.

[126] N. Prencipe and E. Provenzi. Geometric models for color perception. *Cultura e Scienza del Colore - Color Culture and Science*, 13(02):50-56, 2021.

[14] M. Berthier, N. Prencipe, and E. Provenzi. A quantum information-based refoundation of color perception concepts. *SIAM Journal on Imaging Sciences*, 15(4):1944-1976, 2022.

Conferences proceedings

[68] A. Guennec, N. Prencipe, and E. Provenzi. Color correction with lorentz boosts. In *2021 The* 4^{th} *International Conference on Image and Graphics Processing*, ICIGP 2021, page 162-168, New York, NY, USA, 2021. Association for Computing Machinery.

[125] N. Prencipe, and E. Provenzi. Embedding Naka-Rushton's equation in the geometric setting of Möbius transformations. In *2021* 12^{th} *International Symposium on Image and Signal Processing and Analysis (ISPA)*, pages 259-263, 2021.

In particular [124] will be the object of Chapter 2, while the content of [13] will be analyzed in Chapter 4, [14] in Chapter 6, [68] in Chapter 7 and [125] in Chapter 8. Finally [126] is an outreach publication about the content of Chapters 2 and 3.

Chapter 1

About standard colorimetry and related issues

Wittgenstein's 182^{nd} remark on colors states that, when we talk about perceived colors, '*we are not concerned with the facts of physics here except insofar as they determine the laws governing how things appear*', see [160]. In [155] von Neumann, comparing a computer with the human brain, mentions color as an example of *complex information* that the brain elaborates.

Colorimetry and color appearance models deal with the issues of measuring, representing and predicting color *information*, in other words they are about understanding *the laws governing how* colors *appear*.

The aim of this chapter is to provide a brief introduction to standard colorimetry, color appearance models, color attributes and perceptual phenomena. The idea is to point out the problematic aspects of modeling color perception and, in particular, to focus on the mathematical ideas behind trichromacy-based colorimetry in order to motivate our novel mathematical approach to color, that will be treated in the following chapters. Giving an exhaustive description of the state of the art is out of the purposes of this chapter. Several books treat the mentioned topics in detail, among them [88, 85, 49, 137, 163, 66, 120].

In particular we will conclude that our work essentially arises from the necessity of a well-founded mathematical color appearance model based on Hering's opponent mechanism.

1.1 An overview of trichromacy-based colorimetry

Physical and perceived colors

Color perception in humans is originated by reflected or emitted light spectra, which are superpositions of finite-energy electromagnetic waves with wavelengths in the visual spectrum, usually taken to be the interval $\Lambda = [380, 780]$, measured in nanometers, and their mathematical representation is given by positive-valued elements of $L^2(\Lambda)$, let us call this set $L^2_+(\Lambda)$ from now on. Thus the space of physical colors is a space of functions corresponding to light spectra having finite energy, represented by their L^2-norm. Functions with a Dirac-like behavior around a single wavelength are called *narrow-band* light spectra or monochromatic lights.

The fact that light spectra, also called color *stimuli*, and color *sensations* are two very distinct concepts has been known since the nineteenth century. Indeed in 1801 Young exposed to the Royal Society his theory about the existence of three portions of cells sensitive to different light wavelength in the retina. He formulated this hypothesis on the basis of the work of painters, who could reproduce a huge number of color sensations using only three '*primary pigments*'. More than fifty years later, Maxwell formalized the color matching technique which extended the previous result from pigments to light spectra (see later for more details).

Maxwell's experimental results were extremely convincing and were a source of inspiration for Helmholtz, who rescued Young's ideas from oblivion and gave them a mathematical formalization. The resulting theory is nowadays called Young-Helmholtz trichromatic model of color perception. It is also important to notice that color matching was also used by Grassmann as an operative way to apply and test his newly discovered equations of what nowadays is called linear algebra.

In mathematical terms, while the space of physical light spectra is an infinite dimensional space, that of perceived colors is generally confined in a convex region with finite volume, called *color solid*, inside a three-dimensional vector space. About the definition of color solids, in [88], Koenderink and van Doorn make the following considerations: '*That there exist so many colour solids is largely the result of human fancy. The one feature that is common to (almost) all colour solids that have been proposed is that they are convex, finite bodies with pronounced singularities at the white and black poles. This feature, at least, has firm roots in colorimetry*'.

Nowadays, thanks to physiological evidences, that confirmed Young's hypothesis, we know that the biological reason underlying this huge dimensional reduction is that the variability of our photoreceptors is limited to the three LMS cones (where the letters L,M,S are used to represent the *Long*, *Middle* and *Short* wavelengths corresponding to the three sensitivity peaks of the cone photoreceptors) and that infinitely different light spectra produce the same LMS outputs, thus igniting the same chain of events that leads to a color sensation. This phenomenon is synthetically referred to as *metamerism*. As Hardin underlines in [70] '*the eye is a very imperfect analyzer of wavelengths*'. It is important to stress that the post-cones visual chain includes the interlacing of LMS signals, mainly performed by ganglion cells, which gives rise to the achromatic plus color opponent encoding that is sent to the visual cortex and which provides the biological explanation of Hering's theory and also its compatibility with trichromacy.

Opponent color theory was introduced by E. Hering in [72], in [91] Krantz describes it as follows: '*E. Hering noted that colors can be classified as reddish or greenish or neither, but that redness and greenness are not simultaneously attributes of a color. If we add increasing amounts of a green light to a reddish light, the redness of the mixture decreases, disappears, and gives way to greenness. At the point where redness is gone and greenness is not yet present, the color may be yellowish, bluish, or achromatic. We speak of a partial chromatic equilibrium, with respect to red/green... Similarly, yellow and blue are identified as opponent hues...*'.

In the following we are going to briefly mention the physiological mechanism of opponent neural coding, as summarized in Section 7.1 of [12], for further details see [133, 38, 36, 35].

As stated before the vision pipeline starts with the signals obtained by the LMS cone photoreceptors, the physiological basis of trichromacy, while the opponent process takes place later on in the chain, at the level of ganglion cells. These cells receive the input signal from the so-called bipolar and amacrine cells and transmit it to the lateral geniculate nucleus through ganglion axons. Ganglion cells function in the following way: they are activated in case light falls in the center of their receptive fields, while they are inhibited when light falls in the surround of the receptive field. They are referred to as on-center and off-surround. Off-center and on-surround ganglion cells exist as well, and they work in the opposite way.

There are two types of spectral opponent interactions: the first one produces the L-M and M-L spectral opposition and is obtained by the activity rate of midget ganglion cells of the fovea, while the second one produces the S-(L+M) and (L+M)-S spectral opposition and is given by the activity rate of bistratified ganglion cells. It exists as well another type of spectral non-opponent signal obtained by the activity rate of the parasol ganglion cells, which encodes the L+M and -(L+M) information.

To underline the fundamental role of opposition in creating the sensation of color, we quote this sentence taken from [38]: '*It is very misleading to consider the cones as color receptors or give them color names* [...] *The specific information about color comes from lateral neural interactions which in every case involve a comparison of activity in different receptors* [...] *although this fact is hidden by tenacious old theories and the continued use of color names for receptor types*'.

Hering's opponent process theory for color vision has been confirmed by both physiological and psychophysical evidences. However still a lot of aspects about it remain unclear, e.g. the exact hues involved in the opposition, or how to properly integrate it in the construction of color solids. The latter problematic will be better discussed later on in this chapter.

By colorimetry we mean the science of measuring perceived colors. The *International Commission on Illumination* (CIE, for the french *Commission Internationale de l'Éclairage*) is the international authority on colorimetry. Its main purpose is to provide standards for light, illumination, color, and color spaces, in order to allow universal color representation and reproducibility for scientific or industrial purposes.
Evaluating color perception is an extremely complex task, that can be accomplished only under a very controlled experimental context. Indeed it is impossible to measure colors in an absolute way, many factors come to play, to mention just some: background, illumination, total or partial adaptation to the illumination, the nature of the color stimulus (additive or subtractive) etc. Even fixing the viewing conditions it is still challenging to quantify a color stimulus. However evaluating color differences, under fixed viewing conditions, turns out to be a much easier and robust task to accomplish for the human visual system (HVS from now on). This led to the development of the so-called *color matching experiments*. in which a human tester is positioned in a dark room in front of a bipartite field as in Figure 1.1. The left part

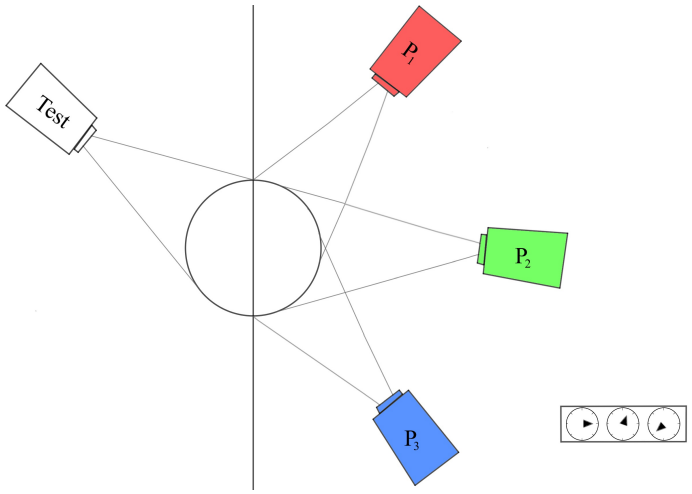

Figure 1.1: Color matching experimental apparatus: test stimulus on the left side of the bipartite champ, on the right side 3 primaries P_1, P_2, P_3, whose intensities can be set by the observer in order to obtain the match with the test stimulus.

contains the light of a reference stimulus, called *test*, from a projector equipped with a filter (nowadays, most often stimuli come from a computer monitor). On the right, the stimulus comes from the superposition of three lights that the observer can modulate in intensity until the edge between the two parts of the field vanishes. When this condition is reached the stimuli are said to *match*. It has been proven that for some stimuli, color matching is not possible in this configuration. In these particular cases, only two lights are superposed on the right side, and the third one is superposed on the test stimulus. The three lights allowing color match

turn out to have the property of being independent, i.e. none of them can be matched by mixing the other two. Any three lights satisfying this feature are called *primaries*.

Wright and Guild in 1928-29 and 1931, respectively, independently carried out two sets of observations (on 10 and 7 observers, respectively) that confirmed and extended Maxwell's experimental findings: for any test stimulus, three independent lights are necessary and sufficient to obtain the match. Either the superposition of three independent lights matches the test stimulus, or the superposition of this stimulus and one of the three lights matches the two remaining lights.

A thorough description of *color solids* is beyond the scope of this chapter, in the following we will limit ourselves to describe the mathematical procedure behind trichromatic colorimetry.

Trichromatic colorimetry

In this paragraph we are going to briefly recall the widely used CIE construction to perform the dimensional reduction from the space of light stimuli $L^2_+(\Lambda)$ to a color solid equipped with a coordinate system.

This procedure has been embedded in a rigorous mathematical framework by Krantz in [90] and by Dubois in [44]. In particular, they used Grassmann's laws [67, 163] to give a mathematical structure to the space of light spectra and related it to a cone embedded in a three-dimensional vector space, which they proved to be unique up to a change of basis. Each basis is related to a different way of coding metamerism. In [90], Krantz defines what he calls code in the following way: *'By a color code (or color mechanism in the sense of Stiles, 1967) we mean some response or function that subserves color discrimination'*. In other words he calls *color code*, or just *code* each coordinate system in a three-dimensional vector space induced by three linearly independent functions of $L^2_+(\Lambda)$.

Let us describe the CIE procedure properly. Let $C \in L^2_+(\Lambda)$ be a color stimulus and S_i, $i =$ L,M,S, be the spectral sensitivity functions of the LMS cones. The *cone activation coefficients* related to C are

$$\alpha_i(C) = \int_\Lambda C(\lambda) S_i(\lambda) \mathrm{d}\lambda, \quad i = \mathrm{L,M,S} \tag{1.1.1}$$

and the set of triplets $(\alpha_i(C))_{i=\mathrm{L,M,S}}$, as C varies in the space of color stimuli, is called the LMS space. CIE switched the interest away from the LMS space by fixing three primaries P_k and by defining the *tristimulus values* of C associated to them, denoted with $T_k(C)$, as the three scalar coefficients that permit to combine the primaries P_k in order to color match C, i.e. those satisfying the following equation

$$\alpha_i(C) = \sum_{k=1}^{3} T_k(C) \int_\Lambda P_k(\lambda) S_i(\lambda) \mathrm{d}\lambda = \sum_{k=1}^{3} T_k(C) \alpha_i(P_k), \tag{1.1.2}$$

where $i = L, M, S$ and $\alpha_i(P_k)$ are the cone activation coefficients related to the primaries P_k, with $k = 1, 2, 3$, obtained as in Equation (1.1.1).
CIE defined the so-called *color matching functions*, $T_k : \Lambda \to \mathbb{R}$ as those satisfying

$$T_k(C) = \int_\Lambda C(\lambda) T_k(\lambda) \mathrm{d}\lambda, \quad k = 1, 2, 3. \tag{1.1.3}$$

If we compare Equations (1.1.1) and (1.1.3) we see that color matching functions are to tristimulus values what cone sensitivity functions are to cone activation values, but, while the latter functions are fixed, color matching functions can vary by selecting different primaries.

As we are going to see, the possibility to modify the basis of functions accordingly to different needs has been exploited in several occasions. In the following we are going to start mentioning two relevant classic examples of curves proposed by the CIE, that led to the RGB and XYZ color spaces.

- In 1931, CIE defined the 'standard observer' by fixing the so-called Wright primaries, see e.g. [163], or, equivalently, a set of three specific color matching functions denoted with $\bar{r}, \bar{g}, \bar{b}$, see Figure 1.1 (a). The associated tristimulus values are the elements of the famous CIE RGB space, used e.g. in [86]. It is important to stress that this basis is obtained from three physical primaries which has no perceptual meaning, in the sense that there is no differentiation between the three coordinates, all of them are of the same kind.

- Not pleased with the negative lobe of $\bar{r}$, CIE modified the primaries and defined other, completely positive, color matching functions, denoted with $\bar{x}, \bar{y}, \bar{z}$, depicted in Figure 1.1 (b), giving rise to the equally famous CIE XYZ space, in which Y plays the role of 'luminance', an attribute roughly associated with the intensity of a color stimulus, which can then be seen as an achromatic component. Indeed the color matching function $\bar{y}$ is more or less the normalized S_M. However there is no such perceptual interpretation of the two other tristimulus values X,Z. This is due to the fact that this basis is obtained from the selection of three virtual primaries, and it does not allow to describe perceptual features. Nevertheless, CIE XYZ is widely used, see e.g. [80, 144, 156].

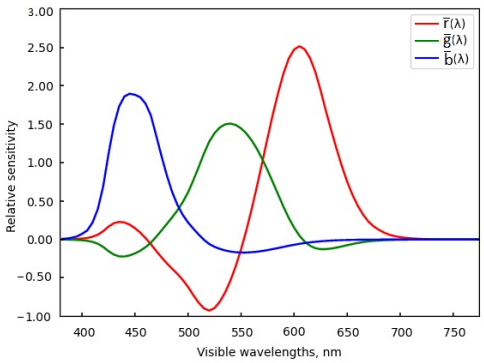

(a) CIE 1931 $\bar{r}, \bar{g}, \bar{b}$ color matching functions.

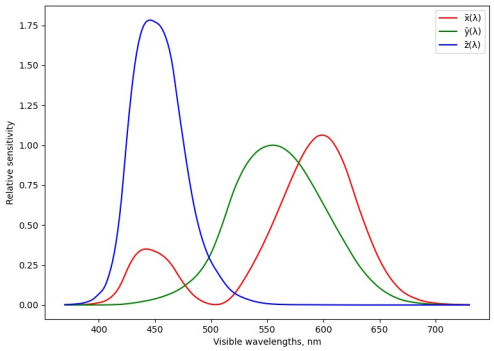

(b) CIE 1931 $\bar{x}, \bar{y}, \bar{z}$ color matching functions.

Figure 1.2: Two classic examples of color matching functions.

Most of the state of the art color solids, as e.g. HSL, HSV, HSI, LCh(ab), LCh(uv) and so on, do actually rely on the dimension reduction performed with respect to these two examples of color matching functions, and are then obtained by, not always perceptually justified, manipulations of the RGB or XYZ coordinates. It is really important to stress that with this setting the starting point is a color space that is trichromacy-based, in the sense that it is built from three information that are all of the same kind. Integrating Hering's opponent mechanism a posteriori (like in the CIELab color space), on a space which is intrinsically trichromatic is extremely complicated.

The choice of a basis, with respect to which one performs the dimension reduction, is arbitrary and is obtained in different ways in literature.

Lenz et al. in [99, 100] and as well Buchsbaum et al. in [25] make use of a principal component analysis (PCA) on a database of light spectra to obtain the basis with respect to which perform the reduction. Clearly the PCA procedure depends on the adopted dataset. It is interesting that in both cases the curves obtained with this technique seem to go in the direction of representing two degrees of opponency and an achromatic information.

There are some other interesting choices of basis functions in literature, made with the intent of translating Hering's opponent mechanism in the coordinates system of the color solid and thus to differentiate what is perceptually considered as achromatic from what is chromatic. Drösler in [42] defines a color solid using as basis the Gaussian, which minimizes the uncertainty principle, and its two first moments, for more details see [122]. Yilmaz also makes the same choice in Section 4 of [165]. He remarks that '*his three sensitivity functions become the first three eigenfunctions of linear harmonic oscillator*'. He calls $\bar{\alpha}, \bar{\beta}$ the first two moments of the linear harmonic oscillator, representing the theoretical opponent sensitivity functions (red-green and yellow-blue respectively). The brightness sensitivity function $\bar{\gamma}$, representing the theoretical achromatic information, is a Gaussian, with maximum around the green part of the visual spectrum at 552 nm, vanishing at 400 nm and 800 nm. An explicit expression of the sensitivity curves proposed by Drösler and Yilmaz, plotted in Figure 1.3, is the following:

$$\bar{\alpha}(\lambda) = -\sqrt{2}u(\lambda)e^{-\frac{u(\lambda)^2}{2}}, \qquad \bar{\beta}(\lambda) = -\frac{1}{\sqrt{2}}(2u(\lambda)^2 - 1)e^{-\frac{u(\lambda)^2}{2}}, \qquad \bar{\gamma}(\lambda) = e^{-\frac{u(\lambda)^2}{2}}, \quad (1.1.4)$$

where $u(\lambda) = 7500(\frac{1}{\lambda} - \frac{1}{552})$.

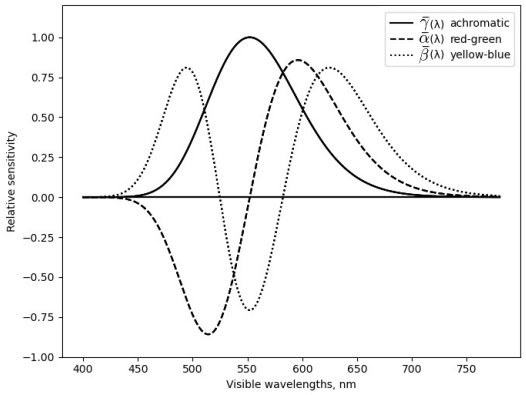

Figure 1.3: An illustration of the sensitivity curves $\bar{\alpha}, \bar{\beta}, \bar{\gamma}$ proposed by Drösler and Yilmaz: eigenfunctions of the harmonic oscillator.

In [165] Yilmaz underlines the similarity of the proposed theoretical curves with experimental curves of Hering's opponent theory. A remarkable experimental work with the objective of quantifying Hering's opponent mechanism was realized in the $50's$ by the couple of scientists Jameson and Hurvich in a series of articles [74, 75, 76, 77] entitled *Some quantitative aspects of an opponent-colors theory.* In particular, in [75], they proposed experimentally based *response curves* for color opponency obtained via hue cancellation experiments. They propose two sensitivity functions corresponding to the red-green and yellow-blue chromatic response, respectively. Let us call them $\overline{rg}, \overline{yb}$. They are given as linear combinations of the color matching functions $\bar{x}, \bar{y}, \bar{z}$ as follows:

$$\begin{cases} \overline{rg}(\lambda) = 1.0065\bar{x}(\lambda) - 1.0006\bar{y}(\lambda) - 0.0051\bar{z}(\lambda) \\ \overline{yb}(\lambda) = -0.0039\bar{x}(\lambda) + 0.3998\bar{y}(\lambda) - 0.3999\bar{z}(\lambda) \end{cases} . \quad (1.1.5)$$

Figure 1.4 illustrates both the original Jameson and Hurvich's plot of the curves $\overline{rg}$ and $\overline{yb}$, and a plot obtained via linear operations of Equation (1.1.5) on the color matching functions $\bar{x}, \bar{y}, \bar{z}$ in Figure 1.1 (b).

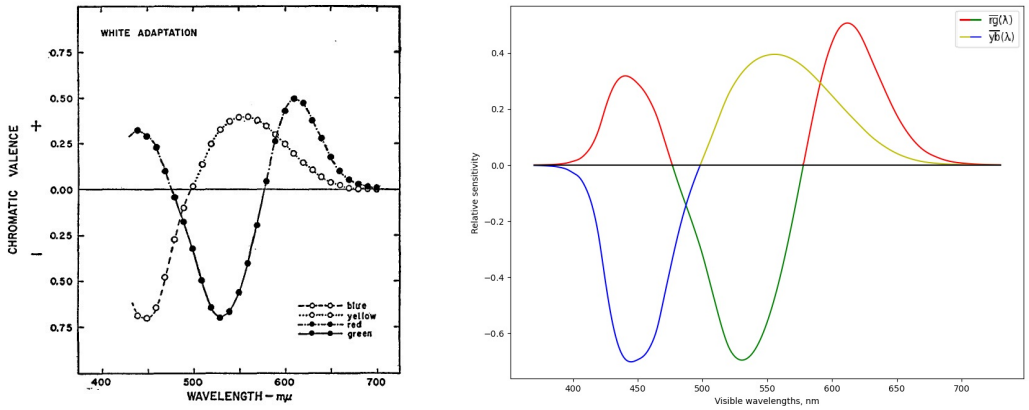

Figure 1.4: *Left*: Jameson and Hurvich sensitivity curves to color opponency under adaptation to neutral illuminant, as reported in [75]. *Right*: plot of the same sensitivity functions obtained from $\bar{x}, \bar{y}, \bar{z}$, using Equation (1.1.5).

Coherently with what Yilmaz stated in [165], the sensitivity curves $\bar{\alpha}, \bar{\beta}, \bar{\gamma}$, actually qualitatively look like e.g. the functions $\overline{rg}, \overline{yb}, \bar{y}$, where $\bar{y}$ comes from the CIE color matching functions $\bar{x}, \bar{y}, \bar{z}$, see Figures 1.3, 1.4 and 1.1 (b). In Chapter 9 we will talk about the idea of using the functions $\overline{rg}, \overline{yb}, \bar{y}$ to define an opponent color solid.

As Jameson and Hurvich stress in [76], this kind of curves are obtained under fixed adaptation condition to neutral illuminant. Hence they might change under adaptation to different illumination conditions. It is important to stress that all the color solids in literature have this feature: they were built under fixed conditions, thus it is not correct to use them to describe colors perceived under other viewing conditions. As Fairchild states in [49], citing note 6 on the CIELAB space from CIE publication 15.2: '*These spaces are intended to apply to comparisons of differences between objects colours of the same size and shape, viewed in identical white or middle-grey surroundings, by an observer photopically adapted to a field of chromaticity not too different from that of average daylight*'. This is the main reason that led to the development of color appearance models, which will be briefly discussed in Section 1.3.

Chromaticity diagrams

The color solid is not a useful or intuitive representation to identify perceived colors, this is the reason that led to the introduction of the concept of *chromaticity diagram*. As stated by its name, a chromaticity diagram, is a two-dimensional area which contains the chromatic features of a perceived color, which are supposed to be perceptually easier to identify. This identification should be performed through attributes that are 'perceptually friendly', like Munsell's ones: hue and chroma or hue and saturation, see Section 1.3 about color attributes.

The concept of chromaticity diagram was firstly introduced by Maxwell in his Cambridge years (1850-1856). Defining a chromaticity diagram in a three-dimensional space of perceived colors means, implicitly, stating that the chromatic part of a perceived color has dimension 2, thus that there exists a mono-dimensional achromatic color coordinate. The chromatic part of a perceived color is isolated by discarding in some sense the achromatic part. Given a certain

color solid the construction of the chromaticity diagram is as arbitrary as the choice of the basis of functions, mentioned in at the end of the previous section, to construct the color solid. It is essentially an operation of dimensional reduction from 3 to 2 and there is not an unique way to perform it. The most common way used in literature is through a normalization of the coordinates. The choice of the normalizing factor as well as the two coordinates to normalize, however, still remains arbitrary.

A typical example is how the CIE defined the chromaticity coordinates in the XYZ space as $x = X/(X+Y+Z)$, $y = Y/(X+Y+Z)$, $z = Z/(X+Y+Z)$ and defined the color space xyY as the set of all chromaticity coordinates (x, y) together with the luminance Y of all color stimuli. The choice of the plane (x, y) is arbitrary, we could have chosen analogously the coordinates (x, z) for instance. Other classic CIE chromaticity diagrams were obtained applying Möbius transformations to the xy coordinates, such as CIE 1960 UCS (Uniform Color Space) whose coordinates are called uv and CIE 1976 UCS with $u'v'$ coordinates. Figure 1.5 shows CIE xy, uv and $u'v'$ chromaticity diagrams. The idea of these successive deformations of the xy chromaticity diagram was one hand to transform MacAdam ellipses into circles all of the same size, on the other hand to have a radial and angular coordinate more similar to perceived saturation and hue. Both problems will be treated in the following sections. Notice that in none of these chromaticity diagrams Hering's opponency is present.

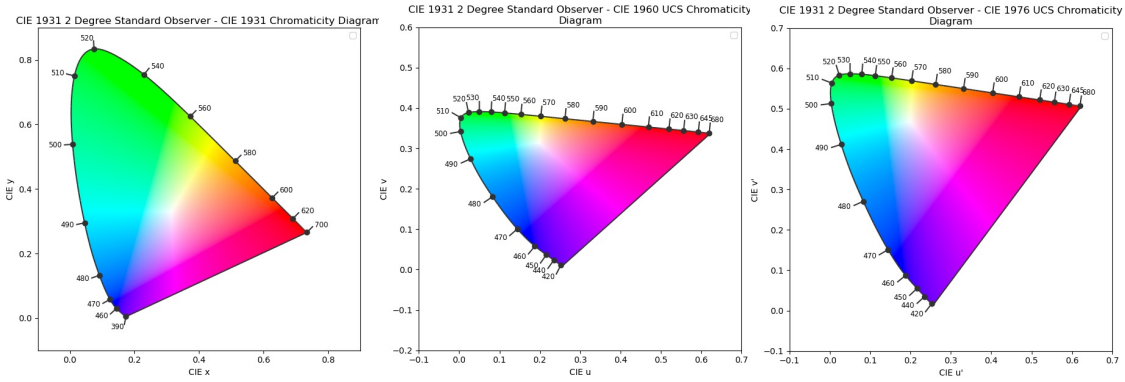

Figure 1.5: *Left*: CIE 1931 xy chromaticity diagram. *Center*: CIE 1960 UCS uv chromaticity diagram. *Right*: CIE 1976 UCS $u'v'$ chromaticity diagram. These figures have been created using the open-source Python package *Colour*, see https://colour.readthedocs.io/en/develop/.

Drösler in [42] was the first one to interpret this standard procedure of normalization in terms of *projective geometry*. Indeed those kind of normalizations can be seen as different choices of affine charts of a projective space of dimension 2. In his paper Drösler justifies his choice of a particular chromaticity diagram stating that it is not restrictive, since different planes are mathematically equivalent. Indeed, given two projective planes, it always exists a projective transformation, i.e. cross-ratio preserving (as we will see in Chapter 3, this implies that it preserves the Klein metric), that maps one into the other.

Constructing a proper perceptual chromaticity diagram is problematic. Indeed, to do that, we need to postulate the existence of an achromatic information, expressed in the coordinates of the color solid*, to find a privileged normalization. Thence we can correctly isolate the chromatic part of a perceived color or, equivalently, eliminate its achromatic part, through a division by this achromatic coordinate. Lenz, in [100], constructs his chromaticity diagram in this way. Nevertheless many of the chromaticity diagrams adopted in literature lack of

*In [145] there are several classic choices for the achromatic coordinates used in literature such as $\frac{R+G+B}{3}$, or the Y coordinate from the XYZ color space, or the so-called value $V = \max\{R, G, B\}$.

perceptual pertinence, i.e. they are not constructed by discarding what they do identify as achromatic information.

The concept of perceptual pertinence of a chromaticity diagram is controversial, not just because of the difficult procedure of identifying and discarding the achromatic coordinate, but also the chromatic coordinates are problematic. Ideally, the radial and angular coordinate should correspond to perceived saturation (or chroma, in some cases) and hue. However, as we will see in the following sections, there is no clear correspondence between these perceptual attributes and existing chromaticity coordinates, and the interdependence phenomena between these two perceptual attributes are not fully understood.

1.2 Evidences of hyperbolic structures in color science

Several works in literature suggest the underlying intrinsic hyperbolic nature of color spaces. Most of them, based on the intuition that Euclidean geometry is not suitable to describe color dissimilarity[†], propose new hyperbolic color metrics defined on existing color solids or chromaticity diagrams. This subsection is about the state of the art on the use of hyperbolic structures in color science, as presented in Section 1.1 of [13].

There are two main experimental facts that suggest the hyperbolic nature of color: MacAdam ellipses and the *hue super importance* phenomenon pointed out by Judd.

The first phenomenon was discovered in 1942 by MacAdam: in [106] he showed that the *just-noticeable difference*, JND from now on,[‡] contours in the CIE xy chromaticity diagram are not circles, as one would expect if the perceptual distance were Euclidean, but are much better approximated by ellipses, see Figure 1.6. In other words the colors inside an ellipse are indistinguishable to an average observer. This work had an immediate influence on Silberstein, who, in his 1943 paper [144], defined a perceptual hyperbolic metric, i.e. a perceptual line element, from the MacAdam ellipses i.e. he searched for a metric defined on the CIE 1931 xy chromaticity diagram, with respect to which MacAdam ellipses are circles of the same radius.

MacAdam's work also impacted von Schelling: in the 1956 paper [156] he proposed the first, up to our knowledge, explicit hyperbolic metric, with the aim of approximating the MacAdam ellipses. CIELab itself was a color space built with the purpose of deforming XYZ in such a way to transform MacAdam ellipses into circles, and as well the CIE uv and $u'v'$ chromaticity diagrams.

A further evidence in favor of the non-Euclidean nature of a perceptual color metric was provided by Judd in 1970 [80]: an experimental setup to implement von Helmholtz's line element theory showed that the JND of chroma is larger than the JND of hue, i.e. that *humans are more sensitive to changes in hue than in chroma.* To describe this phenomenon, Judd coined the term *super-importance of hue differences*, also known as *hue super-importance.* This work inspired Farup and Nölle et al. Farup, in [51], proposed to equip the a^*b^* chromaticity diagram of the CIELab space with the Poincaré metric, showing that this is coherent with both MacAdam's and Judd's results. Nölle et al., in [118] defined a new space that takes into account perceptual attributes in the choice of the coordinates and the hue super-importance. Their color solid is a three-dimensional complex manifold embedded in a four-dimensional complex vector space. The Euclidean metric of the four-dimensional complex space turns to be hyperbolic if expressed in the coordinates parametrizing the three-dimensional manifold.

[†]Up to our knowledge, all the evidences lead to hyperbolic geometry and not to other non-Euclidean geometries.

[‡]The term JND, as defined e.g. in Chapter 1 of [128], generally refers to '*the least perceptible intensity change*' of a stimulus.

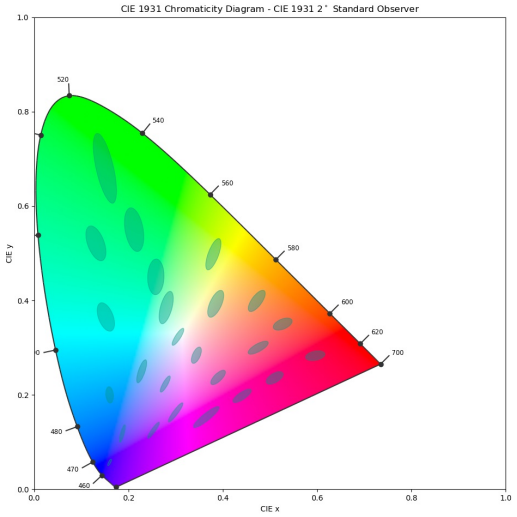

Figure 1.6: MacAdam ellipses for one of MacAdam's test participants, plotted ten times their actual size on the CIE 1931 xy chromaticity diagram. This figure has been created using the open-source Python package *Colour*.

Finally, Lentz et al., in [99, 100], showed the compatibility of data concerning the path of a point in an image under smooth changes of the illuminant with the geodesics of the Poincaré hyperbolic metric on the chromaticity diagram.

Some authors [156, 166, 86] defined the hyperbolic metric on the whole three-dimensional color solid, but the great majority of them, especially the most recent ones, focus on the problem of defining a metric on the chromaticity diagram that they have constructed. While the CIExy chromaticity diagram is sometimes tacitly assumed to inherit the Euclidean metric, several hyperbolic proposals have been done in literature, introduced with different justifications.

Two main different approaches can be identified: a first one more conceptually-based on Weber-Fechner's law, a second one more empirical.

Silberstein, in 1938, pursuing the line element method initiated by von Helmholtz in [152], theorized in [143] that a perceptual metric on an abstract projective chromaticity diagram should not be Euclidean if one assumes Weber-Fechner's law to hold, i.e.

$$\Delta S = k\frac{\Delta I}{I}, \tag{1.2.1}$$

where ΔS is the JND in brightness sensation provoked by the modification of light intensity ΔI w.r.t. a fixed background intensity I, k being a positive real constant.

Notice that Weber-Fechner's law says that the line element must be invariant w.r.t. homothetic transformations. Starting from this statement, Drösler in [42, 43] got the intuition that the space of perceived colors is projective. In particular he stated that Weber-Fechner's law in dimension 1 represents a projective line element that can be generalized to the whole three-dimensional space in [43] and to the chromaticity diagram in [42]. On this last, because of its projective nature, the metric turns out to be the Klein metric. Indeed, as we will see in Chapter 3, Klein's metric can be expressed as function of the cross-ratio, i.e. the only projective invariant, hence this metric is preserved under projective transformations and it is a natural metric for a projective structure.

Koenderink and his collaborators in [86] implement Weber-Fechner's law in the RGB color coordinates and come up to a Klein-like metric as Drösler. This means that implementing

Weber-Fechner's law is equivalent to have a projective model and metric. Koenderink and his collaborators [86] have actually an hybrid approach (both conceptual and empirical), because some parameters in the metric that they propose are set to fit with the Bezold-Brüke effect, i.e. the perceptual change in hue when the intensity of a color stimulus is modified, see also Chapter 10 of Koenderink's book [85] and Section 1.3. Without proposing a metric as such, Ennis and Zaidi have also shown in [47] that experiments on perceptual barycenters in several state-of-the art color spaces lead to the consideration that their results do not fit with Euclidean geometry and suggest the use of a hyperbolic one.

To conclude, many authors, in different ways, came up to the conclusion that a hyperbolic metric is a pertinent distance to measure perceptual dissimilarity. However nowadays the Euclidean distance is still widely used in many applications, mostly for reasons of computational convenience more than perceptual pertinence.

1.3 Phenomenology of color perception

In Section 1.1, talking about color solid and chromaticity diagrams, we started describing colors in terms of coordinates, the tristimulus values like RGB, XYZ, and attributes, hue, saturation etc. In this section we are going to introduce the state-of-the art glossary of color perceptual attributes and briefly underline the problems caused by the attempt of turning them into coordinates of practical color solids. Most of these problems are due to two main reasons: the fact that it is not clear whether it is possible to associate a perceptual attribute to a color solid's coordinate and the interdependence between perceptual color attributes. Interdependence phenomena, known in literature as perceptual effects, fall in the category of the so-called color appearance phenomena. We are going to mention some of the most well-known color appearance phenomena, focusing in particular on the ones that will be described in the framework of our model in the following chapters. The conclusion that color solids are not enough to describe color appearance phenomena led to the development of color appearance models. An excellent reference for the topics mentioned in this section is Fairchild's book [49].

1.3.1 Color appearance attributes

The following list provides the official definitions, that we quote *verbatim*, of color perceptual attributes, see e.g. Chapter 6 (page 487) of [163], Chapter 4 of [49], or the official website https://cie.co.at/e-ilv.

- *Color*: is that aspect of visual perception by which an observer may distinguish differences between two structure-free fields of view of the same size and shape, such as may be caused by differences in the spectral composition of the radiant energy concerned in the observation.

- *Related color*: it is a color perceived to belong to an area or object seen *in relation to other colors*.

- *Unrelated color*: it is a color perceived to belong to an area or object seen *in isolation from other colors*.

- *Hue*: is the attribute of a color perception denoted by blue, green, yellow, red, purple and so on. *Unique hues* are hues that cannot be further described by the use of the hue names other than its own. There are four unique hues: red, green, yellow and blue. The *hueness* of a color stimulus can be described as combinations of two unique hues; for

example, orange is yellowish-red or reddish-yellow. Nonunique hues are also referred to as *binary hues*.

- *Chromatic color*: it is a color perceived possessing hue.
- *Achromatic color*: it is a color perceived devoid of hue.
- *Brightness*: attribute of a visual sensation according to which an area appears to be more or less intense; or, according to which the area in which the visual stimulus is present appears to emit more or less light. Variations in brightness range from *bright* to *dim*.
- *Lightness*: attribute of a visual sensation according to which the area in which the visual stimulus is presented appears to emit more or less light in proportion to that emitted by a similarly illuminated area perceived as a white stimulus. In a sense, lightness may be referred to as *relative brightness*. Variations in lightness range from *light* to *dark*.
- *Colorfulness*: attribute of a visual sensation according to which the perceived color of an area appears to be more or less chromatic.
- *Chroma*: attribute of a visual sensation which permits a judgment to be made of the degree to which a chromatic stimulus differs from an achromatic stimulus of the same brightness. In a sense, chroma is *relative colorfulness*.
- *Saturation*: attribute of a visual sensation which permits a judgment to be made of the degree to which a chromatic stimulus differs from an achromatic stimulus regardless of their brightness.

In [49], the relationship between some of the attributes defined above is resumed in the following *intuitive* equations:

$$\text{Lightness} = \frac{\text{Brightness}}{\text{Brightness(White)}}, \tag{1.3.1}$$

where 'White' refers of course to a surface that is perceived as white.

$$\text{Chroma} = \frac{\text{Colorfulness}}{\text{Brightness(White)}}, \tag{1.3.2}$$

$$\text{Saturation} = \frac{\text{Colorfulness}}{\text{Brightness}}. \tag{1.3.3}$$

There exist analytical formulae to express attributes as hue, saturation, chroma and so on both in the classical CIE spaces and in the color appearance ones, see e.g. [163, 66], which gave rise to a plethora of color spaces, as e.g. HSL, HSV, HSI, LCh(ab), LCh(uv) and so on. All of them were built in the attempt of associating a coordinate in a color solid to a perceptual attribute. An example is given by the different achromatic coordinates used in literature, see e.g. [145], usually obtained as arbitrary combinations of the XYZ or RGB tristimulus values. They are examples of achromatic coordinates which are supposed to represent a perceived achromatic attribute, but indeed it is even not clear whether they are representing perceived brightness or lightness.

One of the main problems about currently used color spaces is the fact that color attributes (or coordinates) interdependence is not fully understood. We must stress that there is a difference between interdependence of perceptual color attributes and interdependence of color coordinates. While the first type of interdependence is a perceptual phenomenon, the second

one is affected by the (arbitrary) way a certain color coordinate of a color solid (e.g. H in HSV) was associated to a perceptual color attribute (e.g. perceived hue as in the glossary above). Of course the first type influences the second one, and both of them affect applications. Talking about intrinsic interdependence of the perceptual attributes, means describing perceptual effects, see the next subsection.

As regards the interdependence of color coordinates in current color solids, in [121], Ottosson provides several concrete examples similar to the ones depicted in Figure 1.7 and Figure 1.8.

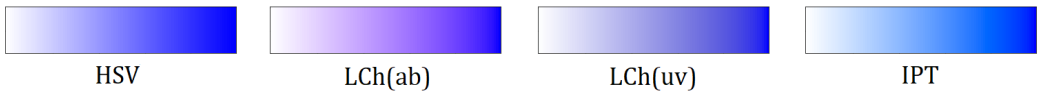

Figure 1.7: In this figure, similar to the test provided by Ottosson in [121], some state-of-the art color spaces, having coordinates representing hue, saturation (or chroma) and an achromatic coordinate, are considered. The depicted color gradients have been obtained fixing the hue to blue (the blue of RGB coordinates $(0, 0, 255)$ represented in each color space) and letting vary the other two coordinates. One can clearly see that, although the hue coordinate was fixed to blue, in some cases clear hue-shifts towards purple appear.

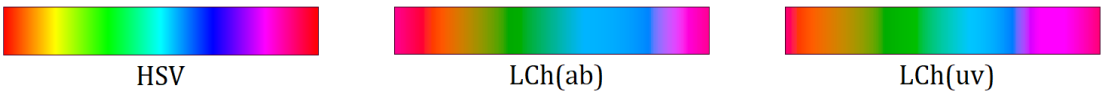

Figure 1.8: Let us consider again some state-of-the art color spaces where one can identify the hue coordinate. One can create hue gradients as follows: fixing all the other coordinates and letting vary the hue uniformly. Notice that even if the hue was varying uniformly in some cases clearly the perceived hue is not varying uniformly, e.g. in the case of HSV there is some kind of 'acceleration' around the zones of yellow, cyan and magenta. One might say as well that e.g. even if the other coordinates (achromatic and saturation or chroma) were fixed, the perceived saturation or lightness is not the same for every part of the gradient.

These kind of phenomena have a high impact on color image processing algorithms, e.g. for color enhancement purposes, if the aim is to desaturate an oversaturated image, we do not want to have hue shifts in doing so, as in the example of Figure 1.7.

1.3.2 Color appearance phenomena

Perceptual effects

Perceptual effects are due to interdependence relations between perceived color appearance attributes. In some cases they are caused as well by mismatches with their physical counterparts (e.g. dominant wavelength or luminance of a light stimulus). Here we are going to briefly mention some ot them.

- The Bezold-Brüke effect proves that the common assumption for which the hue of a perceived color can be described by the dominant wavelength of the visual stimulus is wrong. In fact, the so-called Bezold-Brüke hue shift shows that when a monochromatic stimulus is observed while changing its luminance, the hue perception does not remain constant.

- The Abney effect establishes that mixing a monochromatic light with an achromatic one, in order to decrease its physical colorimetric purity, leads to a modification of the perceived hue.

- As observed in chapter 6 of [49], the Helmholtz-Kohlrausch effect, HK effect from now on, is another demonstration of the inadequacy of standard colorimetry to fit color appearance phenomena. In fact, the Y coordinate of the XYZ space agrees with the luminance of a stimulus and it is erroneously assumed to be a direct estimate of perceived brightness. However, the HK effect shows that, even when two light stimuli have the same luminance, some appear brighter than others, see Figure 1.9. In particular, colored lights tend to appear brighter to human observers than achromatic light. The HK effect is particularly visible at high luminance levels.

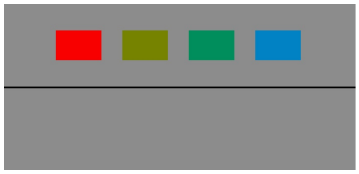

Figure 1.9: An illustration of the Helmholtz-Kohlrausch effect: all the patches in the first row have the same luminance level, as shown in the second row, but clearly they have different brightness (perceived luminance).

- The Hunt effect states that colorfulness increases with brightness. In [17, 19] Berthier and Provenzi provided a mathematical explanation of the Hunt effect, using the tools that will be introduced in Chapters 3 and 5.

Lightness constancy

We are going to describe a bit more in detail the lightness constancy phenomenon, as in [14], since in Chapter 6 we will provide an explanation of this phenomenon within our novel framework.

In order to fix the ideas, we wish to quote the following description of lightness constancy offered by [92]: '*Lightness constancy refers to the observation that we continue to see an object in terms of the proportion of light it reflects rather than the total amount of light it reflects. That is, a gray object will be seen as gray across wide changes in illumination. A white object remains white in a dim room, while a black object remains black in a well-lit room. In this sense, lightness constancy serves a similar function as color constancy in that it allows us to see properties of objects as being the same under different conditions of lighting. Consider an object that reflects 25% of the light that hits its surface. This object will be seen as a rather dark gray. If we leave it in a dim room that receives only 100 units of light, it will reflect 25% units of light. However, if we place it in a room that is better lit, it will still reflect the same 25%. If there are now 1,000 units of light, it will reflect 250 units of light. But we still see it as approximately the same gray, despite the fact that the object is reflecting much more light. Similarly, an object that reflects 75% of ambient light will be seen as a light gray in the dim room, even though it reflects less total light than it does in the bright room. Thus, lightness constancy is the principle that we respond to the proportion of light reflected by an object rather than the total light reflected by an object*'.

To visually illustrate the difference between lightness and brightness judgment, let us consider the scene depicted in Figure 1.10: the horizontal stripes of the building on the left and on the right of the yellow entrance are built with the same material, thus they have the

same reflectance, however, some parts are exposed to sunlight and some other are not, due to the shadow projected by the tree.

If we had to make a *brightness judgment*, we would describe them as brighter and dimmer, respectively. Instead, if we had to express a *lightness judgment*, we would state that all of them are 'white', implicitly meaning that the parts directly hit by sunlight and those covered by the tree shadow *would appear identical if they were lit in the same way*. This is an instance of the lightness constancy property of the human visual system.

The same analysis can be repeated for the parts of the yellow entrance covered or not by the tree shadow. So, thanks to lightness constancy, an observer would exclude the possibility that the part of horizontal stripes or the entrance in shadow are painted with a darker shade of gray or yellow, respectively, but that the perceptual difference is merely due to a different intensity in the lighting condition.

Figure 1.10: A visual scene used to illustrate the lightness constancy phenomenon.

The psycho-physiological reasons underling lightness constancy are still debated; we refer the reader to e.g. [45] for further information.

Color constancy

The chromatic counterpart of lightness constancy is called *color constancy*, i.e. the (imperfect) robustness of the human visual system to describe perceived colors with the same chromatic attributes in spite of changes in the spectral composition of the illuminant. It is due to the phenomenon of chromatic adaptation to the illumination conditions. The famous 'Mondrian experiments' discussed in [95] provide a proof of this property: two patches with identical reflectance and same surround, placed in different parts of a Mondrian-like tableau are lit in very different ways with the declared purpose of inducing two different color sensations to an observer. However, in spite of that, the two patches are still reported to be perceived with the same color. We quote a clear example of chromatic adaptation, provided by Fairchild in [49]: '*consider a piece of white paper illuminated by daylight. When such a piece of paper is moved to a room with incandescent light, it still appears white despite the fact that the energy reflected from the paper has changed from predominantly blue to predominantly yellow*'.

In the following chapters we will come back discussing about this phenomenon, in particular in Chapter 7 we will talk about computational color constancy and chromatic adaptation transforms.

1.4 Conclusion: the need of a mathematical model for color opponency

Tristimulus-based colorimetry works well for color matching under fixed and very restrained viewing conditions, but fails at predicting color appearance, and does not deal well with a correct description of perceptual attributes and their related phenomena. The term *color appearance model* was introduced by CIE referring to any model that tries to overcome these limitations, taking into account viewing conditions and color appearance phenomena. Existing color appearance models aim at enriching color solids structures, e.g. adding parameters specifying the vision conditions, rather than questioning the way they were built, see Chapter 10 of [49].

In [87], Koenderink and van Doorn describe the current state of the art on colorimetry as follows: '*As the field is presented in the standard texts it is somewhat of a chamber of horrors: colorimetry proper is hardly distinguished from a large number of elaborations (involving the notion of 'luminance' and of absolute color judgments for instance) and treatments are dominated by virtually ad hoc definitions (full of magical numbers and arbitrarily fitted functions). We know of no text where the essential structure is presented in a clean fashion. Perhaps the best textbook to obtain a notion of colorimetry is still Bouma's of the late 1940's*'.

In the previous sections we have seen that *arbitrary choices* are present at many different levels in classic trichomacy-based colorimetry: from the choice of the basis of functions with respect to which perform the reduction, to the construction of chromaticity diagrams, to the association of color coordinates to perceptual attributes.

Another fundamental aspect is the way Hering opponent mechanism is (not) taken into account. In current color solids and chromaticity diagrams Hering opponent mechanism is most of the times absent, and, when present, it is added a posteriori, often in an arbitrary way, and it is not part of the mathematical construction of the color solid or of the chromaticity diagram, which is still trichromacy-based. Indeed all the current color solids are based on a reduction procedure with respect to three primaries which are all of the same kind, the split between chromaticity diagram and achromatic information, when present, is always added a posteriori.

The construction of chromaticity diagrams itself is controversial. As we have seen in Section 1.1 one needs to postulate the existence of a perceptual achromatic attribute and then associate it to a color coordinate to be discarded via a normalization procedure. In [88] Koenderink and Van Doorn question even the need of a perceptual achromatic attribute. Indeed, they describe luminance as '*a purely formal entity*', moreover they say that '*it doesn't have any meaning in terms of the perceptual attributes of patches. In this chapter we will ignore the topic of luminance altogether; in our opinion (and in full agreement with Schrödinger's elegant treatment [138]), it doesn't belong to colorimetry proper*'.

Concerning hyperbolicity, in Section 1.2 we have seen that hyperbolic structures proposed in literature are, as Hering's mechanism, added a posteriori on trichromacy-based color solid, and often only justified by the aim of fitting MacAdam or Judd's data. We will see, in Chapter 3, that, in our formulation, the Hibert-Klein hyperbolic metric arises from the theoretical model.

To resume: the mathematical construction behind tristimulus-based colorimetry does not naturally contain Hering's opponent mechanism, nor has hyperbolic features. Our work aims at proposing a mathematical framework coherently integrating all this aspects.

The main paradigm shift that we propose lies in the fact that the measurement procedure is fundamental in the search for color information, thus we should not model colors in terms of coordinates, but interpreting color information as the result of a measurement procedure by the HVS. Motivations of our approach will be explained in detail in Chapter 3, here we limit ourselves to quote the words of B. Russell [136] and P.A.M. Dirac [40].

Russell's: '*When, in ordinary life, we speak of the colour of the table, we only mean the sort of colour which it will seem to have to a normal spectator from an ordinary point of view under usual conditions of light. But the other colours which appear under other conditions have just as good a right to be considered real; and therefore, to avoid favoritism, we are compelled to deny that, in itself, the table has any one particular colour*'.

Dirac's: *'Science is concerned only with observable things and that we can observe an object only by letting it interact with some outside influence. An act of observation is thus necessary accompanied by some disturbance of the object observed"*, and also: *"Questions about what decides the photon's direction of polarization when it does go through cannot be investigated by experiment and should be regarded as outside the domain of science'*.

Citing Hardin [70] again: '*It is time for a new look at color, taken from the perspective of the opponent process theory*'.

Chapter 2

Yilmaz's relativistic model

Yilmaz's papers [165, 166] belong to a surprisingly rich list of contributions to color theory by theoretical physicists. One of the founding fathers of quantum mechanics, E. Schrödinger is among the most famous, with his benchmark axiomatic work on color perception [138]. In more recent years, also S. Weinberg [158] and A. Ashtekar and collaborators [3], to quote but two, wrote papers about color. They share the common interest in understanding the geometrical structure of the space of perceived colors.

In the previous chapter we already mentioned Yilmaz's work, in Section 1.1, concerning the choice of the basis $\bar{\alpha}, \bar{\beta}, \bar{\gamma}$ with respect to which performing the dimension reduction, in order to obtain a color solid representing the space of perceived colors, let us call it $\mathscr{C}$ for the rest of this chapter. The originality of Yilmaz contribution lies in the identification of the striking structural similarity between $\mathscr{C}$ and the future light cone of special relativity theory. This intuition allowed him to determine, on the base of three results that he claimed coming from experiments, a law for the perceptual effect on color perception induced by a change of illuminant. This law turns out to be the direct analogous of Lorentz transformations.

In this chapter we are going to provide a mathematical formalization of Yilmaz's argument about the relationship between Lorentz transformations and the perceptual effect of illuminant changes. In the conclusions we will focus on the problematic aspects of his approach due to its not clear experimental basis. However in this chapter we will proceed assuming the experimental results claimed by Yilmaz to be true. In Chapter 4 we will see how it is possible to avoid them and obtain the same result from a completely theoretical approach.

Concerning the notation in this chapter we are going to use the one adopted by Yilmaz, while we will need to change it in Chapter 4, to recast his results in the framework of the quantum model described in Chapter 3. The main adopted references here will be Yilmaz's originals papers [166, 165] and our first publication [124].

2.1 Yilmaz's experiments

We are going to introduce the experiments on which Yilmaz based his model. For the sake of clarity, we first introduce the notation and nomenclature used in this chapter.

2.1.1 Coordinates of Yilmaz's model

To develop his model, Yilmaz considered trichromatic observers and the color space $\mathscr{C}$ embedded in the closed upper half-space in the Euclidean three-dimensional space, i.e. $\mathscr{H} :=$

$\{(\alpha,\beta,\gamma)|(\alpha,\beta)\in\mathbb{R}^2,\gamma\geq 0\}$. The coordinates (α,β,γ) are the components of a color $F\in\mathscr{C}$ described with respect to a basis $(\hat{\alpha},\hat{\beta},\hat{\gamma})$ of $\mathbb{R}^3$.

The coordinates on the vector space are obtained from the dimension reduction with respect to a basis of functions $\bar{\alpha},\bar{\beta},\bar{\gamma}$. In a first moment, when he talks about *an idealized model*, Yilmaz makes a simple choice for these three functions*, while in the paragraph '*A more realistic model*' he chooses them to be the first three eigenfunctions of the harmonic oscillator, as we have detailed in Section 1.1. The question about how the coordinates are obtained is somehow separate with respect to the discussion about $\mathscr{C}$ and its transformations. In this chapter we will focus on the latter problematic.

The coordinates (α,β) are called chromaticity coordinates and γ is the achromatic one, called *lightness* in [165]. The polar coordinates in the so-called hue-chroma plane are (ϕ,ρ), where $\alpha=\rho\cos\phi$ and $\beta=\rho\sin\phi$, ϕ being associated to the *hue* and ρ to the *chroma* of $F\in\mathscr{C}$. It is customary to identify the hue corresponding to particular values of ϕ with the following standard hues: $\phi=0$ is red R, $\phi=\pi/2$ is yellow Y, $\phi=\pi$ is green G and $\phi=3\pi/2$ is blue B. Coherently with this identification, from now on, as shown in Figure 2.1.1 (a), the $\hat{\alpha}$ axis will be identified with the $R-G$ direction and the $\hat{\beta}$ axis with the $Y-B$ direction.

Following the standard colorimetric definition, Yilmaz relates color *saturation* σ with ρ and γ via $\sigma=\rho/\gamma$.
On the plane defined by $\gamma=1$, ρ and σ can be identified and they represent the radial distance from the γ axis. The half-line defined by $\gamma\geq 0$, $\rho=0$, is called *achromatic axis*, the maximum perceivable value for γ is denoted with $\gamma_{\max}$. For all the values $\gamma>\gamma_{\max}$ cone receptors are saturated due to *glare*. For the sake of simplicity let us normalize $\gamma_{\max}$ to 1. The origin O corresponds to the sensation of black.

It is a known fact gathered by psychophysical experiments that the saturation of spectral colors, i.e. narrow-band lights, is maximal. Yilmaz denoted with Σ_ϕ the maximal saturation sensation induced by a narrow-band light perceived with a hue ϕ.

The existence of a maximal saturation Σ_ϕ implies that the value $1/\sigma$ has a lower bound given by $1/\Sigma_\phi$. More precisely we can see $1/\sigma$ as the slope of a straight half-line passing by the origin in the upper-half plane defined fixing the hue ϕ.
It is not hard to see that this saturation constraint implies that the effective available space for perceived colors, in Yilmaz's setting, is the volume contained in the *cone* shown in Figure 2.1.1 (b), denoted by $\mathscr{C}\subset\mathscr{H}$ and described by the equation:

$$\mathscr{C}=\{F=(\phi,\rho,\gamma)\in\mathscr{H}\,|\,\rho\leq\Sigma_\phi\gamma\}. \tag{2.1.1}$$

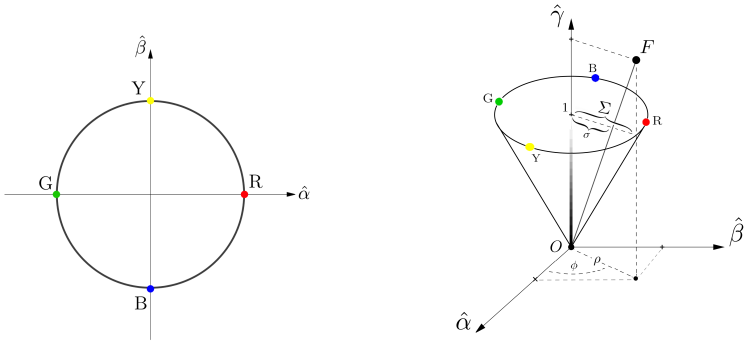

(a) The (α,β)-plane, $\gamma=1$. (b) Depiction of the cone $\mathscr{C}$.

Figure 2.1: Visual representations of the color solid considered by Yilmaz.

*He considers the following functions: $\bar{\alpha}(\lambda)=\frac{1}{\sqrt{\pi}}\sin(\phi(\lambda))$, $\frac{1}{\sqrt{\pi}},\bar{\beta}(\lambda)=\cos(\phi(\lambda)),\bar{\gamma}(\lambda)=\frac{1}{\sqrt{2\pi}}$, where $\phi(\lambda)$ is a suitable function mapping the interval of visible wavelengths Λ into $[0,2\pi]$.

2.1.2 Yilmaz's three experiments

The generic apparatus for the experiments described by Yilmaz in [166] is shown in Figure 2.2, where we can see two identical rooms R_1 and R_2, separated by a common wall with a thin hole and illuminated by the sources of light S_1 and S_2. Both rooms are painted with a non-selective Lambertian white paint. A piece of white paper is divided in two parts and each one is placed in one of the rooms, so that an observer can perceive them simultaneously. The key point is that one piece is seen directly and the other through the hole.

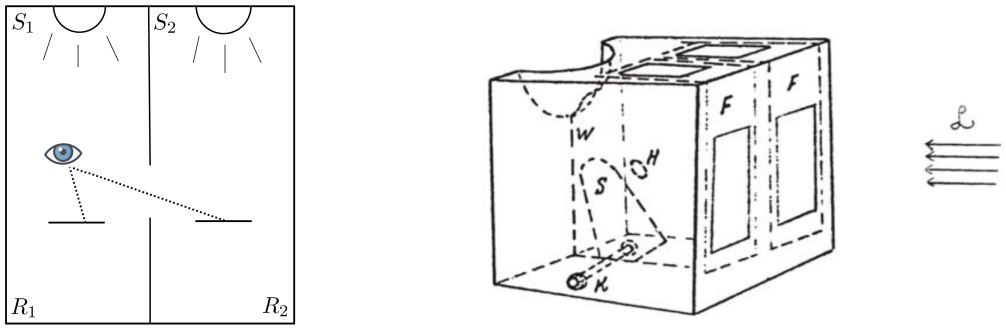

Figure 2.2: *Left*: The experimental apparatus considered by Yilmaz. *Right*: This image is from Inter-Society Color Council News, Issue 419, Jan/Feb 2006, by kind concession of M. H. Brill, whom we would like to thank for sharing this reference with us for [13].

The illumination S_1 of room R_1 will always be provided by near-daylight broadband illuminants. Instead, the illumination of room R_2 will be provided by a light source S_2 that can also be narrow-band. The perceived colors are compared with the help of a set of Munsell chips enlighted by the same illuminant under which the observer is adapted. For some details about adaptation to an illuminant we refer to Subsection 1.3.2 of the previous chapter.

The first experiment

In this first experiment, the sources S_1 and S_2 are chosen to be two different broadband illuminants of near-daylight chromaticity, I and I', respectively. An observer placed in R_i will adapt to S_i and the piece of paper placed in R_i will be perceived as white, $i = 1, 2$. However, Yilmaz noticed that, if an observer, placed in one of the two rooms, looks at the piece of paper in the adjacent room through the thin hole, then it will appear with a certain hue ϕ and saturation σ. By switching the rooms, the piece of paper in the adjacent room will be matched with a Munsell chip of opposite hue, i.e. $\pi + \phi$, but with approximately the same saturation σ [†]. To fix the ideas we choose the hues ϕ and $\pi + \phi$ to be red and green, respectively.

This experiment is extremely interesting because the thin hole in the wall is a trick that permits to show how an observer's reference for white changes when the illumination varies. The immediate consequence is that *color perception is a relative phenomenon*, which depends on the illuminant to which the observer is adapted.

It is worth underlining that this experiment must be performed in such a way that *local retinal adaptation* is prevented in the area covered by the thin hole. This can be done, for example, by allowing only a limited time aperture of the thin hole with the help of a suitable time-dependent shutter.

[†]In the original description of this experiment, Yilmaz made a little abuse of notation using the symbol $-\sigma$, in spite of the fact that saturation is a non-negative quantity. He explained it in the following way: '*the minus sign indicating that the hue is complementary to the former hue*'.

The second experiment

In the second experiment Yilmaz chooses S_2 to be a narrow-band source with a spike in the red region of the visual spectrum. Yilmaz reported that, if an observer in R_1 is adapted to the broadband near-daylight illuminant I and looks at the piece of paper in R_2, he/she will perceive it as having same hue $\phi = 0$ and with maximal saturation Σ_R. If we change the illuminant I with the illuminant I' used in the first experiment and we wait for the adaptation of the observer in R_1 to the new illuminant, then the piece of paper in R_2, seen through the hole, will still be perceived as having same hue $\phi = 0$ and maximal saturation Σ_R.

Yilmaz justifies experimentally this claim by saying that, in both cases, the perceived saturation is reported to be too high to be replicated by any of the Munsell chips, i.e., the observer is able to identify the perceived hue as red, but all of the Munsell chips have saturation strictly smaller than the perceived one. From the first experiment, we know that the change of perceived hue caused by the transformation from I to I' acts on the red-green axis.

The particular choice of the red-green axis seems to be the only one really tested by Yilmaz, however, theoretically, nothing prevents to choose any other direction on the chromatic plane.

The third experiment

This final experiment is similar to the second one, but with an important difference. Here S_2 is chosen to be a narrow-band source of light with spike in the yellow part of the spectrum, i.e., whose hue direction is orthogonal with respect to the $R - G$ axis, see Figure 2.1.1 (a). The observer is always placed in R_1. When S_1 is equal to I he/she perceives S_2 through the hole with yellow hue, i.e, $\phi = \pi/2$, and with a saturation which is, again, too high to be found among the set of Munsell chips and then it is set to Σ_Y. When the illuminant S_1 changes from I to I', no variation in saturation is reported, it is still maximal and equal to Σ_Y, but the hue perception of the piece of paper in R_2 seen from the hole changes by an amount φ such that

$$\sin\varphi \simeq \sigma/\Sigma_Y. \tag{2.1.2}$$

At page 12 of [166], Yilmaz writes: '[...] *these conclusions based on experiment are* [...] *only approximate* [...]', from this we understand that experiments have in fact been performed and data have been gathered. However, it is also clear that such a precise formula as Equation (2.1.2) to determine the hue shift φ is, at least, doubtful. We will turn back on this issue in Section 2.5.

The aim of this chapter is to mathematically analyze Yilmaz's model and its consequences, for this reason, in spite of this debated issue, we in the following section we will consider this data as rigorous, while we will discuss the issues related to the feasibility of these experiments in Section 2.5. However, it is clear that further psychophysical experiments would be extremely valuable to confirm or confute Equation (2.1.2) and Yilmaz model in general.

2.2 Recasting Yilmaz's model in a mathematical framework

In section IV '*Transformation formulae*' of his paper [166], Yilmaz's looked for *a transformation from the coordinates of a color described by an observer adapted to a broadband illuminant I to those of an observer adapted to different broadband illuminant I'*. He deduced, from the three experiments previously discussed, what he claimed to be a linear approximation of this transformation. Clearly such a transformation leaves the black point O fixed.

Unfortunately, Yilmaz's exposition about how to obtain Lorentz boosts as illuminant transformations from the results of the three experiments, is too concise and lacks of rigor. As we

did in [124], our contribution in this Section is to introduce a suitable notation in order to provide a more clean mathematical description of Yilmaz's procedure.

We start with the definition of visual stimuli and by fixing some notations.

- We call *visual stimulus* in Yilmaz's experiment the spectrum of visible light reflected by either a piece of white paper, or a Munsell chip illuminated by a visible light representing an illuminant[‡] entering the eye of an observer;
- F, F' will denote a visual stimulus provided by the visible light reflected by an object enlighted by the illuminant I or I', respectively. The object surface can be either the piece of white paper, and in that case we will write W, W', or a Munsell chip;
- $\tilde{R}, \tilde{Y}$ will indicate the visual stimulus provided by the piece of white paper illuminated by the narrow-band illuminants with spike in the red or yellow region, respectively.

Yilmaz assumed that an observer adapted to a broadband illuminant, I or I', analyzing colors by the comparison with a set of Munsell chips enlighted by *the same* illuminant, defines a vector basis of $\mathbb{R}^3$, $\mathscr{B} = \{\hat{\alpha}, \hat{\beta}, \hat{\gamma}\}$ or $\mathscr{B}' = \{\hat{\alpha}', \hat{\beta}', \hat{\gamma}'\}$, respectively. Thus, the use of $\mathscr{B}$ and $\mathscr{B}'$ will be always implicitly correlated with a triple given by an illuminant, an observer adapted to it and a set of Munsell chips used for color comparison. Notice that while in the first experiment the observer is able to pick a Munsell chip in accordance with the stimulus that he/she perceives, it is not the case for the second and third experiment.

Thus we will assume that color sensations obtained via a matching with a Munsell chip will correspond to elements of the interior of the cone $\mathscr{C}$, defined by Equation (2.1.1).
On the other hand, since it is impossible for an observer to replicate with a Munsell chip the maximal saturation Σ_ϕ of a narrow band visual stimulus, we consider the color sensation produced by such a visible light as a point belonging to the surface $\partial\mathscr{C} = \{F = (\phi, \rho, \gamma) \in \mathscr{H} \,|\, \rho = \Sigma_\phi \gamma\}$ of the cone $\mathscr{C}$. Furthermore we assume Σ_ϕ to be the same for all observers adapted to any illuminant.

The symbols $\mathscr{B}$ and $\mathscr{B}'$ will be used as a subscript for the visual stimuli to indicate the illuminant to which the observer is adapted[§]: $\mathscr{B}$ for I and $\mathscr{B}'$ for I'. Note that the basis subscript is extremely important because it underlines the central role of the observer, i.e., the basis with respect to which the coordinates are written. Without an observer a *perceived color* is just a *stimulus*, in the same way as a point of a vector space is just an abstract (coordinate-free) concept without a basis which describes it in terms of coordinates.

Yilmaz considers the change of basis from $\mathscr{B}$ to $\mathscr{B}'$ to be the linear approximation of the illuminant transformation from I to I', indeed he supposes that a more precise description of the transformation should involve other nonlinear terms. He denotes the associated matrix as[¶] $\Omega \equiv \Omega_{II'} \in GL(3, \mathbb{R})$. Ω is naturally required to be invertible because we can reverse the transformation by switching the two illuminants, i.e. $\Omega^{-1} = \Omega_{II'}^{-1} = \Omega_{I'I}$.

In order to determine the coefficients of Ω, Yilmaz considered the following equations:

$$\begin{cases} \Omega W_{\mathscr{B}} = W_{\mathscr{B}'} \\ \Omega^{-1} W'_{\mathscr{B}'} = W'_{\mathscr{B}} \end{cases} \quad \text{and} \quad \begin{cases} \Omega \tilde{R}_{\mathscr{B}} = \tilde{R}_{\mathscr{B}'} \\ \Omega \tilde{Y}_{\mathscr{B}} = \tilde{Y}_{\mathscr{B}'}. \end{cases}$$

[‡]More precisely, the piece of white paper will be illuminated by both broadband and narrow-band illuminants, while the Munsell chips will only be illuminated by broadband illuminants.

[§]As a consequence they will refer as well to the illuminant enlightening the set of Munsell chips with respect to which the observer makes his/her comparisons.

[¶]We recall that $GL(n, \mathbb{R})$ indicates the so-called general linear group of degree n over $\mathbb{R}$, which is the set of all the invertible matrices $n \times n$ with entries in $\mathbb{R}$.

These equations are the translation of the three Yilmaz experiments in our notation.

If we denote with $(\alpha, \beta, \gamma)^t$ or $(\alpha', \beta', \gamma')^t$ the coordinates of a color perceived by an observer adapted to I or I', respectively, then

$$\begin{pmatrix} \alpha' \\ \beta' \\ \gamma' \end{pmatrix} = \begin{pmatrix} \Omega_{11} & \Omega_{12} & \Omega_{13} \\ \Omega_{21} & \Omega_{22} & \Omega_{23} \\ \Omega_{31} & \Omega_{32} & \Omega_{33} \end{pmatrix} \begin{pmatrix} \alpha \\ \beta \\ \gamma \end{pmatrix}. \tag{2.2.1}$$

At page 14 of [166], Yilmaz analyzes, among all possible illuminant changes, the situation in which the couple I and I' produces a color coordinate transformation only along the α-axis, i.e. the $R - G$ direction, being stable on the (α, γ)-plane and leaving the β-axis unaffected. This hypothesis implies that the coefficients of Ω must fulfill the following conditions: $\Omega_{21} = \Omega_{23} = \Omega_{12} = \Omega_{32} = 0$ and $\Omega_{22} = 1$. So, the matrix Ω has the following form:

$$\Omega = \begin{pmatrix} \Omega_{11} & 0 & \Omega_{13} \\ 0 & 1 & 0 \\ \Omega_{31} & 0 & \Omega_{33} \end{pmatrix}. \tag{2.2.2}$$

The remaining coefficients, i.e. Ω_{ij}, $i, j = 1, 3$, will be determined by translating into formulae the three Yilmaz's experiments.

2.2.1 Coefficients from the first experiment: the white point transformation

Yilmaz's first experiment contains information about the coordinate change associated to the stimuli W and W', i.e. $\Omega W_{\mathscr{B}} = W_{\mathscr{B}'}$ and $\Omega W'_{\mathscr{B}} = W'_{\mathscr{B}'}$, as depicted in Figure 2.3.

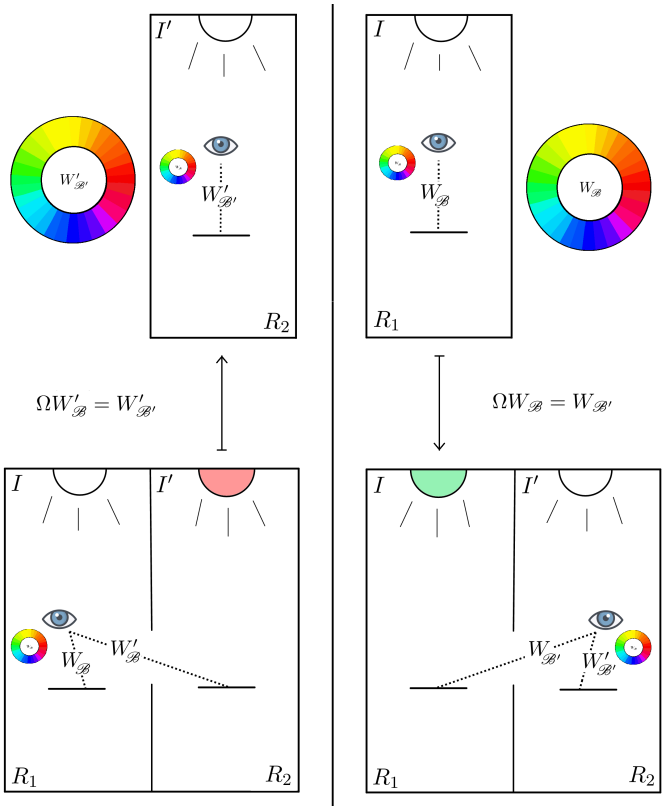

Figure 2.3: Illustration of Yilmaz's first experiment with the notation established in Section 2.2.

Our aim is to write the coordinates of the four points $W_{\mathscr{B}}$, $W_{\mathscr{B}'}$, $W'_{\mathscr{B}}$ and $W'_{\mathscr{B}'}$ to determine constraints among the coefficients Ω_{ij}.

An observer adapted to I or I', respectively, perceives the piece of white paper enlightened by the same illuminant to which he/she is adapted to be of the same placed under the same illuminant as the same white. In terms of coordinates, this means that $W_{\mathscr{B}} = W'_{\mathscr{B}'}$.
According to what said in Subsection 2.1.1, since the white is achromatic, it must belong to the γ-axis, so its α and β coordinates are null. The third coordinate remains free and we can normalize its value to 1, and associate it to the intensity of white, hence $W_{\mathscr{B}} = W'_{\mathscr{B}'} = (0, 0, 1)^t$.

Let us now look for the coordinates of $W_{\mathscr{B}'} = (\alpha', \beta', \gamma')$ and $W'_{\mathscr{B}} = (\alpha, \beta, \gamma)$. As indicated by the notation, $W_{\mathscr{B}'}$ represents the color sensation of an observer adapted to I' when he/she looks at the piece of white paper illuminated by I and compares it with the Munsell chips illuminated by I'. The description of $W'_{\mathscr{B}}$ is analogous, with I and I' switched. As reported in Section 2.1.2, $W_{\mathscr{B}'}$ is perceived as greenish, i.e. with hue π and saturation σ, while $W'_{\mathscr{B}}$ is perceived as reddish, i.e. with hue equals to 0 and saturation σ. In all Yilmaz's three experiments color sensations are described in terms of only two coordinates: hue and saturation, we will come back to this point in Chapter 4. In particular the γ-coordinates $W_{\mathscr{B}'}$ and $W'_{\mathscr{B}}$ are not reported by Yilmaz, thus we are led to introduce two unknown parameters[‖] $\Gamma, \tilde{\Gamma} \in \mathbb{R}^+$ such that $\gamma' = \Gamma$ and $\gamma = \tilde{\Gamma}$.

The psycho-visual color matching experiments performed by Burnham et al. in the paper [26], imply that the two parameters Γ and $\tilde{\Gamma}$ are actually different from 1. The test results reported in [26] led to the determination of matrices that permit, once the XYZ coordinates of a light patch (i.e. a source of light directly emitting a spectrum) perceived by an observer adapted to I are known, to predict the XYZ coordinates of a different light patch having the same appearance for an observer adapted to I'. In particular, experimental data showed that a patch perceived with the same appearance of white by an observer adapted to the CIE standard illuminants C and A, i.e. $W_{\mathscr{B}} = W'_{\mathscr{B}'}$, has different colorimetric specifications, thus $\gamma_{W_{\mathscr{B}}} \neq \gamma_{W'_{\mathscr{B}}}$. Hence, if we normalize $\gamma_{W_{\mathscr{B}}}$ to 1, the value of $\gamma_{W'_{\mathscr{B}}} = \Gamma$ (and vice versa $\gamma_{W_{\mathscr{B}'}} = \tilde{\Gamma}$) must be different than 1.

Since the perceived hue of $W_{\mathscr{B}'}$ is greenish, it must lie on the α'-axis, i.e. $\beta' = 0$, thence $\rho' = \sqrt{\alpha'^2 + \beta'^2} = |\alpha'|$. By definition, $\sigma' = \rho'/\gamma' = |\alpha'|/\Gamma$, but, as reported by Yilmaz, $\sigma' = \sigma$, which gives $|\alpha'| = \sigma\Gamma$. Finally, since greenish hues lies in the negative part of the α'-axis, the value of α' is given by $\alpha' = -\sigma\Gamma$. So, $W_{\mathscr{B}'} = (-\sigma\Gamma, 0, \Gamma)^t$. Analogously, we obtain $W'_{\mathscr{B}} = (\sigma\tilde{\Gamma}, 0, \tilde{\Gamma})^t$, where the positive sign of $\sigma\tilde{\Gamma}$ is due to the fact that, this time, $W'_{\mathscr{B}}$ is perceived as reddish.

We can now write explicitly the systems $\Omega W_{\mathscr{B}} = W_{\mathscr{B}'}$ and $\Omega^{-1} W'_{\mathscr{B}'} = W'_{\mathscr{B}}$, by obtaining, respectively:

$$\begin{pmatrix} \Omega_{11} & 0 & \Omega_{13} \\ 0 & 1 & 0 \\ \Omega_{31} & 0 & \Omega_{33} \end{pmatrix} \begin{pmatrix} 0 \\ 0 \\ 1 \end{pmatrix} = \begin{pmatrix} -\sigma\Gamma \\ 0 \\ \Gamma \end{pmatrix} \iff \begin{cases} \Omega_{13} = -\sigma\Omega_{33} \\ \Omega_{33} = \Gamma \end{cases}, \tag{2.2.3}$$

$$\begin{pmatrix} \Omega_{11} & 0 & -\sigma\Omega_{33} \\ 0 & 1 & 0 \\ \Omega_{31} & 0 & \Omega_{33} \end{pmatrix} \begin{pmatrix} \sigma\tilde{\Gamma} \\ 0 \\ \tilde{\Gamma} \end{pmatrix} = \begin{pmatrix} 0 \\ 0 \\ 1 \end{pmatrix} \iff \begin{cases} \Omega_{11} = \Omega_{33} \\ \Omega_{31} = \frac{1}{\sigma}\left(\frac{1}{\tilde{\Gamma}} - \Omega_{33}\right) \end{cases}. \tag{2.2.4}$$

[‖] $\Gamma, \tilde{\Gamma} \in \mathbb{R}^+$ are just auxiliary parameters that merely appear in these intermediate computations and not in the final form of the matrix coefficients of Ω.

The only relevant information to retain from the previous equations, in order to determine Ω, is given by the formulae $\Omega_{11} = \Omega_{33} = \Gamma$, $\Omega_{13} = -\sigma\Omega_{11}$, which allow us to write Ω as follows:

$$\Omega = \begin{pmatrix} \Omega_{11} & 0 & -\sigma\Omega_{11} \\ 0 & 1 & 0 \\ \Omega_{31} & 0 & \Omega_{11} \end{pmatrix}. \tag{2.2.5}$$

To determine the remaining parameters we will use the results of the second and the third experiment.

2.2.2 Coefficients from the second experiment: the red point transformation

Our aim here is to determine the coordinates of $\tilde{R}_{\mathscr{B}}$ and $\tilde{R}_{\mathscr{B}'}$. Let us denote with $R_{\mathscr{B}}$ and $R'_{\mathscr{B}'}$ the maximally saturated Munsell chips with a hue matching that of $\tilde{R}_{\mathscr{B}}$ and $\tilde{R}_{\mathscr{B}'}$, respectively. The perceived saturation of $R_{\mathscr{B}}$ and $R'_{\mathscr{B}'}$ is strictly inferior than Σ_R, see the depiction in Figure 2.4.

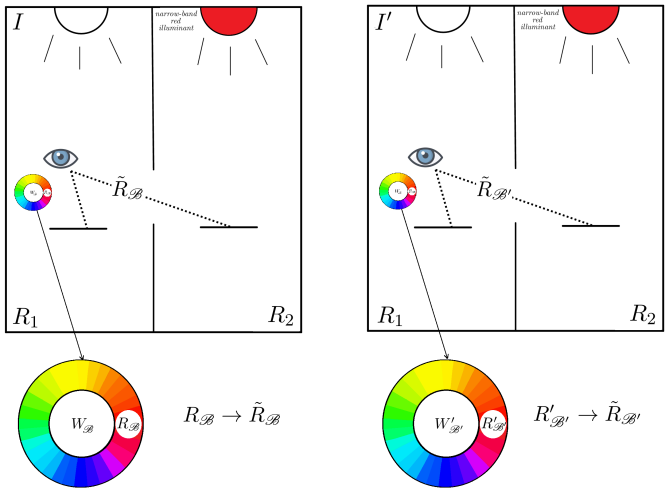

Figure 2.4: Depiction of Yilmaz's second experiment with the notation established in Section 2.2.

In our mathematical framework, a perceived color is a sensation that can be described in terms of coordinates which come from a match with a set of Munsell chips. The coordinates of $\tilde{R}_{\mathscr{B}}$ and $\tilde{R}_{\mathscr{B}'}$ will surely depend on Σ_R, which cannot be quantified in the Yilmaz's setting, thus $\tilde{R}_{\mathscr{B}}$ and $\tilde{R}_{\mathscr{B}'}$ do not belong to the interior of $\mathscr{C}$, but to its boundary $\partial\mathscr{C}$.

The reason why we consider $\tilde{R}_{\mathscr{B}}$ and $\tilde{R}_{\mathscr{B}'}$ on the boundary of $\mathscr{C}$ and not inside $\mathscr{C}$ is that we can imagine $\tilde{R}_{\mathscr{B}}$ and $\tilde{R}_{\mathscr{B}'}$ as resulting from a limit procedure in which a sequence of Munsell chips with increasing saturation approaches their saturation.

The β-coordinate of both $\tilde{R}_{\mathscr{B}}$ and $\tilde{R}_{\mathscr{B}'}$ is surely 0 because they lie on the α axis. Moreover, their α and γ-coordinates will be $\Sigma_R\gamma$ and γ, for $R_{\mathscr{B}}$, and $\Sigma_R\gamma'$ and γ', with $R_{\mathscr{B}}$, $\gamma, \gamma' \in \mathbb{R}^+$. The unknown parameters γ and γ' are introduced exactly for the same reason as Γ and $\tilde{\Gamma}$, i.e. we do not know their lightness. As a consequence, $\tilde{R}_{\mathscr{B}} = (\Sigma_R\gamma, 0, \gamma)^t$ and $\tilde{R}_{\mathscr{B}'} = (\Sigma_R\gamma', 0, \gamma')^t$.

The equation $\Omega\tilde{R}_{\mathscr{B}} = \tilde{R}_{\mathscr{B}'}$ can be written explicitly as follows:

$$\begin{pmatrix} \Omega_{11} & 0 & -\sigma\Omega_{11} \\ 0 & 1 & 0 \\ \Omega_{31} & 0 & \Omega_{11} \end{pmatrix} \begin{pmatrix} \Sigma_R\gamma \\ 0 \\ \gamma \end{pmatrix} = \begin{pmatrix} \Sigma_R\gamma' \\ 0 \\ \gamma' \end{pmatrix} \iff \Omega_{31} = -\frac{\sigma}{\Sigma_R^2}\Omega_{11}, \tag{2.2.6}$$

which implies

$$\Omega = \begin{pmatrix} \Omega_{11} & 0 & -\sigma\Omega_{11} \\ 0 & 1 & 0 \\ -\frac{\sigma}{\Sigma_R^2}\Omega_{11} & 0 & \Omega_{11} \end{pmatrix}. \tag{2.2.7}$$

The explicit form of Ω_{11} will be obtained thanks to the data gathered from the third experiment.

2.2.3 Coefficients from the third experiment: the yellow point transformation

When interpreting the third experiment, we will use the same approach as for the second one. We will denote with $Y_{\mathscr{B}}$ the maximally saturated Munsell chip with a hue matching that of $\tilde{Y}_{\mathscr{B}}$. Differently than the second experiment, here, when an observer changes the adaptation state from I to I', the perceived hue of the narrow band stimulus changes from yellow to a greenish yellow, see Figure 2.5. For this reason, we denote with $G'_{\mathscr{B}'}$ the maximally saturated Munsell chip that best approximates $\tilde{Y}_{\mathscr{B}'}$.

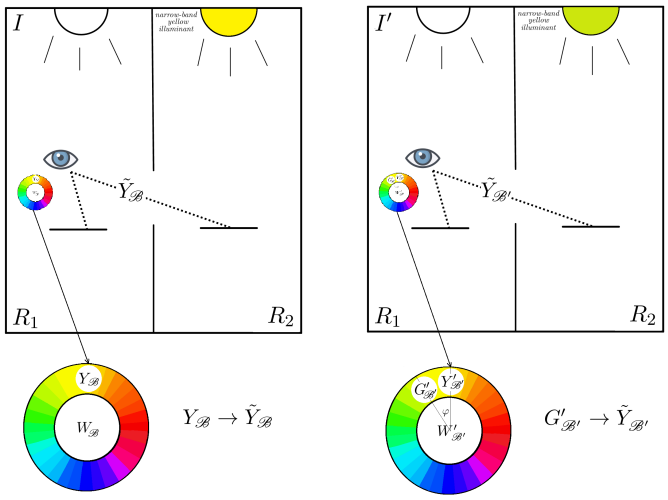

Figure 2.5: Depiction of Yilmaz's third experiment with the notation established in Section 2.2.

By using the same arguments of the previous subsections, we write the coordinates of $\tilde{Y}_{\mathscr{B}}$ as follows: $\tilde{Y}_{\mathscr{B}} = (0, \Sigma_Y\tilde{\gamma}, \tilde{\gamma})^t$, $\tilde{\gamma} \in \mathbb{R}^+$. Since the hue of $\tilde{Y}_{\mathscr{B}'}$ increased by an angle φ which satisfies (2.1.2), the coordinates of $\tilde{Y}'_{\mathscr{B}'}$ are $\tilde{Y}_{\mathscr{B}'} = (-\sin\varphi\Sigma_Y\tilde{\gamma}', \cos\varphi\Sigma_Y\tilde{\gamma}', \tilde{\gamma}')^t$, $\tilde{\gamma}' \in \mathbb{R}^+$, where the presence of $-\sin\varphi$ and $\cos\varphi$ comes from the expression of the hue change in Cartesian coordinates. The equation $\Omega\tilde{Y}_{\mathscr{B}} = \tilde{Y}_{\mathscr{B}'}$ can be then written explicitly as follows:

$$\begin{pmatrix} \Omega_{11} & 0 & -\sigma\Omega_{11} \\ 0 & 1 & 0 \\ -\frac{\sigma}{\Sigma_R^2}\Omega_{11} & 0 & \Omega_{11} \end{pmatrix} \begin{pmatrix} 0 \\ \Sigma_Y\tilde{\gamma} \\ \tilde{\gamma} \end{pmatrix} = \begin{pmatrix} -\sin\varphi\Sigma_Y\tilde{\gamma}' \\ \cos\varphi\Sigma_Y\tilde{\gamma}' \\ \tilde{\gamma}' \end{pmatrix}. \tag{2.2.8}$$

By direct computation one obtains the following system of equations:

$$\begin{cases} -\sigma\Omega_{11}\tilde{\gamma} = -\sin\varphi\Sigma_Y\tilde{\gamma}' \\ \tilde{\gamma} = \cos\varphi\tilde{\gamma}' \\ \Omega_{11}\tilde{\gamma} = \tilde{\gamma}' \end{cases} \iff \begin{cases} -\sigma\Omega_{11} = -\sin\varphi\Sigma_Y\Omega_{11} \\ \Omega_{11} = \frac{1}{\cos\varphi} = \frac{\tilde{\gamma}'}{\tilde{\gamma}} \end{cases}. \tag{2.2.9}$$

Notice that the first equation in the latter system, since $\Omega_{11} = \Gamma \neq 0$, becomes $\sigma = \sin\varphi\Sigma_Y$, i.e. we have obtained Yilmaz's hypothesis stated by Equation (2.1.2). We will come back to this point in Section 2.5.

On the other hand the second equation allows us to determine the last parameter

$$\Gamma = \Omega_{11} = \frac{1}{\cos\varphi} = \frac{1}{\sqrt{1 - \left(\frac{\sigma}{\Sigma_Y}\right)^2}}, \tag{2.2.10}$$

in order to finally obtain the following explicit expression of Ω

$$\Omega = \begin{pmatrix} \Gamma & 0 & -\sigma\Gamma \\ 0 & 1 & 0 \\ -\frac{\sigma}{\Sigma_R^2}\Gamma & 0 & \Gamma \end{pmatrix}, \tag{2.2.11}$$

with Γ as in Equation (2.2.10).

The variation of the yellow hue effect is said to be '*similar to the aberration effect in special relativity*', by Yilmaz in [166] at page 132. We will discuss this aspect in Section 2.4. In Section 2.3, we will point out the analogy between Ω and the matrix that represents Lorentz's transformations in Einstein's theory of special relativity. For more details about special relativity theory and Lorentz boosts see Appendix A.

2.3 Similarities and differences between Yilmaz's model and special relativity

Table 2.1 provides the list of analogies between Yilmaz's model and the standard mathematical framework of special relativity.

Special relativity	**Yilmaz's color perception model**
Observer in an inertial frame	Observer adapted to a broadband illuminant
Event $e = (t, \mathbf{x}) \in \mathbb{R}^4$	Perceived color $F = (\phi, \rho, \gamma) \in \mathscr{C}$
Time coordinate $t \in \mathbb{R}$	Lightness coordinate $\gamma \in \mathbb{R}^+$
Spatial coordinates $(x^1, x^2, x^3) \in \mathbb{R}^3$	Chromatic coordinates $(\rho, \phi) \in \mathbb{R}^+ \times [0, 2\pi)$
Speed of light in vacuum c	Maximal perceived saturation Σ
Lorentz transformations (A.0.7)	Yilmaz transformations (2.2.11)

Table 2.1: Analogies between special relativity and Yilmaz's model.

Among the similarities listed above, some evident differences between special relativity and Yilmaz's model of color perception can be remarked.

1. The Helson-Judd effect, see e.g. [49], shows that human color perception experiences an *incomplete adaptation* to narrow-band illuminants. However in Yilmaz model the case of incomplete adaptation is not taken into account, thus, in the previous table, the analogy between inertial frames and observers occurs only in case of complete adaptation to broadband illuminants.

2. While time t can be extended to the whole $\mathbb{R}$ with the identification of negative values of t as the 'past', a negative lightness is meaningless. So, only the upper part of the cone $\mathscr{C}$ makes sense in color perception. Moreover, and most importantly, this cone is not infinite: in fact, it is bounded from above by the glare limit defined by $\gamma_{\max}$ and from

below for two reasons: the first is the Purkinje effect [163] when we pass from photopic to scotopic vision via the mesopic range**, and the second is the intensity threshold of the retinal rods. Thus, $\mathscr{C}$ is a *truncated cone* at height γ_{max}. In Chapter 5 we will see that the concept of quantum *effects* will provide a better way to bound the color solid.

3. While events in the Minkowski spacetime have four components, perceived colors have only three.

2.4 Relativistic aberration and Yilmaz's third experiment

In this section, we want to discuss Yilmaz's most ambiguous assumption, represented by the result of the third experiment, in a relativistic framework and show that it is the translation, in the colorimetric context, of the relativistic aberration effect. This phenomenon expresses how the angle of incidence of a ray of light changes with the inertial frame of reference and it is a direct application of Lorentz transformations. For more details about the basic concepts and notation of special relativity see Appendix A.

Let $\mathscr{R}$ and $\mathscr{R}'$ be two inertial reference frames, with $\mathscr{R}'$ moving with respect to $\mathscr{R}$ with constant speed v along the x-direction. Without loss of generality we can consider a photon moving towards the origin of the frame and whose spatial trajectory is a straight line contained in the plane $z = 0$. Clearly, in both $\mathscr{R}$ and $\mathscr{R}'$, the speed of the photon will be c.

We suppose that its trajectory forms the angle α (resp. α') in $\mathscr{R}$ (resp. $\mathscr{R}'$), with the x-direction shared by both $\mathscr{R}$ and $\mathscr{R}'$. Our aim is to show how α and α' are related to each other. In $\mathscr{R}$ the photon's world-line is given by $(t, x, y, z) = (t, -tc\cos\alpha, -tc\sin\alpha, 0)$, to obtain it with respect to $\mathscr{R}'$ we need to apply the so-called Lorentz boost as follows:

$$\begin{cases} t' = \Gamma(t - \frac{v}{c^2}x) \\ x' = \Gamma(x - vt) \\ y' = y \\ z' = z \end{cases}, \tag{2.4.1}$$

with $\Gamma = \frac{1}{\sqrt{1-v^2/c^2}}$.
In particular, since the world line of the photon in $\mathscr{R}'$ is analogously given by $(t', x', y', z') = (t', -t'c\cos\alpha', -t'c\sin\alpha', 0)$, we obtain that $x' = \Gamma(-vt - ct\cos\alpha) = -ct'\cos\alpha'$ and $y' = y = -ct\sin\alpha = -ct'\sin\alpha'$. Hence

$$\tan\alpha' = \frac{y'}{x'} = \frac{c\sin\alpha}{\Gamma(c\cos\alpha + v)} = \frac{\sin\alpha\sqrt{1 - v^2/c^2}}{\cos\alpha + \frac{v}{c}}. \tag{2.4.2}$$

By a straightforward computation we obtain

$$\cos^2\alpha' = \frac{1}{1 + \tan^2\alpha'} = \frac{(\cos\alpha + \frac{v}{c})^2}{(1 + \frac{v}{c}\cos\alpha)^2}, \tag{2.4.3}$$

thus

$$\cos\alpha' = \frac{\cos\alpha + \frac{v}{c}}{1 + \frac{v}{c}\cos\alpha}, \tag{2.4.4}$$

**In the photopic range the three retinal cones are activated, in the scotopic range only the retinal rods are, while in the mesopic both photoreceptors function simultaneously.

where only the positive determination of the square root is compatible with the fact that, if $v = 0$, then we must have $\cos\alpha' = \cos\alpha$. Moreover

$$\cos\alpha' - \cos\alpha = \frac{\frac{v}{c}\sin^2\alpha}{1 + \frac{v}{c}\cos\alpha} > 0, \tag{2.4.5}$$

indeed $0 < v < c$, so $\cos\alpha' > \cos\alpha$ and $\alpha' < \alpha$.

We have now all the information to discuss Yilmaz's third experiment: taking into account the analogies underlined in Section 2.3 together with Equation (2.4.4), we have that

$$\cos\phi' = \frac{\Sigma\cos\phi + \sigma}{\Sigma + \sigma\cos\phi}. \tag{2.4.6}$$

For the spectral yellow, we have that $\phi = \pi/2$, so Equation (2.4) becomes $\cos\phi' = \frac{\sigma}{\Sigma}$, but since $\varphi = \phi - \phi'$, we get

$$\sin\varphi = \sin\left(\frac{\pi}{2} - \phi'\right) = \cos\phi' = \frac{\sigma}{\Sigma} \tag{2.4.7}$$

which corresponds to the Equation (2.1.2) reported by Yilmaz, concerning the hue variation of the spectral yellow.

2.5 Critical aspects in Yilmaz's model

In Section 2.2 our aim was to recast Yilmaz's model in a rigorous framework, with respect to both its colorimetric interpretation and its mathematical development, remaining as close as possible to what Yilmaz reported. In particular, concerning the notation, we decided to keep Yilmaz's one, enriching it in order to better structure our proof. In Chapter 4 we will need to translate Yilmaz's result in the notation of Chapter 3. In fact, while this section is about pointing out some critical issues about Yilmaz's model, in 4 we will see how the quantum model allows us to overcome these issues.

The fist problematic aspect is the use of Munsell chips in its experiments. The mentioned piece of white paper is used as a sort of ideal non-selective Lambertian reflector for the illuminant. A clear problem arises from the fact that it is not possible to compare for match a Munsell chip with a narrow band illuminant reflected by the piece of white paper.
While the set of Munsell chips was an obvious choice in 1962, the year of publishing of Yilmaz's paper, nowadays we can replace it without effort with an emitting display that will also allow us performing comparisons with narrow-band lights. With such a modern experimental apparatus, the color sensations $\tilde{R}_{\mathscr{B}}, \tilde{R}_{\mathscr{B}'}, \tilde{Y}_{\mathscr{B}}$ and $\tilde{Y}_{\mathscr{B}'}$ will be effectively measurable.

In a footnote at page 15 of [166], Yilmaz mentions the fact that '*there is no necessity for* Σ *to be the same for all directions*'. For this reason in Sections 2.1 and 2.2 we decided to keep the dependence of Σ on the hue ϕ, using the symbols $\Sigma_\phi, \Sigma_R, \Sigma_Y$. As underlined in Appendix A the speed of light is the same for all the directions, so the question becomes whether this is true as well for Σ. The saturation of a color sensation is defined as a percentage: 100% representing the absence of a washed-out sensation, as it happens for a narrow-band light, and 0% corresponding to the totally washed-out sensation of achromatic stimuli. These measurements are made with fixed hue ϕ, and it is not clear whether changing the hue would lead to a re-scaling of the interval of the possible saturation values. In other words it seems to be problematic understanding how to compare the saturation scales of colors with different hues. It seems more correct to remain faithful to the original definition of saturation and

consider it to be *normalized* in the same way for all the hues[††]. Thus, Equations (2.2.10) and (2.2.11), called by Yilmaz '*more general formulae*', will become:

$$\Omega = \begin{pmatrix} \Gamma & 0 & -\sigma\Gamma \\ 0 & 1 & 0 \\ -\frac{\sigma}{\Sigma^2}\Gamma & 0 & \Gamma \end{pmatrix} \qquad \text{with } \Gamma = \frac{1}{\sqrt{1-\left(\frac{\sigma}{\Sigma}\right)^2}}. \tag{2.5.1}$$

In Section 2.2 we proceeded assuming the experimental results claimed by the author to be true, however it still remains unclear if the results claimed by Yilmaz have been obtained after actual observations or if they are the results of a *gedankenexperiment*, i.e. a thought experiment. In the first case, Yilmaz does not report any experimental data and they do not seem to be found anywhere else, this, of course, raises more than a doubt about their validity.

In the second case, it is clear that Yilmaz pushed the gedankenexperiment technique way too far: a thought experiment is used to check what known results of a given theory would predict in an experimental configuration that is not possible to test with the current available technology. No known colorimetric result can be used to predict the outcomes of the three experiments, in particular, we notice that the hue shift in the third experiment represented by Equation (2.1.2) is unlikely to have been obtained via psychophysical experiments, seems to be somehow forced to have the desired analytical expressions that permitted him to determine the matrix Ω. However, as one can see in Equation 2.2.9, Yilmaz's experimental hypothesis corresponds to the first equation of the second system, hence, in the proof that we provided in Section 2.2, it seems that it does not need to be imposed as an hypothesis.

In spite of the critical issues just underlined, Yilmaz's paper has the great merit of highlighting the theoretical importance of the assumption that the maximal saturation Σ of the color perceived from spectral lights is invariant w.r.t. changes of illuminants.

Finally, it is important to stress that not every aspect of special relativity theory was translated by Yilmaz in a colorimetric context. He only talked about the aspects mentioned in Table 2.1. The crucial point is that he justifies their presence in color theory from a questionable experimental viewpoint. We do believe that he probably got this intuition from the formal similarity of the two theories. In Chapters 4 and 5 we will see how to properly justify the presence of relativistic concepts thanks to the framework that will be provided in Chapter 3.

[††]In Chapter 4 we will see that Σ will be normalized to 1.

Chapter 3

Resnikoff's approach and its quantum interpretation

Yilmaz's speculations, described in the previous chapter, had a strong impact on H.L. Resnikoff who, in the paper [135] published twelve years later, acknowledged him for his intuition. Resnikoff's work on color is particularly remarkable, because it completes the algebraic analysis of color perception started by Grassman and axiomatized by Schrödinger.

In this chapter we will provide an overview and the basic concepts of a recent novel mathematical theory of color perception, based on the quantum reinterpretation of Resnikoff's approach, see [12], which reconciles the concepts of trichromacy and color opponency, already mentioned in Chapter 1. The main references for this chapter will be the several recent contributions of Berthier and Provenzi [15, 129, 12, 16, 18], which treat different aspects of this novel theory in detail.

As we will see in Chapter 4, the framework introduced in this chapter will permit to justify on a purely theoretical basis the relativistic color perception phenomena argued by Yilmaz, overcoming the issues underlined in Chapter 2. Note that further definitions, more related to quantum information theory, will be introduced in Chapter 5 enriching the framework presented in this chapter.

3.1 The trichromacy axiom

The classical, and well established, colorimetric experiences of Newton [116, 117], Grassmann [67], Helmholtz [153] and Maxwell [108] have been resumed by Schrödinger [138] in a set of axioms that describe the structure of a space designed to represent the set of colors from the trichromatic properties of color perception. These axioms stipulate that this space, denoted $\mathcal{C}$ from now on, is a *regular convex cone of real dimension 3*. In particular:

- $\mathcal{C}$ is a *cone* if it is stable w.r.t. multiplications by positive scalars, i.e. for all $c \in \mathcal{C}$ and all $k \in \mathbb{R}^+$, then $kc \in \mathcal{C}$;
- $\mathcal{C}$ is *convex* if, for all $c_1, c_2 \in \mathcal{C}$ and for all $\alpha \in [0,1]$, we have that $\alpha c_1 + (1-\alpha)c_2 \in \mathcal{C}$;
- $\mathcal{C}$ is *regular* if, for any $c \in \mathcal{C}$, $c \neq 0$, then $\nexists\, \tilde{c} \in \mathcal{C}$ such that $c + \tilde{c} = 0$.

In [135], Resnikoff completed the work of Schrödinger and showed that to fully exploit this mathematical structure one needs to add a supplementary axiom, namely the fact that $\mathcal{C}$ is *homogeneous*, which means that there exists a transitive group action on $\mathcal{C}$, see [129] for an extended analysis of the homogeneity axiom. If we add one more property, the *self-duality*

of $\mathcal{C}$, introduced by Berthier in [12], then $\mathcal{C}$ becomes a *symmetric cone* [50]. Let us call $\mathcal{C}$, fulfilling all these axioms, the *trichromacy cone*.

According to the Koecher-Vinberg theorem [8], the trichromacy cone $\mathcal{C}$ can then be seen as the domain of positivity of a formally real Jordan algebra $\mathcal{A}$. This motivates the following:

Axiom (Trichromacy axiom [12]). *The trichromacy cone $\mathcal{C}$ is the domain of positivity of a formally real Jordan algebra of real dimension 3.*

The use of Koecher-Vinberg theorem is of crucial importance since it justifies the use of Jordan algebras and, as we will see, quantum theories in the context of modeling color perception. The idea to recast the study of color perception in the Jordan algebra framework appears already in Resnikoff's contribution [135]. However, Resnikoff was interested in using this concept to understand brightness and he did not mention a possible quantum interpretation of Schrödinger axioms. In the following we are going to mention just some essential definitions about Jordan algebras, for more detailed information on this subject the reader can consult e.g. [8], [50], [84], [109], [110]. Since it is sufficient for our purposes, in the following we are going to consider only finite-dimensional Jordan algebras.

Definition 3.1.1 (Jordan algebra). A Jordan algebra $\mathcal{A}$ is a real vector space equipped with a commutative bilinear product, called *Jordan product*, $\mathcal{A} \times \mathcal{A} \to \mathcal{A}$, $(a, b) \mapsto a \circ b$, satisfying the following so-called *Jordan identity*:

$$(a^2 \circ b) \circ a = a^2 \circ (b \circ a), \tag{3.1.1}$$

where $a^2 := a \circ a$.

The Jordan identity ensures that the power of any element a of $\mathcal{A}$ is well-defined. To prove this we observe that $a^3 := a \circ a \circ a = (a \circ a) \circ a = a^2 \circ a = a \circ a^2 = a \circ (a \circ a)$, so there is no ambiguity in defining a^3; now observe that, by taking $b = a$ in the Jordan identity, we have $a^4 := a^3 \circ a = a^2 \circ a^2$, which eliminates the possible ambiguity and thus also a^4 is well-defined. By induction we have that all powers of $a \in \mathcal{A}$ are well-defined. This implies that $\mathcal{A}$ is always power-associative, in the sense that the sub-algebra generated by any of its elements is associative and $a^m \circ a^n = a^{m+n}$, for all $m, n \in \mathbb{N}$.

Definition 3.1.2 (FRJA). A *Formally real Jordan algebra* (FRJA) is a Jordan algebra $\mathcal{A}$ such that, for any finite set $a_1, a_2, \ldots, a_n \in \mathcal{A}$, it holds true that

$$a_1^2 + a_2^2 + \cdots + a_n^2 = 0 \implies a_1 = a_2 = \cdots = a_n = 0, \tag{3.1.2}$$

just as if the elements $a_1, a_2, \ldots, a_n$ were real, which explains the name. FRJAs are naturally endowed with a partial ordering: given a FRJA $\mathcal{A}$ and two elements $a, b \in \mathcal{A}$, $a \leq b$ if and only if $b - a$ is equal to a sum of squares. This means that the squares of $\mathcal{A}$ are positive. A FRJA can be endowed with the structure of Hilbert space by defining an inner product induced by the Jordan product as follows: $\langle a, b \rangle := \mathrm{Tr}(L_{a \circ b})$, for all $a, b \in \mathcal{A}$ and with $L_{a \circ b}$ being the endomorphism $L_{a \circ b} : \mathcal{A} \to \mathcal{A}$, $c \mapsto (a \circ b) \circ c$, for all $c \in \mathcal{A}$.

FRJAs of finite dimension are classified and decomposed as direct sums of simple Jordan algebras, see [79]. The most surprising consequences of the trichromacy axiom are provided by the classification theorem of Jordan-von Neumann-Wigner, see for instance [8]. According to this theorem there are only two possible choices for $\mathcal{A}$, which are not isomorphic as FRJAs:

1. $\mathbb{R} \oplus \mathbb{R} \oplus \mathbb{R}$, an *associative* Jordan algebra, endowed with the following Jordan product:

$$(t_1 + t_2 + t_3) \circ (s_1 + s_2 + s_3) = (t_1 s_1 + t_2 s_2 + t_3 s_3), \quad t_i, s_i \in \mathbb{R},\ i = 1, 2, 3,$$

whose domain of positivity is $\mathbb{R}^+ \times \mathbb{R}^+ \times \mathbb{R}^+$.

2. $\mathcal{H}(2,\mathbb{R}) \cong \mathbb{R}\oplus\mathbb{R}^2$, two isomorphic *not associative* Jordan algebras, i.e., respectively, the algebra of 2×2 real symmetric matrices and the so-called *spin factor*. Their Jordan products are respectively: the symmetrized matrix product for $\mathcal{H}(2,\mathbb{R})$, i.e. $A\circ B := \frac{1}{2}(AB+BA)$, with $A,B\in\mathcal{H}(2,\mathbb{R})$, and the following product for the spin factor:

$$(\alpha_1,\mathbf{v}_1)\circ(\alpha_2,\mathbf{v}_2) = (\alpha_1\alpha_2+\langle\mathbf{v}_1,\mathbf{v}_2\rangle, \alpha_1\mathbf{v}_2+\alpha_2\mathbf{v}_1), \tag{3.1.3}$$

where $\alpha_i\in\mathbb{R}$, $\mathbf{v}_i\in\mathbb{R}^2, i=1,2$, and $\langle\ ,\ \rangle$ denotes the Euclidean scalar product on $\mathbb{R}^2$. Their domains of positivity are, respectively, $\overline{\mathcal{C}}(\mathcal{H}(2,\mathbb{R})) := \overline{\mathcal{H}^+}(2,\mathbb{R})$ which is the set of positive semi-definite 2×2 matrices, i.e. symmetric matrices with non-negative trace and determinant, and $\overline{\mathcal{C}}(\mathbb{R}\oplus\mathbb{R}^2) := \overline{\mathcal{L}^+} = \{(\alpha,\mathbf{v})^t\in\mathbb{R}\oplus\mathbb{R}^2,\ \alpha\geq 0,\ \alpha^2-\|\mathbf{v}\|^2\geq 0\}$ which is the closure of the *future lightcone*, $\|\ \|$ being the Euclidean norm.

When $\mathbb{R}\oplus\mathbb{R}\oplus\mathbb{R}$ is endowed with the so-called Helmholtz-Stiles metric:

$$ds^2 = \sum_{i=1}^{3} a_i\,(d\xi_i/\xi_i)^2\ , \tag{3.1.4}$$

$a_i,\xi_i\in\mathbb{R}^+$, it represents the metric space used in the standard colorimetry, see e.g. [163]. Since this space has been extensively studied, in the sequel we will concentrate only on the second possibility which, as we will see, contains the quantum structure that we are looking for.

Notice that as a vector space, $\mathbb{R}\oplus\mathbb{R}^2$ can be identified with the 3-dimensional Minkowski space $\mathbb{R}^{1,2}$, that explains the use of the terminology *future lightcone* for its domain of positivity.

As underlined before, the second type of FRJA has two different, isomorphic expressions. The natural isomorphism between $\mathcal{H}(2,\mathbb{R})$ and $\mathbb{R}\oplus\mathbb{R}^2$ is given by:

$$\begin{array}{rccc} \chi: & \mathcal{H}(2,\mathbb{R}) & \xrightarrow{\sim} & \mathbb{R}\oplus\mathbb{R}^2 \\ & \begin{pmatrix}\alpha+v_1 & v_2\\ v_2 & \alpha-v_1\end{pmatrix} & \longmapsto & (\alpha,(v_1,v_2)^t). \end{array} \tag{3.1.5}$$

It is easy to prove that χ is an isomorphism of Jordan algebras, so, in particular, given $A,B\in\mathcal{H}(2,\mathbb{R})$ it respects their respective Jordan products, i.e. $\chi(A\circ B)=\chi(A)\circ\chi(B)$. Furthermore χ induces as well an isomorphism between their domains of positivity, hence $\overline{\mathcal{C}}(\mathcal{H}(2,\mathbb{R}))\cong\overline{\mathcal{C}}(\mathbb{R}\oplus\mathbb{R}^2)$.

An important property of FRJAs is that $\overline{\mathcal{C}}(\mathcal{A})$ is always self-dual, i.e.

$$\overline{\mathcal{C}}(\mathcal{A})\cong\overline{\mathcal{C}}^*(\mathcal{A}) := \{\omega\in\mathcal{A}^*\ :\ \forall b\in\overline{\mathcal{C}}(\mathcal{A}),\ \omega(b)\geq 0\}, \tag{3.1.6}$$

where $\mathcal{A}^*$ denotes the dual vector space of $\mathcal{A}$. As we will see later on, self-duality will play an important role, e.g. in Chapter 5.

3.2 The duality state-observable

Non-associative Jordan algebras have been proven to provide a perfectly valid framework to develop quantum theories in the pioneering paper [79], in the sense that their algebraic description of states and observables is equivalent to the density matrix formalism that can be constructed starting from the ordinary Hilbert space formulation, see e.g. [147, 46]. Non-commutativity of Hermitian operators on a Hilbert space is replaced by non-associativity in the Jordan framework, this is essential to preserve the core of quantum theories, i.e. the

existence of uncertainty relations, which cannot appear if the Jordan algebra of observables is both commutative and associative.

Color perception shares at least two features with quantum theories: first, it makes no sense to talk about color in absolute terms, a color exists only when it is observed in well-specified observational conditions, see e.g. [160, 136]; second, repeated color matching experiments on identically prepared visual scenes do not lead to a sharp selection of a color that matches the test, but to a distribution of selections picked around the most probable one, which is clearly reminiscent of the probabilistic interpretation of quantum mechanics.

The quantum trichromacy axiom implies a radical change of paradigm with respect to classical colorimetry: we no more deal with color in terms of three coordinates belonging to a flat color space, but with a theory of *color states and observables in duality with each other* in which, as we will point out in Chapter 5, *perceived colors are inextricably associated with measurements*, mathematically expressed by the so-called *effects*.

A perceptual observable of a visual scene, or simply an *observable* a, is a sensation that can be measured leading to the registration of an outcome belonging to a certain set that depends on the observable. The algebra of observables $\mathcal{A}$ of our quantum-like theory of color perception is $\mathcal{H}(2,\mathbb{R}) \cong \mathbb{R} \oplus \mathbb{R}^2$ and perceptual colors are particular observables that belong to their domain of positivity.

A perceptual state, or simply a *state* $\mathbf{s}$, coincides, in practice, with the preparation of a visual scene for the measurements of its observables. Two examples of states are the following:

a) a *color state from a light stimulus* is prepared by allowing a naturally or artificially emitted visible radiation to be perceived by an observer;

b) a *color state from an illuminated surface* is prepared by illuminating a colored patch so that it can be perceived by an observer.

Observables characterize a state through their measurements and, vice-versa, the preparation of a particular state characterizes the experimental outcomes that will be obtained. It is common to resume this consideration as the duality state-observable. From a mathematical point of view, the duality state-observable is formalized by the Riesz-Markov representation theorem, see e.g. [132].

It seems natural, at this point, to make an analogy between the notions defining a physical system and color perceptual systems.

Definition 3.2.1 (Nomenclature of physical systems)**.** The following definitions are conventionally assumed in physics, see the classical references [46, 146, 113].

- A physical system $\mathcal{S}$ is described as a setting where one can perform physical measures giving rise to quantitative results in conditions that are as isolated as possible from external influences.
- Observables in $\mathcal{S}$ are the objects of measurements. If they form an associative and commutative algebraic structure, then the physical theory is called classical.
- States of $\mathcal{S}$ are associated with the ways $\mathcal{S}$ is prepared for the measurement of its observables.
- The expectation value of an observable in a given state of $\mathcal{S}$ is the average result of multiple measures of the observable conducted in the physical system $\mathcal{S}$ prepared in the same state.

Regarding this last definition, we notice that this is the standard experimental way of associating a value to an observable both in classical and in quantum physics for two different reasons: in the former we assume that nature is deterministic and observables have precise values, however, we need to introduce the concept of expectation value because all measurements are affected by errors; in the latter we assume that nature is intrinsically probabilistic and the expectation value is needed to associate to every observable the probability that it will take a given value from a set of admissible outcomes.

When we deal with a visual perceptual system, as an illuminated piece of paper, or a light stimulus in a vision box, the definitions above remain valid, with two major differences: first, the instruments used to measure the observables are not physical devices, but the sensory system of a human being; second, the results may vary from person to person, thus the average procedure needed to experimentally define the expectation value of an observable in a given state is, in general, observer-dependent. The response of an *ideal standard observer* can be obtained through a further statistical average on the observer-dependent expectation values of an observable in a given state.

If we specialize this idea to the case of color perception, we may give the following colorimetric definitions.

Definition 3.2.2 (Nomenclature of color perceptual systems)**.**

- A perceptual chromatic state is represented by the preparation of a visual scene for psycho-visual experiments in controlled and reproducible conditions.
- A perceptual color is the perceptual observable identified with a psycho-visual measurement performed in a given perceptual chromatic state.
- A perceived color is the expectation value assumed by a perceptual color after psycho-visual measurements.

We underline that the definition of a perceptual color as an observable associated to a psycho-visual measurement in a given perceptual chromatic state is very different than the physical meaning of the term 'color stimulus', i.e. the spectral distribution of a light signal across the visual interval. In fact, such a color stimulus, presented to an observer in different conditions, e.g. isolated or in context, can be sensed as very different perceived colors. Thus, as we have seen in Chapter 1, it is very ill-posed to identify a perceptual color with a color stimulus, as also mentioned in [163].

3.3 Chromatic states and von Neumann entropy

In the algebraic formulation of quantum mechanics states are described by *density matrices*, i.e. unit-trace positive semi-definite matrices. In the quantum-like theory of color perception, the *chromatic state vectors* $\mathbf{v_s} = (s_1, s_2)^t$ belonging to the unit disk $\mathcal{D}$ parameterize each density matrix $\rho_{\mathbf{s}}$, in fact the perceptual chromatic state space can be identified with:

$$\mathcal{S}(\mathcal{H}(2,\mathbb{R})) = \left\{ \rho_{\mathbf{s}} \equiv \frac{1}{2} \begin{pmatrix} 1+s_1 & s_2 \\ s_2 & 1-s_1 \end{pmatrix},\ \|\mathbf{v_s}\| \leq 1 \right\}, \tag{3.3.1}$$

or, as a consequence of (3.1.5),

$$\mathcal{S}(\mathbb{R} \oplus \mathbb{R}^2) := \chi(\mathcal{S}(\mathcal{H}(2,\mathbb{R}))) = \left\{ \chi(\rho_{\mathbf{s}}) = \frac{1}{2} \begin{pmatrix} 1 \\ \mathbf{v_s} \end{pmatrix},\ \|\mathbf{v_s}\| \leq 1 \right\}. \tag{3.3.2}$$

This is the state space of a *rebit*, the $\mathbb{R}$-version of a qubit, see e.g. [161], and it happens to be the easiest known quantum system.

In this Chapter and in the following ones, to simplify the notation, we will identify a state $\mathbf{s}$ with the unique associated density matrix $\rho_{\mathbf{s}} \in \mathcal{H}(2,\mathbb{R})$ and vector $\chi(\rho_{\mathbf{s}}) \in \mathbb{R} \oplus \mathbb{R}^2$.

The *expectation value* of an observable $a \in \mathcal{H}(2,\mathbb{R})$ on the state $\mathbf{s}$ is the average outcome of repeated and independent measurements of a performed when the system is identically prepared in the state $\mathbf{s}$. It is given by:

$$\langle a \rangle_{\mathbf{s}} = \mathrm{Tr}(\rho_{\mathbf{s}}\, a). \tag{3.3.3}$$

Notice that this is the classical quantum interpretation of the inner product induced on the Jordan product on the FRJA. In particular it is easy to prove that, for $\mathcal{A} = \mathcal{H}(2,\mathbb{R})$, $\mathrm{Tr}(\rho_{\mathbf{s}} \circ a) = \mathrm{Tr}(\rho_{\mathbf{s}} a)$. Indeed it is sufficient to recall that $\rho_{\mathbf{s}} \circ a = \frac{1}{2}(\rho_{\mathbf{s}} a + a\rho_{\mathbf{s}})$ and that $\mathrm{Tr}(\rho_{\mathbf{s}} a) = \mathrm{Tr}(a\rho_{\mathbf{s}})$.
Polar coordinates are the most natural ones in $\mathcal{D}$ and they provide this alternative parameterization of the generic density matrix:

$$\rho_{\mathbf{s}}(r,\vartheta) = \frac{1}{2}\begin{pmatrix} 1 + r\cos\vartheta & r\sin\vartheta \\ r\sin\vartheta & 1 - r\cos\vartheta \end{pmatrix}, \qquad r \in [0,1],\ \vartheta \in [0, 2\pi). \tag{3.3.4}$$

States can be either *mixed* or *pure*, accordingly to the fact that they can be written as a convex combination of other states or not, respectively.

A commonly used descriptor of mixedness of a quantum state is the so-called *von Neumann entropy*. It represents the *expectation of information gain* on a quantum system after a measurement, thus when it is *minimal*, then no information gain can be achieved after a measurement, i.e. we possess all the possible knowledge about the system; while, when it is *maximal*, then the expectation of information gain after a measurement on the system is maximal, which means that we have at disposal the least possible information on the system itself.

Definition 3.3.1 (Von Neumann entropy)**.** Let $\mathbf{s}$ be a mixed state and $\rho_{\mathbf{s}}$ be the density matrix associated to it. The von Neumann entropy $S(\rho_{\mathbf{s}})$ of $\rho_{\mathbf{s}}$ is given by

$$S(\rho_{\mathbf{s}}) = -\,\mathrm{Tr}(\rho_{\mathbf{s}} \log_2 \rho_{\mathbf{s}}) = -\langle \log_2 \rho_{\mathbf{s}} \rangle_{\mathbf{s}}. \tag{3.3.5}$$

This definition actually represents the *normalized* von Neumann entropy, indeed the non-normalized von Neumann entropy is defined by replacing $\log_2$ with log, in that case the maximal value that it reaches is not 1, but $\log 2$. The following proposition provides an equivalent definition for the (normalized) von Neumann entropy.

Proposition 3.3.2. *Let* $\mathbf{s}$ *be a quantum state and* $\rho_{\mathbf{s}}$ *be its density matrix, then*

$$S(\rho_{\mathbf{s}}) = -\sum_k \lambda_k \log_2 \lambda_k. \tag{3.3.6}$$

Where λ_k, $k = 1, 2$, *are the eigenvalues of* $\rho_{\mathbf{s}}$.

Proof. Let the density matrix $\rho_{\mathbf{s}}$ have the following expression:

$$\rho_{\mathbf{s}} = \frac{1}{2}\begin{pmatrix} 1 + r\cos\vartheta & r\sin\vartheta \\ r\sin\vartheta & 1 - r\cos\vartheta \end{pmatrix}. \tag{3.3.7}$$

We want to prove that $\mathrm{Tr}(\rho_{\mathbf{s}} \log_2 \rho_{\mathbf{s}}) = \lambda_1 \log_2 \lambda_1 + \lambda_2 \log_2 \lambda_2$, this is equivalent to proving that $\mathrm{Tr}(\rho_{\mathbf{s}} \log \rho_{\mathbf{s}}) = \lambda_1 \log \lambda_1 + \lambda_2 \log \lambda_2$. The main issue is understanding the expression

$\log \rho_{\mathbf{s}}$. From [34] a real matrix having positive eigenvalues, such as $\rho_{\mathbf{s}}$ since we assumed $\mathbf{s}$ to be a mixed state, admits an unique real logarithm matrix. The issue now becomes obtaining an explicit expression for $\log \rho_{\mathbf{s}}$. Let us start by diagonalizing $\rho_{\mathbf{s}}$ to facilitate this task. Via straightforward computations it is easy to obtain that $P_\vartheta^{-1} \rho_{\mathbf{s}} P_\vartheta = \mathrm{diag}(\lambda_1, \lambda_2)$, with

$$P_\vartheta = \begin{pmatrix} -\sin\vartheta & 1+\cos\vartheta \\ 1+\cos\vartheta & \sin\vartheta \end{pmatrix}, \tag{3.3.8}$$

and $\lambda_1 = (1-r)/2$, $\lambda_2 = (1+r)/2$.

Given a diagonal matrix $D = \mathrm{diag}(a, b)$, with $a, b > 0$, it is easy to prove that its logarithm is given by:

$$\log D = \mathrm{diag}(\log a, \log b) \tag{3.3.9}$$

An easy example is given by Id_2, indeed, as we might expect, $\log Id_2 = \mathbb{O}_2$. Let us consider the density matrix $\frac{1}{2} Id_2$ (it will be needed in the next steps of this proof). Its logarithm is given by

$$\log\left(\frac{1}{2} Id_2\right) = \mathrm{diag}(-\log 2, -\log 2) = -(\log 2) Id_2. \tag{3.3.10}$$

By Theorem 2.8 of [69], for all the matrix A such that $||A - Id||_2 < 1$ the following function

$$\log A = \sum_{k=1}^{+\infty} (-1)^{k+1} \frac{(A - Id)^k}{k}, \tag{3.3.11}$$

is well defined and it is such that $e^{\log A} = A$. In our case, let us call $rR_\vartheta = 2\rho_{\mathbf{s}} - Id_2$. It is easy to prove that $||rR_\vartheta||_2 < 1$, since $0 < r < 1$ and $||R_\vartheta||_2 = 1$. Thus

$$\log(2\rho_{\mathbf{s}}) = \sum_{k=1}^{+\infty} (-1)^{k+1} \frac{(rR_\vartheta)^k}{k}. \tag{3.3.12}$$

Another property of the matrix logarithm states that if A, B are two commuting positive-definite real matrices, then $\log(AB) = \log A + \log B$. This is to say that $\log \rho_{\mathbf{s}} = \log(2\rho_{\mathbf{s}}) + \log\left(\frac{1}{2} Id_2\right)$. Thus, recalling Equation (3.3.10):

$$\log \rho_{\mathbf{s}} = \log(2\rho_{\mathbf{s}}) - (\log 2) Id_2. \tag{3.3.13}$$

Using Equation (3.3.12) the previous equation becomes:

$$\log \rho_{\mathbf{s}} = \sum_{k=1}^{+\infty} (-1)^{k+1} \frac{(rR_\vartheta)^k}{k} - (\log 2) Id_2. \tag{3.3.14}$$

It is easy to show that P_ϑ diagonalizes as well R_ϑ, thus $P_\vartheta^{-1} R_\vartheta P_\vartheta = \mathrm{diag}(-1, 1)$. Let us now

show that P_ϑ diagonalizes also $\log \rho_{\mathbf{s}}$:

$$\begin{aligned}
P_\vartheta^{-1} \log \rho_{\mathbf{s}} P_\vartheta =& P_\vartheta^{-1} \left(\sum_{k=1}^{+\infty} (-1)^{k+1} \frac{(rR_\vartheta)^k}{k} - (\log 2) Id_2 \right) P_\vartheta \\
=& \sum_{k=1}^{+\infty} (-1)^{k+1} \frac{(rP_\vartheta^{-1} R_\vartheta P_\vartheta)^k}{k} - (\log 2) Id_2 \\
=& \sum_{k=1}^{+\infty} (-1)^{k+1} \frac{(r \operatorname{diag}(-1,1))^k}{k} - (\log 2) Id_2 \\
=& \operatorname{diag} \left(\sum_{k=1}^{+\infty} (-1)^{2k+1} \frac{r^k}{k}, \sum_{k=1}^{+\infty} (-1)^{k+1} \frac{r^k}{k} \right) - (\log 2) Id_2 \\
=& \operatorname{diag} \left(-\sum_{k=1}^{+\infty} \frac{r^k}{k}, \sum_{k=1}^{+\infty} (-1)^{k+1} \frac{r^k}{k} \right) - (\log 2) Id_2 \\
=& \operatorname{diag}(\log(1-r), \log(1+r)) - (\log 2) Id_2 \\
=& \operatorname{diag} \left(\log \left(\frac{1-r}{2} \right), \log \left(\frac{1+r}{2} \right) \right) \\
=& \operatorname{diag}(\log \lambda_1, \log \lambda_2),
\end{aligned} \tag{3.3.15}$$

where the second equality holds because of the continuity of the conjugation by P_ϑ.

The above computation shows that $\rho_{\mathbf{s}}$ and $\log \rho_{\mathbf{s}}$ are simultaneously diagonalized by P_ϑ. Let us finally calculate $S(\rho_{\mathbf{s}})$. Using the fact that the trace is invariant under change of basis, we can perform the following computations and obtain the thesis:

$$\begin{aligned}
\operatorname{Tr}(\rho_{\mathbf{s}} \log \rho_{\mathbf{s}}) &= \operatorname{Tr}(P_\vartheta^{-1} \rho_{\mathbf{s}} \log \rho_{\mathbf{s}} P_\vartheta) = \operatorname{Tr}(P_\vartheta^{-1} \rho_{\mathbf{s}} P_\vartheta P_\vartheta^{-1} \log \rho_{\mathbf{s}} P_\vartheta) \\
&= \operatorname{Tr}(\operatorname{diag}(\lambda_1, \lambda_2) \operatorname{diag}(\log \lambda_1, \log \lambda_2)) \\
&= \lambda_1 \log \lambda_1 + \lambda_2 \log \lambda_2.
\end{aligned} \tag{3.3.16}$$

□

Notice that actually we have defined the von Neumann entropy for mixed states only. Indeed the density matrix of a pure state is a rank-1 projector, hence it is not invertible, so it does not fulfill the hypotheses of Theorem 1 in [34], that assures the existence of the logarithm matrix. Even if the log of the density matrix corresponding to a pure state is not defined, it is possible to define its von Neumann entropy as a limit procedure. In fact, by Proposition 3.3.2, for all $r \in [0,1)$ we have that:

$$S(\rho_{\mathbf{s}}) = S(r) = -\frac{1-r}{2} \log_2 \left(\frac{1-r}{2} \right) - \frac{1+r}{2} \log_2 \left(\frac{1+r}{2} \right). \tag{3.3.17}$$

Pure states correspond to the value $r = 1$, where $S(r)$ is not defined. However we can define S at 1, as the limit $S(1) := \lim_{r \to 1^-} S(r) = 0$. Thus the von Neumann entropy has the following expression:

$$S(r) = \begin{cases} -\frac{1-r}{2} \log_2 \left(\frac{1-r}{2} \right) - \frac{1+r}{2} \log_2 \left(\frac{1+r}{2} \right) & r \in [0,1) \\ 0 & r = 1 \end{cases}, \tag{3.3.18}$$

Notice that, after straightforward computations, $S(r)$ can be rewritten as follows:

$$S(r) = \begin{cases} 1 - \left[\frac{1}{2} \log_2(1-r^2) + \frac{r}{2} \log_2 \left(\frac{1+r}{1-r} \right) \right] & r \in [0,1) \\ 0 & r = 1 \end{cases}. \tag{3.3.19}$$

As proven in [71] or [123], the von Neumann entropy is invariant under orthogonal conjugation, which implies that it is a *radial function*, moreover, it is *concave* and, importantly, it provides a characterization of pure states and of the maximally mixed state, denoted with $\rho_{\mathbf{0}}$:

- $\rho_{\mathbf{s}}$ is a pure state if and only if $S(\rho_{\mathbf{s}}) = 0$;
- $\rho_{\mathbf{0}} = \text{argmax}_{\rho_{\mathbf{s}}} S(\rho_{\mathbf{s}})$.

From Equation (3.3.18) we have that $\rho_{\mathbf{0}} = Id_2/2$, where Id_2 is the 2×2 identity matrix, or equivalently, $\chi(\rho_{\mathbf{0}}) = \frac{1}{2}(1, \mathbf{0})^t$, which means that the maximally mixed state is parameterized by the null vector, the center of $\mathcal{D}$, where $S(0) = 1$. Figure 3.3 provides a 2D and a 3D plot of the normalized von Neumann entropy.

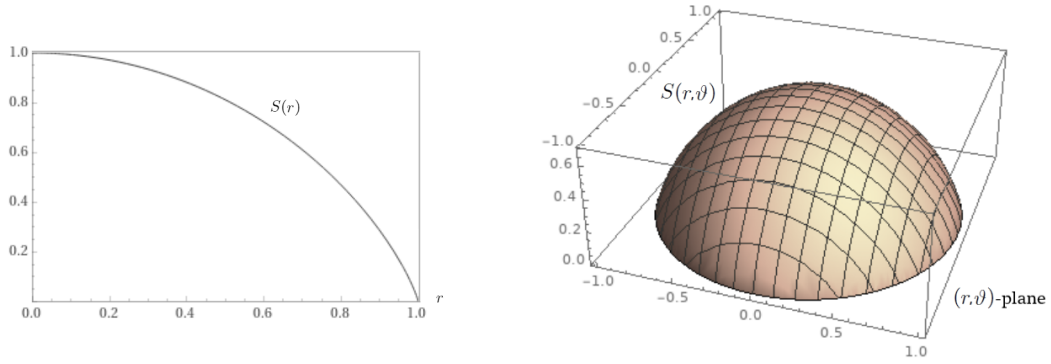

(a) Plot of $S(r)$, fixing ϑ.

(b) Plot of $S(\rho_{\mathbf{s}}) = S(r, \vartheta)$.

Figure 3.1: Plots of the normalized von Neumann entropy.

Since the highest degree of entropy is equivalent to the minimal amount of chromatic information, $\rho_{\mathbf{0}}$ is identified with the *achromatic state*, denoted with $\mathbf{s_a}$. Instead, pure states are parameterized by the points of the border of $\mathcal{D}$ and are identified with the *hues* of perceived colors:

$$\begin{aligned} \mathcal{PS}(\mathcal{H}(2,\mathbb{R})) &= \left\{ \rho_{\mathbf{s}} = \frac{1}{2} \begin{pmatrix} 1+s_1 & s_2 \\ s_2 & 1-s_1 \end{pmatrix}, \ \|\mathbf{v_s}\| = 1 \right\} \\ &= \left\{ \rho_{\mathbf{s}} = \frac{1}{2} \begin{pmatrix} 1+\cos\vartheta & \sin\vartheta \\ \sin\vartheta & 1-\cos\vartheta \end{pmatrix}, \ \vartheta \in [0, 2\pi) \right\}, \end{aligned} \tag{3.3.20}$$

or, equivalently,

$$\mathcal{PS}(\mathbb{R} \oplus \mathbb{R}^2) := \chi(\mathcal{PS}(\mathcal{H}(2,\mathbb{R}))) = \left\{ \chi(\rho_{\mathbf{s}}) = \frac{1}{2} \begin{pmatrix} 1 \\ \mathbf{v_s} \end{pmatrix}, \ \|\mathbf{v_s}\| = 1 \right\}. \tag{3.3.21}$$

In Chapter 6, Section 6.3.3 we will give an argument in favor of the interpretation of pure states as hues.

Recalling the intuitive definition of saturation quoted in Chapter 1, Subsection 1.3.1, it is quite natural to define the saturation Σ of the chromatic state $\rho_{\mathbf{s}}(r, \vartheta)$ as done in [18, 19], using the von Neumann entropy, expressed as in Equation (3.3.19), as follows:

$$\Sigma(r) := 1 - S(r) = \begin{cases} \frac{1}{2}\log_2(1-r^2) + \frac{r}{2}\log_2\left(\frac{1+r}{1-r}\right) & r \in [0,1) \\ 1 & r = 1 \end{cases}, \tag{3.3.22}$$

In this way we have $\Sigma(0) = 0$ and $\Sigma(1) = 1$. We must stress that in Chapter 6 we will come back on the problem of defining the saturation of a perceived color via the von Neumann entropy, in particular we will relate it to the concept of *relative entropy* that will be introduced in Chapter 5.

3.4 Chromatic opponency: Hering's rebit

The next fundamental information to recall is how Hering's chromatic opponency naturally appears in the quantum-like formalism. The following presentation is explicitly based on the canonical decomposition of density matrices known as *Bloch representation*. Given $(e_i)_{i=0}^2$, the canonical basis of $\mathbb{R} \oplus \mathbb{R}^2$, if we define $\sigma_i := \chi^{-1}(e_i)$, then we get

$$\sigma_0 \equiv Id_2, \quad \sigma_1 = \begin{pmatrix} 1 & 0 \\ 0 & -1 \end{pmatrix}, \quad \sigma_2 = \begin{pmatrix} 0 & 1 \\ 1 & 0 \end{pmatrix}, \tag{3.4.1}$$

where σ_1 and σ_2 can be recognized to be the two *real Pauli matrices*. The generic density matrix of $\mathcal{S}(\mathcal{H}(2,\mathbb{R}))$ can be decomposed in terms of the real Pauli matrices as follows:

$$\rho_{\mathbf{s}}(s_1, s_2) = \rho_{\mathbf{0}} + \frac{1}{2}(s_1\sigma_1 + s_2\sigma_2) = \rho_{\mathbf{0}} + \frac{1}{2}\mathbf{v}_{\mathbf{s}} \cdot \vec{\sigma}, \tag{3.4.2}$$

where $\mathbf{v}_{\mathbf{s}} = (s_1, s_2)$ is called the *Bloch vector* associated to $\mathbf{s}$ and $\mathbf{v}_{\mathbf{s}} \cdot \vec{\sigma} := s_1\sigma_1 + s_2\sigma_2$. The set $\{\sigma_0, \sigma_1, \sigma_2\}$ is an orthogonal basis for $\mathcal{H}(2,\mathbb{R})$ with respect to the Hilbert-Schmidt inner product, i.e.

$$\langle \sigma_i, \sigma_j \rangle_{HS} := \mathrm{Tr}(\sigma_i\sigma_j) = 2\delta_{ij}, \qquad i,j = 0,1,2, \tag{3.4.3}$$

so the components of the Bloch vector are the expectation values of the real Pauli matrices on the state $\mathbf{s}$, in fact:

$$\mathbf{v}_{\mathbf{s}} = (s_1, s_2) = (\mathrm{Tr}(\rho_{\mathbf{s}}\,\sigma_1), \mathrm{Tr}(\rho_{\mathbf{s}}\,\sigma_2)) = (\langle\sigma_1\rangle_{\mathbf{s}}, \langle\sigma_2\rangle_{\mathbf{s}}). \tag{3.4.4}$$

As a consequence, Equation (3.4.2) can be re-written as follows:

$$\rho_{\mathbf{s}} = \rho_{\mathbf{0}} + \frac{1}{2}\begin{pmatrix} \langle\sigma_1\rangle_{\mathbf{s}} & \langle\sigma_2\rangle_{\mathbf{s}} \\ \langle\sigma_2\rangle_{\mathbf{s}} & -\langle\sigma_1\rangle_{\mathbf{s}} \end{pmatrix}, \tag{3.4.5}$$

and its polar expression is:

$$\rho_{\mathbf{s}}(r,\vartheta) = \rho_{\mathbf{0}} + \frac{1}{2}\left[r\cos\vartheta\,\sigma_1 + r\sin\vartheta\,\sigma_2\right], \tag{3.4.6}$$

with $r \in [0,1]$ and $\vartheta \in [0, 2\pi)$.

Given two generic angles $\vartheta_1, \vartheta_1 \in [0, 2\pi)$, the pure states $\rho_{\mathbf{s}_k}(1, \vartheta_k)$, $k = 1, 2$, are rank-1 projectors that can be represented as follows:

$$\rho_{\mathbf{s}_k}(1,\vartheta_k) = \frac{1}{2}(Id_2 + \cos\vartheta_k\sigma_1 + \sin\vartheta_k\sigma_2) \equiv \rho_{\mathbf{0}} + \frac{1}{2}\mathbf{v}_{\mathbf{s}_k} \cdot \vec{\sigma}, \tag{3.4.7}$$

with $\mathbf{v}_{\mathbf{s}_k} = (\cos\vartheta_k, \sin\vartheta_k)$, $k = 1, 2$.
Rank-1 projectors are characterized by the following condition: $\rho_{\mathbf{s}}(1,\vartheta) \circ \rho_{\mathbf{s}}(1,\vartheta) = \rho_{\mathbf{s}}(1,\vartheta)$.

Notice that the projector $\rho_{\mathbf{s}_k}(1,\vartheta_k)$ is a projection operator along the direction given by the unit vector $\mathbf{u}_k = (\cos(\vartheta_k/2), \sin(\vartheta_k/2))$. Indeed by straightforward computations we can see that

$$\rho_{\mathbf{s}_k}(1,\vartheta_k) = \frac{1}{2}\begin{pmatrix} 1+\cos\vartheta_k & \sin\vartheta_k \\ \sin\vartheta_k & 1-\cos\vartheta_k \end{pmatrix} = \mathbf{u}_k\mathbf{u}_k^t. \tag{3.4.8}$$

To better understand the following it is important to stress that, given a pure state $\mathbf{s}_k$, its Bloch vector representation $\mathbf{v}_{\mathbf{s}_k}$ does not correspond to the direction of projection $\mathbf{u}_k$ of $\rho_{\mathbf{s}_k}(1, \vartheta_k)$.

In quantum theories, orthogonality with respect to the Hilbert-Schmidt inner product is used to measure *incompatibility between states*, and $\rho_{\mathbf{s}_1}(1, \vartheta_1)$, $\rho_{\mathbf{s}_2}(1, \vartheta_2)$ project on two orthogonal rays in $\mathbb{R}^2$ if and only if their Bloch vectors $\mathbf{v}_{\mathbf{s}_1}, \mathbf{v}_{\mathbf{s}_2}$ are antipodal. Indeed, recalling the fact that $\mathrm{Tr}(\sigma_1) = \mathrm{Tr}(\sigma_2) = \mathrm{Tr}(\sigma_1\sigma_2) = \mathrm{Tr}(\sigma_2\sigma_1) = 0$ and that $\sigma_1^2 = \sigma_2^2 = Id_2$, we obtain:

$$\begin{aligned}
\langle \rho_{\mathbf{s}_1}(1, \vartheta_1), \rho_{\mathbf{s}_2}(1, \vartheta_2) \rangle_{HS} &= \mathrm{Tr}(\rho_{\mathbf{s}_1}(1, \vartheta_1)\rho_{\mathbf{s}_2}(1, \vartheta_2)) \\
&= \frac{1}{4}\,\mathrm{Tr}((Id_2 + \mathbf{v}_1 \cdot \vec{\sigma})(Id_2 + \mathbf{v}_2 \cdot \vec{\sigma})) \\
&= \frac{1}{4}\,\mathrm{Tr}(Id_2 + \mathbf{v}_1 \cdot \vec{\sigma} + \mathbf{v}_2 \cdot \vec{\sigma} + (\mathbf{v}_1 \cdot \vec{\sigma})(\mathbf{v}_2 \cdot \vec{\sigma})) \\
&= \frac{1}{4}\,\mathrm{Tr}(Id_2 + (\cos\vartheta_1\sigma_1 + \sin\vartheta_1\sigma_2)(\cos\vartheta_2\sigma_1 + \sin\vartheta_2\sigma_2)) \\
&= \frac{1}{4}\,\mathrm{Tr}((1 + \cos\vartheta_1\cos\vartheta_2 + \sin\vartheta_1\sin\vartheta_2)Id_2) \\
&= \frac{1}{2}(1 + \cos(\vartheta_1 - \vartheta_2)).
\end{aligned} \tag{3.4.9}$$

The latter expression is equal to 0 if and only if $|\vartheta_1 - \vartheta_2| = \pi$, i.e. the corresponding Bloch vectors $\mathbf{v}_1$ and $\mathbf{v}_2$ are diametrically opposed.

This condition of incompatibility is usually interpreted as the fact that the two states have 0 probability of being simultaneously measured. In other words antipodality of vectors in the Bloch representation correspond to orthogonality with respect to the Hilbert-Shmidt product. For further details see e.g. [71].

In Hering's theory of color perception, see [72], incompatibility between color sensations is called *opposition*, for this reason two pure states $\rho_{\mathbf{s}_1}(1, \vartheta_1)$ and $\rho_{\mathbf{s}_2}(1, \vartheta_2)$ are said to be *chromatically opponent* if incompatible, hence when $|\vartheta_1 - \vartheta_2| = \pi$. The concept of opposition will play a fundamental role in Chapter 6.

Let us immediately use opponency to corroborate our interpretation of $\rho_{\mathbf{0}}$ as the achromatic state: it is easy to prove that the following formula holds

$$\rho_{\mathbf{0}} = \frac{1}{4}\rho_{\mathbf{s}}(1, 0) + \frac{1}{4}\rho_{\mathbf{s}}(1, \pi) + \frac{1}{4}\rho_{\mathbf{s}}\left(1, \frac{\pi}{2}\right) + \frac{1}{4}\rho_{\mathbf{s}}\left(1, \frac{3\pi}{2}\right), \tag{3.4.10}$$

this shows that $\rho_{\mathbf{0}}$ is the mixed state obtained as a convex combination, with exactly the same coefficients, of the balance between two couples of pure opponent chromatic states.

Notice also that the real Pauli matrices can be expressed as follows:

$$\sigma_1 = \rho_{\mathbf{s}}(1, 0) - \rho_{\mathbf{s}}(1, \pi), \quad \sigma_2 = \rho_{\mathbf{s}}\left(1, \frac{\pi}{2}\right) - \rho_{\mathbf{s}}\left(1, \frac{3\pi}{2}\right), \tag{3.4.11}$$

thus Equation (3.4.6) implies the following, fundamental, formula:

$$\rho_{\mathbf{s}}(r, \vartheta) = \rho_{\mathbf{0}} + \frac{1}{2}\left\{ r\cos\vartheta\,[\rho_{\mathbf{s}}(1, 0) - \rho_{\mathbf{s}}(1, \pi)] + r\sin\vartheta\left[\rho_{\mathbf{s}}\left(1, \frac{\pi}{2}\right) - \rho_{\mathbf{s}}\left(1, \frac{3\pi}{2}\right)\right]\right\}. \tag{3.4.12}$$

Equation (3.4.12) is the exact quantum analogue of Hering's representation of color sensations: the generic chromatic state $\mathbf{s}$ identified by the density matrix $\rho_{\mathbf{s}}(r, \vartheta)$ can be interpreted as the *contribution of the achromatic state $\rho_{\mathbf{0}}$ and the balance between two couples of opponent chromatic states*, encoded by the real Pauli matrices σ_1, σ_2.

We must stress that given a density matrix $\rho_{\mathbf{s}}$, one can evaluate the contribution of the red/green opposition degree given by σ_1 by computing $\langle\sigma_1\rangle_{\mathbf{s}} = \mathrm{Tr}(\rho(r,\theta)\circ\sigma_1) = r\cos\theta$, and the same for σ_2. It is quite remarkable that the Bloch disk gives a quantum analogue of the *Hering disk* that describes the color opponency mechanism resulting from the activity of certain retinal neurons [141]. The matrix σ_1 encodes the opposition red/green, while the matrix σ_2 encodes the opposition yellow/blue. We underline that *this quantum justification of the color opponency derives only from the trichromacy axiom when considering the algebra* $\mathcal{H}(2,\mathbb{R})$.

A fundamental remark on color perception made by Hering is that, for unrelated colors, while *the chromatic information is intrinsic*, *the achromatic part can be determined only by means of comparisons with other colors*, see e.g. [73]. An observer can measure the degree of opposition red vs. green and yellow vs. blue of an unrelated color, see e.g. [74], but, due to adaptation mechanisms of the human visual system, he or she cannot establish how bright or dim a perceived unrelated color is (apart from extreme situations close to the visible threshold or the glare limit, that we do not consider here). This ambiguity is represented in Equation (3.4.12) by the fact that $\rho_{\mathbf{0}}$ appears as a sort of 'offset state', independent of the state $\mathbf{s}$.

For clear reasons, we call *Hering's rebit* the quantum-like system that we have just described. This latter can be thought as a mathematical formalization of Newton's chromatic disk, as depicted in Fig. 3.2.

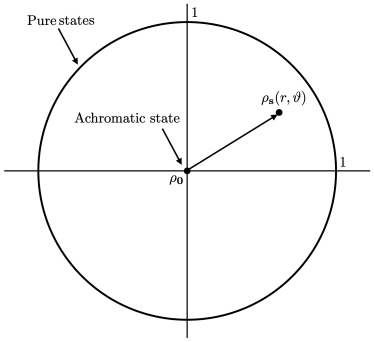

Figure 3.2: Hering's rebit as a quantum-like formalization of Newton's chromatic disk.

In other words we propose, as a theoretically well-founded model for a chromaticity diagram, the Bloch disk representation of Hering's rebit. In the following Chapter we will see that Hering's rebit has a structure of gyrovector space, and the behavior of its elements, the chromatic vectors, allows us to justify Yilmaz's results, already mentioned in Chapter 2.

Chapter 4

Relativity within the quantum model

In this chapter, based on [13], we overcome the problems about Yilmaz's approach presented in Chapter 2 by providing a completely theoretical proof of the experimental outcomes claimed by Yilmaz in the setting of the quantum-like framework for color perception introduced in Chapter 3. In particular we will extend the theory of the previous chapter to incorporate also relativistic phenomena, providing new definitions and adopting the notation of Chapter 3 to describe Yilmaz's model in the terms of the quantum-like one (instead of the one adopted for Chapter 2, more faithful to Yilmaz's original paper).

More specifically the concept of chromatic vector will be of fundamental importance, since Yilmaz's experiments can be explained in terms of Einstein-Poincaré's addition law between chromatic vectors. We have obtained this result by following the hint given by Mermin's alternative reconstruction of the special theory of relativity from Einstein-Poincaré addition law for velocity vectors. Moreover these theoretical results are shown to be coherent with existing experimental data, see Section 4.3.1.

In Chapter 1 we mentioned the presence of hyperbolic metrics in the color literature. In this Chapter we will introduce the Hilbert hyperbolic metric stressing out that, *differently to all the other works that we have consulted, in our model this hyperbolic metric emerges naturally from the mathematical formalism*, see as well [12], *and it is not superimposed to fit experimental data or perceptual effects*. As we will better specify in Section 4.3, the relevance of this metric is due to the fact that it expresses a chromatic constancy property with respect to observer changes.

4.1 Yilmaz relativity of color perception

We must stress that the description of Yilmaz's model, and in particular of the procedure through which he obtained Lorentz transformations in the color context, provided in this chapter, in Subsection 4.1.4, differs from the one of Chapter 2, Section 2.2, in the fact that it is more faithful to Yilmaz's original one. The reason is that we want to focus on the data concerning solely the information about hue and saturation of the color stimuli, in order to better relate it to the algebraic structure of the disk of chromatic vectors that will provide a theoretical justification of Yilmaz's results in Section 4.2.

Yilmaz's work [166, 165] is, to the best of our knowledge, the first contribution that investigates the geometry of color perception from the viewpoint of special relativity. The main Yilmaz goal is to obtain *colorimetric Lorentz transformations* by interpreting mathematically the outcomes of three basic experiments, see Subsection 2.1.2. As we have detailed in Section 2.5, these experiments are quite controversial and this fact gives an even stronger motivation to recast Yilmaz in a mathematical setting where these experiments can be completely bypassed.

4.1.1 Yilmaz colorimetric setting

In this subsection we are going to introduce a notation more in accordance to the one of Chapter 3, for the concepts already presented in Subsection 2.1.1.
In order to analyze the results of *color matching experiments*, Yilmaz considers a conical color space that, in our notation, can be written as follows:

$$\widetilde{\mathcal{C}} = \{(\alpha, x, y) \in \mathbb{R}^3,\ \Sigma^2 - \|\mathbf{v}\|^2 \geq 0,\ \alpha \geq 0\}\ , \tag{4.1.1}$$

where Σ is a non-negative real constant and, when $\alpha > 0$, $\mathbf{v} = (v_1, v_2) = (x/\alpha, y/\alpha)$, otherwise, if $\alpha = 0$, then also $\mathbf{v}$ is null. Notice that $\widetilde{\mathcal{C}}$ is a reparametrization of $\mathscr{C}$ of Chapter 2. A color c of $\widetilde{\mathcal{C}}$ can be viewed both as a point of $\mathbb{R}^3$ with coordinates (α, x, y) and as a couple $(\alpha, \mathbf{v})$, where α is a positive real number and $\mathbf{v}$ is a vector of $\mathbb{R}^2$ with Euclidean norm given by $v = \|\mathbf{v}\|$ less or equal to Σ.

In Yilmaz's context, the norm $v = \sqrt{v_1^2 + v_2^2} = \sqrt{x^2 + y^2}/\alpha$ represents the *saturation* of the color c and satisfies $v \leq \Sigma$, hence Σ is interpreted as the maximal perceivable saturation. Moreover, the angle defined by $\phi = \arctan(y/x) = \arctan(v_2/v_1)$ represents the *hue* of c and the non-negative real α is associated to its *lightness*. The definitions of hue, saturation and lightness of classical colorimetry can be consulted for instance in Chapter 1.

We use the notation $\widetilde{\mathcal{C}}$ instead of the trichromacy cone $\mathcal{C}$ introduced in Chapter 3, because the latter is intrinsically equipped with the rich algebraic structure described in the previous chapter, that is not part of Yilmaz's model.

The existence of a positive real Σ, which plays the role of a *limiting saturation* 'reached by spectral colors', is one of the fundamental assumptions of Yilmaz. The mathematical formula for saturation given above is the analogue of speed (the magnitude of the velocity vector) in mechanics, thus it seems clear that, from Yilmaz's viewpoint, the limiting saturation Σ should be interpreted as an analogue of the speed of light.

We recall that the purpose of the three experiments described in [166] is to show that:

1. color perception is a relativistic phenomenon;
2. the limiting saturation is constant under 'illuminant changes';
3. there exists a colorimetric aberration effect which is the analogue of the relativistic one.

It is worth mentioning that Yilmaz does not use any information related to a hypothetical invariant quadratic form. In physics, the introduction of an invariant metric on the Minkowski spacetime is motivated by the experimental evidence about the constancy of the speed of light in vacuum measured by inertial observers, however an analogous result is not, or at least not yet, available in the colorimetric setting. It is arguable that this is the reason why Yilmaz wanted to bypass the introduction of an invariant metric by introducing the results of the third experimentm, and talking just after obtaining the Lorentz boosts about the Minkowski quadratic form.

Our description and subsequent analysis of Yilmaz's experimental results will be greatly simplified if we set up a novel nomenclature adapted from special relativity.

4.1.2 The nomenclature of the relativity of color perception

Without any further specification, we consider a color c as an abstract *coordinate-free* element of the space $\widetilde{\mathcal{C}}$. This interpretation is the exact analogue to what we do in Galilean mechanics when we consider the position as an abstract element of the space $\mathbb{R}^3$ without coordinates. For color sensations induced by non-self luminous stimuli, a coordinate system can be introduced in $\widetilde{\mathcal{C}}$ by considering an illuminant which allows us to identify c and to perform measurements on it. For this reason, here we propose the following definition.

Definition 4.1.1 (Illuminant)**.** An illuminant is *a reference frame I of the space $\widetilde{\mathcal{C}}$.*

It is well-known, see e.g. [49, 63], that when a person is embedded for a sufficient time in a visual scene illuminated by I, he/she will perceive the surface of an object having non-selective reflectance properties without a color saturation. In this case, we call that person *adapted* to I. This consideration naturally leads to the following definition.

Definition 4.1.2 (Observer)**.** We call any couple $o = (c, I)$, such that the color $c \in \widetilde{\mathcal{C}}$ has zero saturation in the reference frame I, an observer adapted to the illuminant I, or simply an observer.

Given the analogy between the saturation of a color and the speed of a velocity vector for a mechanical system, we can say that an observer $o = (c, I)$ is characterized by the fact that the color c appears 'at rest' in the reference frame I. Carrying on the analogy with mechanics, we propose the following final definition.

Definition 4.1.3 (Inertial observers)**.** We call $o_1 = (c_1, I_1)$ and $o_2 = (c_2, I_2)$ two inertial observers and we denote by $(\alpha^1, x^1, y^1) = (\alpha^1, \boldsymbol{v}_1)$ and $(\alpha^2, x^2, y^2) = (\alpha^2, \boldsymbol{v}_2)$ the coordinates of a generic color in the reference frame I_1 and I_2, respectively.

By definition of observer, we have that $c_i^i = (\alpha^i, 0, 0) = (\alpha^i, \mathbf{0})$, $i = 1, 2$. However, given $i, j = 1, 2$, $i \neq j$, c_j will be described by o_i with a color c_j^i represented by

$$c_j^i = (\alpha, \mathbf{v}_{ij}), \tag{4.1.2}$$

where $\alpha \geq 0$ is a suitable non-negative scalar and $\mathbf{v}_{ij} = \mathbf{v}_{c_j^i}$ verifies $v_{ij} = \|\mathbf{v}_{ij}\| \leq \Sigma$.

4.1.3 Yilmaz experiments revisited

Thanks to the nomenclature just introduced, we are now able to give a concise description of Yilmaz experiments, for the original description see [166, 124] or Subsection 2.1.2.
In all three experiments, Yilmaz considers only the case of two inertial observes $o_1 = (c_1, I_1)$ and $o_2 = (c_2, I_2)$ such that only the first component of the vector $\mathbf{v}_{12}$ is non-zero, i.e. $\mathbf{v}_{c_2^1} = \mathbf{v}_{12} = (v_{12}, 0)$.

The first experiment is intrinsic in the system given by the two inertial observes: each one describes the color that is perceived at rest by the other. The outcome claimed by Yilmaz is the following:

$$\mathbf{v}_{c_1^2} = -\mathbf{v}_{c_2^1} \ . \tag{4.1.3}$$

If we assume this result to be correct, then it follows that *color perception is a relativistic phenomenon* and so an absolute description of the sensation of color is meaningless.

The second and the third experiment involve the two inertial observers defined above in the act of observing a particular color $c \in \tilde{\mathcal{C}}$ which is described by o_1 as having maximal saturation, i.e. $\|\mathbf{v}_{c^1}\| = \Sigma$, thanks to the contribution of only one component of the vector $\mathbf{v}_{c^1}$, the other being zero. The position of the non-null component distinguishes the second from the third experiment. Specifically, the outcome of the second experiment can be summarized as follows:

$$\mathbf{v}_{c^1} = (\Sigma, 0) \Longrightarrow \mathbf{v}_{c^2} = (\Sigma, 0) \ , \tag{4.1.4}$$

i.e., if $c \in \tilde{\mathcal{C}}$ is described by o_1 has having maximal saturation thanks to the sole contribution of the first component of $\mathbf{v}_{c^1}$, then the description of $c \in \tilde{\mathcal{C}}$ performed by o_2 is identical.

Instead, the outcome of the third experiment is the following:

$$\mathbf{v}_{c^1} = (0, \Sigma) \Longrightarrow \mathbf{v}_{c^2} = (-\Sigma \sin\varphi, \Sigma \cos\varphi) \ , \tag{4.1.5}$$

with $\sin\varphi = v_{12}/\Sigma$, so, if $c \in \tilde{\mathcal{C}}$ is described by o_1 has having maximal saturation thanks to the sole contribution of the second component of $\mathbf{v}_{c^1}$, then c will be still described by o_2 as having maximal saturation since $\|\mathbf{v}_{c^2}\| = \left(\Sigma^2(\sin^2\varphi + \cos^2\varphi)\right)^{1/2} = \Sigma$, but the hue description will be different.

As already mentioned in Section 2.4, the third experiment is meant to mimic the relativistic aberration effect. We are going to see that this experiment is crucial for the derivation of the colorimetric Lorentz transformations performed by Yilmaz.

Finally, we underline that, if Yilmaz outcomes are assumed to be true, then *colors with limiting saturation are perceived as such by all inertial observers*, which is in clear analogy of the fact that the speed of light is measured as constant by all inertial observers.

4.1.4 Yilmaz derivation of colorimetric Lorentz transformations

We explain now how to obtain the colorimetric Lorentz transformations from Equations (4.1.3), (4.1.4) and (4.1.5). In [166] the coordinate change between o_1 and o_2 is supposed to be linear. When we take into account the specific choices made by Yilmaz, the coordinate change is given by:

$$\begin{pmatrix} \alpha^2 \\ x^2 \\ y^2 \end{pmatrix} = \begin{pmatrix} a_{11} & a_{12} & 0 \\ a_{21} & a_{22} & 0 \\ 0 & 0 & 1 \end{pmatrix} \begin{pmatrix} \alpha^1 \\ x^1 \\ y^1 \end{pmatrix} . \tag{4.1.6}$$

Proposition 4.1.4. *With the notations introduced before, the color coordinate transformation corresponding to an illuminant change is the Lorentz boost along the x-direction described by the following equation:*

$$\begin{pmatrix} \alpha^2 \\ x^2 \\ y^2 \end{pmatrix} = \begin{pmatrix} \frac{1}{\sqrt{1-(v_{12}/\Sigma)^2}} & \frac{-v_{12}/\Sigma^2}{\sqrt{1-(v_{12}/\Sigma)^2}} & 0 \\ \frac{-v_{12}}{\sqrt{1-(v_{12}/\Sigma)^2}} & \frac{1}{\sqrt{1-(v_{12}/\Sigma)^2}} & 0 \\ 0 & 0 & 1 \end{pmatrix} \begin{pmatrix} \alpha^1 \\ x^1 \\ y^1 \end{pmatrix} . \tag{4.1.7}$$

Proof. Using Equation (4.1.6) and by calculating its inverse, after straightforward computations, we obtain:

$$\frac{x^2}{\alpha^2} = \frac{a_{21}\alpha^1 + a_{22}x^1}{a_{11}\alpha^1 + a_{12}x^1}, \quad \frac{x^1}{\alpha^1} = \frac{-a_{21}\alpha^2 + a_{11}x^2}{a_{22}\alpha^2 - a_{12}x^2} . \tag{4.1.8}$$

As it can be checked in more detail in [124] or Section 2.2, the fact that $\mathbf{v}_{12} = (v_{12}, 0)$ and Equation (4.1.3) are equivalent to:

$$\frac{a_{21}}{a_{11}} = -v_{12}, \quad \frac{-a_{21}}{a_{22}} = v_{12} . \tag{4.1.9}$$

This shows that: $a_{11} = a_{22}$ and $a_{21} = -v_{12}a_{22}$.

The result of the second experiment, Equation (4.1.4), is equivalent to:

$$\Sigma = \frac{a_{21} + a_{22}\Sigma}{a_{11} + a_{12}\Sigma} , \tag{4.1.10}$$

which gives: $a_{12} = -(v_{12}a_{22})/\Sigma^2$.

From the third experiment, Equation (4.1.5), we have:

$$-\tan\varphi = \frac{a_{21}\alpha^1 + a_{22}x^1}{y^1} = \frac{a_{21}}{\Sigma} . \tag{4.1.11}$$

Since $\sin\varphi = v_{12}/\Sigma$, this implies:

$$a_{22} = \frac{1}{\sqrt{1-(v_{12}/\Sigma)^2}} . \tag{4.1.12}$$

□

It is worth noticing that the derivation of these colorimetric Lorentz transformations proposed by Yilmaz relies only on information given by the **v**-component of colors, the only one appearing in Equations (4.1.3), (4.1.4) and (4.1.5). As we will see, in the quantum framework these **v**-components correspond to the perceptual chromatic vectors that will be introduced in Subsection 4.2.1.

4.1.5 Issues about Yilmaz approach

Without calling into question the great originality of Yilmaz's ideas and the relevance of his results, we deem necessary to underline some issues about the approach that we have reported above. As mentioned before, the derivation of the colorimetric Lorentz transformations is essentially based on the following assumptions:

- the space of *perceived colors* is the cone $\tilde{\mathcal{C}}$, and, in particular, there exists a limiting saturation Σ;
- the coordinate changes between inertial observers are linear transformations;
- the results obtained from the three experiments are considered as valid.

However, as we have underlined in Section 2.5, no experimental result, nor apparatus description is available in [166] and this naturally raises doubts about the actual implementation of the three experiments. Furthermore, while the results of the first two experiments are plausible, the outcome of the third seems completely illusory. In fact, Yilmaz defines the limiting saturation of a color $c = (\alpha, x, y) \in \widetilde{\mathcal{C}}$ as a value Σ of $\|v\|$ that cannot be perceptually matched with that of any Munsell chip, thus, while this definition permits to *identify* the limiting saturation of a color, it does not allow its *measurement*. As a consequence, Equation (4.1.5), with its precise analytical form, seems to be an ad-hoc formula used to single out the colorimetric Lorentz transformations (4.1.7), more than the real outcome of a psycho-physical experiment.

It may be tempting to adopt a more conventional approach to obtain the desired transformations starting, for instance, from the fact that there exists a limiting saturation invariant under observer changes and that the color space is isotropic and homogeneous. However, to go further, it is necessary to introduce an analogue of the Minkowski metric, which Yilmaz circumvents. One may choose to follow the standard path used in special relativity, see e.g. [96, 97], to justify the existence of such a metric. However, while the assumptions that go along with this approach rely on a solid experimental basis for what concerns the Minkowski spacetime, they are far from being either obvious or simple to be tested for the space of perceived colors.

For this reason, we consider a better solution to follow less conventional, but fully equivalent, approaches to special relativity as, e.g., that of the remarkable Mermin's paper [112], whose main focus is the Einstein-Poincaré velocity addition law and not Lorentz transformations. This alternative approach seems more suitable because the colorimetric effects reported by Yilmaz involve the sole **v**-components (or, equivalently, the sole perceptual chromatic vectors that will be defined in Subsection 4.2.1). The appropriateness of Mermin's approach is also justified by the fact that, as already declared by the emblematic title 'Relativity without light', he deals with relativity without specifically considering the physics of electromagnetic waves, thus providing a more general approach that can also be used in our case.

We will show how to recover Yilmaz's results from a purely theoretical point of view, thus avoiding the issues discussed in this Subsection, thanks to the quantum framework of color perception presented in Chapter 3.

4.2 Einstein-Poincaré's addition law for chromatic vectors

In this section we show that the outcomes of the first two experiments quoted by Yilmaz in his model can be rigorously derived from the fact that the so-called perceptual chromatic vectors, that will be introduced in Subsection 4.2.1, satisfy the Einstein-Poincaré addition law.

As we have done in Subsection 4.1.2, in order to show in the clearest way how to obtain the results stated above, we first need to introduce several notions in Subsection 4.2.1. The notions introduced in Chapter 3 will be needed as well.

4.2.1 The nomenclature perceptual color attributes in the quantum colorimetric framework

We recall that a *perceptual color* c is an element of the trichromacy cone $\mathcal{C}$, i.e. explicitly $c = (\alpha, \mathbf{v})$ with $\alpha^2 - \|\mathbf{v}\|^2 \geq 0$ and $\alpha \geq 0$.

Definition 4.2.1 (Magnitude of a perceptual color)**.** Let $c = (\alpha, \mathbf{v}) \in \mathcal{C}$ be a perceptual color. The positive real α is called the *magnitude* of c.

Recalling that $\rho_{\mathbf{0}} = Id_2$ the magnitude can be equivalently defined as the evaluation of c on the state of maximal entropy, as follows

$$\alpha := \langle c \rangle_{\rho_{\mathbf{0}}} = \mathrm{Tr}(c \circ \rho_{\mathbf{0}}). \tag{4.2.1}$$

In this chapter we prefer to use the term magnitude, instead of the term *lightness*, adopted by Yilmaz because of possible confusion. A more thoughtful discussion about this issue is the object of Chapter 6.

Since the cone $\mathcal{C}$ is self-dual, c can also be considered as an element of the dual cone $\mathcal{C}^*$. The case when c has magnitude $\alpha = 1/2$ is special, in fact, as previously seen, thanks to the isomorphism defined in Equation (3.1.5), c can naturally be associated to a density matrix representing its state. This justifies the following definition.

Definition 4.2.2 (Perceptual color state)**.** If the perceptual color $c = (\alpha, \mathbf{v})$ has magnitude $\alpha = 1/2$, then c is called a *perceptual color state* and denoted with c_s. Thus, every perceptual color state has the following expression:

$$c_s := (1/2, \mathbf{v}), \text{ with } \|\mathbf{v}\| \leq 1/2. \tag{4.2.2}$$

If we want to associate a perceptual color c with magnitude $\alpha \geq 0$, $\alpha \neq 1/2$, to a density matrix, we must proceed in two steps: the first consists in dividing c by twice the magnitude, i.e. $c/2\alpha = (1/2, \mathbf{v}/2\alpha)$, which belongs to $\mathcal{D}_{1/2} = \{c \in \mathcal{C},\ \alpha = 1/2\} \cong \{\mathbf{u} \in \mathbb{R}^2 \ :\ \|\mathbf{u}\| \leq 1/2\}$. In this way, the new magnitude is correctly set to $1/2$, coherently with Equation (3.3.1), but we need a second steps to restore the variability of the vector part inside the unit disk, which is easily accomplished by considering $2\mathbf{v}_c \in \mathcal{D}_1 \cong \{\mathbf{u} \in \mathbb{R}^2 \ :\ \|\mathbf{u}\| \leq 1\}$.

The simple procedure just described leads to the following two definitions.

Definition 4.2.3 (Perceptual chromatic vector)**.** Let $c = (\alpha, \mathbf{v}) \in \mathcal{C}$, then $\mathbf{v}_c := \mathbf{v}/2\alpha \in \mathcal{D}_{1/2}$ is called the perceptual chromatic vector of c.

The reason for the name that we have chosen is that $\mathbf{v}_c$ carries only information about the chromatic attributes of c and not about its magnitude. Notice that this procedure of descarding the achromatic component α via division is reminiscent of the construction of the chromaticity diagrams mentioned in Section 1.1.

Definition 4.2.4 (Perceptual chromatic state)**.** For every perceptual color $c = (\alpha, \mathbf{v}) \in \mathcal{C}$, the density matrix $\rho(2\mathbf{v}_c)$

$$\rho(2\mathbf{v}_c) = \frac{1}{2}\begin{pmatrix} 1 + 2v_{c,1} & 2v_{c,2} \\ 2v_{c,2} & 1 - 2v_{c,1} \end{pmatrix} . \tag{4.2.3}$$

is called perceptual chromatic state of c.

The difference between a perceptual *color* state and a perceptual *chromatic* state is represented by the fact that, in the first case, the density matrix associated to a color c with magnitude $1/2$ contains all the information about the state of c, magnitude included, which is not the case for a chromatic state, where the magnitude α of c does not play any role.

Two noticeable conditions about perceptual chromatic states can be singled out, as formalized in the following definition.

Definition 4.2.5 (Pure and achromatic perceptual states and colors)**.** Let $c = (\alpha, \mathbf{v}) \in \mathcal{C}$ be a perceptual color:

- the density matrix $\rho(2\mathbf{v}_c)$ describes a pure perceptual chromatic state if $\|\mathbf{v}_c\| = 1/2$. If that is the case, then c is called a pure perceptual color;
- the density matrix $\rho(2\mathbf{v}_c)$ describes the state of maximal von Neumann entropy if $\mathbf{v}_c = \mathbf{0}$. If that is the case, then c is said to be an achromatic perceptual color.

Geometrically, pure perceptual colors are in one-to-one correspondence with the points of the boundary of the disk $\mathcal{D}_{1/2}$, while the center of the disk $\mathcal{D}_{1/2}$ represents achromatic perceptual colors. Notice that $\mathcal{D}_{1/2}$, or analogously $\mathcal{D}_1$, can be considered the quantum-like version of Newton's disk and of the concept of chromaticity. As we will see, their geometry is not Euclidean because they can be naturally endowed with the Klein hyperbolic metric.

We now introduce the *chromaticity descriptors*, that we will call purities and quantities. For a closer coherence with Yilmaz first two experiments, see Subsection 4.1.3, we will consider only colors c whose perceptual chromatic vectors are of the form $\mathbf{v}_c = (v_c, 0)$ with $-1/2 \leq v_c \leq 1/2$.

Definition 4.2.6 (Pure opponent chromatic vectors)**.** The two chromatic vectors $\mathbf{v}_+ = (1/2, 0)$ and $\mathbf{v}_- = (-1/2, 0)$ are called pure opponent chromatic vectors.

Given a color c, its chromatic vector $\mathbf{v}_c$ divides the segment connecting $\mathbf{v}_-$ and $\mathbf{v}_+$ (extremes excluded) in two parts, whose lengths are denoted by $p^-(c)$ and $p^+(c)$, where:

$$p^-(c) = \frac{1}{2} - v_c = \frac{1 - 2v_c}{2} \in [0, 1], \qquad p^+(c) = v_c - \left(-\frac{1}{2}\right) = \frac{1 + 2v_c}{2} \in [0, 1]. \tag{4.2.4}$$

Definition 4.2.7 ($\pm$ purity of a perceptual color)**.** $p^-(c)$ and $p^+(c)$ will be called the $-$ purity and the $+$ purity of a perceptual color c, respectively.

The sum of the $-$ and $+$ purity of c is 1, so $\mathbf{v}_c$ can be written as the convex combination of the pure opponent chromatic vectors $\mathbf{v}_-$ and $\mathbf{v}_+$ with weights given by p^- and p^+, respectively, i.e.

$$\mathbf{v}_c = p^-(c)\mathbf{v}_- + p^+(c)\mathbf{v}_+. \tag{4.2.5}$$

Figure 4.1 provides a depiction of the $\pm$ purities defined above.

The term 'purity' is particularly appropriate, not only because it involves the pure opponent chromatic vectors, but also because it is reminiscent of the same term appearing in classical CIE colorimetry. Indeed, also the definition of 'excitation purity' p_e of a color c carries the information about its position on a straight line, precisely the one joining the equienergy

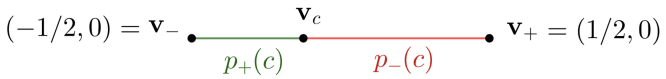

Figure 4.1: Purities.

point w (achromatic color) of the CIE 1931 chromaticity diagram with the so-called dominant wavelength of c (represented by a point belonging to the border of the chromaticity diagram). See [163] for more details.

Definition 4.2.8 (Purity ratio)**.** Given a perceptual color $c \in \mathcal{C}$, such that $|v_c| \neq 1/2$, the non-negative real number

$$r(c) = \frac{p^-(c)}{p^+(c)} = \frac{1 - 2v_c}{1 + 2v_c}, \tag{4.2.6}$$

is called the *purity ratio* of the color c.

It is easy to see that:

$$v_c = \frac{1}{2}\left(\frac{p^+(c) - p^-(c)}{p^+(c) + p^-(c)}\right). \tag{4.2.7}$$

It is obvious that, given two colors c and d, we have:

$$\mathbf{v}_c = \mathbf{v}_d \iff p^+(c) = p^+(d) \iff p^-(c) = p^-(d), \tag{4.2.8}$$

so, two colors with the same purity may differ only by their magnitude. For this reason, it is useful to define a color attribute analogue to purity but which takes into account also the magnitude information that has been lost after the projection on $\mathcal{D}_{1/2}$. This is done as follows.

Definition 4.2.9 ($\pm$ quantity of a perceptual color)**.** Let $c = (\alpha, \mathbf{v})$ be a perceptual color. We define the $-$ *quantity* $q^-(c)$ and the $+$ *quantity* $q^+(c)$ of c by the following two non-negative real numbers:

$$q^-(c) = 2\alpha p^-(c) = \alpha(1 - 2v_c), \quad q^+(c) = 2\alpha p^+(c) = \alpha(1 + 2v_c). \tag{4.2.9}$$

Clearly perceptual colors with magnitude equal to $1/2$, i.e. perceptual color states, are characterized by the fact that their purities and quantities coincide.

4.2.2 Einstein-Poincaré addition law and Yilmaz experiments

Now we discuss our main issue: *is there a rigorous way to compare two given colors c and d in $\mathcal{C}$?* The answer to this question that seems more natural and coherent with the concepts previously defined is to compare $q^-(c)$ with $q^-(d)$ and $q^+(c)$ with $q^+(d)$, that is to compare their $-$ and $+$ *quantities*. For this, we have to introduce the following concept.

Definition 4.2.10 (Quantity ratios)**.** Given two perceptual colors c and d, such that $|v_d| \neq 1/2$, the $\pm$ quantity ratios are defined as:

$$s^+(c, d) = \frac{q^+(c)}{q^+(d)} \quad \text{and} \quad s^-(c, d) = \frac{q^-(c)}{q^-(d)}. \tag{4.2.10}$$

Let us consider two arbitrary perceptual colors c and d whose magnitudes and perceptual chromatic vectors are, respectively, α_c and α_d, and $\mathbf{v}_c$ and $\mathbf{v}_d$, with $v_c > v_d$. We have:

$$s^+(c, d) = \frac{\alpha_c p^+(c)}{\alpha_d p^+(d)} \quad \text{and} \quad s^-(c, d) = \frac{\alpha_c p^-(c)}{\alpha_d p^-(d)}. \tag{4.2.11}$$

Now we arrive to a key definition.

Definition 4.2.11 (Relative perceptual chromatic vector)**.** Let $c, d \in \mathcal{C}$ be two perceptual colors, then, the relative perceptual chromatic vector is given by $\mathbf{v}_c^d = (v_c^d, 0)$, where

$$v_c^d := \frac{1}{2}\left(\frac{s^+(c,d) - s^-(c,d)}{s^+(c,d) + s^-(c,d)}\right) . \tag{4.2.12}$$

The definition of $\mathbf{v}_c^d$ is clearly inspired from Equation (4.2.7), but here quantity ratios play the role of purities. We also remark that the second coordinate of the relative perceptual chromatic vector is 0 because of our choice to consider only perceptual chromatic vectors of the type $\mathbf{v}_c = (v_c, 0)$, as Yilmaz did in his first two experiments.

Proposition 4.2.12. *With the notation introduced before, it holds that*

$$v_c^d = \frac{v_c - v_d}{1 - 4v_c v_d} , \tag{4.2.13}$$

or, equivalently,

$$v_c = \frac{v_c^d + v_d}{1 + 4v_c^d v_d}. \tag{4.2.14}$$

Proof. Thanks to Equation (4.2.11) we obtain:

$$v_c^d = \frac{1}{2}\left(\frac{q^+(c)q^-(d) - q^-(c)q^+(d)}{q^+(c)q^-(d) + q^-(c)q^+(d)}\right) , \tag{4.2.15}$$

and, since the ratio cancels out the proportionality between quantities and purities, we obtain:

$$v_c^d = \frac{1}{2}\left(\frac{p^+(c)p^-(d) - p^-(c)p^+(d)}{p^+(c)p^-(d) + p^-(c)p^+(d)}\right) . \tag{4.2.16}$$

We now notice that:

$$\frac{v_c - v_d}{1 - 4v_c v_d} = \frac{\frac{1}{2}\left(\frac{p^+(c)-p^-(c)}{p^+(c)+p^-(c)}\right) - \frac{1}{2}\left(\frac{p^+(d)-p^-(d)}{p^+(d)+p^-(d)}\right)}{1 - \frac{p^+(c)-p^-(c)}{p^+(c)+p^-(c)} \cdot \frac{p^+(d)-p^-(d)}{p^+(d)+p^-(d)}} , \tag{4.2.17}$$

straightforward manipulations lead to

$$\frac{v_c - v_d}{1 - 4v_c v_d} = \frac{1}{2}\left(\frac{p^+(c)p^-(d) - p^-(c)p^+(d)}{p^+(c)p^-(d) + p^-(c)p^+(d)}\right) = v_c^d, \tag{4.2.18}$$

and, consequently, to Equation (4.2.14). □

In special relativity, the Einstein-Poincaré addition law between two collinear velocity vectors with speed u_1 and u_2 can be written as follows:

$$u_1 \oplus u_2 = \frac{u_1 + u_2}{1 + \frac{u_1 u_2}{c^2}}, \tag{4.2.19}$$

where $\oplus$ is the symbol used to denote the relativistic sum and c is the speed of light. As we have already remarked in section 4.1, in Yilmaz's model the analogous of c is the limiting saturation Σ that, in the context of perceptual chromatic vectors, is equal to $1/2$. This explains the presence of the factor 4 in Equations (4.2.13) and (4.2.14), which are the exact analogue of the Einstein-Poincaré addition law for perceptual chromatic vectors written with our nomenclature. In particular, Equation (4.2.14) establishes that, given any two perceptual colors c and d, the relativistic sum of v_d with the relative perceptual chromatic vector v_c^d leads to v_c.

4.2.3 A theoretical proof of Yilmaz experiments

Thanks to Equations (4.2.13) and (4.2.14), we can prove the first two outcomes of Yilmaz's experiments in a purely theoretical manner. The proof of the first one is extremely simple, in fact, by exchanging c and d in Equation (4.2.13) we immediately find that

$$v_c^d = -v_d^c, \tag{4.2.20}$$

which is nothing but an alternative way of writing Equation (4.1.3), i.e. the first experimental outcome claimed by Yilmaz. The theoretical proof of the second experimental outcome claimed by Yilmaz, i.e. (4.1.4), is a bit trickier. First of all, we must recall that the second Yilmaz experiment involves two inertial observers $o_1 = (c_1, I_1)$ and $o_2 = (c_2, I_2)$ perceiving a maximally saturated color, which gives rise to the two vectors $\mathbf{v}_{c^1} = (\Sigma, 0)$ and $\mathbf{v}_{c^2} = (\Sigma, 0)$, together with the vector $\mathbf{v}_{c_2^1}$, which encodes how o_1 describes the color c_2. Instead, in this section, we deal with two perceptual colors $c, d \in \mathcal{C}$, which are associated to the perceptual chromatic vectors $\mathbf{v}_c, \mathbf{v}_d \in \mathcal{D}_{1/2}$, respectively, together with the relative perceptual chromatic vector $\mathbf{v}_c^d \in \mathcal{D}_{1/2}$. Thus, if we want to find a correlation, we must first operate suitable identifications among the three vectors appearing in the two situations. The correct identifications are the following:

$$\begin{cases} \mathbf{v}_{c^1} \equiv \mathbf{v}_c \\ \mathbf{v}_{c^2} \equiv \mathbf{v}_c^d \\ \mathbf{v}_{c_2^1} \equiv \mathbf{v}_d \end{cases}, \tag{4.2.21}$$

in fact, if, for the reasons explained above, we replace Σ with $1/2$ and we introduce $v_c = 1/2$ in Equation (4.2.13), we find that $v_c^d = 1/2$ independently of v_d. This is the precise way in which the second outcome claimed by Yilmaz must be interpreted within the formalism of perceptual chromatic vectors.

The case of the third Yilmaz's experiment is more complex, since related to the relativistic aberration effect already underlined in Section 2.4, but it is possible to obtain it using the general formula of the Einstein-Poincaré addition law for non collinear vectors. We must stress that the presence of the general relativistic addition law between chromatic vectors will be fully justified in Section 5.2 of the next chapter.

Recalling Equation (4.1.5), we know that $\mathbf{v}_{c^1} = (0, \Sigma)$ and $\mathbf{v}_{c_2^1} = (v_{12}, 0)$. According to Yilmaz's third experiment this implies that $\mathbf{v}_{c^2} = (-\Sigma \sin\varphi, \Sigma \cos\varphi)$, with $\sin\varphi = v_{12}/\Sigma$. As we did for the second experiment let us replace Σ with $1/2$ and do the same associations as in (4.2.21). Thus the description of the third experiment becomes:

$$\mathbf{v}_c = \mathbf{v}_{c^1} = (0, 1/2) \Longrightarrow \mathbf{v}_c^d = \mathbf{v}_{c^2} = (-\sin\varphi/2, \cos\varphi/2) \ , \tag{4.2.22}$$

with $\sin\varphi = 2v_{12}$. Notice that $\mathbf{v}_d = \mathbf{v}_{c_2^1} = (v_{12}, 0)$.

Let us start by assuming the statement of Proposition 4.2.12 to be true also for the general expression of the relativistic addition law, see Section 5.3 of the next chapter, thus, in particular, that the general equivalent of Equations (4.2.14) and (4.2.13) will be $\mathbf{v}_c = \mathbf{v}_c^d \oplus \mathbf{v}_d$ and $\mathbf{v}_c^d = \mathbf{v}_c \ominus \mathbf{v}_d$, respectively. To obtain the outcome of Yilmaz's third experiment we will use the latter equation. Explicit formulas for the two components of the vector $\mathbf{v}_c^d$ are the following:

$$(\mathbf{v}_c \ominus \mathbf{v}_d)_x = \frac{(\mathbf{v}_c)_x - v_{12}}{1 - 4v_{12}(\mathbf{v}_c)_x}, \qquad (\mathbf{v}_c \ominus \mathbf{v}_d)_y = \frac{\sqrt{1 - 4v_{12}^2}(\mathbf{v}_c)_y}{1 - 4v_{12}(\mathbf{v}_c)_x}, \tag{4.2.23}$$

see e.g. [149]. Notice that $\oplus$ is commutative for the collinear case, while it is not commutative in the general configuration. Using the fact that $\mathbf{v}_c = (0, 1/2)$ and the formulas provided in

Equation (4.2.23), one obtains the following expression for the vector $\mathbf{v}_c^d$:

$$\mathbf{v}_c^d = \mathbf{v}_c \ominus \mathbf{v}_d = \frac{1}{2}\left(-2v_{12}, \sqrt{1-4v_{12}^2}\right). \tag{4.2.24}$$

From the expression above it is easy to check that $||\mathbf{v}_c^d|| = 1/2$. Moreover comparing it with the expression of $\mathbf{v}_c^d$ of Equation (4.2.22), one can easily conclude that $\sin\varphi = 2v_{12}$.

4.3 The Hilbert metric

In this section we prove that, quite remarkably, the Einstein-Poincaré additivity law satisfied by perceptual chromatic vectors permits to coherently equip the space of such vectors with the so-called Hilbert metric. In Subsection 4.3.1, we show that this metric is compatible with the results of well-established psycho-visual experiments.

Let us start by recalling that, given four collinear points a, p, q, and b of $\mathbb{R}^2$, with $a \neq p$ and $q \neq b$, the *cross ratio* $[a, p, q, b]$ is defined by [31]:

$$[a, p, q, b] = \frac{\|q-a\|}{\|p-a\|} \cdot \frac{\|p-b\|}{\|q-b\|}\ , \tag{4.3.1}$$

where $\|\cdot\|$ denotes the Euclidean norm. Given two points p and q of the closed disk $\mathcal{D}_{1/2}$ such that the points $(-1/2, 0) = a_-$, p, q, and $(1/2, 0) = a_+$ are collinear with the segment $[p, q]$ contained in the segment $[a_-, a_+]$, the $\mathcal{D}_{1/2}$-Hilbert distance $d_H(p, q)$ is given by [31]:

$$d_H(p, q) = \frac{1}{2}\ln\left[a_-, p, q, a_+\right]\ , \tag{4.3.2}$$

where the choice of the points involved in the cross ratio above guarantees that the argument of ln is strictly positive.

We consider now three chromatic vectors $\mathbf{v}_c$, $\mathbf{v}_d$ and $\mathbf{v}_c^d$ of $\mathcal{D}_{1/2}$ with $\mathbf{v}_c = (v_c, 0)$, $\mathbf{v}_d = (v_d, 0)$ and $\mathbf{v}_c^d = (v_c^d, 0)$. We have the following result (see for instance [57] for related topics).

Proposition 4.3.1. *With the notations introduced above, it holds that:*

$$d_H((0,0),(v_c^d,0)) = d_H((v_d,0),(v_c,0)) \iff v_c = \frac{v_c^d + v_d}{1 + 4v_c^d v_d}\ . \tag{4.3.3}$$

Proof. By definition, the equality $d_H((0,0),(v_c^d,0)) = d_H((v_c,0),(v_d,0))$ holds if and only if $\left[a_-,(0,0),(v_c^d,0),a_+\right] = [a_-,(v_d,0),(v_c,0),a_+]$. Equivalently:

$$d_H((0,0),(v_c^d,0)) = d_H((v_c,0),(v_d,0)) \iff \frac{1/2 - v_c}{1/2 + v_c} = \frac{1/2 - v_c^d}{1/2 + v_c^d} \cdot \frac{1/2 - v_d}{1/2 + v_d}\ . \tag{4.3.4}$$

By a straightforward computation, it can be checked that the right-hand side of (4.3.4) is equivalent to that of (4.3.3). □

By using the vector notation, (4.3.3) can be re-written as follows

$$d_H(\mathbf{0}, \mathbf{v}_c^d) = d_H(\mathbf{v}_d, \mathbf{v}_c) \iff v_c = \frac{v_c^d + v_d}{1 + 4v_c^d v_d}, \tag{4.3.5}$$

i.e. the relative perceptual chromatic vector $\mathbf{v}_c^d$ appears in the relativistic sum expressed by (4.2.14) together with the perceptual chromatic vectors $\mathbf{v}_c$ and $\mathbf{v}_d$ if and only if the *Hilbert length* $d_H(\mathbf{0}, \mathbf{v}_c^d)$ of $\mathbf{v}_c^d$ is equal to the Hilbert distance between $\mathbf{v}_c$ and $\mathbf{v}_d$.

The colorimetric interpretation is the following: since the relativistic sum (4.2.14) has been previously proven to hold true, this result implies that our hypothesis that $\mathbf{v}_c^d$ contains information about the perceptual dissimilarity between the colors c and d is verified if and only if we consider the chromatic vectors as elements of the metric space $(\mathcal{D}_{1/2}, d_H)$, thus promoting the Hilbert distance to a mathematically coherent candidate for a perceptual metric of chromatic attributes.

Remarkably, see e.g. [10], the Hilbert metric on $\mathcal{D}_{1/2}$ coincides precisely with the *Klein hyperbolic metric* defined by:

$$ds^2_{\mathcal{D}_{1/2}} = \frac{(1/4 - v_2^2)dv_1^2 + 2v_1v_2dv_1dv_2 + (1/4 - v_1^2)dv_2^2}{(1/4 - \|v\|^2)^2} \ . \tag{4.3.6}$$

The geodesics with respect to this metric are straight chords of $\mathcal{D}_{1/2}$.

A geometric representation of this result is provided by the so-called Chasles theorem on cross ratios of cocyclic points, see Figure 4.2, which provides a graphical method to construct the relativistic sum of two vectors in one dimension. An alternative interpretation of formula

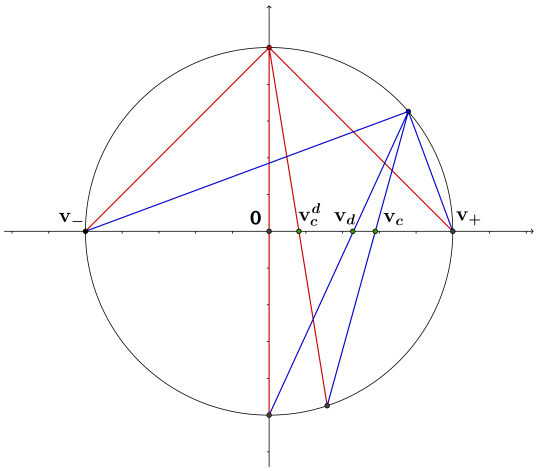

Figure 4.2: Illustration of the result of Proposition 4.3.1 by Chasles theorem on the cross ratios of cocyclic points. $\mathbf{v}_c$, $\mathbf{v}_d$ and $\mathbf{v}_c^d$ satisfy Equation (4.3.5).

(4.3.5) is possible by recasting it in the context of the inertial observers framework introduced in Section 4.1. To remain coherent with the assumption of Section 4.2.1, we will consider only chromatic vectors of the type $\mathbf{v}_c = (v_c, 0)$.

Considering again the notation of Section 4.1.2, let $o_1 = (c_1, I_1)$ and $o_2 = (c_2, I_2)$ be two inertial observers*, then, by definition, $\mathbf{v}_{11} = (0, 0)$ and $\mathbf{v}_{22} = (0, 0)$. However, using the notation introduced in Equation (4.1.2), the inertial observer o_1 perceives c_2 with a non-zero saturation, i.e. $\mathbf{v}_{12} = (v_{12}, 0)$, with $v_{12} \neq 0$, and, thanks to Equation (4.2.20), $\mathbf{v}_{21} = (-v_{12}, 0)$.

Furthermore, fixed $F \in \mathcal{C}$, let $\mathbf{v}_{1F} = (v_{1F}, 0)$ and $\mathbf{v}_{2F} = (v_{2F}, 0)$ be the chromatic vectors corresponding to the description of F performed by the inertial observers o_1 and o_2, respectively.

Coherently with the analysis made in Section 4.2.3, we perform the following identifications between the chromatic vector components of the colors c and d appearing in formula (4.3.5)

*We recall that, for the sake of a simpler phrasing, we implicitly assume that the inertial observer o_i is adapted to the illuminant I_i, $i = 1, 2$, without explicitly specifying it.

and those of c_1, c_2 and F:

$$\begin{cases} \mathbf{v}_d \equiv \mathbf{v}_{12} \\ \mathbf{v}_c \equiv \mathbf{v}_{1F} \\ \mathbf{v}_c^d \equiv \mathbf{v}_{2F} \end{cases},$$

then formula (4.3.5) implies the equality

$$d_H(\mathbf{v}_{22}, \mathbf{v}_{2F}) = d_H(\mathbf{v}_{12}, \mathbf{v}_{1F}), \tag{4.3.7}$$

notice that the arguments of the Hilbert distance in the left-hand side are relative to the color description performed by o_2 and those in the right-hand side are relative to o_1. Since $v_{22} = 0$, we can also write

$$d_H(\mathbf{0}, \mathbf{v}_{2F}) = d_H(\mathbf{v}_{12}, \mathbf{v}_{1F}). \tag{4.3.8}$$

The interpretation of formula (4.3.8) gives a rigorous meaning to the sentence in the introduction to this chapter about the fact that the Hilbert distance provides a '*chromatic constancy property with respect to observer changes*'. In fact, if we interpret the Hilbert distance as a perceptual metric, Equation (4.3.8) says that the perceptual chromatic difference between F and an achromatic color sensed by o_2 is the same as the one that o_1 experiences between F and the chromatic vector $\mathbf{v}_{12}$ representing the saturation shift due to the observer change from o_1 to o_2.

We stress that we have implicitly assumed the illuminants I_1 and I_2 to be broadband, so the previous interpretation is valid as long as the quantity $v_d = v_{12}$ is relatively small.

4.3.1 Compatibility of the Hilbert metric with psycho-visual experimental data

Now we address the important issue of the compatibility between the Hilbert metric on $\mathcal{D}_{1/2}$ and psychovisual measurements. This is not an easy task because of two reasons: firstly, experimental data on color perception are very scarce, secondly, psychovisual measurements are always affected by subjective variations which imply the use of averaging procedures that inevitably reduce the measure accuracy. Some useful psychovisual results consistent with our framework are those reported in [26] and [33].The authors conducted their tests with the help of the standard CIE illuminants C (near-daylight, $(x_C, y_C) = (0.3125, 0.3343)$) and A (tungsten, $(x_A, y_A) = (0.4475, 0.4084)$) and added a third one, denoted with G (greenish, $(x_G, y_G) = (0.3446, 0.4672)$). The values (x, y) represent the CIE xyY chromaticity coordinates of C, A and G, respectively, Figure 4.3 shows their position in the chromaticity diagram. In what follows, observers adapted to the illuminants C, A and G, respectively, will be denoted by $o_1 = (c, C)$, $o_2 = (a, A)$ and $o_3 = (g, G)$. A haploscope is used to compare the color perception of one eye always adapted to the illuminant C and the other eye adapted to C, A and G.

Figure 4.3 shows, in the xyY diagram, three families of curves obtained by the tests performed in [33]:

- the first is composed by three contours surrounding C that correspond to color stimuli with fixed Munsell value, different hue but with the same perceived Munsell chroma in $\{2, 4, 8\}$. By normalizing these data between 0 and 0.5 we obtain $\{0.1, 0.2, 0.4\}$, which are the norms of the chromatic vectors $\mathbf{v}_{1c}$ of the colors associated to the corresponding stimuli observed by o_1;
- the second and the third are given by two contours surrounding A, resp. G, that correspond to colors c with varying hues and whose Munsell chroma belong to the set $\{2, 4\}$. The chromatic vectors $\mathbf{v}_{2c}$, resp. $\mathbf{v}_{3c}$, of these colors observed from o_2, resp. o_3, have norms belonging to the set $\{0.1, 0.2\}$.

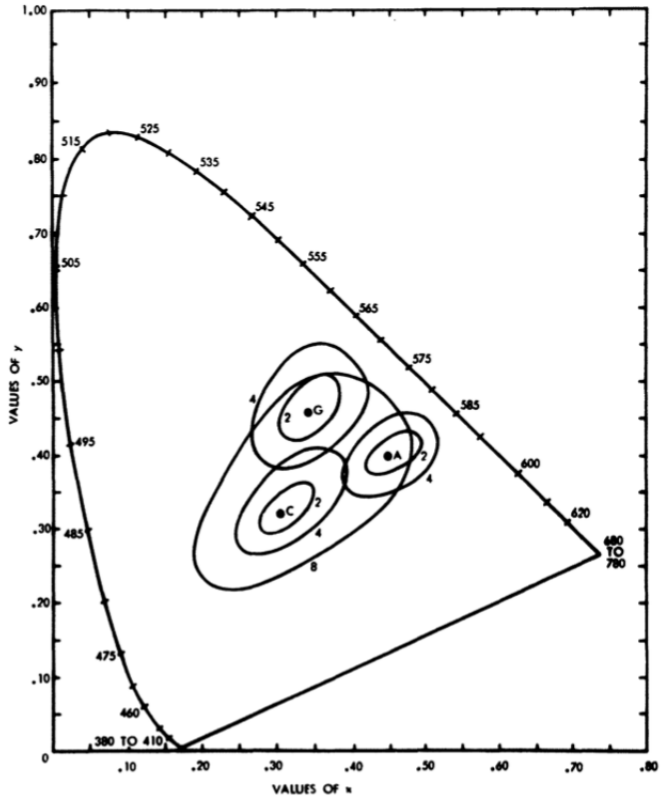

Figure 4.3: The iso Munsell chroma contours found by [33] in the xyY diagram.

As discussed above, the psychovisual data reported in [26] and [33] are only averaged, thus, the only kind of information that we have from Figure 4.3 is, for example, that the xyY coordinates of standard illuminant A are between the curves of chroma 4 and 8 of the observer o_1. Thus, the norm of the chromatic vectors is not possible to be achieved with accuracy. An approximation is given by $\|\mathbf{v}_{1a}\| \simeq 6.76/20 = 0.338$.

In Figure 4.4(a), we denote by F and F' the xyY coordinates of the points in the xyY diagram obtained by the intersection between the line connecting A and C with the iso-chroma contours for o_1 and o_2, respectively. The color F is perceived by o_1 as having a chromatic vector $\mathbf{v}_{1F}$ with norm $\|\mathbf{v}_{1F}\| = 0.2$. By construction, we determine F', the color perceived by o_2 with chromatic vector $\mathbf{v}_{2F'}$ such that $\mathbf{v}_{2F'} = \mathbf{v}_{1F}$. The norm of the chromatic vector $\mathbf{v}_{1F'}$ corresponding to the color F' perceived by o_1, is approximated by $\|\mathbf{v}_{1F'}\| \simeq 3.76/20 = 0.188$. Fig. 4.4(b) shows all the chromatic vectors in the disk $\mathcal{D}_{1/2}$. One can easily check, as illustrated by Chasles theorem, that:

$$d_H(\mathbf{v}_{1F}, \mathbf{v}_{1c}) = d_H(\mathbf{v}_{2F'}, \mathbf{v}_{2a}) = d_H(\mathbf{v}_{1F'}, \mathbf{v}_{1a}) \ . \tag{4.3.9}$$

The same reasoning applied to the situation depicted in Figure 4.5(a), where the points F_2 and F_2' belong to another iso-chroma contour, leads to:

$$d_H(\mathbf{v}_{1F_2}, \mathbf{v}_{1c}) = d_H(\mathbf{v}_{2F_2'}, \mathbf{v}_{2a}) = d_H(\mathbf{v}_{1F_2'}, \mathbf{v}_{1a}) \ , \tag{4.3.10}$$

see Fig. 4.5(b).

Finally, we consider the quite more complicated situation depicted in Figure 4.6(a). It is precised in [26] that '*A change from a blue (C) adaptation to a yellow (A) adaptation shows vectors running in a blue-yellow direction, a change from a blue (C) adaptation to a green*

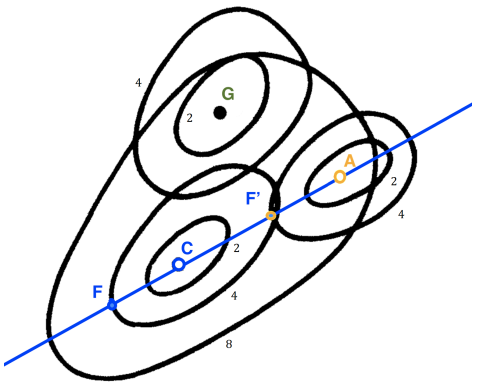

(a) The illuminants C and A and the colors F and F' in the xy chromaticity diagram.

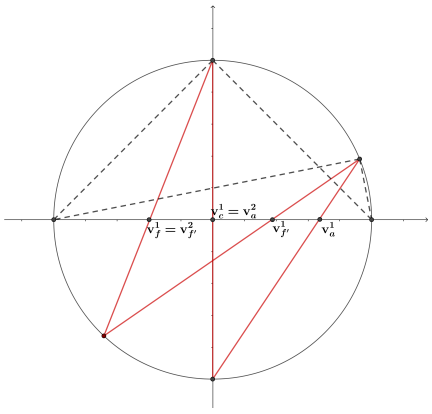

(b) Illustration of the equalities of Equation (4.3.9) in the disk $\mathcal{D}_{1/2}$.

Figure 4.4: Invariance of the Hilbert distance under observer changes: illuminants C and A, and colors F and F'.

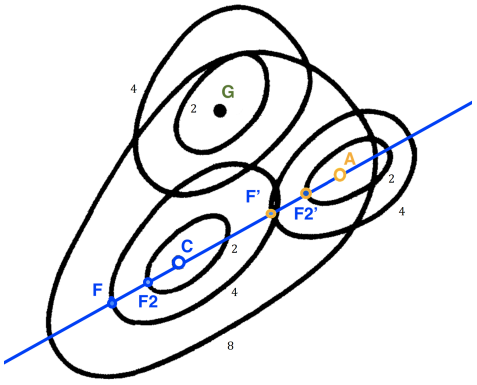

(a) The illuminants C and A and the colors F and F', and F_2 and F_2' in the CIE xy chromaticity diagram.

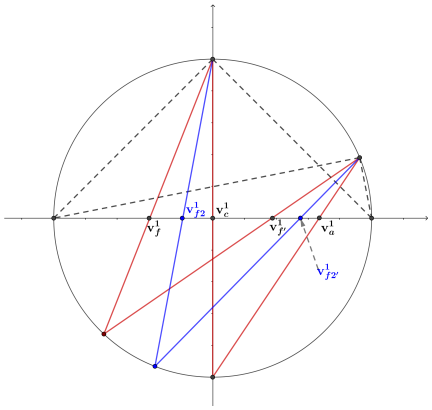

(b) Illustration of the equalities of Equation (4.3.10) in the disk $\mathcal{D}_{1/2}$.

Figure 4.5: Invariance of the Hilbert distance under observer changes: illuminants C and A, and colors F, F', F_2, and F_2'.

(G) adaptation shows vectors running in a blue-green direction.' This means that the angle between $\mathbf{v}_{1a}$ and $\mathbf{v}_{1g}$ is equal to $\pi/4$. From Figure 4.6(a) we can approximate the norm of the chromatic vector $\mathbf{v}_{1g}$: $\|\mathbf{v}_{1g}\| \simeq 0.32$. The chromatic vectors $\mathbf{v}_{1H}$ and $\mathbf{v}_{3H''}$ of the two colors H and H'' marked on Fig. 4.6(a) are equal. Once again, one can easily check that:

$$d_H(\mathbf{v}_{1H}, \mathbf{v}_{1c}) = d_H(\mathbf{v}_{3H''}, \mathbf{v}_{3g}) = d_H(\mathbf{v}_{1H''}, \mathbf{v}_{1g}) \ , \tag{4.3.11}$$

see Fig. 4.6(b).

These discussions show clearly that the Hilbert metric is compatible with the reported psychovisual data. Here we have reported only three cases, but other three configurations related to Figure 4.3 can be studied and our computations showed that they give rise to the same conclusions. We have only treated the case when colors, e.g. F and F', have chromatic vectors collinear to the new observer chromatic vector, e.g. $\mathbf{v}_{1F}$ and $\mathbf{v}_{1F'}$ are collinear to $\mathbf{v}_{1a}$ in this first situation. Dealing with arbitrary colors needs the use ot Einstein-Poincaré addition law for non-collinear vectors. We prefer to postpone the study of the general case for future

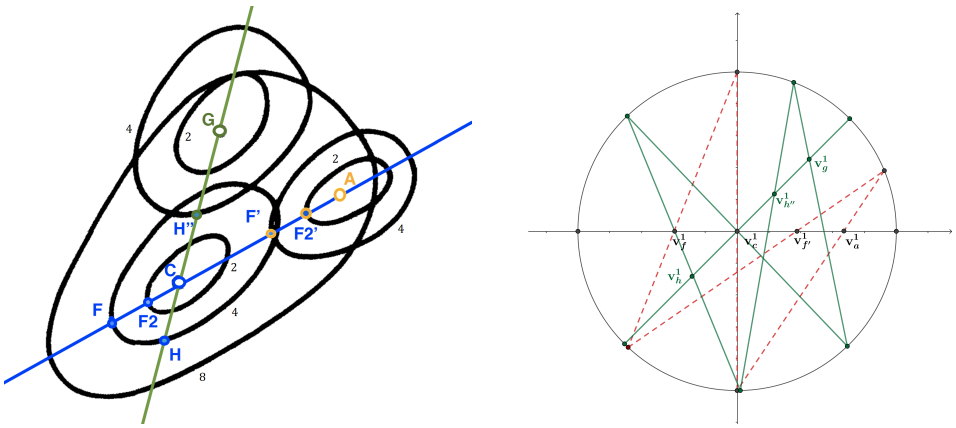

(a) The three illuminants C, A and G, and the colors F and F', F_2 and F_2', and H and H'' in the xyY diagram.

(b) Illustration of the equalities of Equation (4.3.11) in the disk $\mathcal{D}_{1/2}$.

Figure 4.6: Invariance of the Hilbert distance under observer changes: illuminants C and G, and colors H and H'', compared with illuminants C and A, and colors F and F'.

research, since the formulas are more complicated and more accurate psychovisual date would be needed.

Chapter 5

Quantum effects for color measurement

In this chapter we will introduce some concepts coming from quantum information theory, that will enrich the framework described in Chapter 3. The crucial one is the concept of *effect*. Indeed it encodes the probabilistic nature of quantum measurements and lies at the very core of modern quantum theories, see e.g. the classical books [93, 27, 71] for an overview on this topic. We will define as well post-measurement generalized states, Lüders operations and relative quantum entropy. In particular, in Section 5.2, we will see that the action of Lüders operations on the disk of chromatic vectors corresponds to Einstein-Poincaré addition law. We recall that the general case of the relativistic addition law was needed to prove Yilmaz's third result, as announced in Subsection 4.2.3. For more details the main reference will be [19] for a thoughtful discussion, or Section 3.3 of [14] for a quick overview. As we will see in Chapter 6, the concepts introduced here will be fundamental to establish definitions of color attributes within the quantum-like model.

5.1 Effect space of the rebit

The quantum trichromacy axiom, see Section 3.1, refers to an *ideal* normal trichromatic observer, capable of a non-trivial response to light stimuli of any intensity, no matter how dim or intense. However, the visible threshold and glare limits, see e.g. [88, 127, 129], imply that the space of perceived colors perceived by a *real* normal trichromatic observer is actually a finite convex subset, called *color solid*, see as well Chapter 1, of the infinite cone $\overline{\mathcal{C}}(\mathcal{A})$, where $\mathcal{A} = \mathcal{H}(2, \mathbb{R})$ or $\mathbb{R} \oplus \mathbb{R}^2$.

A naïve way to obtain a bounded volume could be, as in Chapter 2, to 'cut' $\overline{\mathcal{C}}(\mathcal{A})$ at height corresponding to the glare limit, however in the following we are going to introduce a more profound and meaningful construction, relying on the concept of quantum-effects and on the self-duality of $\overline{\mathcal{C}}(\mathcal{A})$, that leads to a bounded volume.

As first argued in [12], a finite-volume color solid can be obtained in a natural way in the quantum-like framework by first re-writing $\overline{\mathcal{C}}(\mathcal{A})$ to make states appear explicitly as follows, let us call it the state cone

$$\overline{\mathcal{C}}(\mathcal{H}(2,\mathbb{R})) = \left\{ 2\alpha\rho_{\mathbf{s}} = \begin{pmatrix} \alpha(1+s_1) & \alpha s_2 \\ \alpha s_2 & \alpha(1-s_1) \end{pmatrix},\ \alpha \geq 0,\ \mathbf{v_s} = (s_1, s_2) \in \mathcal{D} \right\} \tag{5.1.1}$$

and

$$\overline{\mathcal{C}}(\mathbb{R} \oplus \mathbb{R}^2) = \left\{ 2\alpha\chi(\rho_{\mathbf{s}}) = \begin{pmatrix} \alpha \\ \alpha\mathbf{v_s} \end{pmatrix},\ \alpha \geq 0,\ \mathbf{v_s} \in \mathcal{D} \right\}, \tag{5.1.2}$$

Let us call them *state cones* $\overline{\mathcal{C}}(\mathcal{A}) = \overline{\mathcal{C}}(\mathcal{S}(\mathcal{A}))$ with $\mathcal{A} = \mathcal{H}(2,\mathbb{R})$ or $\mathbb{R}\oplus\mathbb{R}^2$, as they are the domains of positivity of their respective FRJAs re-parametrized using the states of $\mathcal{D}$. By $\mathcal{D}$ we mean the unit disk, called $\mathcal{D}_1$ in the previous chapter.

In quantum information, the concept of *effect* refers to a measurement apparatus that produces an outcome. The duality between states and effects means essentially that when a state and an effect are specified, one can compute a probability distribution which is the only meaningful information that we can obtain about the experiment. Let us now understand how to represent effects and their action on $\mathcal{S}(\mathcal{A})$.

We identify an effect with an element $\eta_{\mathbf{e}}$ of $\overline{\mathcal{C}}(\mathcal{H}(2,\mathbb{R}))$ bounded between the null and the identity 2×2 matrix (with respect to the ordering of positive semi-definite matrices) or, equivalently, $\chi(\eta_{\mathbf{e}}) \in \overline{\mathcal{C}}(\mathbb{R}\oplus\mathbb{R}^2)$.

It is useful to adopt a general symbol to denote an effect $\mathbf{e}$ when it is not important to know if it is realized as the matrix $\eta_{\mathbf{e}}$ or the vector of the spin-factor $\chi(\eta_{\mathbf{e}})$. We will use the following notation:

$$\mathbf{e} := (e_0, \mathbf{v_e}), \tag{5.1.3}$$

where e_0 and $\mathbf{v_e}$, called *effect magnitude* and *effect chromatic vector*, respectively, play the role of α and $\mathbf{v_s}$ in Equation (5.1.1), respectively. It is convenient to define the effect vector as follows:

$$\mathbf{v_e} := \left(\frac{e_1}{e_0}, \frac{e_2}{e_0}\right)^t, \tag{5.1.4}$$

$e_0, e_1, e_2 \in \mathbb{R}$, because then the matrix $\eta_{\mathbf{e}}$ can be written in this way

$$\eta_{\mathbf{e}} = \begin{pmatrix} e_0+e_1 & e_2 \\ e_2 & e_0-e_1 \end{pmatrix}, \tag{5.1.5}$$

and

$$\chi(\eta_{\mathbf{e}}) := e_0 \begin{pmatrix} 1 \\ \mathbf{v_e} \end{pmatrix}. \tag{5.1.6}$$

Whenever $\mathbf{v_e} = \mathbf{0}$, we will write $\mathbf{e} = \mathbf{e_a}$ and we will call it an *achromatic effect*. It is clear that $\eta_{\mathbf{e_a}} = e_0\sigma_0$. We recall that, from (3.4.1), $\sigma_0 = Id_2$.

The matrix $\eta_{\mathbf{e}}$ defines an effect if and only if $\mathbf{0} \leq \eta_{\mathbf{e}} \leq \sigma_0$, this double inequality is equivalent to the request that the determinant and the trace of both $\eta_{\mathbf{e}}$ and $\sigma_0 - \eta_{\mathbf{e}}$ are non-negative. From $\det(\eta_{\mathbf{e}}) \geq 0$ we obtain $\mathbf{v_e} \in \mathcal{D}$ and, by considering all the other constraints, we find that the effect space, or perceived color space, can be geometrically characterized in an explicit way as follows:

$$\mathcal{E} = \left\{ (e_0, e_1, e_2) \in \mathbb{R}^3,\ e_0 \in [0,1],\ e_1^2 + e_2^2 \leq \min_{e_0\in[0,1]} \left\{(1-e_0)^2, e_0^2\right\} \right\}. \tag{5.1.7}$$

$\mathcal{E}$ is a *closed convex double cone* with a circular basis of radius $1/2$ located height $e_0 = 1/2$ and vertices in $(0,0,0)$ and $(1,0,0)$, associated to *the null and the unit effect*, respectively. Notice that with this expression for $\mathcal{E}$ we do not have to specify whether we are using the matrix representation $\eta_{\mathbf{e}}$ or the spin-factor one $\chi(\eta_{\mathbf{e}})$. In case we need to specify it we will use the notation $\mathcal{E}(\mathcal{S}(\mathcal{A}))$ with $\mathcal{A} = \mathcal{H}(2,\mathbb{R})$ or $\mathbb{R}\oplus\mathbb{R}^2$, as in [19].

The geometry of $\mathcal{E}$, depicted in Figure 5.1, happens to be in agreement with that of the perceived color spaces advocated by Ostwald and De Valois, see e.g. [37].

By self duality of $\overline{\mathcal{C}}(\mathcal{A})$ it is possible to see effects as affine maps acting on chromatic states, see [19] for more details:

$$\mathcal{E} \cong \{\mathbf{e} : \mathcal{S}(\mathcal{A}) \to [0,1],\ \mathbf{e}(\mathbf{s}) = e_0 + e_1 s_1 + e_2 s_2\}, \tag{5.1.8}$$

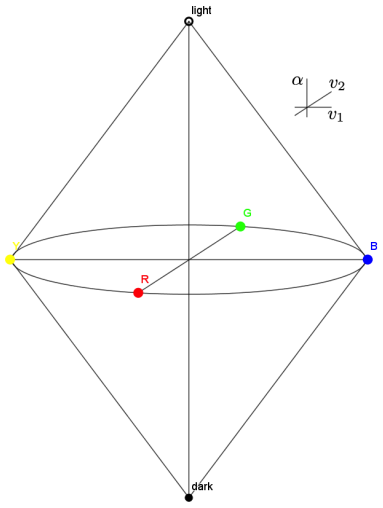

Figure 5.1: The double cone of effects $\mathcal{E}(\mathcal{S}(\mathbb{R} \oplus \mathbb{R}^2))$.

$\mathbf{e}(\mathbf{s})$ is interpreted as the probability to register the outcome (e_0, e_1, e_2) after a color measurement on the visual scene prepared in the state $\mathbf{s}$, i.e. $\mathbf{e}(\mathbf{s})$ coincides with the expectation value $\langle \mathbf{e} \rangle_{\mathbf{s}}$, which can be written as follows:

$$\langle \mathbf{e} \rangle_{\mathbf{s}} = \mathrm{Tr}(\rho_{\mathbf{s}}\, \eta_{\mathbf{e}}) = e_0 + e_1 s_1 + e_2 s_2 = e_0(1 + \mathbf{v}_{\mathbf{e}} \cdot \mathbf{v}_{\mathbf{s}}) = 2\chi(\rho_{\mathbf{s}}) \cdot \chi(\eta_{\mathbf{e}}). \tag{5.1.9}$$

The so-called *achromatic effect* is $\mathbf{e_a} := e_0(1, \mathbf{0})$, with $e_0 \in [0, 1]$, it is characterized by a null effect vector $\mathbf{v}_{\mathbf{e_a}} = \mathbf{0}$, so that

$$\eta_{\mathbf{e_a}} = e_0 \sigma_0. \tag{5.1.10}$$

If we consider the achromatic state $\mathbf{s_a}$, with $\mathbf{v}_{\mathbf{s_a}} = \mathbf{0}$, and we compute the expectation value of an arbitrary effect $\mathbf{e}$ on it we obtain:

$$\langle \mathbf{e} \rangle_{\mathbf{s_a}} = e_0, \tag{5.1.11}$$

which shows that *the first component* e_0 *of* $\mathbf{e}$ *represents its achromatic attribute*, or *magnitude*.

5.2 Lüders operations and post-measurement generalized states

Effects parameterize a fundamental class of state transformations called *Lüders operations*, which are *convex-linear positive functions* $\psi_{\mathbf{e}}$ defined on the state space $\mathcal{S}(\mathcal{H}(2, \mathbb{R}))$ and satisfying the constraint:

$$0 \leq \mathrm{Tr}(\psi_{\mathbf{e}}(\rho_{\mathbf{s}})) \leq 1, \quad \text{for all } \rho_{\mathbf{s}} \in \mathcal{S}(\mathcal{H}(2, \mathbb{R})). \tag{5.2.1}$$

This implies that, since $\mathcal{S}(\mathcal{H}(2, \mathbb{R})) \subset \psi_{\mathbf{e}}(\mathcal{S}(\mathcal{H}(2, \mathbb{R})) =: \tilde{\mathcal{S}}(\mathcal{H}(2, \mathbb{R}))$, i.e. $\rho_{\mathbf{s}}$ will lose the property of having unit trace* after a Lüders operation, becoming a so-called *generalized density matrix* representing a *post-measurement generalized state*. From the identification between states and density matrices it follows that

$$\psi_{\mathbf{e}}(\mathbf{s}) \equiv \psi_{\mathbf{e}}(\rho_{\mathbf{s}}) \in \tilde{\mathcal{S}}(\mathcal{H}(2, \mathbb{R})), \tag{5.2.2}$$

*We recall that, for all $\rho_{\mathbf{s}} \in \mathcal{S}(\mathcal{H}(2, \mathbb{R}))$, $\mathrm{Tr}(\rho_{\mathbf{s}}) = 1$, see Equation (3.3.1) in Section 3.3.

so

$$\mathrm{Tr}(\psi_{\mathbf{e}}(\mathbf{s})) \in [0,1]. \tag{5.2.3}$$

The analytical expression of the post-measurement generalized state $\psi_{\mathbf{e}}(\mathbf{s})$, see e.g. [27] page 37, is:

$$\psi_{\mathbf{e}}(\mathbf{s}) = \eta_{\mathbf{e}}^{1/2}\rho_{\mathbf{s}}\eta_{\mathbf{e}}^{1/2}, \tag{5.2.4}$$

$\eta_{\mathbf{e}}^{1/2}$ is called *Kraus operator* associated to $\mathbf{e}$ and it is the square root of $\eta_{\mathbf{e}}$, i.e. the only symmetric and positive semi-definite matrix such that $\eta_{\mathbf{e}}^{1/2}\eta_{\mathbf{e}}^{1/2} = \eta_{\mathbf{e}}$. Thanks to the cyclic property of the trace we have that:

$$\mathrm{Tr}(\psi_{\mathbf{e}}(\mathbf{s})) = \mathrm{Tr}(\rho_{\mathbf{s}}\,\eta_{\mathbf{e}}) = \langle \mathbf{e}\rangle_{\mathbf{s}} = e_0(1 + \mathbf{v}_{\mathbf{e}} \cdot \mathbf{v}_{\mathbf{s}}), \tag{5.2.5}$$

so

$$\varphi_{\mathbf{e}}(\mathbf{s}) := \frac{\psi_{\mathbf{e}}(\mathbf{s})}{\langle \mathbf{e}\rangle_{\mathbf{s}}} \tag{5.2.6}$$

is a density matrix corresponding to a state belonging to $\mathcal{S}(\mathcal{H}(2,\mathbb{R}))$.

By convex-linearity, Lüders operations can be naturally extended to generalized states, thus elements of the state cone $\overline{\mathcal{C}}(\mathcal{S}(\mathcal{A}))$, as follows:

$$\psi_{\mathbf{e}}(s_0\mathbf{s}) = s_0\psi_{\mathbf{e}}(\mathbf{s}), \qquad \forall s_0 \in [0,1]. \tag{5.2.7}$$

By linearity of the trace this implies that:

$$\langle \mathbf{e}\rangle_{s_0\mathbf{s}} = \mathrm{Tr}(\psi_{\mathbf{e}}(s_0\mathbf{s})) = \mathrm{Tr}(s_0\psi_{\mathbf{e}}(\mathbf{s})) = s_0\langle \mathbf{e}\rangle_{\mathbf{s}} = e_0 s_0(1 + \mathbf{v}_{\mathbf{e}} \cdot \mathbf{v}_{\mathbf{s}}), \tag{5.2.8}$$

so

$$\varphi_{\mathbf{e}}(s_0\mathbf{s}) = \frac{\psi_{\mathbf{e}}(s_0\mathbf{s})}{\langle \mathbf{e}\rangle_{s_0\mathbf{s}}} = \frac{s_0\psi_{\mathbf{e}}(\mathbf{s})}{s_0\langle \mathbf{e}\rangle_{\mathbf{s}}} = \varphi_{\mathbf{e}}(\mathbf{s}), \tag{5.2.9}$$

thus the post-measurement chromatic state depends solely on $\mathbf{s}$ and not on s_0. This implies a formula that will be often used in this chapter and in the following one:

$$\psi_{\mathbf{e}}(s_0\mathbf{s}) = e_0 s_0(1 + \mathbf{v}_{\mathbf{e}} \cdot \mathbf{v}_{\mathbf{s}})\,\varphi_{\mathbf{e}}(\mathbf{s}). \tag{5.2.10}$$

This formula shows explicitly how the chromatic information about the state $\mathbf{s}$ and the expectation value of the effect $\mathbf{e}$ on $\mathbf{s}$ are *fused together* in the post-measurement generalized state $\psi_{\mathbf{e}}(s_0\mathbf{s})$.

In the case of an achromatic effect $\mathbf{e_a}$, for which $\mathbf{v}_{\mathbf{e_a}} = \mathbf{0}$, the previous formula gives

$$\psi_{\mathbf{e_a}}(s_0\mathbf{s}) = e_0 s_0\,\varphi_{\mathbf{e_a}}(\mathbf{s}), \tag{5.2.11}$$

but $\eta_{\mathbf{e_a}}^{1/2} = \sqrt{e_0}\sigma_0$ so, by Equation (5.2.4),

$$\psi_{\mathbf{e_a}}(s_0\mathbf{s}) = e_0 s_0 \rho_{\mathbf{s}}, \tag{5.2.12}$$

hence $\varphi_{\mathbf{e_a}}(\mathbf{s}) = \rho_{\mathbf{s}}$, or, by identifying $\rho_{\mathbf{s}}$ with the chromatic state $\mathbf{s}$,

$$\varphi_{\mathbf{e_a}}(\mathbf{s}) = \mathbf{s}, \tag{5.2.13}$$

this means that the post-measurement state induced by the action of an achromatic effect coincides with the original state.

In [19], it has been shown that *the state change* $\mathbf{s} \mapsto \psi_{\mathbf{e}}(\mathbf{s})$ *induced by the act of observing a color* is implemented through a 3-dimensional normalized Lorentz boost in the direction of $\mathbf{v}_{\mathbf{e}}$. This formally justifies the presence of Lorentz boosts, already mentioned in Chapters 2

and 4, within the quantum model. Here we refer only to the result *(ii)* of Corollary 4.1, that will be needed in Chapter 7 for an application to automatic white balance, for a proof and further details see [19].

Let $\mathbf{e}$ be an effect whose chromatic vector is such that $||\mathbf{v_e}|| < 1$, then the expression of the Lüders operation relative to $\mathbf{e}$ within the state cone of the spin-factor, of Equation (5.2.21), can be re-written in the following way:

$$\chi(\psi_{\mathbf{e}}(\mathbf{s})) = \frac{e_0}{\gamma_{\mathbf{v_e}}} B(\mathbf{v_e}) \frac{1}{2} \begin{pmatrix} 1 \\ \mathbf{v_s} \end{pmatrix} \equiv B_N(\mathbf{e}) \frac{1}{2} \begin{pmatrix} 1 \\ \mathbf{v_s} \end{pmatrix}, \tag{5.2.14}$$

where $B(\mathbf{v_e})$ is the Lorentz boost associated to the chromatic vector $\mathbf{v_e}$, whose associated matrix is:

$$[B(\mathbf{v_e})] = \begin{pmatrix} \gamma_{\mathbf{v_e}} & \gamma_{\mathbf{v_e}} \mathbf{v_e}^t \\ \gamma_{\mathbf{v_e}} \mathbf{v_e} & \sigma_0 + \frac{\gamma_{\mathbf{v_e}}^2}{1+\gamma_{\mathbf{v_e}}} \mathbf{v_e} \mathbf{v_e}^t \end{pmatrix}, \tag{5.2.15}$$

$\gamma_{\mathbf{v_e}}$ is the Lorentz factor defined by

$$\gamma_{\mathbf{v_e}} := \frac{1}{\sqrt{1 - \|\mathbf{v_e}\|^2}}, \tag{5.2.16}$$

and where we define the normalized Lorentz boost associated to $\mathbf{e}$ as follows:

$$B_N(\mathbf{e}) \equiv \frac{e_0}{\gamma_{\mathbf{v_e}}} B(\mathbf{v_e}). \tag{5.2.17}$$

Clearly Equation (5.2.14) holds as well for generalized states

$$\chi(\psi_{\mathbf{e}}(s_0\mathbf{s})) = \frac{s_0 e_0}{\gamma_{\mathbf{v_e}}} B(\mathbf{v_e}) \frac{1}{2} \begin{pmatrix} 1 \\ \mathbf{v_s} \end{pmatrix} = B_N(\mathbf{e}) \frac{s_0}{2} \begin{pmatrix} 1 \\ \mathbf{v_s} \end{pmatrix}, \tag{5.2.18}$$

In Chapter 7 we will use this latter equation to propose a novel chromatic adaptation transform (CAT).

In the same way as Hamilton's quaternions are used to reproduce rotations in $\mathbb{R}^3$, it is possible to use the so-called *split quaternions*, see e.g. [64, 78] to reproduce the action of (normalized) Lorentz boosts, i.e. hyperbolic rotations. There are both theoretical and applied implications of this fact. Indeed, on the theoretical side, this means that $\mathbb{R} \oplus \mathbb{R}^2$ and $\mathcal{H}(2, \mathbb{R})$ are isomorphic as Jordan algebras to a certain sub-algebra of the split quaternions. From an applied point of view, a faster version of the CAT proposed in Chapter 7 can be obtained using this different formalism.

As also proven in [19], the post-measurement chromatic state vector is the Einstein-Poincaré relativistic sum of $\mathbf{v_e}$ and $\mathbf{v_s}$, i.e.

$$\mathbf{v}_{\varphi_{\mathbf{e}}(\mathbf{s})} = \mathbf{v_e} \oplus \mathbf{v_s}, \tag{5.2.19}$$

or,

$$\chi(\varphi_{\mathbf{e}}(\mathbf{s})) = \frac{1}{2} \begin{pmatrix} 1 \\ \mathbf{v_e} \oplus \mathbf{v_s} \end{pmatrix} \in \mathcal{S}(\mathbb{R} \oplus \mathbb{R}^2), \tag{5.2.20}$$

and so

$$\chi(\psi_{\mathbf{e}}(\mathbf{s})) = e_0(1 + \mathbf{v_e} \cdot \mathbf{v_s}) \frac{1}{2} \begin{pmatrix} 1 \\ \mathbf{v_e} \oplus \mathbf{v_s} \end{pmatrix} \in \tilde{\mathcal{S}}(\mathbb{R} \oplus \mathbb{R}^2), \tag{5.2.21}$$

where the relativistic sum $\mathbf{v_e} \oplus \mathbf{v_s}$ is defined as follows: if $\|\mathbf{v_e}\| < 1$, then

$$\mathbf{v_e} \oplus \mathbf{v_s} := \frac{1}{1 + \mathbf{v_e} \cdot \mathbf{v_s}} \left\{ \mathbf{v_e} + \frac{1}{\gamma_{\mathbf{v_e}}} \mathbf{v_s} + \frac{\gamma_{\mathbf{v_e}}}{1 + \gamma_{\mathbf{v_e}}} (\mathbf{v_e} \cdot \mathbf{v_s}) \mathbf{v_e} \right\}, \tag{5.2.22}$$

where $\gamma_{\mathbf{v_e}}$ is defined as in Equation (5.2.16) and, if $\|\mathbf{v_e}\| = 1$,

$$\mathbf{v_e} \oplus \mathbf{v_s} := \mathbf{v_e}. \tag{5.2.23}$$

Comparing Equations (5.2.18) and (5.2.20) we may notice that a the action of $B_N(\mathbf{e})$ on the state cone corresponds to performing a left-relativistic addition law with $\mathbf{v_e}$ on the space of chromatic vectors. This shows the link between Lorentz boosts and Einstein-Poincaré addition law.

Apart from the case of collinear vectors, the composition of Lüders operations is neither associative nor commutative due to the action of the so-called *Thomas gyration operator*, see [149] for more details. This is particularly important to keep in mind[†] when we write the expression of a post-measurement generalized state issued by a sequential Lüders operation as the following:

$$\chi(\psi_{\mathbf{e}^2}(\psi_{\mathbf{e}^1}(s_0\mathbf{s}))) = e_0^1 e_0^2 s_0 (1 + \mathbf{v}_{\mathbf{e}^1} \cdot \mathbf{v}_\mathbf{s})(1 + \mathbf{v}_{\mathbf{e}^2} \cdot (\mathbf{v}_{\mathbf{e}^1} \oplus \mathbf{v}_\mathbf{s}))\frac{1}{2}\begin{pmatrix} 1 \\ \mathbf{v}_{\mathbf{e}^2} \oplus (\mathbf{v}_{\mathbf{e}^1} \oplus \mathbf{v}_\mathbf{s}) \end{pmatrix}. \tag{5.2.24}$$

We recall as well the fundamental chromatic matching equation, that will be applied in Section 6.4 of the next chapter to obtain the characterization of lightness constancy. From [19] we have the following result: given two couples of chromatic states-effects $(\mathbf{s}^1, \mathbf{e}^1)$ and $(\mathbf{s}^2, \mathbf{e}^2)$, the equation

$$\varphi_{\mathbf{e}^1}(\mathbf{s}^1) = \varphi_{\mathbf{e}^2}(\mathbf{s}^2), \tag{5.2.25}$$

or, equivalently,

$$\mathbf{v}_{\mathbf{e}^1} \oplus \mathbf{v}_{\mathbf{s}^1} = \mathbf{v}_{\mathbf{e}^2} \oplus \mathbf{v}_{\mathbf{s}^2}, \tag{5.2.26}$$

represents the *chromatic matching equation* between $(\mathbf{s}^1, \mathbf{e}^1)$ and $(\mathbf{s}^2, \mathbf{e}^2)$ that establishes the perception of the same chromatic information.

5.3 Relativistic sum and the Hilbert-Klein metric

Fock, Mermin and Ungar [57, 112, 149] studied deeply the relationship with the Einstein-Poincaré addition law and the structures of hyperbolic geometry. Ungar, in particular, introduced the so called *gyro-structures* to describe the algebraic properties of the Bloch disk. In particular $(\mathcal{D}, \oplus, \otimes)$, is said to be a gyro-vector space where $\mathcal{D}$ is endowed with the Einstein-Poincaré addition law $\oplus$ as sum, defined in Equation (5.2.22), and the so-called Einstein scalar multiplication $\otimes$ is defined [29] as follows:

$$r \otimes \mathbf{v} = \frac{(1 + ||\mathbf{v}||)^r - (1 - ||\mathbf{v}||)^r}{(1 + ||\mathbf{v}||)^r + (1 - ||\mathbf{v}||)^r}\frac{\mathbf{v}}{||\mathbf{v}||} = \tanh(r \tanh^{-1} ||\mathbf{v}||)\mathbf{v}, \quad r \in \mathbb{R}, \mathbf{v} \in \mathcal{D}. \tag{5.3.1}$$

The notation $\ominus\mathbf{v}$ is used to mean $\ominus\mathbf{v} = -\mathbf{v}$ and so $\mathbf{u} \ominus \mathbf{v} = \mathbf{u} \oplus (-\mathbf{v})$, with $\mathbf{u}, \mathbf{v} \in \mathcal{D}$. Unlike vector spaces, the sum is not commutative nor associative and it is not bilinear with respect to the scalar multiplication, see [29, 148, 149].

In Proposition 4.3.3 of Chapter 4, we have mentioned the use of the Hilbert-Klein metric as a metric expressing the perceptual distance invariant under changes of observers for the case of collinear chromatic vectors.

[†]It will be needed in Section 6.4 to check that the proposed derivation also applies for the case of two illuminants which are not achromatic.

We recall that in Chapter 4 the Hilbert-Klein metric on $\mathcal{D}_{1/2}$ was expressed either using the cross-ratio as in Equation (4.3.2), or, equivalently, as the line element in Equation (4.3.6). Another equivalent expression for the Hilbert-Klein distance on $\mathcal{D}$, see [131], is the following:

$$\cosh(d_{\mathcal{K}}(x,y)) = \frac{1 - x \cdot y}{\sqrt{1-|x|^2}\sqrt{1-|y|^2}}, \quad x, y \in \mathcal{D}. \tag{5.3.2}$$

Here we generalize the result of Proposition 4.3.3 to the case of not necessarily collinear vectors. Let us start by showing how the Hilbert-Klein distance is related to Einstein-Poincaré addition law. The statement of the following proposition is mentioned in Equation (5.12) of [19], here we provide a short proof.

Proposition 5.3.1. *Let $\mathbf{u}, \mathbf{v} \in \mathcal{D}$, then their Klein distance is related to their Einstein-Poincaré addition law in the following way:*

$$d_{\mathcal{K}}(\mathbf{u}, \mathbf{v}) = \tanh^{-1} || - \mathbf{u} \oplus \mathbf{v}||. \tag{5.3.3}$$

Proof. Let us start by the following formula [29] involving relativistic correction factors:

$$\gamma_{\mathbf{u}\oplus\mathbf{v}} = \gamma_{\mathbf{u}}\gamma_{\mathbf{v}}(1 + \mathbf{u} \cdot \mathbf{v}). \tag{5.3.4}$$

By definition of relativistic correction factor we have that

$$\gamma_{\mathbf{u}\oplus\mathbf{v}} = \frac{1}{\sqrt{1 - ||\mathbf{u} \oplus \mathbf{v}||^2}}. \tag{5.3.5}$$

Inverting the previous formula we obtain:

$$||\mathbf{u} \oplus \mathbf{v}||^2 = 1 - \frac{1}{\gamma^2_{\mathbf{u}\oplus\mathbf{v}}} \overset{(5.3.4)}{=} 1 - \frac{1}{\gamma^2_{\mathbf{u}}\gamma^2_{\mathbf{v}}(1 + \mathbf{u} \cdot \mathbf{v})} = 1 - \frac{(1 - ||\mathbf{u}||^2)(1 - ||\mathbf{v}||^2)}{1 + \mathbf{u} \cdot \mathbf{v}}. \tag{5.3.6}$$

We use now the definition of the Hilbert-Klein metric $d_{\mathcal{K}}$ given by Equation (5.3.2) obtaining:

$$||\mathbf{u} \oplus \mathbf{v}||^2 = 1 - \frac{(1 - ||\mathbf{u}||^2)(1 - ||\mathbf{v}||^2)}{1 + \mathbf{u} \cdot \mathbf{v}} = 1 - \frac{1}{\cosh^2(d_{\mathcal{K}}(-\mathbf{u}, \mathbf{v}))} = \tanh^2(d_{\mathcal{K}}(-\mathbf{u}, \mathbf{v})), \tag{5.3.7}$$

then we can conclude that:

$$||\mathbf{u} \oplus \mathbf{v}|| = \tanh(d_{\mathcal{K}}(-\mathbf{u}, \mathbf{v})). \tag{5.3.8}$$

□

More technical proofs of this result can be found in [57] page 39, or [149] page 239. Notice that formula (5.3.6) implies as well that $||\mathbf{v} \oplus \mathbf{u}|| = ||\mathbf{u} \oplus \mathbf{v}||$ and that $|| - \mathbf{u} \oplus \mathbf{v}|| = ||\mathbf{u} \ominus \mathbf{v}||$, for all $\mathbf{u}, \mathbf{v} \in \mathcal{D}$.
An analogous version of this results for the angular coordinate of $\mathbf{v} \oplus \mathbf{u}$, instead of the radial one, is detailed in the Appendix B.

Now we can report Proposition 5.2 of [19], which is the generalization of Proposition 4.3.3.

Proposition 5.3.2 (Chromaticity constancy)**.** *Given $(\mathbf{e}^1, \mathbf{s}^1)$ and $(\mathbf{e}^2, \mathbf{s}^2)$, as in Equation (5.2.26), so*

$$\varphi_{\mathbf{e}^1}(\mathbf{s}^1) = \varphi_{\mathbf{e}^2}(\mathbf{s}^2) \quad \Longleftrightarrow \quad \mathbf{v}_{\mathbf{e}^1} \oplus \mathbf{v}_{\mathbf{s}^1} = \mathbf{v}_{\mathbf{e}^2} \oplus \mathbf{v}_{\mathbf{s}^2}, \tag{5.3.9}$$

then

$$\mathbf{v}_{\mathbf{s}^1} \ominus \mathbf{v}_{\mathbf{s}^2} = -\mathbf{v}_{\mathbf{e}^1} \oplus \mathbf{v}_{\mathbf{e}^2} \tag{5.3.10}$$

and

$$d_{\mathcal{K}}(\mathbf{v}_{\mathbf{s}^1}, \mathbf{v}_{\mathbf{s}^2}) = d_{\mathcal{K}}(\mathbf{v}_{\mathbf{e}^1}, \mathbf{v}_{\mathbf{e}^2}). \tag{5.3.11}$$

Clearly Equation (5.3.10) implies Equation (5.3.11), thanks to Proposition 5.3.1. Most importantly, Proposition 5.3.2 shows that if two colors, i.e. generalized post-measurement states, are in chromatic matching, this means that the Hilbert-Klein dissimilarity between the chromaticity vectors associated to the states $\mathbf{s}^1$ and $\mathbf{s}^2$ is the same as the one between the chromatic vectors associated to the effects $\mathbf{e}^1$ and $\mathbf{e}^2$.

5.4 Relative entropy

In quantum information theory the notion of *relative entropy* is used as a measure of distinguishability between states. We introduce this concept here, because it will be of fundamental importance to provide the definitions of quantum-like color attributes in Chapter 6. In particular the attributes of hue, saturation, chroma and colorfulness will be defined using relative entropy.

Definition 5.4.1 (Relative entropy)**.** Let $\mathbf{s}, \mathbf{t}$ be two quantum states and $\rho_{\mathbf{s}}, \rho_{\mathbf{t}}$ be their associated density matrices. The relative entropy between $\rho_{\mathbf{s}}$ and $\rho_{\mathbf{t}}$ is given by

$$R(\rho_{\mathbf{s}}||\rho_{\mathbf{t}}) := \mathrm{Tr}[\rho_{\mathbf{s}} \log_2 \rho_{\mathbf{s}} - \rho_{\mathbf{s}} \log_2 \rho_{\mathbf{t}}] \tag{5.4.1}$$

Actually, the so-called *Klein inequality*, establishes a sort of 'definite positivity' for R in the following sense: $R(\rho_{\mathbf{s}}||\rho_{\mathbf{t}}) \geq 0$ for all $\rho_{\mathbf{s}}$ and $\rho_{\mathbf{t}}$ and $R(\rho_{\mathbf{s}}||\rho_{\mathbf{t}}) = 0$ if and only if $\rho_{\mathbf{s}} = \rho_{\mathbf{t}}$.

Notice that R is not symmetric, hence it does not constitute a metric on Hering's rebit, see Chapter 9.

One of the most important reasons why we will consider the relative entropy so inherently natural in the analysis of chromatic attributes in the quantum-like framework of the next chapter is that it can also be defined on generalized state density matrices. In fact, for all $\lambda > 0$, R satisfies the following property:

$$R(\lambda\rho_{\mathbf{s}}||\lambda\rho_{\mathbf{t}}) = \lambda R(\rho_{\mathbf{s}}||\rho_{\mathbf{t}}). \tag{5.4.2}$$

Unlike the von Neumann entropy, relative entropy 'behaves well' with respect to scalar multiplication, it is thanks to this feature that, in Chapter 6, we will be able to build a coherent system of linearly related definitions of saturation, chroma and colorfulness, which are the same quantity up to a scalar factor, as shown by the Equations (1.3.2) and (1.3.3) in Subsection 1.3.1.

To obtain an explicit expression for R, let us consider two density matrices $\rho_{\mathbf{s}}$ and $\rho_{\mathbf{t}}$ with chromatic state vectors $\mathbf{v}_{\mathbf{s}} = (s_1, s_2)$ and $\mathbf{v}_{\mathbf{t}} = (t_1, t_2)$, respectively, i.e.

$$\rho_{\mathbf{s}} = \frac{1}{2}\begin{pmatrix} 1+s_1 & s_2 \\ s_2 & 1-s_1 \end{pmatrix}, \quad \rho_{\mathbf{t}} = \frac{1}{2}\begin{pmatrix} 1+t_1 & t_2 \\ t_2 & 1-t_1 \end{pmatrix}. \tag{5.4.3}$$

Let us also denote $r_{\mathbf{s}} := \|\mathbf{v}_{\mathbf{s}}\|$, $r_{\mathbf{t}} := \|\mathbf{v}_{\mathbf{t}}\|$, and $\cos\vartheta_{\mathbf{s},\mathbf{t}} := \mathbf{v}_{\mathbf{s}} \cdot \mathbf{v}_{\mathbf{t}} / r_{\mathbf{s}} r_{\mathbf{t}}$.

Technical computations lead to the following explicit expression:

$$\begin{aligned} R(\rho_{\mathbf{s}}||\rho_{\mathbf{t}}) = {} & \frac{1}{2}\log_2(1-r_{\mathbf{s}}^2) + \frac{r_{\mathbf{s}}}{2}\log_2\left(\frac{1+r_{\mathbf{s}}}{1-r_{\mathbf{s}}}\right) \\ & - \frac{1}{2}\log_2(1-r_{\mathbf{t}}^2) - \frac{r_{\mathbf{s}}\cos\vartheta_{\mathbf{s},\mathbf{t}}}{2}\log_2\left(\frac{1+r_{\mathbf{t}}}{1-r_{\mathbf{t}}}\right). \end{aligned} \tag{5.4.4}$$

As a particularly important case of Equation (5.4.4), if $\mathbf{t} = \mathbf{s_a}$, i.e. $\rho_{\mathbf{t}} = \rho_{\mathbf{0}}$, the achromatic state, then $r_{\mathbf{t}} = 0$ and:

$$R(\rho_{\mathbf{s}}||\rho_{\mathbf{0}}) = \frac{1}{2}\log_2(1 - r_{\mathbf{s}}^2) + \frac{r_{\mathbf{s}}}{2}\log_2\left(\frac{1 + r_{\mathbf{s}}}{1 - r_{\mathbf{s}}}\right) = \Sigma(r_{\mathbf{s}}), \tag{5.4.5}$$

where, as in Equation (3.3.22) of Section 3.3, $\Sigma(r_{\mathbf{s}}) = 1 - S(\rho_{\mathbf{s}})$, $S(\rho_{\mathbf{s}})$ being the von Neumann entropy of the state $\mathbf{s}$.

Notice that the relative entropy between $\rho_{\mathbf{s}}$ and the achromatic state agrees with the definition of saturation based on the von Neumann proposed in Section 3.3, as well as in [18, 19]. We will come back to the problem of defining the saturation in Section 6.3.2 of the next chapter, where we will use the notion of relative entropy.

Chapter 6

A quantum information-based vocabulary for color attributes

In Subsection 1.3.1 of Chapter 1 we have presented the state-of-the art color appearance attributes and treated the issue of expressing them into coordinates of a color solid.
Understanding the mathematical expression of color appearance attributes is a fundamental question also because they are involved in the so called color appearance phenomena, mentioned in Subsection 1.3.2, and, of course, because of their high impact on applications. We must stress that both problems of finding coordinates to associate to color appearance attributes and a mathematical description of color appearance phenomena are still unsolved and debated topics in the literature.

In Chapter 5 we have seen a paradigm shift according to which a perceived color is not described in terms of coordinates, but it is intended as a generalized post-measurement state, i.e. the outcome of a measurement procedure involving the interaction of an effect and a generalized state. The aim of this chapter, whose content is based on [14], is to provide definitions of color perception attributes using the tools from quantum information theory introduced in the previous one, such as generalized quantum states, Lüders transformations and effects. We will see that these new definitions are in accordance with the ones provided in Subsection 1.3.1. An illustration of the potential of these new system of definitions is provided by the rigorous derivation of the so-called *lightness constancy* phenomenon, already introduced in Subsection 1.3.2 of Chapter 1.

6.1 The basic definitions: observer, illuminant, perceptual patch and perceived color from emitted and reflected light

In this section we provide the formalization of the most basic entities of our color perception theory. We must stress that the definition given in this section are coherent with the ones given in Subsection 4.1.2 of Chapter 4, but they are enriched and expressed using the tools provided in Chapter 5, new concepts will be introduced as well.
The modeling rules that we will follow are listed below:

- any quantity whose chromatic features manifest themselves multiplied by a scalar factor in $[0, 1]$ will be described through a *generalized state*;
- any act of (physical or perceptual) color measurement and the (physical or perceptual) medium used to perform it will be associated to an *effect*;
- the measurement outcome will be identified with the *post-measurement generalized state* induced by the action of the effect via Lüders transformations.

Our formalization starts with this very simple remark: *a perceived color is the result of the measurement of a physical color stimulus performed by the visual system of a human observer.*

This means that a human observer is the medium through which a perceptual color measurement takes place, for this reason we model it as an effect.

Definition 6.1.1 (Observer)**.** *An observer o measuring a color stimulus is identified with an effect $\mathbf{o} = (o_0, \mathbf{v_o}) \in \mathcal{E}$, $o_0 \in [0,1]$ and $\mathbf{v_o} \in \mathcal{D}$.*

The color stimulus hitting the eyes of o can be either a light *emitted* by a source of radiation or a light *reflected* from the patch of a surface lit by an illuminant. Let us first formalize the former situation.

Definition 6.1.2 (Emitted light stimulus)**.** *An emitted light stimulus ℓ is identified with the generalized state $\ell_0\boldsymbol{\ell}$, $\ell_0 \in [0,1]$ and $\boldsymbol{\ell} \in \mathcal{S}(\mathcal{H}(2,\mathbb{R}))$. The real quantity ℓ_0 is the normalized light intensity and $\boldsymbol{\ell}$ carries the intrinsic chromatic features.*

Definition 6.1.3 (Achromatic and white light)**.** *An achromatic light is an emitted light stimulus with $\ell_0 \in [0,1]$ and $\boldsymbol{\ell} = \mathbf{s_a}$. If, in particular, $\ell_0 = 1$, then we call it a white light and we write $\boldsymbol{\ell}^W = \mathbf{s_a}$.*

The act of measuring an emitted light stimulus ℓ by an observer o produces a perceived color through the Lüders operation associated to the effect $\mathbf{o}$.

Definition 6.1.4 (Perceived color from a light stimulus)**.** *Given an observer o and an emitted light stimulus ℓ, i.e. the couple $(\mathbf{o}, \ell_0\boldsymbol{\ell})$, the color perceived by o from ℓ is the post-measurement generalized state $\psi_{\mathbf{o}}(\ell_0\boldsymbol{\ell}) \in \tilde{\mathcal{S}}(\mathcal{H}(2,\mathbb{R}))$.*

Notice that this definition is coherent with the three-dimensional nature of perceived colors, in fact Equations (5.2.10) and (5.2.6) imply:

$$\psi_{\mathbf{o}}(\ell_0\boldsymbol{\ell}) = o_0\ell_0(1 + \mathbf{v_o} \cdot \mathbf{v}_{\boldsymbol{\ell}})\, \varphi_{\mathbf{o}}(\boldsymbol{\ell}) = \langle \mathbf{o} \rangle_{\ell_0\boldsymbol{\ell}}\ \varphi_{\mathbf{o}}(\boldsymbol{\ell}), \tag{6.1.1}$$

with $\langle \mathbf{o} \rangle_{\ell_0\boldsymbol{\ell}} \in [0,1]$ and $\varphi_{\mathbf{o}}(\boldsymbol{\ell}) \in \mathcal{S}(\mathcal{H}(2,\mathbb{R}))$.

Thanks to Equation (5.2.13), we know that if an observer o_{a} is associated to an achromatic effect $\mathbf{o_a}$, then

$$\varphi_{\mathbf{o_a}}(\boldsymbol{\ell}) = \boldsymbol{\ell}, \tag{6.1.2}$$

which means that the chromatic state of the color perceived by o_{a} from the light source $\ell = \ell_0\boldsymbol{\ell}$ is exactly its intrinsic chromatic state $\boldsymbol{\ell}$.

Formula (6.1.1) shows explicitly the role played by the effect magnitude o_0 and by the effect chromatic vector $\mathbf{v_o}$: o_0 describes *how the observer perceives the intensity* of the color stimulus, while $\mathbf{v_o}$ describes *the adaptation state of the observer.*

Let us now turn our attention to color stimuli from non-emitting surfaces. While the perceptual measurement of an emitted light stimulus consists simply in the act of observing it, a non-emitting surface needs an additional step: before being observed, it must be illuminated. For this reason, the formalization of the concept of perceived color from a reflected light requires the preliminary definition of illuminant. Being the medium that permits to perform a measurement process, an illuminant is identified with an effect*.

Definition 6.1.5 (Illuminant and achromatic illuminant)**.** *An illuminant ι needed to light up a non-emitting surface in order to measure its color is identified with an effect $\boldsymbol{\iota} = (\iota_0, \mathbf{v}_{\boldsymbol{\iota}})$, $\iota_0 \in [0,1]$, $\mathbf{v}_{\boldsymbol{\iota}} \in \mathcal{D}$. The real quantity ι_0 represents the illuminant intensity, while $\mathbf{v}_{\boldsymbol{\iota}}$ carries the chromatic features. If $\mathbf{v}_{\boldsymbol{\iota}} = \mathbf{0}$, ι is called an achromatic illuminant.*

*An observer o can be thought as a *perceptual effect*, an illuminant o can be interpreted as a *physical effect*.

Now let us pass to the definition of patch (or *area*) of a non-emitting surface. Without being illuminated, a surface patch is characterized only by its intrinsic properties that establish how much light the surface reflects and how it interacts with the different spectral components of the incoming radiation. These features are fused together, which motivates the next definition.

Definition 6.1.6 (Patch)**.** *The patch p of a non-emitting surface is identified with a generalized state $p_0\mathbf{p}$, $p_0 \in [0,1]$ and $\mathbf{p} \in \mathcal{S}(\mathcal{H}(2,\mathbb{R}))$. The real quantity p_0 represents the overall proportion of the illuminant intensity that p is able to reflect and $\mathbf{p}$ carries the intrinsic chromatic properties of p.*

Definition 6.1.7 (Achromatic and white patch)**.** A patch $p = p_0\mathbf{p}$ with $\mathbf{p} = \mathbf{s_a}$ is called achromatic. In particular, if $p_0 = 1$, then we call it white patch and we write $\mathbf{p}^W = \mathbf{s_a}$.

When a patch is lit by an illuminant ι it can be observed, becoming a perceptual patch, as defined below.

Definition 6.1.8 (Perceptual patch)**.** *A perceptual patch r is a post-measurement generalized state*[†] *$r_0\mathbf{r}$, $r_0 \in [0,1]$, $\mathbf{r} \in \mathcal{S}(\mathcal{H}(2,\mathbb{R}))$, given by a physical patch p lit by an illuminant ι, i.e. $r_0\mathbf{r} = \psi_{\boldsymbol{\iota}}(p_0\mathbf{p})$.*

This definition is the *perceptual* counterpart of the well-known *physical* formula

$$I_p(\lambda, x) = L(\lambda)R_p(\lambda, x), \tag{6.1.3}$$

typically used in image formation models, see e.g. [60, 128]. $I_p(\lambda, x)$ is the image information about the physical patch p that has been acquired by a spectrophotometer at the wavelength λ and at the spatial position x, $L(\lambda)$ is the luminance of the radiation used to light up the material (supposed to be spatially uniform, which explains the absence of the variable x) and $R_p(\lambda, x)$ is the patch reflectance at the wavelength λ and at the point x. When $I_p(\lambda, x)$ is acquired, the data about L and R are fused together.

We are now ready to give the definition of perceived color of a patch.

Definition 6.1.9 (Perceived color from an illuminated patch)**.** *Given an observer o, a surface patch p and an illuminant ι, i.e. the triple $(\mathbf{o}, \boldsymbol{\iota}, p_0\mathbf{p})$, the color perceived by o from the perceptual patch $r = \psi_{\boldsymbol{\iota}}(p_0\mathbf{p})$ is the post-measurement generalized state $\psi_{\mathbf{o}}(r) = \psi_{\mathbf{o}}(\psi_{\boldsymbol{\iota}}(p_0\mathbf{p})) \in \tilde{\mathcal{S}}(\mathcal{H}(2,\mathbb{R}))$.*

We can interpret the sequential operation $\psi_{\mathbf{o}} \circ \psi_{\boldsymbol{\iota}}$ obtained via the combined action of the (physical) effect $\boldsymbol{\iota}$ and the (perceptual) effect $\mathbf{o}$ as a Lüders operation associated to a single (perceptual) effect $\tilde{\mathbf{o}}$ defined either by the equation

$$\psi_{\tilde{\mathbf{o}}}(p_0\mathbf{p}) := (\psi_{\mathbf{o}} \circ \psi_{\boldsymbol{\iota}})(p_0\mathbf{p}) = \psi_{\mathbf{o}}(r), \tag{6.1.4}$$

or, thanks to Equation (5.2.24), by the more explicit formula

$$\chi(\psi_{\tilde{\mathbf{o}}}(p_0\mathbf{p})) = o_0\iota_0p_0(1 + \mathbf{v}_{\boldsymbol{\iota}} \cdot \mathbf{v}_{\mathbf{p}})(1 + \mathbf{v}_{\mathbf{o}} \cdot (\mathbf{v}_{\boldsymbol{\iota}} \oplus \mathbf{v}_{\mathbf{p}}))\frac{1}{2}\begin{pmatrix} 1 \\ \mathbf{v}_{\mathbf{o}} \oplus (\mathbf{v}_{\boldsymbol{\iota}} \oplus \mathbf{v}_{\mathbf{p}}) \end{pmatrix}. \tag{6.1.5}$$

Thanks to Equations (5.2.11) and (5.2.13), if ι is an achromatic illuminant $\boldsymbol{\iota}_{\mathbf{a}} = (\iota_0, \mathbf{0})$ we have

$$r_{\mathrm{a}} := \psi_{\boldsymbol{\iota}_{\mathbf{a}}}(p_0\mathbf{p}) = \iota_0p_0\varphi_{\boldsymbol{\iota}_{\mathbf{a}}}(\mathbf{p}) = \iota_0p_0\mathbf{p}, \tag{6.1.6}$$

If, moreover, the observer o is represented by an achromatic effect $\mathbf{o_a}$, then

$$\varphi_{\mathbf{o_a}}(r_{\mathrm{a}}) = \varphi_{\mathbf{o_a}}(\psi_{\boldsymbol{\iota}_{\mathbf{a}}}(p_0\mathbf{p})) = \varphi_{\mathbf{o_a}}(\iota_0p_0\mathbf{p}) = \mathbf{p}, \tag{6.1.7}$$

[†]The letter r reminds the fact that the generalized state $r_0\mathbf{r}$ is issued by the light reflected by p.

thus, *such an observer perceives the chromatic state of a physical patch lit by an achromatic illuminant as it is.*

We must stress that the concepts of color perceived by an observer from an emitted light stimulus, see Definition 6.1.4, and from an illuminated surface patch, see Equation (6.1.4), in spite of having different interpretations, can be characterized by *the same mathematical object*: a post-measurement generalized state. For this reason, hereinafter, when it is not meaningful to distinguish between the two cases, we will deal with a perceived color by using the abstract and unifying notation represented by $\psi_{\mathbf{e}}(s_0\mathbf{s})$.

Notice that in [19] a perceived color has been defined as a an effect, while in the present section we have identified it with a post-measurement generalized state induced by an effect. These two apparently different definitions are actually linked. In fact, if $\mathbf{e} := (e_0, \mathbf{v_e})$ is an effect, then one can associate to $\mathbf{e}$ the perceived color $\psi_{\mathbf{e}}(\mathbf{s_a}) = e_0\varphi_{\mathbf{e}}(\mathbf{s_a})$, this correspondence being clearly one-to-one and onto.

6.2 Definition of the achromatic attributes: brightness and lightness

Defining a meaningful terminology to describe the achromatic component of a perceived color is a delicate issue. The title of [83] emblematically refers to it as an *unrelenting controversy*. This confusion is particularly evident when one reads names as lightness, brightness, luminance, luma, value or intensity used as synonyms to describe the achromatic attribute in image processing. For the definitions of brightness and lightness as color appearance attributes check Subsection 1.3.1 of Chapter 1. Notice that the definitions provided in this section will be sufficient to formalize the lightness constancy phenomenon in Section 6.4.

In this section we will provide a mathematically rigorous proposal for the definitions of brightness and lightness. To motivate our proposals, we start by reporting the following two descriptions that refer to the case of light reflected by a physical patch lit by an illuminant.

Quoting [62]: '*the physical counterpart of lightness is the permanent property of a surface that determines what percentage of light the surface reflects. Surfaces that appear white reflect about* 90% *of the light striking them. Black surfaces reflect about* 3%*. In short, lightness is perceived reflectance*'.

Quoting [83] : '*the physical counterpart of brightness is called luminance, that is, the absolute intensity of light reflected in the direction of the observer's eye by a surface (or at least coming from a certain part of the visual field). In short, if lightness is perceived reflectance, brightness is perceived luminance. The reflectance of an object is a relatively permanent property, whereas its luminance is transient*'.

The basic information brought by the references quoted above is that in order to extract lightness from the perceived color $\psi_{\mathbf{e}}(s_0\mathbf{s})$, we must be able to meaningfully extract a percentage out of it which has to verify suitable perceptual robustness properties. On the other hand brightness should represent the perceived absolute intensity of light. As we have seen in Chapter 5, the most immediate information that one can extract from a perceived color $\psi_{\mathbf{e}}(s_0\mathbf{s})$ is the evaluation $\langle\mathbf{e}\rangle_{s_0\mathbf{s}}$, see Equation (5.2.8), thus it seems natural to define brightness as follows.

Definition 6.2.1 (Brightness of a perceived color from an emitted light)**.** *Given an observer* o*,* $\mathbf{o} = (o_0, \mathbf{v_o})$*, the brightness of the color* $\psi_{\mathbf{o}}(\ell_0\boldsymbol{\ell})$ *perceived by* o *from an emitted light stimulus* $\ell_0\boldsymbol{\ell}$ *is given by*

$$\mathcal{B}(\psi_{\mathbf{o}}(\ell_0\boldsymbol{\ell})) := \mathrm{Tr}(\psi_{\mathbf{o}}(\ell_0\boldsymbol{\ell})) = o_0\ell_0(1 + \mathbf{v_o}\cdot\mathbf{v}_{\boldsymbol{\ell}}). \tag{6.2.1}$$

The following result is immediate, we state it for white light because we need it to define

lightness, but it can be extended to an arbitrary achromatic emitted light $\ell_0 \mathbf{s_a}$, obtaining $\ell_0 o_0$, $\ell_0 \in [0,1]$, instead of o_0 in the following proposition.

Proposition 6.2.2 (Robustness of the white light brightness)**.** *Given any observer* $\mathbf{o} = (o_0, \mathbf{v_o})$*, the brightness perceived by* o *from the white light* $\boldsymbol{\ell}^W$ *is:*

$$\mathcal{B}(\psi_{\mathbf{o}}(\boldsymbol{\ell}^W)) = o_0, \tag{6.2.2}$$

so the brightness of the white light does not depend on the effect vector of o*.*

Now we treat the case of reflected light.

Definition 6.2.3 (Brightness of a perceived color from a reflected light)**.** *Given a couple observer-illuminant* (o, ι)*,* $\mathbf{o} = (o_0, \mathbf{v_o})$*,* $\boldsymbol{\iota} = (\iota_0, \mathbf{v}_{\boldsymbol{\iota}})$*, the brightness of the color* $\psi_{\mathbf{o}}(\psi_{\boldsymbol{\iota}}(p_0\mathbf{p}))$ *perceived by* o *from a patch* $p_o\mathbf{p}$ *lit by* ι *is:*

$$\mathcal{B}(\psi_{\mathbf{o}}(\psi_{\boldsymbol{\iota}}(p_0\mathbf{p})) = o_0\iota_0 p_0(1 + \mathbf{v}_{\boldsymbol{\iota}} \cdot \mathbf{v_p})(1 + \mathbf{v_o} \cdot (\mathbf{v}_{\boldsymbol{\iota}} \oplus \mathbf{v_p})). \tag{6.2.3}$$

The equivalent of Proposition 6.2.2 in the case of reflected light is the following result, which can be extended to achromatic patches lit by achromatic lights by replacing $o_0\iota_0$ with $o_0\iota_0 p_0$.

Proposition 6.2.4 (Robustness of white patch brightness under achromatic illuminant)**.** *Given a couple observer-illuminant* (o, ι)*,* $\mathbf{o} = (o_0, \mathbf{v_o})$*,* $\boldsymbol{\iota} = (\iota_0, \mathbf{v}_{\boldsymbol{\iota}})$*, the brightness perceived by* o *from the white patch* $\mathbf{p}^W$ *lit by* ι *is:*

$$\mathcal{B}(\psi_{\mathbf{o}}(\psi_{\boldsymbol{\iota}}(\mathbf{p}^W)) = o_0\iota_0(1 + \mathbf{v_o} \cdot \mathbf{v}_{\boldsymbol{\iota}}), \tag{6.2.4}$$

hence, the brightness of the white patch does not depend on the effect vector of o *if and only if* ι *is an achromatic illuminant* ι_a*, in which case we have:*

$$\mathcal{B}(\psi_{\mathbf{o}}(\psi_{\boldsymbol{\iota_a}}(\mathbf{p}^W)) = o_0\iota_0. \tag{6.2.5}$$

Let us now pass to the definition of lightness. The following reasoning will give a more substantiated basis to the intuitive equation proposed in [49], recalled in Chapter 1, Equation (1.3.1).

An observer cannot distinguish an isolated chromatic patch lit by an achromatic illuminant from an achromatic one lit by a chromatic illuminant. The physical counterpart of this statement is the impossibility of recovering the reflectance $R_p(\lambda, x)$ from the sole knowledge of $I_p(\lambda, x)$ in formula (6.1.3): it is clear that, without any further hypothesis on $R_p(\lambda, x)$, or on the luminance $L(\lambda)$, this problem is ill-posed.

This is the reason why several hypotheses, e.g. white patch, gray world, gray edge and so on, have been formulated in order to solve this problem, see e.g. [60, 128] for an overview. Among them, the only hypothesis that can be meaningfully applied to unrelated colors is the white patch (because unrelated colors, by definition, do not have a surround), i.e. the physical assumption that there exists a patch p^W, among those observed under the same illuminant, that has perfect reflectance, i.e. such that $R_{p^W}(\lambda, x) \equiv 1$.

If this hypothesis is satisfied, then formula (6.1.3) gives $I_{p^W}(\lambda, x) = L(\lambda)$, i.e. the image information acquired from the white patch p^W agrees with the luminance of the illuminant, hence we can retrieve the reflectance of each patch p from the image information $I_p(\lambda, x)$ simply dividing it by $I_{p^W}(\lambda, x)$, i.e.

$$R_p(\lambda, x) = \frac{I_p(\lambda, x)}{I_{p^W}(\lambda, x)}. \tag{6.2.6}$$

As before, we distinguish our definition of lightness for emitted and reflected light, starting by the former case.

Definition 6.2.5 (Lightness of a perceived color from an emitted light)**.** *Given an observer o, $\mathbf{o} = (o_0, \mathbf{v_o})$, the lightness of the color $\psi_{\mathbf{o}}(\ell_0\boldsymbol{\ell})$ perceived by o from an emitted light stimulus $\ell_0\boldsymbol{\ell}$ is given by the ratio between its brightness, Equation* (6.2.1)*, and the brightness of the white light, Equation* (6.2.2)*, i.e.*

$$\mathcal{L}(\psi_{\mathbf{o}}(\ell_0\boldsymbol{\ell})) := \frac{\mathcal{B}(\psi_{\mathbf{o}}(\ell_0\boldsymbol{\ell}))}{\mathcal{B}(\psi_{\mathbf{o}}(\boldsymbol{\ell}^W))} = \ell_0(1 + \mathbf{v_o} \cdot \mathbf{v}_{\boldsymbol{\ell}}). \tag{6.2.7}$$

The lightness perceived from an achromatic emitted light coincides with its intensity ℓ_0 independently of the observer:

$$\mathcal{L}(\psi_{\mathbf{o}}(\ell_0\mathbf{s_a})) = \ell_0, \quad \forall \mathbf{o}. \tag{6.2.8}$$

In particular, the lightness of the white light is equal to 1.

When $\mathbf{v_o} = \mathbf{0}$, the lightness of any color perceived from an emitted light coincides with the light intensity independently of the chromatic state of the emitted light:

$$\mathcal{L}(\psi_{\mathbf{o_a}}(\ell_0\boldsymbol{\ell})) = \ell_0, \quad \forall \boldsymbol{\ell}. \tag{6.2.9}$$

Definition 6.2.6 (Lightness of a perceived color from a reflected light)**.** *Given a couple observer-illuminant (o, ι), $\mathbf{o} = (o_0, \mathbf{v_o})$, $\boldsymbol{\iota} = (\iota_0, \mathbf{v}_{\boldsymbol{\iota}})$, the lightness of the color $\psi_{\mathbf{o}}(\psi_{\boldsymbol{\iota}}(p_0\mathbf{p}))$ perceived by o from the patch $p_0\mathbf{p}$ lit by ι is given by the ratio between its brightness, Equation* (6.2.3)*, and the brightness of the white patch lit by the same illuminant ι, Equation* (6.2.4)*, i.e.*

$$\mathcal{L}(\psi_{\mathbf{o}}(\psi_{\boldsymbol{\iota}}(p_0\mathbf{p})) := \frac{\mathcal{B}(\psi_{\mathbf{o}}(\psi_{\boldsymbol{\iota}}(p_0\mathbf{p}))}{\mathcal{B}(\psi_{\mathbf{o}}(\psi_{\boldsymbol{\iota}}(\mathbf{p}^W))} = p_0\frac{(1 + \mathbf{v}_{\boldsymbol{\iota}} \cdot \mathbf{v_p})(1 + \mathbf{v_o} \cdot (\mathbf{v}_{\boldsymbol{\iota}} \oplus \mathbf{v_p}))}{1 + \mathbf{v_o} \cdot \mathbf{v}_{\boldsymbol{\iota}}}. \tag{6.2.10}$$

Notice that the lightness of an achromatic patch coincides with p_0, the overall percentage of illuminant intensity that the patch is able to reflect, regardless of the chromaticity of the illuminant ι and the effect vector of the observer o:

$$\mathcal{L}(\psi_{\mathbf{o}}(\psi_{\boldsymbol{\iota}}(p_0\mathbf{s_a})) = p_0, \quad \forall(\mathbf{o}, \boldsymbol{\iota}). \tag{6.2.11}$$

In particular, the lightness of the white patch is normalized to 1.

Differently from the case of emitted light, the lightness of a surface color perceived by an observer with $\mathbf{v_o} = \mathbf{0}$ is not simply p_0 but

$$\mathcal{L}(\psi_{\mathbf{o_a}}(\psi_{\boldsymbol{\iota}}(p_0\mathbf{p})) = p_0(1 + \mathbf{v}_{\boldsymbol{\iota}} \cdot \mathbf{v_p}), \tag{6.2.12}$$

this quantity reduces to p_0 when ι is an achromatic illuminant:

$$\mathcal{L}(\psi_{\mathbf{o_a}}(\psi_{\boldsymbol{\iota_a}}(p_0\mathbf{p})) = p_0. \tag{6.2.13}$$

As a final remark, we notice that the fact that brightness and lightness differ by the multiplicative constant represented by the brightness of the perceived white area is coherent with the Weber-Fechner's law, mentioned in Equation (1.2.1) Section 1.2, see as well [65]. This might justify the choice of ds/s, which is invariant under scalar multiplication of s, as metric for the achromatic component of a color. In other words lightness is invariant under linear rescalings of brightness.

6.3 Definition of perceptual chromatic attributes: colorfulness, saturation, chroma and hue

In this section we discuss two possible ways of defining the chromatic attributes of colorfulness, chroma and saturation. We recall that the intuitive definitions of these color appearance attributes are reported in Subsection of Chapter 1. We must stress that the role of chromatic opponency, introduced in Chapter 3 is fundamental to characterize chromatic attributes.

As we will see, there are different ways to provide definitions of the chromatic attributes using color opponency: in Subsection 6.3.1 we will provide the most simple one using the Euclidean distance, while in Subsections 6.3.2 and 6.3.3 we will employ the concept of relative quantum entropy, introduced in Section 5.4 of Chapter 5.

6.3.1 Chromatic opponency and Euclidean definition of colorfulness, saturation and chroma of a perceived color

As already mentioned in Section 3.4, the expectation values of the real Pauli matrices σ_1, σ_2 on a chromatic state, and analogously on a generalized state, provide its degrees of opponency. Our aim here is to define the chromatic attributes of *colorfulness*, *chroma* and *saturation* using only the information about chromatic opponency.

Moreover, we want to translate into rigorous equations the intuitive formulae (1.3.3) and (1.3.2) of Subsection 1.3.1, that we recall here:

$$\text{Saturation} = \frac{\text{Colorfulness}}{\text{Brightness}} \quad \text{and} \quad \text{Chroma} = \frac{\text{Colorfulness}}{\text{Brightness(White)}}. \tag{6.3.1}$$

Since in the previous section we have already defined the concept of brightness, what remains to be defined is just the colorfulness. In fact, given the perceived color $\psi_{\mathbf{e}}(s_0\mathbf{s})$, if we know how to define its colorfulness $\text{Col}(\psi_{\mathbf{e}}(s_0\mathbf{s}))$, then its saturation 'Sat' and chroma 'Chr' are, respectively,

$$\text{Sat}(\psi_{\mathbf{e}}(\text{s}_0\mathbf{s})) = \frac{\text{Col}(\psi_{\mathbf{e}}(s_0\mathbf{s}))}{\mathcal{B}(\psi_{\mathbf{e}}(s_0\mathbf{s}))} \quad \text{and} \quad \text{Chr}(\psi_{\mathbf{e}}(\text{s}_0\mathbf{s})) = \frac{\text{Col}(\psi_{\mathbf{e}}(s_0\mathbf{s}))}{\mathcal{B}(\psi_{\mathbf{e}}(\mathbf{s_a}))}. \tag{6.3.2}$$

Alternatively, if we knew how to define saturation, we could define colorfulness and chroma as follows:

$$\text{Col}(\psi_{\mathbf{e}}(s_0\mathbf{s})) = \beta\,\text{Sat}(\psi_{\mathbf{e}}(\text{s}_0\mathbf{s})) \quad \text{and} \quad \text{Chr}(\psi_{\mathbf{e}}(s_0\mathbf{s})) = \lambda\,\text{Sat}(\psi_{\mathbf{e}}(\text{s}_0\mathbf{s})), \tag{6.3.3}$$

where

$$\begin{cases} \beta := \mathcal{B}(\psi_{\mathbf{e}}(s_0\mathbf{s})) \\ \lambda := \mathcal{L}(\psi_{\mathbf{e}}(s_0\mathbf{s})) = \mathcal{B}(\psi_{\mathbf{e}}(s_0\mathbf{s}))/\mathcal{B}(\psi_{\mathbf{e}}(\mathbf{s_a})) \end{cases} . \tag{6.3.4}$$

We will exploit this remark in the next subsection.

Let us start with a preliminary definition.

Definition 6.3.1 (i-th degrees of opponency of a perceived color)**.** Let $\psi_{\mathbf{e}}(s_0\mathbf{s})$ be a perceived color. Then, for $i = 1, 2$, its:

- *i-th degree of colorfulness opponency* is

$$\text{Col}_i(\psi_{\mathbf{e}}(s_0\mathbf{s})) := \langle\sigma_i\rangle_{\psi_{\mathbf{e}}(s_0\mathbf{s})} \; ; \tag{6.3.5}$$

- *i-th degree of saturation opponency* is

$$\text{Sat}_i(\psi_{\mathbf{e}}(s_0\mathbf{s})) := \frac{\langle\sigma_i\rangle_{\psi_{\mathbf{e}}(s_0\mathbf{s})}}{\text{Tr}(\psi_{\mathbf{e}}(s_0\mathbf{s}))} \; ; \tag{6.3.6}$$

- *i-th degree of chroma opponency* is

$$\mathrm{Chr}_i(\psi_{\mathbf{e}}(s_0\mathbf{s})) := \frac{\langle\sigma_i\rangle_{\psi_{\mathbf{e}}(s_0\mathbf{s})}}{\mathrm{Tr}(\psi_{\mathbf{e}}(\mathbf{s_a}))}. \tag{6.3.7}$$

Now we have to face the problem of suitably combine the i-th degree of opposition of these chromatic attributes in order to obtain a positive real number that defines the attribute itself. If we had to follow the Euclidean choice of classical colorimetry we would give the following definitions.

Definition 6.3.2 (Euclidean definitions of colorfulness, saturation and chroma of a perceived color)**.** Given the perceived color $\psi_{\mathbf{e}}(s_0\mathbf{s})$, its:

- colorfulness is

$$\mathrm{Col}(\psi_{\mathbf{e}}(s_0\mathbf{s})) = \sqrt{[\mathrm{Col}_1(\psi_{\mathbf{e}}(s_0\mathbf{s}))]^2 + [\mathrm{Col}_2(\psi_{\mathbf{e}}(s_0\mathbf{s}))]^2}\,; \tag{6.3.8}$$

- saturation is

$$\mathrm{Sat}(\psi_{\mathbf{e}}(s_0\mathbf{s})) = \sqrt{[\mathrm{Sat}_1(\psi_{\mathbf{e}}(s_0\mathbf{s}))]^2 + [\mathrm{Sat}_2(\psi_{\mathbf{e}}(s_0\mathbf{s}))]^2}\,; \tag{6.3.9}$$

- chroma is

$$\mathrm{Chr}(\psi_{\mathbf{e}}(s_0\mathbf{s})) = \sqrt{[\mathrm{Chr}_1(\psi_{\mathbf{e}}(s_0\mathbf{s}))]^2 + [\mathrm{Chr}_2(\psi_{\mathbf{e}}(s_0\mathbf{s}))]^2}. \tag{6.3.10}$$

With such definitions the linear relations of Equation (6.3.2) are satisfied.

We now pass to the discussion of a second possible way to define chromatic attributes that we deem more coherent with the quantum-like theory of color perception that lies at the basis of our work.

6.3.2 Definition of colorfulness, saturation and chroma of a perceived color via relative quantum entropy

Here we propose an alternative description of the perceptual chromatic attributes based on the notion of relative (quantum) entropy, for more information about this concept we refer to Chapter 5 or [32, 7] and also to [119] or [6] for the proofs of its properties that we shall quote here.

Now, in order to define the saturation of the perceived color $\psi_{\mathbf{e}}(s_0\mathbf{s})$ we simply consider the chromatic state $\varphi_{\mathbf{e}}(s_0\mathbf{s}) = \varphi_{\mathbf{e}}(\mathbf{s})$ associated to it and we compute the relative entropy between its density matrix and $\rho_{\mathbf{0}}$, see as well Equation (5.4.5), as formalized in the following definition.

Definition 6.3.3 (Saturation of a perceived color)**.** Given the perceived color $\psi_{\mathbf{e}}(s_0\mathbf{s})$, its saturation is

$$\begin{aligned}\mathrm{Sat}(\psi_{\mathbf{e}}(s_0\mathbf{s})) &= R(\rho_{\varphi_{\mathbf{e}}(\mathbf{s})}||\rho_{\mathbf{0}}) = 1 - S(\rho_{\varphi_{\mathbf{e}}(\mathbf{s})}) = \Sigma(r_{\varphi_{\mathbf{e}}(\mathbf{s})}) \\ &= \frac{1}{2}\log_2(1 - r^2_{\varphi_{\mathbf{e}}(\mathbf{s})}) + \frac{r_{\varphi_{\mathbf{e}}(\mathbf{s})}}{2}\log_2\left(\frac{1 + r_{\varphi_{\mathbf{e}}(\mathbf{s})}}{1 - r_{\varphi_{\mathbf{e}}(\mathbf{s})}}\right),\end{aligned} \tag{6.3.11}$$

with $r_{\varphi_{\mathbf{e}}(\mathbf{s})} = \|\mathbf{v}_{\varphi_{\mathbf{e}}(\mathbf{s})}\|$, where $\mathbf{v}_{\varphi_{\mathbf{e}}(\mathbf{s})} = (\langle\sigma_1\rangle_{\varphi_{\mathbf{e}}(\mathbf{s})}, \langle\sigma_2\rangle_{\varphi_{\mathbf{e}}(\mathbf{s})})$ is the chromatic state vector of $\varphi_{\mathbf{e}}(\mathbf{s})$ which contains the intrinsic information about its degrees of chromatic opposition.

Hence, $\mathrm{Sat}(\psi_{\mathbf{e}}(s_0\mathbf{s}))$ depends only on the chromatic vector of the effect $\mathbf{e}$ that permits the observation of the color and on its chromatic features, embedded in $r_{\varphi_{\mathbf{e}}(\mathbf{s})}$, but *not on* s_0, nor on e_0.

Remark 6.3.4. We must stress that with this second approach the chromatic attribute of saturation refers no more to a particular, arbitrarily chosen, coordinate on the chromaticity disk, since it is obtained by the computation of a trace, it is independent on the coordinate system. This definition, via the relative entropy aims at measuring the distinguishability of the state with the achromatic state. In this sense, the saturation characterizes some information that it is not related to a special coordinate. In other words saturation is not a coordinate, in a fixed coordinate system, but an intrinsic attribute, independent on the choice of the coordinate system.

Now that we have provided a definition of saturation, it is easy to define colorfulness and chroma following Equations (6.3.3). Note that both of them depend on the coefficient s_0.

Definition 6.3.5 (Colorfulness of a perceived color)**.** Given the perceived color $\psi_{\mathbf{e}}(s_0\mathbf{s})$ with brightness $\beta = \mathcal{B}(\psi_{\mathbf{e}}(s_0\mathbf{s})) = \mathrm{Tr}(\psi_{\mathbf{e}}(s_0\mathbf{s}))$, its *colorfulness* is

$$\mathrm{Col}(\psi_{\mathbf{e}}(s_0\mathbf{s})) = R(\beta\rho_{\varphi_{\mathbf{e}}(s_0\mathbf{s})}||\beta\rho_{\mathbf{s_a}}) = \beta\,\mathrm{Sat}(\psi_{\mathbf{e}}(s_0\mathbf{s})). \tag{6.3.12}$$

Definition 6.3.6 (Chroma of a perceived color)**.** Let $\psi_{\mathbf{e}}(s_0\mathbf{s})$ be a perceived color with lightness given by $\lambda = \mathcal{L}(\psi_{\mathbf{e}}(s_0\mathbf{s})) = \mathrm{Tr}(\psi_{\mathbf{e}}(s_0\mathbf{s}))/\,\mathrm{Tr}(\psi_{\mathbf{e}}(\mathbf{s_a}))$, then its *chroma* is

$$\mathrm{Chr}(\psi_{\mathbf{e}}(s_0\mathbf{s})) = R(\lambda\rho_{\varphi_{\mathbf{e}}(s_0\mathbf{s})}||\lambda\rho_{\mathbf{s_a}}) = \lambda\,\mathrm{Sat}(\psi_{\mathbf{e}}(s_0\mathbf{s})). \tag{6.3.13}$$

We must stress that both definitions above rely on the property of the relative entropy stated by Equation (5.4.2) in Chapter 5.

6.3.3 Definition of hue of a perceived color via relative quantum entropy

As lightness and brightness, perceptual hue has a physical counterpart: the concept of *dominant wavelength* of a color stimulus. As presented in [163], the dominant wavelength of a color stimulus is '*the wavelength of monochromatic stimulus that, when mixed with some specified achromatic stimulus, matches the given stimulus in color*'. In other words, the dominant wavelength characterizes any light mixture in terms of the monochromatic spectral light that elicits the same perception of hue. In the CIE chromaticity diagram, see e.g. Figure 1.5, the dominant wavelength is the point of its border determined by the intersection with the straight line that passes through the white point and the one associated to the given color.

In order to express this concept within the quantum-like perceptual framework, motivated by the results of the previous subsection, we replace the concept of nearest Euclidean distance to the border of the CIE chromaticity diagram with that of minimal relative entropy between a given chromatic state and a pure state parameterized by a point of the border of $\mathcal{D}$.

These considerations lead naturally to the following definition of hue.

Definition 6.3.7 (Hue of a perceived color)**.** Given $\psi_{\mathbf{e}}(s_0\mathbf{s})$, a non-achromatic perceived color, its hue is the pure chromatic state $\varphi^*_{\mathbf{e}}(\mathbf{s})$ defined by

$$\varphi^*_{\mathbf{e}}(\mathbf{s}) := \underset{\rho\in\mathcal{PS}(\mathcal{H}(2,\mathbb{R}))}{\arg\min}\; R(\rho||\rho_{\varphi_{\mathbf{e}}(\mathbf{s})}). \tag{6.3.14}$$

Notice that *the hue of* $\psi_{\mathbf{e}}(s_0\mathbf{s})$ *does not depend on* s_0 because of the property $\varphi_{\mathbf{e}}(s_0\mathbf{s}) = \varphi_{\mathbf{e}}(\mathbf{s})$ for all $s_0 \in [0,1]$. For an explicit expression of $\mathcal{PS}(\mathcal{H}(2,\mathbb{R}))$ see Equation (3.3.20).

Of course, we must verify that the definition is well-posed, i.e. that the solution to the minimization problem defined by Equation (6.3.14) exists and it is unique. Thanks to the Klein inequality, see Section 5.4, the relative entropy is null if and only if $\rho = \varphi_{\mathbf{e}}(\mathbf{s})$, so let us avoid this trivial case and also the achromatic condition (since achromatic colors lack of hue by definition) by supposing that $0 < r_{\varphi_{\mathbf{e}}(\mathbf{s})} < 1$.

Let us notice that, thanks to Definition 5.4.1, Equations (5.4.4) and (3.3.19) we get:

$$R(\rho_{\mathbf{s}}||\rho_{\mathbf{t}}) = 1 - S(\rho_{\mathbf{s}}) - \frac{1}{2}\log_2(1 - r_{\mathbf{t}}^2) - \frac{r_{\mathbf{s}}\cos\vartheta_{\mathbf{s},\mathbf{t}}}{2}\log_2\left(\frac{1 + r_{\mathbf{t}}}{1 - r_{\mathbf{t}}}\right). \tag{6.3.15}$$

Now we must replace the generic density matrix $\rho_{\mathbf{s}}$ with one, ρ, associated to a pure state, so that $S(\rho_{\mathbf{s}}) = 0$ and $r_{\mathbf{s}} = 1$, and $\mathbf{t}$ with $\varphi_{\mathbf{e}}(\mathbf{s})$, thus obtaining:

$$R(\rho||\rho_{\varphi_{\mathbf{e}}(\mathbf{s})}) = 1 - \frac{1}{2}\log_2(1 - r_{\varphi_{\mathbf{e}}(\mathbf{s})}^2) - \frac{\cos\vartheta_{\rho,\varphi_{\mathbf{e}}(\mathbf{s})}}{2}\log_2\left(\frac{1 + r_{\varphi_{\mathbf{e}}(\mathbf{s})}}{1 - r_{\varphi_{\mathbf{e}}(\mathbf{s})}}\right). \tag{6.3.16}$$

Since $0 < r_{\varphi_{\mathbf{e}}(\mathbf{s})} < 1$, $-\frac{1}{2}\log_2(1 - r_{\varphi_{\mathbf{e}}(\mathbf{s})}^2) > 0$ and $\log_2\left(\frac{1+r_{\varphi_{\mathbf{e}}(\mathbf{s})}}{1-r_{\varphi_{\mathbf{e}}(\mathbf{s})}}\right) > 0$. Given that $R(\rho||\rho_{\varphi_{\mathbf{e}}(\mathbf{s})}) > 0$ and that $r_{\varphi_{\mathbf{e}}(\mathbf{s})}$ is fixed, the computation of the arg min in Equation (6.3.14) is equivalent to the maximization of $\cos\vartheta_{\rho,\varphi_{\mathbf{e}}(\mathbf{s})}$, i.e. *we can reformulate the definition of hue of* $\psi_{\mathbf{e}}(s_0\mathbf{s})$ *as follows*:

$$\varphi_{\mathbf{e}}^*(\mathbf{s}) := \underset{\rho\in\mathcal{PS}(\mathcal{H}(2,\mathbb{R}))}{\arg\max}\ \cos\vartheta_{\rho,\varphi_{\mathbf{e}}(\mathbf{s})}. \tag{6.3.17}$$

Recalling that $\vartheta_{\rho,\varphi_{\mathbf{e}}(\mathbf{s})}$ is the angle between the chromatic vectors $\mathbf{v}_\rho$ of the pure state associated to ρ (so that $r_\rho = \|\mathbf{v}_\rho\| = 1$) and $\mathbf{v}_{\varphi_{\mathbf{e}}(\mathbf{s})}$, which is fixed, we get:

$$\cos\vartheta_{\rho,\varphi_{\mathbf{e}}(\mathbf{s})} = \frac{\mathbf{v}_\rho \cdot \mathbf{v}_{\varphi_{\mathbf{e}}(\mathbf{s})}}{r_{\varphi_{\mathbf{e}}(\mathbf{s})}}, \tag{6.3.18}$$

which is maximized when $\mathbf{v}_\rho$ is parallel to $\mathbf{v}_{\varphi_{\mathbf{e}}(\mathbf{s})}$.

Hence, given the state $\varphi_{\mathbf{e}}(\mathbf{s})$ corresponding to the perceived color $\psi_{\mathbf{e}}(s_0\mathbf{s})$ associated to the density matrix

$$\rho_{\varphi_{\mathbf{e}}(\mathbf{s})} = \frac{1}{2}\begin{pmatrix} 1 + r_{\varphi_{\mathbf{e}}(\mathbf{s})}\cos\vartheta_{\varphi_{\mathbf{e}}(\mathbf{s})} & r_{\varphi_{\mathbf{e}}(\mathbf{s})}\sin\vartheta_{\varphi_{\mathbf{e}}(\mathbf{s})} \\ r_{\varphi_{\mathbf{e}}(\mathbf{s})}\sin\vartheta_{\varphi_{\mathbf{e}}(\mathbf{s})} & 1 - r_{\varphi_{\mathbf{e}}(\mathbf{s})}\cos\vartheta_{\varphi_{\mathbf{e}}(\mathbf{s})} \end{pmatrix}, \tag{6.3.19}$$

its hue is the pure state $\varphi_{\mathbf{e}}^*(\mathbf{s})$ defined by the density matrix:

$$\rho_{\varphi_{\mathbf{e}}^*(\mathbf{s})} = \frac{1}{2}\begin{pmatrix} 1 + \cos\vartheta_{\varphi_{\mathbf{e}}(\mathbf{s})} & \sin\vartheta_{\varphi_{\mathbf{e}}(\mathbf{s})} \\ \sin\vartheta_{\varphi_{\mathbf{e}}(\mathbf{s})} & 1 - \cos\vartheta_{\varphi_{\mathbf{e}}(\mathbf{s})} \end{pmatrix}. \tag{6.3.20}$$

What just proven not only shows that our definition of hue is well-posed, but it is also in perfect agreement with the interpretation of pure states as hues already discussed in Section 3.3 of Chapter 3.

We emphasize the fact that the two definitions of saturation and hue by means of relative quantum entropy are much more significant from the perception viewpoint than those involving *ad hoc* coordinates of classical colorimetric spaces. The relative entropy between two states is a measure of their *distinguishability*. This precisely means that the saturation of a perceived color is a measure of how it can be distinguished from the achromatic state. In the same way, the hue of a perceived color is the closest, from the distinguishability point of view, pure chromatic state to the given perceived color. We also insist on the fact that the above computations make use of the Bloch parameters of the state space of the rebit which are not the coordinates of the color appearance models of the CIE.

As a consequence, the novel definitions of perceptual attributes that we propose constitute not only a meaningful formalization of the CIE definitions given in Subsection 1.3.1, but they are also mathematically operative in the quantum-like framework presented in Chapters 3, 5. They provide a rigorous explanation of the intuitive representation that one may have of the perceived color solid. In the next section, we illustrate the potential of this novel system of definitions on the specific example of the lightness constancy phenomenon. We do believe these new definitions to be a good starting point to understand and model also other color appearance phenomena, as the ones mentioned in Subsection 1.3.2.

6.4 Characterization of lightness constancy in the quantum-like framework

In this section we analyze the important property of lightness constancy, introduced in Subsection 1.3.2 from the point of view of the quantum-like framework and we characterize it through a matching equation involving generalized states. In particular we will use the novel definitions of brightness and lightness given in Section 6.2 of the present chapter.

The two perceptual patches of interest are given by the two generalized states $p^1 = p_0^1\mathbf{p}^1$ and $p^2 = p_0^2\mathbf{p}^2$, where $p_0^1, p_0^2 \in [0,1]$ and $\mathbf{p}^1, \mathbf{p}^2$ are two chromatic states. We first consider the case where the two (physical) effects corresponding to the two illuminants are achromatic, i.e. represented by $\boldsymbol{\iota}^1 = (\iota_0^1, \mathbf{0})$ and $\boldsymbol{\iota}^2 = (\iota_0^2, \mathbf{0})$. In classical colorimetry, this amounts to considering a D65 illuminant, see e.g. [163].

The two reflected lights of interest are thus given by the two generalized states

$$r^1 = \psi_{\boldsymbol{\iota}^1}(p_0^1\mathbf{p}^1) = \iota_0^1 p_0^1\mathbf{p}^1, \quad r^2 = \psi_{\boldsymbol{\iota}^2}(p_0^2\mathbf{p}^2) = \iota_0^2 p_0^2\mathbf{p}^2. \tag{6.4.1}$$

We consider now an observer o associated to a (perceptual) achromatic effect $(o_0, \mathbf{0})$. As explained before, see Equation (6.1.7), this observer perceives the chromatic information of the two reflected lights 'as they are', which means that there is no variation between the chromatic features of the reflected lights and the chromatic features of the perceived colors. More precisely, we have

$$\psi_{\mathbf{o}}(r^1) = o_0\iota_0^1 p_0^1\mathbf{p}^1, \quad \psi_{\mathbf{o}}(r^2) = o_0\iota_0^2 p_0^2\mathbf{p}^2. \tag{6.4.2}$$

Recalling Equation (6.2.13), the lightness of the perceived colors $\psi_{\mathbf{o}}(r^1)$ and $\psi_{\mathbf{o}}(r^2)$ is

$$\mathcal{L}(\psi_{\mathbf{o}}(r^1)) = p_0^1, \quad \mathcal{L}(\psi_{\mathbf{o}}(r^2)) = p_0^2. \tag{6.4.3}$$

It makes sense to consider the phenomenon of lightness constancy only when two perceived colors share the same chromatic information. In the present case, the chromatic matching Equation (5.2.25) leads trivially to $\mathbf{p}^1 = \mathbf{p}^2 =: \mathbf{p}$. As a consequence,

$$r^1 = \iota_0^1 p_0^1\mathbf{p}, \quad r^2 = \iota_0^2 p_0^2\mathbf{p}, \tag{6.4.4}$$

and

$$\psi_{\mathbf{o}}(r^1) = o_0\iota_0^1 p_0^1\mathbf{p}, \quad \psi_{\mathbf{o}}(r^2) = o_0\iota_0^2 p_0^2\mathbf{p}. \tag{6.4.5}$$

The two reflected lights r^1 and r^2 come from the two different illuminants ι^1 and ι^2, and the observer has to compensate the difference between these two illuminants in order to compare the initial perceptual patches p^1 and p^2, i.e. to compare the lightnesses p_0^1 and p_0^2. This means that the observer must find a way to recover the reflected lights as if they where lit by the same illuminant.

Let the observer o change his/her (perceptual) effect from $(o_0, \mathbf{0})$ to $(o_0^1, \mathbf{0})$ to define a new observer o^1 perceiving the reflected light r^1. In the same way, let the observer o change his/her (perceptual) effect from $(o_0, \mathbf{0})$ to $(o_0^2, \mathbf{0})$ to define a new observer o^2 perceiving the reflected light r^2. We have

$$\psi_{\mathbf{o}^1}(r^1) = o_0^1 \iota_0^1 p_0^1 \mathbf{p}, \quad \psi_{\mathbf{o}^2}(r^2) = o_0^2 \iota_0^2 p_0^2 \mathbf{p}. \tag{6.4.6}$$

These two perceived colors are those obtained from a measurement of *only one observer associated to an achromatic effect* from the reflected lights produced by the two perceptual patches p^1 and p^2 *lit with the same achromatic illuminant* if and only if $o_0^1 \iota_0^1 = o_0^2 \iota_0^2$. If, for instance, $o^1 = (\iota_0^2, \mathbf{0})$ and $o^2 = (\iota_0^1, \mathbf{0})$, then

$$\psi_{\mathbf{o}^1}(r^1) = \iota_0^2 \iota_0^1 p_0^1 \mathbf{p}, \quad \psi_{\mathbf{o}^2}(r^2) = \iota_0^1 \iota_0^2 p_0^2 \mathbf{p} \tag{6.4.7}$$

are the perceived colors measured by the observer $o = (1, \mathbf{0})$ from the reflected lights $\widetilde{r}^1 = \iota_0^1 \iota_0^2 p_0^1 \mathbf{p}$ and $\widetilde{r}^2 = \iota_0^1 \iota_0^2 p_0^1 \mathbf{p}$ obtained by illuminating the perceptual patches p^1 and p^2 with the same achromatic illuminant $(\iota_0^1 \iota_0^2, \mathbf{0})$. Using the equation $o_0^1 \iota_0^1 = o_0^2 \iota_0^2$, it appears clearly that the two perceived colors $\psi_{\mathbf{o}^1}(r^1)$ and $\psi_{\mathbf{o}^2}(r^2)$ are equal if and only if the two lightnesses p_0^1 and p_0^2 are equal.

The above analysis of lightness constancy requires two measurements performed by the observers o^1 and o^2, with the condition $o_0^1 / o_0^2 = \iota_0^2 / \iota_0^1$, in order to make some comparison. This means that the lightness constancy phenomenon requires that the observer is able to evaluate the ratio ι_0^2 / ι_0^1 between the two magnitudes of the illuminants ι^2 and ι^1.

It is easy to check that the proposed derivation also applies when the two illuminants are no more achromatic but still share the same chromatic features expressed by their effect vector. In fact let $\boldsymbol{\iota}^1 = (\iota_0^1, \mathbf{v}_\iota)$ and $\boldsymbol{\iota}^2 = (\iota_0^2, \mathbf{v}_\iota)$ be the two illuminants, with o^i, p^i as before, $i = 1, 2$, then we obtain the following perceived colors

$$\psi_{\mathbf{o}^1}(r^1) = o_0^1 \iota_0^1 p_0^1 (1 + \mathbf{v}_\iota \cdot \mathbf{v}_\mathbf{p})(\mathbf{v}_\iota \oplus \mathbf{v}_\mathbf{p}), \quad \psi_{\mathbf{o}^2}(r^2) = o_0^2 \iota_0^2 p_0^2 (1 + \mathbf{v}_\iota \cdot \mathbf{v}_\mathbf{p})(\mathbf{v}_\iota \oplus \mathbf{v}_\mathbf{p}). \tag{6.4.8}$$

Notice that, from Definition 6.2.6 their lightness is given by

$$\mathcal{L}(\psi_\mathbf{o}(r^1)) = p_0^1 (1 + \mathbf{v}_\iota \cdot \mathbf{v}_\mathbf{p}), \quad \mathcal{L}(\psi_\mathbf{o}(r^2)) = p_0^2 (1 + \mathbf{v}_\iota \cdot \mathbf{v}_\mathbf{p}). \tag{6.4.9}$$

The perceived colors in Equation (6.4.8) are those obtained from a measurement of only one observer associated to an achromatic effect from the reflected lights produced by the two perceptual patches p^1 and p^2 lit with the same illuminant of chromaticity $\mathbf{v}_\iota$ if and only if $o_0^1 \iota_0^1 = o_0^2 \iota_0^2$. Thus the following perceived colors

$$\psi_{\mathbf{o}^1}(r^1) = \iota_0^2 \iota_0^1 p_0^1 (1 + \mathbf{v}_\iota \cdot \mathbf{v}_\mathbf{p})(\mathbf{v}_\iota \oplus \mathbf{v}_\mathbf{p}), \quad \psi_{\mathbf{o}^2}(r^2) = \iota_0^1 \iota_0^2 p_0^2 (1 + \mathbf{v}_\iota \cdot \mathbf{v}_\mathbf{p})(\mathbf{v}_\iota \oplus \mathbf{v}_\mathbf{p}), \tag{6.4.10}$$

can be seen as the perceived colors measured by $o = (1, \mathbf{0})$ from the reflected lights $\widetilde{r}^1 = \iota_0^1 \iota_0^2 p_0^1 (1 + \mathbf{v}_\iota \cdot \mathbf{v}_\mathbf{p})(\mathbf{v}_\iota \oplus \mathbf{v}_\mathbf{p})$ and $\widetilde{r}^2 = \iota_0^1 \iota_0^2 p_0^2 \mathbf{p} (1 + \mathbf{v}_\iota \cdot \mathbf{v}_\mathbf{p})(\mathbf{v}_\iota \oplus \mathbf{v}_\mathbf{p})$ obtained by illuminating the patches p^1 and p^2 with the same illuminant $(\iota_0^1 \iota_0^2, \mathbf{v}_\iota)$. It is clear that the two perceived colors $\psi_{\mathbf{o}^1}(r^1)$ and $\psi_{\mathbf{o}^2}(r^2)$ are perceived as equal if and only if their lightnesses in Equation (6.4.9) are equal.

Chapter 7

Related applications: a CAT for AWB

This chapter is about the very first application to color image processing of the new model described in the previous chapters. In Chapter 2 we have seen Yilmaz's original association between chromatic adaptation and Lorentz boosts, in Chapters 4 and 5 we formally motivated the presence of relativistic concepts within the quantum-like framework, finally, in the present chapter, we will see how to use a normalized Lorentz boost as a chromatic adaptation transform.

As references for the content of the present chapter one might look at [68] for a detailed exposition of the first version of the algorithm, and at Subsection 3.3.3 of [14] for an overview of the most recent one, where the links with the concepts exposed in Chapter 5, in particular Lüders operations and effects, are stressed out. Details about the last version of the algorithm and a first quantitative evaluation of its performance are presented here for the first time. Future projects involving this algorithm will be mentioned in Chapter 9.

7.1 Color constancy and white balance

Many aspects in color image processing are inspired by features of the HVS*. In Chapter 1 we have seen that trichromacy-based color spaces are inspired by the presence of three types of cone photoreceptors, while in Chapter 8 we will see that tone mapping algorithms are made to imitate visual adaptation. In the same spirit, white balance algorithms are meant to emulate the capability of the HVS to adapt to non-neutral illumination conditions. This phenomenon, known as *chromatic adaptation*, occurs at the level of both retinal cells and higher brain mechanisms, see [49] for further details about the physiological aspects of chromatic adaptation.

Chromatic adaptation is usually explained in terms of independent variations of the cone sensitivity functions, however, as underlined in [49], it is restrictive to consider it an early-level process, in fact also higher levels of the vision pipeline are involved, in particular the opponent level, see e.g. [76], and even the object recognition level.

Chromatic adaptation is the reason behind the so-called *color constancy* phenomenon, already mentioned in Subsection 1.3.2, i.e. the robustness of the HVS to describe perceived colors with the same chromatic attributes in spite of illuminant changes. Roughly speaking, from an evolutionary point of view, it is convenient for the HVS to perceive an object with a stable color under different illumination conditions, in order to better recognize and track it.

Automatic White Balance, AWB from now on, refers to the process of automatic detection and removal of an unwanted color cast on a digital image generated by the presence of a

*Acronym for Human Visual System.

non-neutral illuminant in the scene that is represented in the picture. The term *automatic* refers to the fact that the illuminant estimation is performed automatically. The aim of AWB algorithms is to recover an image representing the scene as it was enlightened by a neutral illuminant, or as if the scene was seen by an observer fully adapted to the non-neutral illuminant. More precisely AWB consists of two steps:

- an illuminant estimation algorithm, that identifies the illuminant(s) in the scene associating to it (each of them) a 3-dimensional vector $\vec{L}$;
- a Chromatic Adaptation Transform (CAT), parametrized by $\vec{L}$ that eliminates the presence of the illuminant returning an image as if the scene was lit by a neutral illuminant.

Modeling chromatic adaptation is a complex issue for several reasons: first of all the psychophysical phenomenon itself is very elaborate involving different levels of the visual chain, then, as we will see in following, the detection of the illuminant(s) to discard is an ill-posed problem, moreover the objective, as already underlined for the case of the lightness constancy, is to recover the *perceived* reflectance of the scene, and not the physical one. By perceived reflectance we mean, ideally, taking into account not just the cone response functions, but as well the opponent mechanism and other levels of the visual chain that are involved. Of course, the task becomes even more complex if one considers the case of incomplete adaptation to the illuminant.

In the following we are going to present the classic image formation model widely used in literature, underlining the assumptions on which it is based upon.

7.1.1 Image formation model

Let us start by fixing the notations. We call $\mathscr{I} \subset \mathbb{R}^2$ is the 2-dimensional support of a RGB digital image $\vec{I} = (I_R, I_G, I_B)$, where I_c is the RGB color channel of $\vec{I}$, with $c \in \{R, G, B\}$. The position of a generic pixel belonging to $\mathscr{I}$ will be denoted by $x = (x_1, x_2)$ and the image intensity $I_c(x)$ is supposed to be normalized in $[0, 1]$.

We must stress that this is essentially a physically-based model that aims at reconstructing the physical reflectance of the objects, in which the only perceptually-inspired element is the presence of the three camera sensitivity functions.

In the dichromatic reflection model [139, 61, 128], the scene elements are supposed to have both a specular and a diffused reflectance. A specular reflection is only visible if the normal vector of a shiny object is oriented precisely halfway between the direction of incoming light and the direction of the camera sensor. The diffused reflectance is due to the scattering between the light and the surface particles of an object, which produces an isotropic reflection of light. We denote by $m_s(x)$ and $m_d(x)$ the scale factors that weight the relative amount of specular and diffused reflectance, respectively, contributing to the overall light reflected at the location x. Let Λ be the visible spectrum, let $S_c(\lambda)$, with $c \in R, G, B$ and $\lambda \in \Lambda$, be the spectral sensitivity functions of the camera, and let $\rho = \rho(x, \lambda)$, with $x \in \mathscr{I}, \lambda \in \Lambda$, being the reflectance. Let $E(\lambda)$ be the illuminant spectrum, then the intensity of the pixel x is given by:

$$I_c(x) = m_d(x) \int_\Lambda \rho(x, \lambda) S_c(\lambda) E(\lambda) \mathrm{d}\lambda + m_s(x) L_c, \quad \forall c \in \{R, G, B\}, \tag{7.1.1}$$

where $L_c = \int_\Lambda S_c(\lambda) E(\lambda) \mathrm{d}\lambda$. If we point the camera towards the light source, we obtain the light vector $\vec{L} = (L_R, L_G, L_B)$ associated to the illuminant. In the Lambertian reflection

models, the specular reflection term is ignored, so that $m_d(x) \equiv 1$ and $m_s(x) \equiv 0$, and the resulting image formation model reduces to:

$$I_c(x) = \int_\Lambda \rho(x,\lambda) S_c(\lambda) E(\lambda) \mathrm{d}\lambda, \quad \forall c \in \{R,G,B\}, \tag{7.1.2}$$

The Lambert image formation model used in literature about AWB of single-illuminant digital images is based on the following assumption:

$$I_c(x) = \rho_c(x) L_c, \qquad \forall c \in \{R,G,B\}, \tag{7.1.3}$$

where ρ_c is the c-component of the reflectance of the point in the scene represented by the pixel x and L_c is c-component of the illuminant present in the scene. It is very important to stress that, in spite of the appealing simplicity of this formula, Equation (7.1.3) is far from being an accurate description of the real image formation process. In fact, to pass from the more accurate dichromatic model of Equation (7.1.1) to Equation (7.1.3), one needs to state the following three hypotheses:

1. there is no specular reflection in the scene;
2. the supports of the camera spectral sensitivity functions S_c are mutually disjoint;
3. the reflectance $\rho(x,\lambda)$ is constant for every $\lambda \in \mathrm{supp}(S_c)$, in such a way that $\rho(x,\lambda)$ becomes separated into $\rho_R(x), \rho_G(x), \rho_B(x)$.

Notice that we are excluding the particular case in which $\rho(x,\lambda) = \rho(x)$ for all $\lambda \in \Lambda$, in that case there is no need for the camera spectral sensitivity functions to have mutually disjoint supports. We are not considering as well the case in which the camera spectral sensitivity functions are dirac-like functions, in that case there is no need for the third hypothesis.

Both of the above cases are however unlikely to happen: the first one because too restrictive on the reflectance, the second one because it is not realistic in conventional digital photography.

Most of the AWB algorithms based on the image formation model represented by Equation (7.1.3) work in the same way: starting from the knowledge of $I_c(x)$ they want to estimate L_c in order to eliminate its presence, and so the unwanted color cast, by simple division. Of course, the illuminant estimation problem is ill-posed because in Equation (7.1.3) there is only one known quantity, i.e. $I_c(x)$, versus two unknown quantities, i.e. $\rho_c(x)$ and L_c.

We must stress that the perceptual aspect of the model described above is only the presence of the camera spectral sensitivity functions, in particular Hering opponent mechanism is not taken into account.

The scope of this chapter is to propose a new prototype of CAT arising from the theoretical model described in the previous chapters. In the following paragraphs we are going to provide a brief overview of existing illuminant estimation methods and CATs.

7.1.2 Illuminant estimation

To solve the ill-posed problem of Equation (7.1.3) various solutions have been proposed in the literature, see [61, 128]. Here we just consider the two most simple widely used, which are based on the white-patch (WP) and the gray-world (GW) hypotheses.

The first assumes that there is at least one patch with perfect reflectance in the visual scene, i.e. it exists $\bar{x}_c \in \mathscr{I}$ such that $\rho_c(\bar{x}_c) = 1$, so that $I_c(\bar{x}_c) = L_c$ for all $c \in \{R,G,B\}$. Let us call $L_c^{WP} = I_c(\bar{x}_c)$ for all $c \in \{R,G,B\}$ the illuminant estimation obtained with the WP method.

The latter hypothesis assumes that the spatial average reflectance in a visual scene is achromatic [24]. If we denote with $\bar{I}_c$ the spatial average of the image in the fixed chromatic channel c, then, it can be proven, see e.g. [128] that, the estimated illuminant is given by $L_c^{GW} = \bar{I}_c/k$ for all $c \in \{R, G, B\}$, with $k \in [0, 1]$. We stress that real-world images do not satisfy these hypothesis all the time: a simple example is given by a close-up image, which will typically show uniform areas that violate the assumptions above.

Clearly more advanced methods for global and local the illuminant estimation exist, see [61] for a good overview, the most recent ones are obtained using Machine Learning techniques. Notice that, for the case of multiple sources of illumination the illuminant vector depends on the pixel, thus $\vec{L} = \vec{L}(x)$.

7.1.3 Chromatic adaptation transforms

A CAT is meant to mimic the adaptation process, more precisely it takes as input an estimated illuminant vector[†] $\vec{L}$, and the input image $\vec{I}(x)$, with $x \in \mathscr{I}$ representing a scene enlightened by the estimated illuminant, and returns as output an image $\vec{I}'(x)$ representing how the scene would appear to an observer fully adapted to the illuminant.

The output image should represent the perceived reflectance of the scene, i.e. $I'_c(x) = \rho_c(x)$ for all $c \in \{R, G, B\}$, $x \in \mathscr{I}$. In other words $\vec{I}'(x)$ represents the scene as it was lit by a neutral illuminant. Equation (7.1.3), suggests that, given $\vec{I}(x)$ and knowing $\vec{L}$, then for all $x \in \mathscr{I}$ $\vec{I}'(x)$ is obtained via the pointwise multiplication

$$\begin{pmatrix} I'_R(x) \\ I'_G(x) \\ I'_B(x) \end{pmatrix} = \begin{pmatrix} 1/L_R & 0 & 0 \\ 0 & 1/L_G & 0 \\ 0 & 0 & 1/L_B \end{pmatrix} \begin{pmatrix} I_R(x) \\ I_G(x) \\ I_B(x) \end{pmatrix}. \tag{7.1.4}$$

Notice that this is equivalent to linearly rescale the spectral sensitivity functions $S_c(\lambda)$, $c \in \{R, G, B\}$ obtaining the new sensitivity functions $S'_c(\lambda)$ of an observer adapted to $\vec{L}$ are given by $S'_c(\lambda) = S_c(\lambda)/L_c$, $c \in \{R, G, B\}$, $\lambda \in \Lambda$.

Furthermore, notice that the RGB illuminant vector $\vec{L}$ is mapped into $(1, 1, 1)^t$ which is the white in RGB.

The diagonal correction method of Equation (7.1.4) is generally known as *von Kries* CAT [154]. This method is widely used in literature and applications, because of its simplicity and low computational cost. Usually, in the image processing pipeline, the CAT is applied on linear RGB images after demosaicing.

As underlined in Chapter 9 of [49], it is more correct to apply the von Kries CAT in the LMS domain, i.e. the estimated illuminant $\vec{L}$, the input image $\vec{I}(x)$ and the corrected one $\vec{I}'(x)$ should be represented using LMS coordinates, in particular this means using the LMS spectral sentitivity functions $S_c(\lambda)$ with $c \in \{L, M, S\}$ in Equation (7.1.2), instead of the camera sensitivity functions $S_c(\lambda)$ with $c \in \{R, G, B\}$.

For computational convenience the von Kries CAT is usually applied in the linear RGB domain. As stated in [61] about the von Kries CAT in RGB: '*Although this model is merely an approximation of illuminant change and might not accurately be able to model photometric changes, it is widely accepted as color correction model* [159, 56, 58, 162, 22] *and it underpins many color constancy algorithms*'. In both cases of LMS and linear RGB, the idea is that, since chromatic adaptation is approximately an early-level process in the vision pipeline, the CAT should be applied in a color domain describing the the early stage of vision, hence LMS,

[†]For the case of multi illuminant estimation it works in the same way, taking as input $\vec{L}(x)$.

or, by analogy, at the early stage of the image processing pipeline, thus in the linear RGB domain.

With the aim of providing a more accurate computational model for chromatic adaptation, several alternative CATs are present in literature, most of them are linear in the RGB or LMS domain. Often they are proposed as modifications of the von Kries CAT, e.g. [20]. For further details several CATs are described by Fairchild in Chapter 9 of [49], and a good survey about the state of the art chromatic adaptation transforms, methods and datasets was provided by the CIE in 2004 [1].

7.2 The normalized boost CAT in HCV

7.2.1 Preliminary assumptions and link with the theoretical model

The idea here is to use a normalized Lorentz boost, as defined in Chapter 5, as a CAT, to do so we are going to start by recalling some concepts mentioned in Chapter 5 to better contextualize the algorithm that we propose.

As we have seen in Chapter 5, Lüders operations act on generalized states. More precisely let us recall Equation (5.2.18), expressing the link between Lüders operations and normalized Lorentz boosts. Let $\mathbf{e} = (e_0, e_1, e_2) \in \mathcal{E}$ be an effect, let $\mathbf{v_e} \in \mathcal{D}$ be its chromatic vector such that $||\mathbf{v_e}|| < 1$. Let $s_0\mathbf{s}$ be a generalized state, then the Lüders operation parametrized by $\mathbf{e}$, acting on $s_0\mathbf{s}$, can be expressed as a linear operation on the state cone of the spin factor $\overline{\mathcal{C}}(\mathbb{R} \oplus \mathbb{R}^2)$ as follows:

$$\chi(\psi_{\mathbf{e}}(s_0\mathbf{s})) = \frac{s_0 e_0}{\gamma_{\mathbf{v_e}}} B(\mathbf{v_e}) \frac{1}{2} \begin{pmatrix} 1 \\ \mathbf{v_s} \end{pmatrix} = B_N(\mathbf{e}) \frac{s_0}{2} \begin{pmatrix} 1 \\ \mathbf{v_s} \end{pmatrix}, \tag{7.2.1}$$

with

$$\gamma_{\mathbf{v_e}} := \frac{1}{\sqrt{1 - \|\mathbf{v_e}\|^2}}. \tag{7.2.2}$$

$B(\mathbf{v_e})$ is the Lorentz boost parametrized by $\mathbf{v_e}$, and $B_N(\mathbf{e})$ is the normalized boost parametrized by $\mathbf{e}$. Let us recall as well that the explicit expression $B_N(\mathbf{e})$, as in Equations (5.2.15) and (5.2.17), is given by

$$[B_N(\mathbf{e})] = \frac{e_0}{\gamma_{\mathbf{v_e}}} [B(\mathbf{v_e})] = \frac{e_0}{\gamma_{\mathbf{v_e}}} \begin{pmatrix} \gamma_{\mathbf{v_e}} & \gamma_{\mathbf{v_e}} \mathbf{v_e}^t \\ \gamma_{\mathbf{v_e}} \mathbf{v_e} & \sigma_0 + \frac{\gamma_{\mathbf{v_e}}^2}{1+\gamma_{\mathbf{v_e}}} \mathbf{v_e} \mathbf{v_e}^t \end{pmatrix}, \tag{7.2.3}$$

We recall that in Yilmaz's model, see Chapter 2 or [166, 165], he proposed a simple boost to model chromatic adaptation. Brill and West [23] underlined the necessity of a normalizing factor, we justify its presence through the theoretical model, in particular by Equation (7.2.1).

Let us now understand how to use $B_N(\mathbf{e})$ as a CAT. Notice that $B_N(\mathbf{e}) : \overline{\mathcal{C}}(\mathbb{R} \oplus \mathbb{R}^2) \to \overline{\mathcal{C}}(\mathbb{R} \oplus \mathbb{R}^2)$ acts linearly on the state cone of the spin factor $\overline{\mathcal{C}}(\mathbb{R} \oplus \mathbb{R}^2)$. If one considers $B_N(\mathbf{e})$ as acting on $\mathbb{R} \oplus \mathbb{R}^2$, then it is stable on $\overline{\mathcal{C}}(\mathbb{R} \oplus \mathbb{R}^2)$. Let us recall Equation (5.1.2), expressing the parametrization of $\overline{\mathcal{C}}(\mathbb{R} \oplus \mathbb{R}^2)$:

$$\overline{\mathcal{C}}(\mathbb{R} \oplus \mathbb{R}^2) = \left\{ \begin{pmatrix} \alpha \\ \alpha \mathbf{v_s} \end{pmatrix}, \ \alpha \geq 0, \ \mathbf{v_s} \in \mathcal{D} \right\}. \tag{7.2.4}$$

Furthermore, since $||\mathbf{v_e}|| < 1$, the matrix $B(\mathbf{v_e})$ is invertible and it is easy to prove that $B(\mathbf{v_e})^{-1} = B(-\mathbf{v_e})$, hence

$$B_N(\mathbf{e})^{-1} = \frac{\gamma_{\mathbf{v_e}}}{e_0} B(-\mathbf{v_e}). \tag{7.2.5}$$

Since $\gamma_{\mathbf{v_e}} = \gamma_{-\mathbf{v_e}}$, an explicit expression for $B_N(\mathbf{e})^{-1}$ is given by

$$[B_N(\mathbf{e})^{-1}] = \frac{\gamma_{\mathbf{v_e}}}{e_0}[B(-\mathbf{v_e})] = \frac{\gamma_{\mathbf{v_e}}}{e_0} \begin{pmatrix} \gamma_{\mathbf{v_e}} & -\gamma_{\mathbf{v_e}} \mathbf{v_e}^t \\ -\gamma_{\mathbf{v_e}} \mathbf{v_e} & \sigma_0 + \frac{\gamma_{\mathbf{v_e}}^2}{1+\gamma_{\mathbf{v_e}}} \mathbf{v_e} \mathbf{v_e}^t \end{pmatrix}. \tag{7.2.6}$$

Let us underline one last property of the theoretical model, that will be used in the following. Let us consider the effect $\mathbf{e}$, by self-duality we can associate to it a generalized state $e_0\mathbf{s_e}$, where $\mathbf{s_e}$ is a state whose chromatic vector is $\mathbf{v_e}$. Let us consider the representation of $e_0\mathbf{s_e}$ as an element of $\overline{\mathcal{C}}(\mathbb{R} \oplus \mathbb{R}^2)$, then it is not hard to prove, via straightforward computations using Equation (7.2.6), that

$$B_N(\mathbf{e})^{-1} \begin{pmatrix} e_0 \\ e_0 \mathbf{v_e} \end{pmatrix} = \begin{pmatrix} 1 \\ \mathbf{0} \end{pmatrix}. \tag{7.2.7}$$

In other words *the generalized state* $e_0\mathbf{s_e}$ *is mapped into the achromatic state of maximal entropy* $\mathbf{s_a}$.

Now we are ready to relate the concepts and properties recalled above to the problem of defining a CAT. As in Section 7.1, let $\vec{I}(x) = (I_R(x), I_G(x), I_B(x))^t$ be the input image, not white balanced, represented in the RGB domain, with $x \in \mathscr{I}$ on which we want to apply the CAT. Let $\vec{L} = (L_R, L_G, L_B)^t$ be the estimated illuminant vector[‡]. Let $\vec{I}'(x) = (I'_R(x), I'_G(x), I'_B(x))^t$ be the output image after the application of the CAT.

For all $x \in \mathscr{I}$ we want to perform the following associations:

- $\vec{I}(x)$ and $\vec{I}'(x)$ to elements of $\overline{\mathcal{C}}(\mathbb{R} \oplus \mathbb{R}^2)$;
- $\vec{L}$ to $\mathbf{e}$, or equivalently, by self-duality, to the generalized state $e_0\mathbf{s_e}$ described before.

As we have seen for the von Kries CAT in RGB, the main idea underlying a CAT is that it should map the illuminant vector $\vec{L}$ to the white. Suppose we are able to perform the associations above, then $B_N(\mathbf{e})^{-1}$ is a good candidate for a CAT, because, by Equation (7.2.7), it maps the vector $(e_0, e_0\mathbf{v_e})^t$, associated to the illuminant vector $\vec{L}$, into $(1, \mathbf{0})^t$ corresponding to the state of maximal entropy $\mathbf{s_a}$, representing white in $\overline{\mathcal{C}}(\mathbb{R} \oplus \mathbb{R}^2)$.

It is important to stress that $\overline{\mathcal{C}}(\mathbb{R} \oplus \mathbb{R}^2)$ is not a color space in the sense of the state-of-the art trichromacy based color solids, see Section 1.1 of Chapter 1, but it provides the basic mathematical framework on which the theoretical model detailed in Chapters 3, 4 and 5 is built. Nevertheless, the association between elements of $\overline{\mathcal{C}}(\mathbb{R} \oplus \mathbb{R}^2)$ and coordinates of trichromacy-based color solids (or their modifications) is fundamental to start implementing concrete applications to color image processing. Clearly, it is a non trivial aspect with a great margin of improvement. On the long term we do believe that the support of psychovisual data and ML techniques will be necessary to fully accomplish this task. Some first simple steps in this direction can be found in Section 7.3, or in Chapter 9. As we will see in the rest of this chapter, even tests of the model performed in an approximated color domain give satisfactory first results.

RGB is not a suitable color domain to perform easy associations with elements of $\overline{\mathcal{C}}(\mathbb{R} \oplus \mathbb{R}^2)$. Hence we need to change color domain to represent $\vec{I}(x)$, $\vec{I}'(x)$ and $\vec{L}$. An adequate choice

[‡]We recall that the multi-illuminant case is analogous, with $\vec{L} = \vec{L}(x)$.

should be a conic-shaped color solid with circular section, as e.g. the one depicted in Figure 2.1.1 (b). Clearly several options are available in literature, however most of the recently developed color spaces do not have circular section. The simplest choice, furfilling these properties, is given by the classic HCV (Hue Chroma Value) color space. We will discuss about the absence of Hering's opponency in HCV and some simple solutions to this issue in Section 7.3. Moreover, another candidate for a new color solid in which it would be possible to test the CAT proposed in this chapter will be mentioned among the future projects in Chapter 9.

We consider now $\vec{I}(x)$, $\vec{I}'(x)$ represented in the HCV color space, for all $x \in \mathscr{I}$, thus $I_c(x), I'_c(x)$, with $c \in \{H, C, V\}$. In the following we will omit the dependence on the pixel x and use the notation $H = I_H, C = I_C, V = I_V, H' = I'_H, C' = I'_C, V' = I'_V$.

We are ready now to perform associations between $\overline{\mathcal{C}}(\mathbb{R} \oplus \mathbb{R}^2)$ and the HCV color space. Let us recall that in HCV the value V represents the achromatic coordinate, moreover the HCV color space is converted in the HSV where S is the saturation obtained from C and V via $S = C/V$.

Let us consider an element of $\overline{\mathcal{C}}(\mathbb{R} \oplus \mathbb{R}^2)$, $(s_0, s_0\mathbf{v_s})^t$ with $s_0 \geq 0$ and $\mathbf{v_s} \in \mathcal{D}$. Let $r_\mathbf{s}, \vartheta_\mathbf{s}$ be the polar coordinates of the vector $\mathbf{v_s}$. We perform the following associations:

$$\begin{cases} \vartheta_\mathbf{s} \equiv H \\ s_0 r_\mathbf{s} \equiv C \\ s_0 \equiv V \\ r_\mathbf{s} \equiv S \end{cases} . \tag{7.2.8}$$

The same holds for the primed variables. Thanks to the associations above, we are now able to identify the input and output images $(H(x), C(x), V(x))^t$ and $(H'(x), C'(x), V'(x))^t$, for $x \in \mathscr{I}$, with elements of $\overline{\mathcal{C}}(\mathbb{R} \oplus \mathbb{R}^2)$.

Analogously, let us consider the illuminant vector $\vec{L}$, represented in the HSV domain, hence L_c, with $c \in \{H, S, V\}$. In the following we will use the notation $L_H = \phi$, $L_S = \sigma, L_V = \varepsilon$. We can perform analogous identifications between $\vec{L}$ and $\mathbf{e}$ as follows

$$\begin{cases} \vartheta_\mathbf{e} \equiv \phi \\ e_0 \equiv \varepsilon \\ r_\mathbf{e} \equiv \sigma \end{cases} , \tag{7.2.9}$$

$r_\mathbf{e}, \vartheta_\mathbf{e}$ being the polar coordinates of $\mathbf{v_e}$. Doing the same for the Lorentz factor we obtain

$$\gamma_{\mathbf{v_e}} \equiv \Gamma, \qquad \text{with} \qquad \Gamma = \frac{1}{\sqrt{1 - \sigma^2}}. \tag{7.2.10}$$

In the same way we can associate to $[B_N(\mathbf{e})^{-1}]$ a matrix, let us call it Ω. $B_N(\mathbf{e})^{-1}$ is parametrized by $\mathbf{e}$, and, in the same way Ω will be parametrized by the HSV coordinates of $\vec{L}$, i.e. $\phi, \sigma, \varepsilon$. Before writing the explicit expression for Ω we must make two remarks: the first one is that $B_N(\mathbf{e})^{-1}$ is applied on the Cartesian components of the vector $s_0\mathbf{v_s}$. Let us call $\alpha(x), \beta(x)$ and $\alpha'(x), \beta'(x)$ the Cartesian coordinates of $H(x), C(x)$ and $H'(x), C'(x)$, respectively, for all $x \in \mathscr{I}$. Then $(\alpha', \beta', V')^t = \Omega(\alpha, \beta, V)^t$. The second remark is that in the parametrization of $\overline{\mathcal{C}}(\mathbb{R} \oplus \mathbb{R}^2)$ the magnitude of the generalized state is in the first position, while in α, β, V the achromatic is placed in the last one.

Writing $[B_N(\mathbf{e})^{-1}]$ as the achromatic coordinate occupied the last position would lead to the following matrix, that we want to identify with Ω:

$$\frac{\gamma_{\mathbf{v_e}}}{e_0}\begin{pmatrix}\sigma_0+\frac{\gamma_{\mathbf{v_e}}^2}{1+\gamma_{\mathbf{v_e}}}\mathbf{v_e}\mathbf{v_e}^t & -\gamma_{\mathbf{v_e}}\mathbf{v_e}\\ -\gamma_{\mathbf{v_e}}\mathbf{v_e}^t & \gamma_{\mathbf{v_e}}\end{pmatrix}\equiv\Omega. \tag{7.2.11}$$

Using the identifications of Equations (7.2.11) and (7.2.10), it is possible, after some computations, to obtain the following explicit expression for Ω:

$$\Omega=\frac{\Gamma}{\varepsilon}\begin{pmatrix}\Gamma\cos^2\phi+\sin^2\phi & (\Gamma-1)\cos\phi\sin\phi & -\sigma\Gamma\cos\phi\\ (\Gamma-1)\cos\phi\sin\phi & \Gamma\sin^2\phi+\cos^2\phi & -\sigma\Gamma\sin\phi\\ -\sigma\Gamma\cos\phi & -\sigma\Gamma\sin\phi & \Gamma\end{pmatrix}, \tag{7.2.12}$$

where Γ is as in Equation (7.2.10). Notice that Ω is fully determined by the HSV coordinates of the illuminant vector ϕ,σ,ε.

7.2.2 The normalized Lorentz boost CAT

In the previous subsection we have underlined the motivations and conditions under which the theoretical model lead to a CAT. This subsection is dedicated to a succinct exposition of the steps needed to implement it and some qualitative considerations about the outputs.

Let $\vec{I}(x)=(R(x),G(x),B(x))$, with $x\in\mathscr{I}$ be the input RGB image, let $\vec{L}=(L_R,L_G,L_B)$ be the estimated illuminant vector[§]. Let $\vec{I'}(x)=(R'(x),G'(x),B'(x))$, with $x\in\mathscr{I}$, be the corrected output image. We will use unprimed coordinates to represent the image before applying the CAT Ω and primed coordinates to represent the image after applying Ω.

In the sequel we will need to use conversion formulas from RGB to HSV or HCV and viceversa. These transformations are customary in literature and implemented in several open source Python packages. Here we mention just the map from RGB to HCV, for its inverse function and further details see e.g. Appendix B in [167], or [145]. Let $R,G,B\in[0,1]^3$ and $H\in[0,2\pi)$, $C,V\in[0,1]^2$ then:

$$\begin{cases}C:=\max(R,G,B)-\min(R,G,B)\\ V:=\max(R,G,B)\\ H:=\frac{\pi}{3}\begin{cases}0 & \text{if } C=0\\ \frac{G-B}{C} & \text{if } V=R\\ \frac{B-R}{C}+2 & \text{if } V=G\\ \frac{R-G}{C}+4 & \text{if } V=B\end{cases}\end{cases}. \tag{7.2.13}$$

Let us now show the steps to obtain the corrected RGB image $\vec{I'}(x)$, given an input RGB image $\vec{I}(x)$ and the estimated illuminant $\vec{L}$.

1. We start by calculating the HSV coordinates of the RGB illuminant vector:

$$\vec{L}=\begin{pmatrix}L_R\\L_G\\L_B\end{pmatrix}\longmapsto\begin{pmatrix}L_H\\L_S\\L_V\end{pmatrix}=:\begin{pmatrix}\phi\\\sigma\\\varepsilon\end{pmatrix} \tag{7.2.14}$$

[§] $\vec{L}(x)$ with $x\in\mathscr{I}$ for the multi-illuminant case.

2. Using the parameters $\phi, \sigma, \varepsilon$ we can write the CAT matrix:

$$\Omega = \frac{\Gamma}{\varepsilon} \begin{pmatrix} \Gamma\cos^2\phi + \sin^2\phi & (\Gamma-1)\cos\phi\sin\phi & -\sigma\Gamma\cos\phi \\ (\Gamma-1)\cos\phi\sin\phi & \Gamma\sin^2\phi + \cos^2\phi & -\sigma\Gamma\sin\phi \\ -\sigma\Gamma\cos\phi & -\sigma\Gamma\sin\phi & \Gamma \end{pmatrix}, \qquad \Gamma = \frac{1}{\sqrt{1-\sigma^2}}. \tag{7.2.15}$$

3. Then we convert the input RGB image in HCV coordinates:

$$\vec{I}(x) = \begin{pmatrix} R(x) \\ G(x) \\ B(x) \end{pmatrix} \longmapsto \begin{pmatrix} H(x) \\ C(x) \\ V(x) \end{pmatrix}. \tag{7.2.16}$$

4. We convert the polar coordinates HC into Cartesian coordinates that we call α, β:

$$\begin{pmatrix} H(x) \\ C(x) \\ V(x) \end{pmatrix} \longmapsto \begin{pmatrix} \alpha(x) \\ \beta(x) \\ V(x) \end{pmatrix} := \begin{pmatrix} C(x)\cos H(x) \\ C(x)\sin H(x) \\ V(x) \end{pmatrix}. \tag{7.2.17}$$

5. We apply the matrix Ω calculated in point 2. to the input image represented in $\alpha\beta V$ coordinates, obtaining the corrected image $\vec{I}'(x)$ represented in the $\alpha\beta V$ domain:

$$\begin{pmatrix} \alpha(x) \\ \beta(x) \\ V(x) \end{pmatrix} \longmapsto \begin{pmatrix} \alpha'(x) \\ \beta'(x) \\ V'(x) \end{pmatrix} := \Omega \begin{pmatrix} \alpha(x) \\ \beta(x) \\ V(x) \end{pmatrix}. \tag{7.2.18}$$

6. We come back from the $\alpha\beta V$ domain to RGB, firstly converting $\alpha'\beta'$ into polar coordinates $H'C'$, and then applying the conversion function from HCV to RGB:

$$\begin{pmatrix} \alpha'(x) \\ \beta'(x) \\ V'(x) \end{pmatrix} \longmapsto \begin{pmatrix} H'(x) \\ C'(x) \\ V'(x) \end{pmatrix} = \begin{pmatrix} \arctan\left(\beta'(x)/\alpha'(x)\right) \\ \sqrt{\alpha'^2(x) + \beta'^2(x)} \\ V'(x) \end{pmatrix} \longmapsto \begin{pmatrix} R'(x) \\ G'(x) \\ B'(x) \end{pmatrix}, \tag{7.2.19}$$

The only difference between the single illuminant, and the multi-illuminant case is that the CAT matrix depends as well on the pixel $\Omega = \Omega(x)$.

To summarize, the chain of operations performed, omitting the dependence on x, is

$$\begin{pmatrix} R \\ G \\ B \end{pmatrix} \longmapsto \begin{pmatrix} H \\ C \\ V \end{pmatrix} \longmapsto \begin{pmatrix} \alpha \\ \beta \\ V \end{pmatrix} \longmapsto \begin{pmatrix} \alpha' \\ \beta' \\ V' \end{pmatrix} = \Omega \begin{pmatrix} \alpha \\ \beta \\ V \end{pmatrix} \longmapsto \begin{pmatrix} H' \\ C' \\ V' \end{pmatrix} \longmapsto \begin{pmatrix} R' \\ G' \\ B' \end{pmatrix}. \tag{7.2.20}$$

Figure 7.1 shows some examples of outputs of the algorithm described above, together with the non corrected inputs, and outputs of the classical von Kries CAT for visual comparison.

One common problem of CATs is that, depending on the illuminant estimation, clipping can occur. This supplementary clipping process leads to false colors and artifacts. This is the case as well for the von Kries CAT. We have noticed that in the normalized boost is less affected by this issue than the simple boost that we proposed in [68], and also with respect to the von Kries CAT.

Using the normalized boost CAT the clipped pixels are less numerous than the von Kries CAT and generally placed at e.g. the highlights on highly reflective objects objects or some white parts of the depicted toys. These artifacts are hence not due to a problem in the CAT, but to the fact that there is a single-illuminant vector through which the image is corrected. In other words e.g. the highlights in the image are clipped because they are brighter and whiter than what it was estimated to be the white (in this case the white patch of the color checker). We performed as well tests on images with multi illuminant ground truth maps $\vec{L}(x)$, i.e. a different illuminant vector for each pixel, [82] and this problem does not occur.

There are two common solutions to the clipping issue:

- clipping the affected pixels, hence putting equal to 1 the RGB values of the output image which are greater than 1;
- dividing the image by its maximum, i.e. $\vec{I}'(x)/M$, with $M = \max_{\substack{c\in\{R,G,B\}\\ x\in\mathscr{I}}} I_c(x)$.

For the pictures showed in this chapter we preferred to use the first option, because it gives brighter images, while for the quantitative tests presented in Section 7.4, or in general for image processing applications, is customary to choose the second one. One technical reason is that AWB is generally applied at the early stages of the image processing pipeline, in the RGB RAW linear domain just after demosaicing. In general images in the linear domain are darker, because they will be brightened by applying tone mapping, thus passing to a non-linear domain, later in the chain.

Figure 7.1: *Left*: input image. *Center*: output image after white balance using the von Kries CAT. *Right*: output image after white balance using the normalized Lorentz boost CAT. The white balanced images have been obtained using the same illuminant estimation, performed manually on the white patch of the color checker present in each image. The image of the first row belongs to the ColorChecker Dataset [59, 142], while the others belong to the NUS Indoor Dataset [30].

From a first visual comparisons the CAT that we propose seems to be better at rendering

details in the scene, it is theoretically based and, as underlined before, it is less affected by artifacts, which are only due to the non-globality of the illuminant estimation. Computational time is slightly longer with respect to the von Kries CAT, because color space conversions are needed.

We do believe that this aspect can be improved, e.g. using the linear color domain proposed among the future projects in Chapter 9.

The color rendering seems visually good or comparable with the von Kries CAT. Nevertheless if we pay attention to the red hues, we can see that some of them tend to turn a bit pinkish, this might be better seen in the last picture in Figure 7.1 on the white-red box with a flower depicted on it, whose red looks too turned towards the magenta in the normalized boost CAT output w.r.t. the von Kries one, or the input. In the following section we will see that this issue is related to the use of the HCV color domain, hence we will propose simple alternative color domains that solve this problem, as depicted in Figure 7.2.

7.3 A modified HCV space encoding Hering's opponency

One of the reasons why the HCV color domain is not a good choice to mimic the state cone $\overline{\mathcal{C}}(\mathbb{R} \oplus \mathbb{R}^2)$ is that it lacks of one of the most important properties of the theoretical model: Hering's opponent mechanism.

Indeed, as depicted in Figure 7.3 (a), the HCV color space, or analogously HSV, inherits the hue positioning on the circle from RGB, thus the red, green and blue hues are equidistant on the circle, while the yellow is placed halfway between the red and the green as follows:

$$H(R) = 0, \qquad H(Y) = \frac{\pi}{3}, \qquad H(G) = \frac{2\pi}{3}, \qquad H(B) = \frac{4\pi}{3}. \tag{7.3.1}$$

Thus yellow and blue are diametrically opposed, while red and green are separated by an angle of 60°, so in HCV the opponent hue to red is cyan. It has to be noted that in Hering's opponent theory it is not clear exactly which shades of the four unique hues are opponent, nor if the two opponent axes have to be orthogonal.

With the aim of correcting the problem of red objects slightly shifting to magenta underlined at the end of the previous section, we tried to propose an alternative color domain to HCV in which implement the normalized boost CAT. This new color solid was obtained from the HCV color solid[¶], by modifying only the hue coordinate H. The objective was to obtain a color domain like HCV, but endowed with Hering's opponent mechanism.

To do so we tried several functions, using simple interpolation techniques in 1-dimension, to modify the hue configuration on the circle. The objective was to approximately recover the, not necessarily orthogonal, Hering's opponent axes. We selected the two best performing functions f_1, f_2 on the images. Let us call H_1CV and H_2CV the two color solids obtained from HCV using f_1 and f_2. As one can see in Figure 7.2 the normalized boost CAT implemented in H_1CV or H_2CV does not have anymore the of the slight shift towards magenta of the red objects that occurred in HCV, see in particular the white-red box with a flower depicted on it.

[¶]The same modification should be done as well for the HSV color space, since needed at the step 1. of the algorithm described in Subsection 7.2.2. Since only the hue is involved, the transformation is the same as the one applied to HCV.

Let us explain a but more in detail how f_1 and f_2 have been obtained. Both $f_1, f_2 : [0, 2\pi] \to [0, 2\pi]$ are 2π-periodic and invertible, their plots are illustrated in Figure 7.4. The coordinates H_i to change color space are obtained from the H coordinate of HCV by $H_i = f_i^{-1}(H)$, $i = 1, 2$. In particular

1. f_1 is obtained requiring the red to stay be the same, and the green to be diametrically opposed to the red, hence it is obtained by quadratic interpolation of the points $(0, 0), (2\pi/3, \pi), (2\pi, 2\pi)$. It can be explicitly written as a parabola $f_1(x) = \frac{1}{4}\left(7x - \frac{3}{2\pi}x^2\right)$. As depicted in Figure 7.3 (b), red and green are now opponent, but the blue is diametrically opposed to an orangish yellow. Furthermore these opponent axes are not orthogonal, but are separated by an angle of 30°.

2. f_2 is obtained by fixing again the red and moving the green to be diametrically opposed to it, then moving the yellow and the blue in order to have an angle of 60° between the two opponent axes, as in Figure 7.3 (c). f_2 was obtained via quadratic piece-wise interpolation of the points $(0, 0), (\pi/3, 2\pi/3), (2\pi/3, \pi), (4\pi/3, 5\pi/3), (2\pi, 2\pi)$.

Figure 7.2: *Left*: output of the normalized boost CAT implemented in HCV. *Center*: output of the normalized boost CAT implemented in H_1CV. *Right*: output of the normalized boost CAT implemented in H_2CV. These images have been obtained from the NUS Indoor Dataset [30].

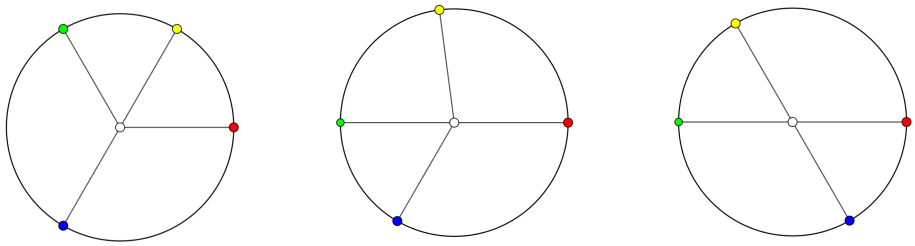

(a) HCV (b) H_1CV (c) H_2CV

Figure 7.3: Red, yellow, green and blue hue positions in the hue-chroma planes of the HCV, H_1CV and H_2CV color spaces.

We have remarked that the normalized boost CAT gives visually slightly better results in H_1CV than in H_2CV. The quantitative evaluations presented in the following section are coherent with this fact. Visually the outputs in H_2CV appear to be a little desaturated w.r.t. the ones in HCV or in H_1CV. This might seem strange, because the only thing that was modified is the hue coordinate, however this is just a case correlation among the coordinates of the state-of-the art color solids, as the ones mentioned in Section 1.3 of Chapter 1.

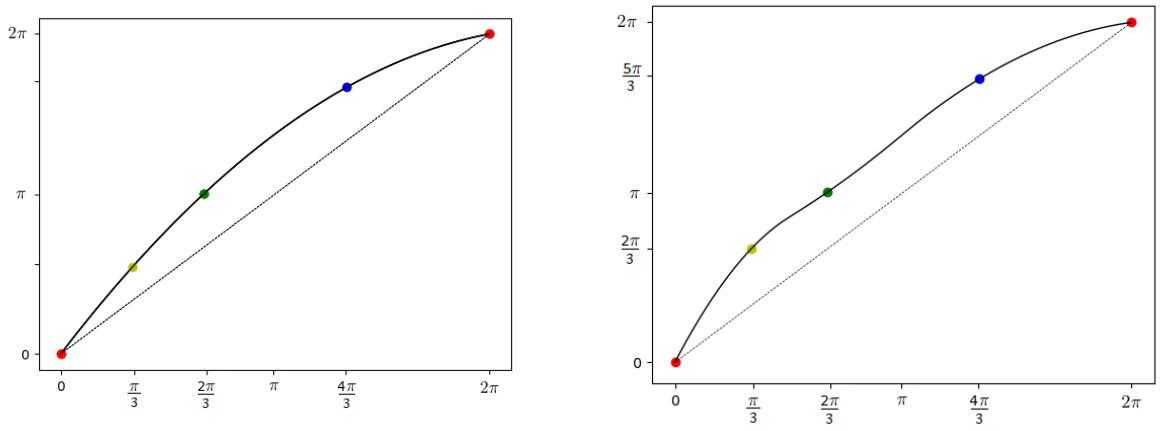

Figure 7.4: Plots of the two functions used to recover Hering's opponent mechanism in the HCV color space. *Left*: plot of f_1. *Right*: plot of f_2.

7.4 A first quantitative evaluation

Generally datasets like the mentioned ones in Figure 7.1, are used with the purpose of performing quantitative tests on single-illuminant estimation algorithms. In this section we are going to talk about a first quantitative evaluation of the normalized Lorentz boost CAT, in particular we want to measure the rendering of the color checker in images corrected using the von Kries CAT, the normalized boost CAT in HCV, and in its modifications H_1CV and H_2CV presented in the previous section, to compare their performances.

We chose to use the NUS Indoor Dataset[‖] (Canon 1Ds Mark III, 105 images) [30]. The procedure that we adopted to obtain the quantitative evaluations of the color checker rendering is schematized in Figure 7.5.

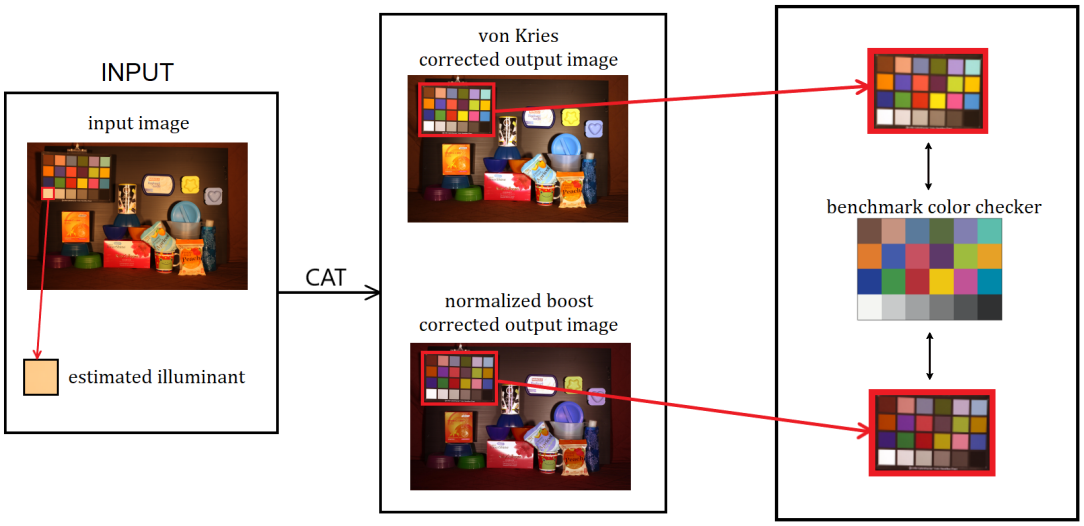

Figure 7.5: Schematic representation of the quantitative evaluation of the color checker rendering of different CATs.

We started by generating linear png images applying linear demosaicing on the RAW

[‖] Available at https://cvil.eecs.yorku.ca/projects/public_html/beyond/beyond.html.

images provided with the dataset. We automatically detected the color checker present in each image and extracted the nineteenth patch (the white one) as ground truth illuminant vector. The automatic detection of the color checker was done using the Checker Detection functions available in the open-source Python package *Colour*[**]. Using the extracted ground truths we corrected the mentioned png images using four different CATs: von Kries, normalized boost in HCV, normalized boost in H_1CV and normalized boost in H_2CV. Clipping cases were managed by dividing the image by its maximum. Then we detected all the color checkers in the output images, still using the Checker Detection functions.

We chose to use some color metrics, more precisely CIE ΔE 1994 [103], DIN99 [4], CIE ΔE 2000 [102, 111], ΔE CIECAM02 [105] and ΔE CIECAM16 [101], as they are implemented in the package *Colour*.

For each CAT we considered the set of detected color checkers and we calculated the distance between each of them and the standard benchmark color checker enlightened by D65 illuminant. This distance was obtained by calculating, for each patch, its distance from the corresponding one in the benchmark color checker and then averaging over the 24 patches. For each CAT we averaged the distances of the color checkers over the 105 images of the dataset, obtaining the values reported by Table 7.1.

metrics	von Kries	L in HCV	L in H_1CV	L in H_2CV
CIE 1994	25.66	25.01	24.86	**24.85**
DIN99	26.25	25.48	**25.28**	25.39
CIEDE 2000	22.53	**22.10**	22.44	22.41
CAM02 UCS	25.99	**25.31**	**25.31**	25.34
CAM02 LCD	33.87	32.99	**32.84**	32.93
CAM16 UCS	26.01	**25.28**	25.31	25.35
CAM16 LCD	33.87	32.99	**32.84**	32.94

Table 7.1: Average distances from the stan, von Kries CAT, normalized Lorentz boost in HCV, normalized Lorentz boost in H_1CV, normalized Lorentz boost in H_2CV.

Lower values in the previous table mean that the color checker rendering of a certain CAT is closer to the benchmark color checker. We can see that, as predicted qualitatively in the previous section, H_1CV is better performing than H_2CV. Furthermore, according to this evaluation, it a bit is better to use the implementation in H_1CV than in HCV, and both of them have better results than the von Kries CAT. However it must be noted that the value differences between the columns are sometimes of the order of decimals. It is known that ΔE values lower than 2 are not noticeable by the human eye. One might see that, however, e.g. the yellow patch of the color checker in the images depicted in Figure 7.1 and 7.2 looks different when corrected with different CATs. This is probably due to the fact that the distance is averaged over all the paches of the color checker.

We want to stress that this is a first simple quantitative evaluation, among the future projects in Chapter 9 we are going to mention the idea of testing the normalized boost CAT, using specific datasets created for CATs: the so-called *corresponding colors*.

[**]See https://colour.readthedocs.io/en/develop/.

Chapter 8

Related applications: Tone Mapping

In this chapter we will start by briefly introducing the problem of tone mapping of high dynamic range (HDR) images and the classic tone mapping operator known as *Naka-Rushton equation*. Then, in Section 8.2 we will provide a geometric interpretation of this equation analyzing it as a Möbius transformation. This is related to the model presented in Chapters 3 and 5, because Möbius transformations can be characterized as cross-ratio preserving maps, and, moreover, they are related to the construction of the classic models of hyperbolic geometry, see e.g. [131]. This part of the chapter will be essentially based on [125]. In Section 8.3 we will propose a work-in-progress tone mapping operator inspired by Klein's disk construction, related to the structure of $\mathcal{S}(\mathcal{A})$, mentioned in Chapter 3.

8.1 The Naka-Rushton equation and its use for tone mapping

High Dynamic Range (HDR) images provide a way to store real-world radiance values, e.g. by combining multiple photos of a scene taken with different time exposures following the classical work of Debevec and Malik [39]. However, since the real-world radiance can span up to 10 orders of magnitude and ordinary displays can only span up to two orders of magnitude, a further 'compression step', called 'Tone Mapping' (TM) is required to properly visualize the information stored in the HDR images.

Following Ward et al. [157], the large majority of tone mapping operators are devised to reproduce detail visibility and emulating as much as possible contrast and color sensation of the real-world scene. Ideally, a perfect model of the Human Visual System (HVS) would satisfy these requests, however the knowledge about human vision is still too vague to permit the construction of such a model, so that simplified and partial HVS descriptions are needed.

In this sense, it is quite remarkable that the sole use of the visual adaptation step already provides a remarkably good tone mapping. The visual adaptation phase, as we will see in the following, occurs when photoreceptors (cones and rods) strongly compress the light range around an average (adaptation) value. This process can be described by the Naka-Rushton equation [114] which has been widely used as a global TM operator, for a thorough review see e.g. [134, 52, 53, 54, 128, 9].

Let us recall how the retina responds to light stimuli. The range of radiances over which the HVS can operate is very large: from 10^{-6}cd/m^2 (scotopic limit) to 10^6 cd/m^2 (glare limit) [163]. The automatic process that allows the HVS to operate over such a huge range is called *visual adaptation* [140].

However, the HVS cannot operate over this entire range simultaneously. Rather, it adapts to an average intensity and handles a smaller magnitude interval. There is no complete agreement in the literature about the precise value of this range, which can vary from two ([140] page 326) up to four orders of magnitude ([81] page 670).

Empirical experiments have shown that visual adaptation occurs mainly in the retina. The experiments to measure this behavior were performed using very simple, non-natural images: brief pulses of light with intensity $\mathcal{I}$ superimposed on a uniform background. When a photoreceptor absorbs $\mathcal{I}$, the electric potential of its membrane changes accordingly to the empirical law known in vision research literature as Naka-Rushton's equation [114, 140, 98]:

$$r(\mathcal{I}) = \frac{\mathcal{I}}{\mathcal{I} + \mathcal{I}_s}, \tag{8.1.1}$$

where $r(\mathcal{I})$ is the normalized response of the retina to $\mathcal{I}$ and $\mathcal{I}_s$ is the light level at which the photoreceptor response is half maximal, called *semisaturation level* and which is usually associated with the level of adaptation. Some authors report the formula writing the γ power of $\mathcal{I}$ and $\mathcal{I}_s$, in this case the equation is called Michaelis-Menten's formula ([98] page 301).

The reason why this formula has received so much attention from the tone mapping community is because it permits to compress any given range of the light stimuli into the interval $[0, 1]$ (since $\mathcal{I}$ and $\mathcal{I}_s$ are light intensity levels, hence they are both positive) in such a way that the details in dark areas are enhanced and the ones in the higher areas are compressed, see Figure 8.2, which is coherent with the well-known Weber-Fechner's law [163].

Let us now see how Naka-Rushton's equation is used in the context of HDR imaging. We denote with $\mathscr{I} \subset \mathbb{R}^2$ the spatial domain of an RGB high dynamic range image $\vec{I} : \mathscr{I} \to (0, +\infty)^3$, $\mathscr{I} \ni x \mapsto (I_R(x), I_G(x), I_B(x))$, I_c being the scalar chromatic component of $\vec{I}$, $c \in \{R, G, B\}$, where $x = (x_1, x_2) \in \mathscr{I}$ is the spatial position of an arbitrary pixel in the image. Generally, tone mapping algorithms operate on either the three RGB channels separately, or on the luminance value of $\vec{I}$, calculated in one of the many possible ways available in literature [134], e.g. the $V = \max(R, G, B)$ in HSV, or the arithmetic average of the three RGB channels. In some cylindrical or conic shaped color spaces the compression of only the achromatic coordinate often leads to oversaturated images. Thus, in general, the compression of the achromatic coordinate comes together with a correction, often a smaller compression, of the saturation or chroma. To mention a few examples: in [150] after applying a TMO on the V, in the HSV color space, S is scaled according to the compression of the V channel, in [107] a TMO is applied on the L channel in the CIELAB space, while the chroma in the a^*b^* plane is rescaled, something similar is done in [2] in the IPT color space.

In any case, it is clear that only a scalar-valued function is considered, let us denote it simply with $\lambda : \mathscr{I} \to (0, +\infty)$.

Since the HDR image represents the radiance map of a scene, it is natural to associate λ with $\mathcal{I}$ and to identify the semisaturation level $\mathcal{I}_S$ with the average value of λ, denoted by μ. In the literature there is no agreement about how μ has to be computed, i.e. via arithmetic average μ_a, geometric average μ_g, median μ_{med}, or combinations of them [134, 52]. For these reasons, we will leave the formal expression of μ unspecified. In Section 8.2 we will see that the parameter μ has a particular geometrical meaning in the decomposition of r as a Möbius transformation.

With the notation just introduced, the expression of the Naka-Rushton equation for tone mapping of HDR images is the following:

$$r(\lambda(x)) = \frac{\lambda(x)}{\lambda(x) + \mu}, \qquad \forall x \in \mathscr{I}. \tag{8.1.2}$$

In the so-called *local* tone mapping algorithms, both the pixel position x and the value of $\lambda(x)$ influence the tone mapping operation, however, for the sake of simplicity, in this chapter we will only deal with a global tone mapping, in which two generic pixels $x, y \in \mathscr{I}$ such that $\lambda(x) = \lambda(y)$ will be tone-mapped in exactly the same value. Thanks to this assumption, Equation (8.1.2) can be simplified as follows:

$$r(\lambda) = \frac{\lambda}{\lambda + \mu}, \qquad \forall \lambda \in [\lambda_{\min}, \lambda_{\max}] \subset (0, +\infty), \tag{8.1.3}$$

with obvious meaning of the symbols $\lambda_{\min}$ and $\lambda_{\max}$ and $r(\mu) = 1/2$. The plot of $r(\lambda)$ is depicted in Figure 8.2. The non-linearity of $r(\lambda)$ is essential, in fact, due to the vast dynamic range of HDR images, a linear tone mapping performed via the formula:

$$\lambda \mapsto \frac{\lambda - \lambda_{\min}}{\lambda_{\max} - \lambda_{\min}} \in [0, 1], \tag{8.1.4}$$

eventually multiplied by 255 to restore the usual 8 bit dynamic range, would set to black all pixels in the image whose λ value is two orders of magnitude smaller than $\lambda_{\max}$, as clearly shown in Figure 8.1.

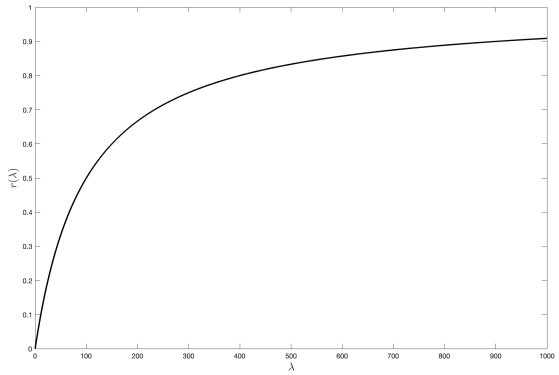

Figure 8.1: Graph of $r(\lambda)$, with $\lambda_{\min} = 0.1$, $\lambda_{\max} = 10^3$ and $\mu = 100$.

Figure 8.2: *Left*: one image of the famous Memorial church sequence. *Right*: result of the linear tone mapping of Equation (8.1.4), where almost all the pixels are set to black apart from those belonging to the brightest areas of the image.

8.2 Analysis of Naka-Rushton's formula as a Möbius transformation

The non-linearity of the Naka-Rushton transformation and the possibility to quite easily control the global brightness of the resulting image by modifying the value of μ are the two most important features of Naka-Rushton based tone mapping that established its successful and widespread use.

Alongside the analytical formula (8.1.3) and the graphical depiction of Figure 8.2, it is possible to analyze the Naka-Rushton transformation from a geometric point of view that happens to give finer information about its behavior. In fact, as we are going to prove in this section, Equation (8.1.3) can be interpreted as the composition of a non-linear map followed by an affine one. In order to prove this, we must first introduce the concepts of reflection, inversion and Möbius transformation.

8.2.1 Möbius transformations

The main reference for this section is Ratcliffe's book [131]. One common way to define the group of Möbius transformations on $\mathbb{R}^n$, denoted by $\mathcal{M}(\mathbb{R}^n)$ is as the subgroup of $\mathrm{Aut}(\mathbb{R}^n) = \{f : \mathbb{R}^n \to \mathbb{R}^n,\ f \text{ bijective}\}$ generated by reflections w.r.t. hyperplanes and inversions w.r.t. hyperspheres.

The concepts of *hyperplane* and *hypersphere* are the generalizations to dimension n of the concepts of plane and sphere in dimension 3 or straight line and circle in dimension 2. It is important to stress that both hyperplanes and hyperspheres are submanifolds of dimension $n-1$ embedded in a space of dimension n.

Definition 8.2.1 (Hyperplane in $\mathbb{R}^n$)**.** Given $a \in \mathbb{R}^n$, $\|a\| = 1$, and $t \geq 0$, the *hyperplane* in $\mathbb{R}^n$ associated to a and t is the set

$$P_{a,t} := \{x \in \mathbb{R}^n,\ \langle x, a\rangle = t\}. \tag{8.2.1}$$

Note that a is the *normal vector* to $P_{a,t}$, and t is the *distance* between $P_{a,t}$ and 0. We denoted with $\langle \cdot, \cdot \rangle$ the Euclidean scalar product.

Definition 8.2.2. A *reflection* in $\mathbb{R}^n$ w.r.t. the hyperplane $P_{a,t}$ is the affine function:

$$\begin{array}{rccl} \rho_{a,t}: & \mathbb{R}^n & \longrightarrow & \mathbb{R}^n \\ & x & \mapsto & \rho_{a,t}(x) := x + 2(t - \langle x, a\rangle)a. \end{array} \tag{8.2.2}$$

Geometrically, the reflection $\rho_{a,t}$ takes any point $x \in \mathbb{R}^n$ at a distance d from $P_{a,t}$ to a point $\rho_{a,t}(x)$ which lies specularly on the other side of $P_{a,t}$ at the same distance d.

Proposition 8.2.3. *Every reflection $\rho_{a,t}$ satisfies the following properties for all $x, y \in \mathbb{R}^n$:*

1. *$\rho_{a,t}(x) = x$ if and only if $x \in P_{a,t}$;*
2. *$\rho^2_{a,t}(x) = x$, i.e. $\rho_{a,t}$ is an involution, and so $\rho^2_{a,t} = id_{\mathbb{R}^n}$, i.e. $\rho_{a,t}$ is a bijection with ${\rho_{a,t}}^{-1} = \rho_{a,t}$;*
3. *$\rho_{a,t}$ is a Euclidean isometry: $\|\rho_{a,t}(x) - \rho_{a,t}(y)\| = \|x - y\|$.*

Definition 8.2.4 (Hypersphere in $\mathbb{R}^n$)**.** Given $c \in \mathbb{R}^n$ and $d > 0$, the *hypersphere*, of dimension $n-1$, in $\mathbb{R}^n$ centered in c of radius d is the set of all the points having distance d from the center c:

$$S_{c,d} := \{x \in \mathbb{R}^n \ :\ \|x - c\| = d\}. \tag{8.2.3}$$

The main difference between reflections and inversions is that the hypersurface w.r.t. the inversion is performed is not a hyperplane, but a hypersphere. While a hyperplane extends towards the infinite, a sphere is bounded, this fact implies that it is impossible to continuously fill the whole outer space to the spherical surface simply by reflecting its interior points w.r.t. the tangent hyperplane to the sphere at a point, a different, non-linear, geometrical operation is needed.

This operation consists in mapping any point x inside the sphere to the unique point $\sigma(x)$ outside the sphere characterized by the following two properties: firstly, $\sigma(x)$ lies on the same line joining x with the center of the sphere; secondly, the norm of $\sigma(x)$ is inverted w.r.t. that of x. More precisely we have the following definition:

Definition 8.2.5. Let $c \in \mathbb{R}^n$ and $d > 0$, then the *inversion* in $\mathbb{R}^n$ w.r.t. the hypersphere $S_{c,d}$ is the non-linear function

$$\begin{array}{rccl} \sigma_{c,d}: & \mathbb{R}^n \setminus \{c\} & \longrightarrow & \mathbb{R}^n \setminus \{c\} \\ & x & \mapsto & \sigma_{c,d}(x) := c + \frac{d^2}{\|x-c\|^2}(x-c). \end{array} \tag{8.2.4}$$

$\sigma_{c,d}(x)$ is said to be the *inverse of* x w.r.t. to the sphere $S_{c,d}$.

Proposition 8.2.6. *Every inversion $\sigma_{c,d}$ w.r.t. a hypersphere $S_{c,d}$ satisfies the following properties for all $x, y \in \mathbb{R}^n \setminus \{c\}$:*

1. *$\sigma_{c,d}(x) = x$ if and only if $x \in S_{c,d}$;*
2. *$\sigma_{c,d}^2(x) = x$, i.e. $\sigma_{c,d}$ is an involution, and so $\sigma_{c,d}$ is invertible with ${\sigma_{c,d}}^{-1} = \sigma_{c,d}$;*
3. *$\|\sigma_{c,d}(x) - \sigma_{c,d}(y)\| = \frac{d^2}{\|x-c\|\|y-c\|}\|x-y\|$.*

Every circular inversion $\sigma_{c,d}$ maps the exterior part of the hypersphere $\overline{B}^c_{c,d} = \{x \in \mathbb{R}^n : \|x-c\| > d\}$ into the inner part $B_{c,d} = \{x \in \mathbb{R}^n : \|x-c\| < d\}$ and viceversa, i.e. $\sigma(\overline{B}^c_{c,d}) = B_{c,d}$ and $\sigma(B_{c,d}) = \overline{B}^c_{c,d}$, while the points of $S_{c,d}$ stay fixed, i.e. $\sigma(S_{c,d}) = S_{c,d}$.

Both reflections w.r.t. hyperplanes and inversions w.r.t. hyperspheres are, essentially, *one-dimensional operations*, in the sense that all the points belonging to the same straight line orthogonal to the hyperplane involved in a reflection are left on this straight line; in the same way, all the points belonging to the straight line passing through the origin of the sphere involved in an inversion are left on that line.

It is possible to extend reflections and inversions to $\widehat{\mathbb{R}}^n := \mathbb{R}^n \cup \{\infty\}$. It is sufficient to define the image of ∞.

Definition 8.2.7. Let $\rho_{a,t}$ be a reflection and $\sigma_{c,d}$ an inversion in $\mathbb{R}^n$. The extension of $\rho_{a,t}$ in ∞ and of $\sigma_{c,d}$ in ∞ and c are defined as follows:

$$\rho_{a,t}(\infty) := \infty \qquad \text{and} \qquad \begin{cases} \sigma_{c,d}(\infty) := c \\ \sigma_{c,d}(c) := \infty \end{cases}. \tag{8.2.5}$$

Möbius transformations arise from the combinations of inversions and reflections of $\widehat{\mathbb{R}}^n$, one of the main interest in combining them is that, when they are fused together, they form a group. Notice that this is not a trivial statement because neither the set of reflections nor the set inversions form a group: we do not have a identity element or any stability.

Definition 8.2.8. A *Möbius transformation* $\phi : \widehat{\mathbb{R}}^n \to \widehat{\mathbb{R}}^n$ is a finite composition of reflections w.r.t. a hyperplane and inversions w.r.t. a sphere in $\widehat{\mathbb{R}}^n$. The group of Möbius transformations is: $\mathcal{M}(\widehat{\mathbb{R}}^n) = \{\phi = \mu_1 \circ \cdots \circ \mu_m : m \in \mathbb{N},\ \mu_i \text{ reflections or inversions of } \widehat{\mathbb{R}}^n,\ i \in \{1, \ldots, m\}\}$.

Another equivalent characterization of Möbius transformations is based on the concept of cross-ratio, already mentioned in Section 4.3 of Chapter 4. Let us define it for the case of points belonging to $\widehat{\mathbb{R}}^n$.

Definition 8.2.9. Let $u, v, x, y \in \widehat{\mathbb{R}}^n$ such that $u \neq y, v \neq x$. The *cross-ratio* of (u, v, x, y) is given by:

$$[u, v, x, y] = \frac{(u - x)(v - y)}{(u - y)(v - x)}. \tag{8.2.6}$$

$\mathcal{M}(\widehat{\mathbb{R}}^n)$ can be characterized as the set of all the transformations preserving the cross-ratio, i.e. $\phi \in \mathcal{M}(\widehat{\mathbb{R}}^n)$ if and only if for all $u, v, x, y \in \widehat{\mathbb{R}}^n$ we have that $[u, v, x, y] = [\phi(u), \phi(v), \phi(x), \phi(y)]$.

Theorem 8.2.10. *Let $\phi \in \mathcal{M}(\widehat{\mathbb{R}}^n)$. Then:*

1. *$\phi(\infty) = \infty$ if and only if ϕ is a similarity of $\widehat{\mathbb{R}}^n$;*
2. *if $\phi(\infty) \neq \infty$, then, there exist:*
   - *a unique hypersphere Σ in $\mathbb{R}^n$ on which ϕ acts as a Euclidean isometry, i.e. for all $x, y \in \Sigma$, $\|\phi(x) - \phi(y)\| = \|x - y\|$;*
   - *a unique inversion σ w.r.t. Σ and a unique Euclidean isometry ψ such that ϕ can be decomposed as follows $\phi = \psi \circ \sigma$.*

8.2.2 Naka-Rushton's formula as a Möbius transformation

Let us consider the real interval $\Lambda := [\lambda_{\min}, \lambda_{\max}]$. The intensity levels of a HDR image belong to Λ, i.e. $\lambda(\mathscr{I}) \subset \Lambda$, where $\mathscr{I}$ is the spatial support of the image. We want to use a parsimonious combination of simple Möbius transformations, i.e. inversions and reflections, to obtain a non-linear compression of the interval Λ, hence at least one inversion is needed. We will see that the search of the simplest monodimensional Möbius transformation r such that:

1. r is non-linear;
2. r is compressive* on Λ;
3. r is monotonically increasing on Λ;

leads naturally to Naka-Rushton's transformation.

In the following we are going to use elements of $\mathcal{M}(\mathbb{R})$, hence $n = 1$. Since the intensity is always positive, we can consider their restriction to $(0, +\infty)$. Notice that when $n = 1$ a hyperplane is just a point $a \in \mathbb{R}$, while a hypersphere is the set of two points having the same distance d from the center c, $S_{c,d} = \{c - d, c + d\}$.

In dimension 1 reflections and inversions have the following easier expressions:

$$\rho_a(\lambda) = 2a - \lambda \quad \text{and} \quad \sigma_{c,d}(\lambda) = c + \frac{d^2}{\lambda - c}, \tag{8.2.7}$$

with $a, c \in \mathbb{R}$ and $d > 0$.

Recalling Theorem 8.2.10 a generic $r \in \mathcal{M}(\mathbb{R})$ is either a similarity or not, and it can be decomposed as $r = \psi \circ \sigma$, where ψ is an isometry of $\mathbb{R}$ and σ is a (unique) circular inversion. Since we are looking for a non-linear transformation and similarities act linearly, we can exclude the first option.

*For all $\lambda_1, \lambda_2 \in \Lambda$ we have that $|r(\lambda_1) - r(\lambda_2)| < |\lambda_1 - \lambda_2|$.

We want r to be compressive on Λ. Since the component ψ is an isometry[†], σ must be compressive on Λ.

Let us consider the simplest case of a circular inversion w.r.t. a sphere centered in 0 of radius 1, $S_{0,1} = \{-1, 1\}$. The circular inversion w.r.t. this sphere is given by $\sigma_{0,1}(\lambda) = \frac{1}{\lambda}$.

Notice that, as an inversion, $\sigma_{0,1}$ maps the inner part of $S_{0,1}$ into the external part and viceversa, i.e. $\sigma_{0,1}((0,1)) = (1, +\infty)$ and $\sigma_{0,1}((1, +\infty)) = (0, 1)$. Since $\sigma_{0,1}(1) = 1$ we can also say that $\sigma_{0,1}([1, +\infty)) = (0, 1]$. In other words, this last equality means that the infinite half line $(1, +\infty)$ is mapped into the bounded segment $(0, 1)$.

This means that, if the interval Λ, which can have arbitrarily large length $l = \lambda_{\max} - \lambda_{\min}$, is contained in the half line $[1, +\infty)$, then $\sigma_{0,1}(\Lambda)$ will be compressed, not linearly, in a segment contained in $(0, 1]$. To ensure that $\Lambda \subset [1, +\infty)$ we preliminary apply the translation $\tau_1(\lambda) = \lambda + 1$, hence $\tau_1(\Lambda) = [\lambda_{\min} + 1, \lambda_{\max} + 1]$.

Up to now, we are applying on Λ the transformation $\sigma_{0,1} \circ \tau_1(\lambda) = \frac{1}{\lambda+1}$, see Figure 8.3. Although this function is non-linear and compressive on Λ, it does not respect the order on Λ, i.e. it is not monotonically increasing. To recover the correct order on the compressed interval we need to apply the reflection w.r.t. the point $\frac{1}{2}$, i.e. $\rho_{1/2}(\lambda) = 1 - \lambda$. Note that, in particular, $\rho_{1/2}$ reverses the segment $[0, 1]$, swapping the segment's extremes: $\rho_{1/2}(0) = 1$ and $\rho_{1/2}(1) = 0$. As a reflection $\rho_{1/2}$ is an isometry thanks to Proposition 8.2.3.

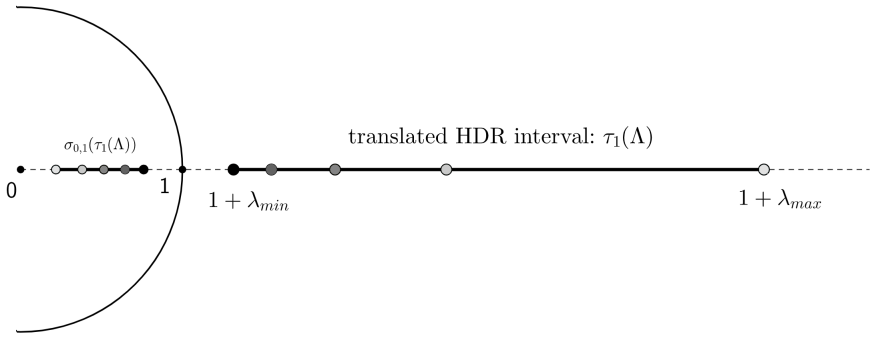

Figure 8.3: Depiction of the action of the transformation $\rho_{1/2} \circ \sigma_{0,1}$ on the interval Λ. Notice that it is more compressive on high intensity levels than on the lower ones.

Let us call $r' = \rho_{1/2} \circ \sigma_{0,1}$ and $r = r' \circ \tau_1$. In this case, without taking into account the preliminary translation τ_1, i.e. considering r' instead of r, r' is decomposed as stated in Theorem 8.2.10, i.e. $r' = \psi \circ \sigma$, with $\psi = \rho_{1/2}$ and $\sigma = \sigma_{0,1}$. Moreover r has the following explicit expression:

$$r(\lambda) = \rho_{1/2} \circ \sigma_{0,1} \circ \tau_1(\lambda) = \rho_{1/2}\left(\frac{1}{\lambda+1}\right) = \frac{\lambda}{\lambda+1}. \tag{8.2.8}$$

Notice that this simple reasoning leads us to a Naka-Rushton transformation with $\mu = 1$.

Let us follow the same reasoning, but starting from a more generic circular inversion $\sigma_{0,\mu}$ w.r.t. a sphere centered in 0 of radius μ, $S_{0,\mu} = \{-\mu, \mu\}$.

To ensure that Λ is placed outside the sphere $S_{0,\mu}$, i.e. $\Lambda \subset [\mu, +\infty)$, before the inversion $\sigma_{0,\mu}$, we preliminary apply the translation $\tau_\mu(\lambda) = \lambda + \mu$.

Up to now, we are considering the transformation $\sigma_{0,\mu} \circ \tau_\mu$. We know that $\sigma_{0,\mu}(\lambda) = \frac{\mu^2 \lambda}{|\lambda|^2}$, but, since we are in dimension 1, $\sigma_{0,\mu}(\lambda) = \frac{\mu^2}{\lambda}$. Hence $\sigma_{0,\mu} \circ \tau_\mu(\lambda) = \frac{\mu^2}{\lambda+\mu}$. Now $\sigma_{0,\mu} \circ \tau_\mu(\Lambda)$ is contained in the segment $[0, \mu]$. To recover the correct order of the intensity levels we need to

[†]For all $\lambda_1, \lambda_2 \in \Lambda$ we have that $|\psi(\lambda_1) - \psi(\lambda_2)| = |\lambda_1 - \lambda_2|$.

apply the reflection $\rho_{\mu/2}(\lambda) = \mu - \lambda$, which reverses the segment$[0, \mu]$. At this point the image of Λ is contained in the segment $[0, \mu]$, we need to rescale it applying a dilation of factor $\frac{1}{\mu}$, $\delta_{1/\mu}(\lambda) = \frac{1}{\mu}\lambda$, which maps $[0, \mu]$ into $[0, 1]$. In this way the image of Λ is contained in $[0, 1]$. Let us call r the composition of all the Möbius transformations introduced up to now:

$$r(\lambda) = \delta_{1/\mu} \circ \rho_{\mu/2} \circ \sigma_{0,\mu} \circ \tau_{\mu}(\lambda) = \frac{\lambda}{\lambda + \mu}.$$

The Möbius transformation r that we have obtained is a Naka-Rushton function and the parameter μ represents the radius of the sphere w.r.t. which we are performing a circular inversion.

Let us call $r' = \rho_{\mu/2} \circ \sigma_{0,\mu}$, hence $r = \delta_{1/\mu} \circ r' \circ \tau_{\mu}$. If we do not consider the preliminary translation τ_{μ} and the dilation $\delta_{1/\mu}$ that we apply a posteriori to recover the range $[0, 1]$, i.e. we consider r' instead of r, then r' agrees with the minimal decomposition stated in Theorem 8.2.10 as $r' = \psi \circ \sigma$, with $\psi = \rho_{\mu/2}$ and $\sigma = \sigma_{0,\mu}$.

One might also think to decompose $r(\lambda) = \frac{\lambda}{\lambda+\mu}$ according to Theorem 8.2.10. After straightforward computations it is easy to obtain that $r = \psi \circ \sigma$ with $\psi(\lambda) = \rho_{\frac{1-\mu}{2}}(\lambda) = 1 - \mu - \lambda$ and $\sigma(\lambda) = \sigma_{-\mu,\sqrt{\mu}}(\lambda) = -\mu + \frac{\mu}{\lambda+\mu}$. Notice that also in this decomposition the parameter μ is related to the radius of the sphere w.r.t. which we are performing an inversion.

8.2.3 Some considerations about Möbius transformations and color

We have identified the non-linear inversion and the affine reflection that make up Naka-Rushton's map as a Möbius transformation. An inversion encodes the non-linear part of the mapping, mapping very dark and bright values of λ in the range $0-255$ with the reversed order between them. For this reason, the composition with a reflection is needed to re-establish the correct intensity order.

The fact that reflections are isometries is particularly important for this step, in fact they do not modify the image relative intensities obtained as output of the inversion step, which is wise because the range has been correctly shrunk and we want to preserve it like it is.

We consider that pointing out this geometric information about tone mapping operator based on Naka-Rushton's formula may give interesting information for future developments of this kind of techniques. In particular, considering the prominent role of Möbius transformations in hyperbolic geometry and the importance played by hyperbolic structures in the model described in Chapters 3, 4, 5 and 6.

Möbius transformations encode many desirable colorimetric properties, e.g. they are conformal maps, i.e. they preserve angles, but they can also be identified with the transformations that preserve the cross-ratio, see e.g. [131].

In this section we treated only 1-dimensional Möbius transformations that can either be applied on the luminance channel of an RGB image, or to each separate chromatic channel. It would be interesting to study also the application of 3-dimensional Möbius transformations, i.e. elements of $\mathcal{M}(\mathbb{R}^3)$, on the whole image content. Some signs in literature that go in this direction are present e.g. in [55], were color holographies, projective maps i.e. cross-ratio preserving, are used for some applications, or the work of Drösler, already mentioned in Chapter 1, which relates cross-ratio to Weber's ratio starting from the mono-dimensional case and treating as well the three dimensional one [42, 43].

As already mentioned in Section 8.1, the interaction between the intensity shrinking and the chromatic components is a non-trivial aspect that affects the color rendering of images after TM. One reason are the correlations phenomena described in Section 1.3. In particular the

chromatic and achromatic part might be correlated because of the attributes representation in a particular color solid, but as well because of perceptual effects like Hunt's one, [2].

8.3 KTMO: a Klein inspired Tone Mapping Operator

In this section we are going to describe a work-in-progress proposal of tone mapping operator inspired from the construction of a classic model of hyperbolic geometry: Klein's disk. We already mentioned in Chapters 4 and 5 the Hilbert-Klein metric on the unit disk $\mathcal{D}$ or on the disk of radius 1/2, $\mathcal{D}_{1/2}$.

As we will see in the following, the Klein disk is constructed via projection from the origin[‡], that maps the hyperboloid leaf, tangent to the center of the disk, onto the disk. The hyperboloid is another classic model of 2-dimensional hyperbolic geometry. It can be proven that, endowing the hyperboloid with the metric given by the arc length computed on its surface and $\mathcal{D}$ with the Hilbert-Klein metric then this projection is an isometry, for more details see [131].

Roughly speaking the Klein projection transforms a hyperboloid leaf, which is an infinite surface into a disk which is bounded. Imagining to represent an HDR image as a set of points belonging to a infinite cone, the idea is to use this transformation as a TMO to non-linearly compress an HDR image in a truncated cone.
Similarly to what we did in the previous chapter for AWB, here we choose a conic-shaped color space, like HCV to be able to apply these techniques on an image. For further details about the issues of relating the theoretical model to applications, see Subsection 7.2.1 in Chapter 7.

8.3.1 Leaves and Klein disks in HCV

Let us start by considering the state-of the art conic-shaped color space HCV. It is a cone of slope 1, truncated at height 1. In this space saturation S is defined as $S = C/V$. On the other hand the HSV color space has a cylindric shape. Let us call φ the coordinate change from HSV to HCV, then $\varphi(H, S, V) = (H, SV, V)$ and $\varphi^{-1}(H, C, V) = (H, C/V, V)$.

Let us now provide a parametrization of the conic volume of the HCV color space without taking into account the constraint of being bounded at height 1. Let us call $\mathcal{C}$ this infinite conic volume, then $\mathcal{C}$ is defined as the set of all points:

$$\mathcal{C} = \{(H, C, V) \in [0, 2\pi) \times \mathbb{R}^+ \times \mathbb{R}^+ \mid V^2 - C^2 \geq 0\}. \tag{8.3.1}$$

Using the HSV coordinates to reparametrize the same set of points $\mathcal{C}$ one obtains:

$$\mathcal{C} = \{(H, S, V) \in [0, 2\pi) \times \mathbb{R}^+ \times \mathbb{R}^+ \mid V^2(1 - S^2) \geq 0\}. \tag{8.3.2}$$

Definition 8.3.1 (Leaf)**.** Let $k \in \mathbb{R}^+$, an *hyperboloid leaf* $\mathcal{L}_k \subset \mathcal{C}$ is defined as the following set of points:

$$\mathcal{L}_k = \{(H, C, V) \in \mathcal{C} \mid \sqrt{V^2 - C^2} = k\}. \tag{8.3.3}$$

Using HSV coordinates a leaf is given by $\mathcal{L}_k = \{(H, S, V) \in \mathcal{C} | V\sqrt{1 - S^2} = k\}$. Notice that $\mathcal{L}_0 = \partial\mathcal{C}$. For every point $x \in \mathcal{C}$ it exists an unique $\mathcal{L}_k$ such that $x \in \mathcal{L}_k$. The cone $\mathcal{C}$ is said to be *foliated* in the set of leaves $\{\mathcal{L}_k\}_{k\in\mathbb{R}^+}$, i.e. $\mathcal{C} = \bigsqcup_{k\in\mathbb{R}^+} \mathcal{L}_k$, see Figure 8.4.

[‡]See as well [16] for the role played by the Klein's disk projection in the theoretical model. Roughly speaking applying Klein's projection on the whole state cone, one obtains a representation of the state space.

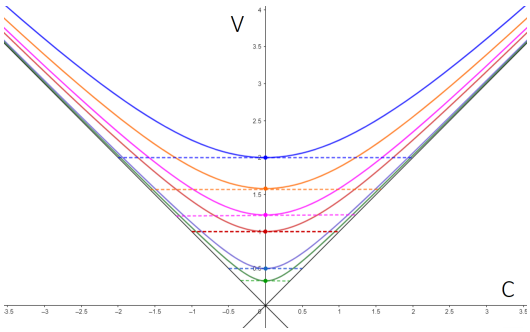

Figure 8.4: Depiction of the leaves and disks in a chroma-value plane in HCV.

Let us consider the set of leaves in represented the HCV domain. Every leaf $\mathcal{L}_k$ intersects the vertical axis V at height k. Let $\mathcal{D}_k$ be the disk of radius k, obtained as $\mathcal{D}_k := \mathcal{C} \cap \pi_k$, where π_k is the plane of equation $V = k$. Note that, as depicted in Figure 8.4, $\mathcal{L}_k$ is tangent to $\mathcal{D}_k$ in $(0, 0, k)$, for every k. We define the *k-Klein projection* κ_k, as the function that maps the hyperboloid leaf $\mathcal{L}_k$ into the disk $\mathcal{D}_k$ in the following way:

$$\begin{array}{rccc} \kappa_k : & \mathcal{L}_k & \longrightarrow & \mathcal{D}_k \\ & (H, C, V)^t & \longmapsto & (H, kC/V, k)^t, \end{array}$$

Since for all $x = (H, C, V) \in \mathcal{L}_k$ we have that $k = \sqrt{V^2 - C^2}$, we can define a function κ acting on the whole $\mathcal{C}$ and such that $\kappa_{|\mathcal{L}_k} = \kappa_k$, for all $k \in \mathbb{R}^+$, as follows:

$$\begin{array}{rccc} \kappa : & \mathcal{C} & \longrightarrow & \mathcal{C} \\ & (H, C, V)^t & \longmapsto & \left(H, \frac{C\sqrt{V^2-C^2}}{V}, \sqrt{V^2 - C^2}\right)^t. \end{array}$$

Note that κ is invertible on $\mathcal{C}$ and transforms each leaf in a disk. For a visual representation of the action of κ in HCV see Figure 8.4.

Let us call $\tilde{\kappa}$ the function κ acting on the HSV domain, thus $\tilde{\kappa} = \varphi^{-1}\kappa\varphi$. Straightforward computations lead to the following explicit expression:

$$\begin{array}{rccc} \tilde{\kappa} : & \mathcal{C} & \longrightarrow & \mathcal{C} \\ & (H, S, V)^t & \longmapsto & \left(H, S, V\sqrt{1 - S^2}\right)^t. \end{array}$$

8.3.2 KTMO

Let us consider an HDR image expressed in HSV coordinates, with S and V not necessarily in $[0, 1]$, but belonging to $[0, R]$, where R is a positive constant determined by the dynamic range of the input image. Let us call $\mathscr{I}$ the spatial domain of the image, every pixel $x \in \mathscr{I}$ is represented by a point of coordinates $H(x), S(x), V(x)$ contained in $\mathcal{C}$.

We recall that the aim of a TMO is to perform a non linear compression of the pixel's coordinates to make the image displayable on a screen. $\tilde{\kappa}$ is a non-linear, compressive function. One might think about defining a TMO in the HSV domain, that is the composition of $\tilde{\kappa}$ with a linear re-normalization, e.g. division by the maximum of the image or the maximum V. However this operation is not sufficiently compressive and the results are almost all dark.

To solve this issue we propose a TMO, that we call Klein TMO (KTMO from now on) that is the composition of $\tilde{\kappa}$ with a simple Naka-Rushton applied on the coordinate V. From Equation (8.1) we recall that the Naka-Rushton has the following expression:

$$x \longmapsto NR(x) = \frac{x}{x + \hat{x}}. \tag{8.3.4}$$

Clearly there is the problem of setting the parameter $\hat{x}$. In this section we follow the choice made in [89]. Let $x_1, \ldots, x_n$ be the values taken by the variable x, then parameter $\hat{x}$ is chosen to be the weighted average between the arithmetic mean $A = A(x_1, \ldots, x_n)$ and the geometric mean $G = G(x_1, \ldots, x_n)$, i.e. $\hat{x} = A^p G^{1-p}$, with p to be set in $[0, 1]$.

Figure 8.5 (Left) shows some examples of outputs of Naka-Rushton applied on the V channel in HSV color space, with $p = 0$.

The KTMO performs the following sequence of operations:

1. starts from an HDR input image expressed in RGB coordinates;
2. passes from RGB to HSV coordinates;
3. applies $\tilde{\kappa}$ to the HSV coordinates, obtaining three coordinates that we will call $H'S'V'$;
4. applies a NR on V', with parameter $\hat{x} = A^p G^{1-p}$, p is a parameter to be set in $[0, 1]$. Let us call $\tilde{V} = NR(V')$;
5. applies a linear normalizaton (division by the maximum $\tilde{V}$) to $\tilde{V}$, to have the output value in $[0, 1]$;
6. converts the image back to RGB.

References about the coordinate changes from RGB to HSV and viceversa can be found e.g. in [167, 145], moreover these functions are already implemented in several Python packages for color image processing. Figure 8.5 (Center) shows some visual examples of KTMO outputs with $p = 0.5$.

8.3.3 Fréchet means

The choice of the parameter $\hat{x}$ appearing in Naka-Rushton's equation is a known non-trivial problem in literature. In order to investigate about alternative choices for $\hat{x}$ for the NR in the KTMO, we introduce here the concept of Fréchet means.

A Fréchet mean is the generalization of the concept of centroid for a generic metric, for further details see e.g. [104].

Definition 8.3.2 (Fréchet variance)**.** Let (M, d) be a complete metric space. Let $x_1, \ldots, x_n \in M$. For every $x \in M$ the Fréchet variance is given by:

$$\psi(x) = \sum_{i=1}^{n} d^2(x, x_i). \tag{8.3.5}$$

Definition 8.3.3 (Karcher and Fréchet mean)**.** A point $m \in M$ that locally minimizes ψ is called *Karcher mean* of the points $x_1, \ldots, x_n$

$$m(x_1, \ldots, x_n) = \arg\min_{x \in M} \psi(x). \tag{8.3.6}$$

If there exists a point $m \in M$ that globally minimizes $\psi(x)$, it is called the *Fréchet mean* of the points $x_1, \ldots, x_n$.

In the following we are going to show that known means are actually particular instances of Fréchet means, with different choices for the metric.

Example 8.3.4 (Arithmetic mean). Let $M \subseteq \mathbb{R}$ open, the arithmetic mean of $x_1, \dots, x_n \in M$ is the Fréchet mean with d being the Euclidean metric d_E:

$$A(x_1, \dots, x_n) = \frac{1}{n} \sum_{i=0}^{n} x_i = \arg\min_{x \in \mathbb{R}} \sum_{i=0}^{n} |x - x_i|^2. \tag{8.3.7}$$

It can be easily verified that $\psi(x) = \sum_{i=0}^{n} |x - x_i|^2$ is globally minimal in $\bar{x} = \frac{1}{n} \sum_{i=0}^{n} x_i$. Indeed, computing the derivative $\psi'(x) = 2 \sum_{i=0}^{n} (x - x_i) = 2nx - 2 \sum_{i=0}^{n} x_i$, we obtain that $\psi'(x) = 0$ if and only if $x = \bar{x}$, $\psi'(x) > 0$ for all $x > \bar{x}$ and $\psi'(x) < 0$ for all $x < \bar{x}$.
It can be proven that the previous example holds true also for $M = \mathbb{R}^m$.

Definition 8.3.5 (f-mean)**.** Let $M, N \subseteq \mathbb{R}$ open and $f : M \longrightarrow N$ an invertible function. Let us consider N as a metric space with the Euclidean distance d_E. Then we can use f to define a metric on M as follows:

$$d_f(x, y) := |f(x) - f(y)|, \qquad \forall x, y \in M. \tag{8.3.8}$$

In this way f is an isometry between the metric spaces (M, d_f) and (N, d_E). Then the **f-mean** of $x_1, \dots, x_n \in M$ is given by

$$A_f(x_1, \dots, x_n) = f^{-1}\left(A(f(x_1), \dots, f(x_n))\right). \tag{8.3.9}$$

Let us verify that it is a good definition.

$$A_f(x_1, \dots, x_n) = \arg\min_{x \in M} \sum_{i=1}^{n} d_f^2(x, x_i) = \arg\min_{x \in M} \sum_{i=1}^{n} |f(x) - f(x_i)|^2. \tag{8.3.10}$$

We have to verify that the last arg min in the previous equation exists and it is unique. For all $x \in M$ the function $\sum_{i=1}^{n} |f(x) - f(x_i)|^2$ is minimized if and only if x is such that $f(x) = \arg\min_{y \in N} \sum_{i=1}^{n} |y - f(x_i)|^2$. From Example 8.3.4 we know that it exists an unique $\bar{y} \in N$ that minimizes $\sum_{i=1}^{n} |y - f(x_i)|^2$ and $\bar{y} = \frac{1}{n} \sum_{i=1}^{n} f(x_i)$, so, since f is invertible it exists an unique point $\bar{x} = f^{-1}(\bar{y})$ that minimizes $\sum_{i=1}^{n} |f(x) - f(x_i)|^2$.

Example 8.3.6 (Arithmetic mean). The arithmetic mean is a trivial example of f-mean, with $f = id_{\mathbb{R}}$.

Example 8.3.7 (Geometric mean). Let $x_1, \dots x_n \in \mathbb{R}^+$, their geometric mean $G(x_1, \dots x_n) = \sqrt[n]{x_1 \cdot \dots \cdot x_n}$ is an f-mean with $f = \log : \mathbb{R}^+ \longrightarrow \mathbb{R}$, i.e. the Fréchet mean obtained choosing the metric $d(x, y) = |\log(x) - \log(y)|$. Indeed using Equation (8.3.9) we can perform the following computations:

$$\begin{aligned} \exp\left(A(\log(x_1), \dots, \log(x_n))\right) &= \exp\left(\frac{1}{n} \sum_{i=0}^{n} \log(x_i)\right) = \exp\left(\frac{1}{n} \log\left(\prod_{i=0}^{n} x_i\right)\right) \\ &= \sqrt[n]{\prod_{i=0}^{n} x_i} = G(x_1, \dots, x_n). \end{aligned} \tag{8.3.11}$$

8.3.4 KTMO and Fréchet means

In a first proposition of the Klein TMO, $\hat{x}$ is chosen to be the weighted product between the arithmetic mean A and the geometric mean G of the values $V(x)$ with $x \in \mathscr{I}$, i.e. $\hat{x} = A^p G^{1-p}$, with $p \in [0, 1]$, as in [89].

Since in the KTMO we apply a Naka-Rushton transformation on the achromatic coordinate, it seems appropriate to set this parameter as a Fréchet mean obtained from a metric that appears naturally in color perception to measure the differences in intensity of a mono-dimensional stimulus. As reported e.g. in [43, 65] variations in intensity of a mono-dimensional stimulus follow Weber-Fechner's law and are well described by the metric ds/s, see as well Subsection 1.2 of Chapter 1. Given $a, b \in \mathbb{R}^+$, their distance is given by $d(a, b) = \left| \int_a^b \frac{\mathrm{d}s}{s} \right| = |\log(a) - \log(b)|$. Hence the Fréchet mean associated to this metric is the geometric mean, see Example 8.3.7. Figure 8.5 (Right) shows the Klein TMO with $\hat{x}$ as the geometric mean.

Figure 8.5: *Left*: NR applied on V in HSV, $\hat{x} = G$. *Center*: KTMO with $\hat{x} = A^p G^{1-p}$ with $p = 0.5$. *Right*: KTMO with $\hat{x}$ as the geometric mean. The HDR inputs used to obtain these images belong to '*Mark Fairchild's HDR Photographic Survey*' [48], available at http://markfairchild.org/HDR.html.

As we can see in Figure 8.5, KTMO seems to be slightly better performing at color rendering than Naka-Rushton's equation applied on the V channel of HSV, e.g. in the red flowers in the bottom left corner of the image in the second line. There is no big difference between the second and the third column, but the use of the geometric mean as parameter of the Naka-Rushton applied within KTMO is better motivated theoretically being related to Weber-Fechner's law as explained before.

On the other hand the results of the KTMO look over-saturated. This happens because, while chroma is modified by the KTMO, saturation stays unchanged, so the saturation of the

low dynamic image is the same as one of the HDR image.

There are different possible ways in literature to integrate a desaturation step in the KTMO, e.g. [150]. We tried as well to desaturate the image using Einstein's scalar multiplication, see Equation (5.3.1) in Chapter 5, but the results were not satisfactory. Similarly to what done in [2], as a future project we would like to propose a desaturation step that takes into account Hunt's effect as quantified in Section 5 of [19].

Chapter 9

Conclusion and future perspectives

We have seen how the novel quantum-like approach that has been described in this thesis has both theoretical and applied implications. Citing Bengtsson and Zyczkowski [11]: '*There are many lessons from colour theory that are of interest in quantum mechanics*'. We might say that the inverse holds as well: there are many lessons from quantum mechanics that are of interest in color theory.

We want to conclude mentioning a few open questions that will constitute the object of further investigations for future works.

About the existence of four unique hues

Recalling the definition of hue mentioned in Subsection 1.3.1, there are only four unique hues (red, yellow, green and blue), and any other hue can be expressed as a combination of two of them. One might ask whether there is a mathematical explanation of the presence of *exactly* four unique hues, e.g. Purves and collaborators, in [130], relate it to the four-color-map problem [28]. In Chapter 3 we have seen that the existence of two couples of opponent hues in opposition is part of the algebraic formulation, encoded in the real Pauli matrices σ_1 and σ_2. In Chapter 5 we showed how Lüders operations act on the disk of chromatic states, in particular they stabilize and do not deform it. It exists a more general set of transformations, of which Lüders operations represent a particular instance, known in quantum information theory as *quantum channels*. In particular the action of a quantum channel can deform the disk of chromatic states in a generic convex set of dimension 2. This means that one can generalize the ideal model described in Chapter 5 to a more realistic one, where a perceived color is obtained as the outcome of a measurement procedure consisting in the action of a quantum channel on a generalized state. Furthermore this process deforms the states space of the observer. Since, in this new setting, the set of chromatic states of a trichromatic observer is a generic convex, then an idea is to explore its link with four-vertex theorem, applied on its border, see [41]. This might provide a mathematical explanation of the existence of four unique hues, corresponding to the local extremas of the border's curvature function.

Perceptual effects and chromatic adaptation

A way to validate the model is to check whether it is coherent with the phenomenology of color perception. In particular, as done in [17, 19] for the Hunt effect, it is important to understand whether it is possible explain via the formalism of the model other known perceptual effects, e.g. Helmholtz-Kohlrausch, Bezold-Brüke, Abney etc., see Subsection 1.3.2.

It is possible that some effects involving a hue-shift, as Bezold-Brüke's one, could be modeled using the angle variation formula obtained in Appendix B, Equation (B.0.13).
We think that the task of modeling perceptual effects is made more difficult by the fact that chromatic adaptation might affect them. Therefore understanding and modeling the perceptual effects means, as well, understanding which is the role of chromatic adaptation in these phenomena.

As the viral phenomenon of *The Dress* proved in 2015 on social media, what exactly chromatic adaptation is, how to correctly model it (taking into account all the involved steps in the vision chain) and how it influences color appearance phenomena is still unclear.

An interesting point of view is given in [164], where a probabilistic interpretation of space perception is used to explain several space perception phenomena. Roughly speaking, among all the possible physical configurations that could lead to the same bi-dimensional visual image, the *most probable* one is chosen by the HVS. It is possible that something similar happens as well for color perception phenomena, e.g. while estimating the chromaticity of a light source (as happened for *The Dress* phenomenon). In fact, some of the scientific explanations [94, 5] of the fact that people were perceiving the dress differently (either black and blue or white and gold) involved chromatic adaptation. Indeed the phenomenon was explained in terms of inter-observers differences in the estimation of the illuminant in the scene, in particular a black/blue dress is seen when the discarded illuminant is yellowish, while a white/yellow one is seen when the observer adapts to a bluish illuminant. As detailed in Chapter 7 illuminant estimation is an ill-posed problem, hence it seems reasonable that, given a visual stimulus, the HVS looks for the *most probable*, in some sense, illuminant to discard.

In the following paragraph we describe a possible way of obtaining a mathematical explanation of why chromatic adaptation happens.

Chromatic adaptation to increase color distinguishability

In Chapter 5 we have mentioned the concept of relative entropy and used it in Chapter 6 to provide definitions of colorimetric attributes within the quantum-like model. In quantum information theory, relative entropy is known to be a measure of *discernability* between states. Another interesting research direction consists at giving a formal explanation of why chromatic adaptation occurs. In particular, we would like do define a measure of distinguishability between colors, given by the relative entropy, or its symmetrized version, between the associated states. Then we would like to provide a simple proof* of the fact that this quantity increases after chromatic adaptation, formalized as in Chapter 5. Roughly speaking this would provide a mathematical explanation of chromatic adaptation: the HVS adapts itself to the specific features of a visual scene in order to better distinguish its colors. Some details and a proof of the collinear case for the symmetrized relative entropy, are presented in the Appendix C.
It would be interesting to investigate if psychovisual data can support this hypothesis.

Defining a Jameson-Hurvich-like color solid JHY

In Chapter 1 we mentioned the chromatic response curves proposed by Jameson and Hurvich within their series of articles about quantifying Hering's opponent process, in particular [75, 76]. The idea here is to use a basis of functions made up by them and a choice for the brightness sensitivity function, let us pick $\bar{y}$ for simplicity, to define a color solid.

Let $C \in L^2_+(\Lambda)$ be a color stimulus, then its tristimulus values obtained performing the reduction with respect to the basis $\overline{rg}, \overline{yb}, \bar{y}$, as in Equation (1.1.3), are given by:

*Notice that this result is known for the case of quantum mechanics, see e.g. [151] for a proof.

$$
\begin{aligned}
J &= \int_\Lambda C(\lambda)\overline{rg}(\lambda)\mathrm{d}\lambda, \\
H &= \int_\Lambda C(\lambda)\overline{yb}(\lambda)\mathrm{d}\lambda, \\
Y &= \int_\Lambda C(\lambda)\bar{y}(\lambda)\mathrm{d}\lambda.
\end{aligned}
\tag{9.0.1}
$$

From Equation (1.1.5), by linearity of the integral we obtain that the first two equalities in Equation (9.0.1), can be rewritten as:

$$
\begin{aligned}
J &= 1.0065\int_\Lambda C(\lambda)\bar{x}(\lambda)\mathrm{d}\lambda - 1.0006\int_\Lambda C(\lambda)\bar{y}(\lambda)\mathrm{d}\lambda - 0.0051\int_\Lambda C(\lambda)\bar{z}(\lambda)\mathrm{d}\lambda, \\
H &= -0.0039\int_\Lambda C(\lambda)\bar{x}(\lambda)\mathrm{d}\lambda + 0.3998\int_\Lambda C(\lambda)\bar{y}(\lambda)\mathrm{d}\lambda - 0.3999\int_\Lambda C(\lambda)\bar{z}(\lambda)\mathrm{d}\lambda.
\end{aligned}
\tag{9.0.2}
$$

Recalling that the XYZ coordinates associated to $C(\lambda)$ are obtained, as in Equation (1.1.3), by

$$
\begin{aligned}
X &= \int_\Lambda C(\lambda)\bar{x}(\lambda)\mathrm{d}\lambda, \\
Y &= \int_\Lambda C(\lambda)\bar{y}(\lambda)\mathrm{d}\lambda, \\
Z &= \int_\Lambda C(\lambda)\bar{z}(\lambda)\mathrm{d}\lambda.
\end{aligned}
\tag{9.0.3}
$$

We obtain that the tristimulus values XYZ are linearly related to the JHY coordinates as follows:

$$
\begin{pmatrix} J \\ H \\ Y \end{pmatrix} = \begin{pmatrix} 1.0065 & -1.0006 & -0.0051 \\ -0.0039 & 0.3998 & -0.3999 \\ 0 & 1 & 0 \end{pmatrix} \begin{pmatrix} X \\ Y \\ Z \end{pmatrix}. \tag{9.0.4}
$$

It seems interesting to define a color model in this way, since it would be a new way of including Hering's opponent mechanism in a color space. Moreover Jameson and Hurvich's curves have been used as well in [115] to give a colorimetric explanation and quantification of the Helmholtz-Kohlrausch effect. This seems promising in the perspective of defining a color model that takes into account and predicts this kind of effects. Furthermore this Jameson-Hurvich-like color solid could be a good color domain candidate to test the CAT proposed in Chapter 7 or the KTMO of Chapter 8.

About the normalized boost CAT

In 2004 the CIE reunited a technical commission, TC 1-52, testing 13 CATs with the purpose of recommending a best performing one, see [1]. As reported in [20], '*The members of the CIE TC 1-52 were unable to agree on a single CAT as some of them required that the adopted transform must be theoretically based*'. For this reason we are interested in keeping ameliorating our proposal of a theoretically based CAT, presented in Chapter 7.

There are two main aspects on which we do believe that there is margin of improvement. The first one consists at finding a better color domain for the implementation. One possible solution is either studying more in detail further modifications of HCV or other state-of-the art color solids, either using the Jameson-Hurvich-like color solid described in the previous paragraph.

The second, very important, aspect is to provide quantitative evaluations of its performance. The state-of-the art benchmark to test CATs are the so-called *corresponding colors* datasets. These experimental data are obtained through different techniques, among them haploscopic matching as the Burnham experiments [26] mentioned in Chapter 4. For a thoughtful description of the available datasets and existing CATs see the CIE report [1], Chapter 9 of [49] or [20]. A couple of corresponding colors consists of two points, represented in a certain chromaticity diagram, which represent the same perceived color under two different adaptation conditions. CATs are meant to predict the corresponding colors couples, some data-based state-of-the art CATs have been created fitting the available corresponding colors datasets. Concerning our model we performed some first tests on e.g. Breneman's data [21], implementing Einstein-Poincaré's addition law (which corresponds to the action of $B_N(\mathbf{e})^{-1}$ on the chromaticity diagram) in the $u'v'$ chromaticity diagram, depicted in Figure 1.5, but the results were not satisfactory. The reason is that the $u'v'$ chromaticity diagram is not a good approximation of the theoretical one. Hence we would like to perform other tests, on Breneman's or other corresponding colors datasets, representing the points in a different chromaticity diagram, e.g. H_1S in the the solid H_1SV defined in Section 7.3, or the chromaticity diagram JH of the Jameson-Hurvich-like color solid described in the previous paragraph.

Appendix A

Elements of special relativity theory

Here we will briefly recap only the basic concepts of special relativity because inherent to Yilmaz's model treated in Chapters 2 and 4. The discussion that follows will be faithful to the standard special relativity formulation, see e.g. [96, 97].

Special relativity is known to be an extension of Galilean relativity, which is based on the following two postulates:

1. space is homogeneous and isotropic and time is homogeneous*;
2. laws of physics† have the same form in all inertial (i.e. not accelerated) reference frames, i.e. no inertial reference frame is privileged.

In special relativity, Einstein considered, along with the motion of objects with mass, also the peculiar behavior of electromagnetic signals by adding the following postulate:

3. the speed of light in vacuum has a constant value $c \in \mathbb{R}^+$ when measured in all inertial reference frames.

In special relativity, we call *event* e a point in $\mathbb{R}^4 = \mathbb{R} \times \mathbb{R}^3$ with coordinates written as‡ $x^\mu = (ct, \mathbf{x})$, where $t \in \mathbb{R}$ and $\mathbf{x} = (x^i)$, $i = 1, 2, 3$, are, respectively, the time instant and the spatial position of the event as measured by an inertial observer with respect to her/his inertial reference frame $\mathscr{R}$. Let us consider, in particular, the following two events: the first, $e_1 = (ct_1, x_1^i)$, consists in a light signal emanating at the time t_1 from the spatial position (x_1^i); the second, $e_2 = (ct_2, x_2^i)$, consists in the same light signal arriving at the time t_2 in the spatial position (x_2^i). Since the signal propagates with constant speed c, the square distance that is traveled is $c^2(t_2 - t_1)^2$. If we equip $\mathbb{R}^3$ with the Euclidean metric, this same square distance is equal to $\sum_{i=1}^{3}(x_2^i - x_1^i)^2$, so the coordinates of the events e_1 and e_2 in the fixed inertial frame $\mathscr{R}$ are related by the equation:

$$c^2(t_2 - t_1)^2 - \sum_{i=1}^{3}(x_2^i - x_1^i)^2 = 0 \iff c^2(t_2 - t_1)^2 - \|\mathbf{x}_2 - \mathbf{x}_1\|^2 = 0, \tag{A.0.1}$$

$\|\cdot\|$ being the Euclidean norm in $\mathbb{R}^3$. Of course, Equation (A.0.1) remains valid for all spacetime differences, also infinitesimal ones, thus we can write the differential version of Equation (A.0.1)

*In this context, isotropy means invariance under rotations, while homogeneity means invariance with respect to translations.

†In Galileian relativity, the laws of physics refer only to the mechanics of objects with mass.

‡Using ct instead of t is customary in special relativity: physically, this amounts at replacing the time t with the corresponding space ct traveled by a ray of light during t.

as $c^2dt^2 - \|d\mathbf{x}\|^2 = 0$. In special relativity, the quantity

$$ds^2 = c^2dt^2 - \|d\mathbf{x}\|^2, \tag{A.0.2}$$

is called *spacetime interval*. From Equation (A.0.1) it follows that the spacetime interval between two events connected by a signal traveling at the speed of light is null. Since the speed of light is an upper limit for velocity, this amounts at promoting it as a reference and at normalizing to 0 the spacetime distance between any two events, no matter how far in space or time, connected by a light-speed signal.

Postulates 1 and 3 imply that the spacetime interval ds^2 between two events described in the inertial reference frame $\mathscr{R}$ and the spacetime interval ds'^2 between the same couple of events described in any other inertial reference frame $\mathscr{R}'$ is exactly the same: $ds'^2 = ds^2$, see e.g. [97], page 7 or [96], page 117, for a rigorous proof.

If we write the infinitesimal difference between any two events as the vector $dx = (dx^\mu)$, then the spacetime interval can be written[§] as the (non positive-definite) quadratic form $ds^2 = dx^\mu \eta_{\mu\nu} dx^\nu = dx^t \eta dx$, where $\eta = (\eta_{\mu\nu})$ is the matrix $\eta = \text{diag}\,(1, -1, -1, -1)$. The metric space $\mathcal{M} = (\mathbb{R}^4, \eta)$ is called *Minkowski spacetime* and η is the matrix associated to the Minkowski quadratic form. The associated pseudo-norm, i.e. $\|u\|^2_{\mathcal{M}} = (u^0)^2 - [(u^1)^2 + (u^2)^2 + (u^3)^2]$ is called *Minkowski norm* of $u \in \mathcal{M}$.

A *world-line* in $\mathcal{M}$ is any connected path composed by events between an initial and a final one. Straight lines in $\mathcal{M}$ correspond to world-lines of inertial movements.

The last information that we must recall is how to relate the coordinates of two inertial frames. First of all, it is simple to deduce from postulate 1 that the coordinate transformation $\omega : \mathbb{R}^4 \to \mathbb{R}^4$, $x^\mu \mapsto x'^\mu = \omega(x^\mu)$ from $\mathscr{R}$ to $\mathscr{R}'$ of an event must be *linear* (under the reasonable hypothesis to be differentiable). In fact, by postulate 1, there are no special instants and positions in $\mathbb{R}^4$, so, the distance between two events remains the same when these are translated by a fixed vector $b \in \mathbb{R}^4$. This is true independently on the coordinate system used to write the events in two arbitrary inertial reference frames $\mathscr{R}$ and $\mathscr{R}'$. Let $x = x^\mu$ and $y = y^\mu$ be the coordinates of the two events in $\mathscr{R}$ and $\omega^\mu(x)$ and $\omega^\mu(y)$ the coordinates of the same events in $\mathscr{R}'$. Since $(x^\mu + b^\mu) - (y^\mu + b^\mu) = x^\mu - y^\mu$, we must have $\omega^\mu(x+b) - \omega^\mu(y+b) = \omega^\mu(x) - \omega^\mu(y)$. If we derive the two sides of the last equation with respect to x^ν, $\nu = 0, 1, 2, 3$, we obtain $\frac{\partial \omega^\mu}{\partial x^\nu}(x + b) = \frac{\partial \omega^\mu}{\partial x^\nu}(x)$, for all $b \in \mathbb{R}^4$, since y does not depend on x. Thanks to the fact that b is arbitrary, $x + b$ represents any vector in $\mathbb{R}^4$, so the function $\frac{\partial \omega^\mu}{\partial x^\nu}$ is constant, which implies that $\frac{\partial \omega^\mu}{\partial x^\nu}(x) = \Lambda^\mu_\nu \in \mathbb{R}$ for all $x \in \mathbb{R}^4$, $\mu, \nu = 0, 1, 2, 3$, i.e.

$$x'^\mu = \omega^\mu(x) = \Lambda^\mu_\nu x^\nu + a^\mu. \tag{A.0.3}$$

The invariance of the spacetime interval imposes a strong constraint on the form of the matrix Λ: to see this, let us write the difference vector dx^μ in the inertial reference frame $\mathscr{R}'$ by using Equation (A.0.3): $dx'^\mu = y'^\mu - x'^\mu = \Lambda^\mu_\nu y^\nu + a^\mu - (\Lambda^\mu_\nu x^\nu + a^\mu) = \Lambda^\mu_\nu dx^\nu$. Thus, on one side,

$$ds'^2 = dx'^\mu \eta_{\mu\nu} dy'^\nu = dx^\alpha \Lambda^\mu_{\ \alpha} \eta_{\mu\nu} \Lambda^\nu_{\ \beta} dy^\beta, \tag{A.0.4}$$

and, on the other side,

$$ds^2 = dx^\alpha \eta_{\alpha\beta} dy^\beta, \tag{A.0.5}$$

so, the equality $ds'^2 = ds^2$ implies:

$$\Lambda^\mu_{\ \alpha} \eta_{\mu\nu} \Lambda^\nu_{\ \beta} = \eta_{\alpha\beta} \iff \Lambda^t \eta \Lambda = \eta. \tag{A.0.6}$$

[§]Here we use of the standard *Einstein's convention* which implicitly assumes a sum over repeated indices *above and below*, e.g. if $i = 1, \ldots, n$, then $a^i b_i := \sum_{i=1}^n a_i b_i$.

The set of all these matrices forms a group, called the *Lorentz group* classically denoted by the symbols $\mathscr{L} \equiv O(1,3) = \{\Lambda \in GL(4,\mathbb{R}) \ : \ \Lambda^t \eta \Lambda = \eta\}$.

Thus, postulates 1 and 3 imply that the coordinates used to describe the same event in two generic inertial reference frames are related by either non-homogeneous linear transformations of the type $x' = \Lambda x + a$, $\Lambda \in O(1,3)$, $a \in \mathbb{R}^4$, called *Poincaré transformations*, or, in the special case when $a = 0$, by linear transformations

$$x' = \Lambda x, \tag{A.0.7}$$

called *Lorentz transformations*.

Appendix B

Angle variation in Einstein-Poincaré's addition law

In Chapter 5 we have underlined the importance of the relativistic addition law between an effect vector and a state vector in describing the process of color measurement and in modeling chromatic adaptation.

Let us consider two vectors $\mathbf{v}, \mathbf{u} \in \mathcal{D}$, with r, ϑ and s, φ being their polar coordinates. Let us call R, Θ the polar coordinates of the vector $\mathbf{u} \oplus \mathbf{v}$. In Proposition 5.3.1 we provided an explicit expression for R. The aim of this appendix is to find an explicit expression for Θ as a function of the polar coordinates of the two involved vectors, i.e. $\Theta = \Theta(r, s, \vartheta, \varphi)$. As mentioned in Chapter 9, the interest of doing so is to use this formula as a possible way to model hue-depending perceptual effects, like Bezold-Brüke's or Abney's one. Furthermore this formula will be used in Appendix C to prove the monotonicity of the symmetrized relative entropy, in the case of collinear vectors.

To find an explicit formula for the angle Θ, our strategy will be to use the relation between relativistic addition law and Lorentz boosts, as we have seen in Chapter 5, in particular in Equations (5.2.18) and (5.2.20). Since we are looking for an angular coordinate, possible normalized versions of the boost, like $B_N(\mathbf{e})$ in Chapter 5, will not affect the result.

A Lorentz boost $B(\mathbf{v})$, parametrized by a generic velocity $\mathbf{v}$, can be decomposed as the product of a boost along the x-direction $B_r := B((r, 0))$ conjugated with a spatial rotation of angle ϑ, as follows:

$$B(\mathbf{v}) = R_\vartheta B_r R_\vartheta^t, \tag{B.0.1}$$

where

$$R_\vartheta = \begin{pmatrix} 1 & 0 & 0 \\ 0 & \cos\vartheta & -\sin\vartheta \\ 0 & \sin\vartheta & \cos\vartheta \end{pmatrix}, \qquad B_r = \begin{pmatrix} \gamma_\mathbf{v} & \gamma_\mathbf{v} r & 0 \\ \gamma_\mathbf{v} r & \gamma_\mathbf{v} & 0 \\ 0 & 0 & 1 \end{pmatrix}, \qquad \gamma_\mathbf{v} = \frac{1}{\sqrt{1 - r^2}}. \tag{B.0.2}$$

In fact the set of Lorentz boosts is not a group, because, in particular, the composition of two Lorentz boosts is not a Lorentz boost. Moreover $B(\mathbf{v})B(\mathbf{u}) \neq B(\mathbf{v} + \mathbf{u})$ and also $B(\mathbf{v})B(\mathbf{u}) \neq B(\mathbf{v} \oplus \mathbf{u})$. Nevertheless given two Lorentz boosts $B(\mathbf{v}_1)$ and $B(\mathbf{v}_2)$, it is true that $B(\mathbf{v}_1) = R_\phi B(\mathbf{v}_2) R_\phi^t$, where ϕ is the angle between $\mathbf{v}_1$ and $\mathbf{v}_2$.

Given a space-time event $(t, x, y)^t$, let us call $(t', x', y')^t$ its image after the action of a Lorentz boost, thus

$$\begin{pmatrix} t' \\ x' \\ y' \end{pmatrix} = B(\mathbf{v}) \begin{pmatrix} t \\ x \\ y \end{pmatrix} = R_\vartheta B_r R_\vartheta^t \begin{pmatrix} t \\ x \\ y \end{pmatrix}. \tag{B.0.3}$$

Let us call $\mathbf{u}$ the velocity vector of $(t,x,y)^t$, obtained as follows:

$$\mathbf{u} = \begin{pmatrix} u_x \\ u_y \end{pmatrix} = \begin{pmatrix} s\cos\varphi \\ s\sin\varphi \end{pmatrix} = \frac{1}{t}\begin{pmatrix} x \\ y \end{pmatrix} = \begin{pmatrix} x/t \\ y/t \end{pmatrix}. \tag{B.0.4}$$

It can be proven that the velocity vector of $(t',x',y')^t$ is actually $\mathbf{v}\oplus\mathbf{u}$. Let us call $\mathbf{u}' := \mathbf{v}\oplus\mathbf{u}$, then

$$\mathbf{v}\oplus\mathbf{u} = \mathbf{u}' = \begin{pmatrix} (\mathbf{v}\oplus\mathbf{u})_x \\ (\mathbf{v}\oplus\mathbf{u})_y \end{pmatrix} = \begin{pmatrix} \mathbf{u}'_x \\ \mathbf{u}'_y \end{pmatrix} = \frac{1}{t'}\begin{pmatrix} x' \\ y' \end{pmatrix} = \begin{pmatrix} x'/t' \\ y'/t' \end{pmatrix}. \tag{B.0.5}$$

We recall that the polar coordinates of the vectors $\mathbf{v},\mathbf{u},\mathbf{u}'$ are $(r,\vartheta),(s,\varphi),(R,\Theta)$, respectively. We are looking for an explicit expression for Θ, more precisely:

$$\Theta(r,s,\vartheta,\varphi) = \operatorname{arctg}\left(\frac{u'_y}{u'_x}\right) = \operatorname{arctg}\left(\frac{y'}{x'}\right) \tag{B.0.6}$$

In the end we will see that actually $\Theta(r,s,\vartheta,\varphi) = \Theta(r,s,\vartheta-\varphi)$.

Let us start from Equation (B.0.3):

$$\begin{pmatrix} t' \\ x' \\ y' \end{pmatrix} = R_\vartheta B_r R_\vartheta^t \begin{pmatrix} t \\ x \\ y \end{pmatrix} = R_\vartheta B_r \begin{pmatrix} t \\ x\cos\vartheta + y\sin\vartheta \\ -x\sin\vartheta + y\cos\vartheta \end{pmatrix}. \tag{B.0.7}$$

Let us call $X := x\cos\vartheta + y\sin\vartheta$ and $Y := -x\sin\vartheta + y\cos\vartheta$. Thus we obtain

$$\begin{pmatrix} t' \\ x' \\ y' \end{pmatrix} = R_\vartheta B_r \begin{pmatrix} t \\ X \\ Y \end{pmatrix} = R_\vartheta \begin{pmatrix} \gamma_\mathbf{v}(t+rX) \\ \gamma_\mathbf{v}(rt+X) \\ Y \end{pmatrix}. \tag{B.0.8}$$

Let us call

$$\begin{pmatrix} \tilde{t} \\ \tilde{x} \\ \tilde{y} \end{pmatrix} := \begin{pmatrix} \gamma_\mathbf{v}(t+rX) \\ \gamma_\mathbf{v}(rt+X) \\ Y \end{pmatrix}. \tag{B.0.9}$$

We are looking for $\Theta = \operatorname{arctg}(y'/x')$. Since it holds that

$$\begin{pmatrix} x' \\ y' \end{pmatrix} = \begin{pmatrix} \cos\vartheta & -\sin\vartheta \\ \cos\vartheta & \sin\vartheta \end{pmatrix}\begin{pmatrix} \tilde{x} \\ \tilde{y} \end{pmatrix}, \tag{B.0.10}$$

it is true that

$$\Theta = \operatorname{arctg}\left(\frac{y'}{x'}\right) = \vartheta + \operatorname{arctg}\left(\frac{\tilde{y}}{\tilde{x}}\right). \tag{B.0.11}$$

We can now perform the following computations:

$$\begin{aligned} \Theta(r,s,\vartheta,\varphi) &= \vartheta + \operatorname{arctg}\left(\frac{Y}{\gamma_\mathbf{v}(rt+X)}\right) = \vartheta + \operatorname{arctg}\left(\frac{-x\sin\vartheta + y\cos\vartheta}{\gamma_\mathbf{v}(rt + x\cos\vartheta + y\sin\vartheta)}\right) \\ &= \vartheta + \operatorname{arctg}\left(\frac{-u_x\sin\vartheta + u_y\cos\vartheta}{\gamma_\mathbf{v}(r + u_x\cos\vartheta + u_y\sin\vartheta)}\right) \\ &= \vartheta + \operatorname{arctg}\left(\frac{-s\cos\varphi\sin\vartheta + s\sin\varphi\cos\vartheta}{\gamma_\mathbf{v}(r + s\cos\varphi\cos\vartheta + s\sin\varphi\sin\vartheta)}\right) \\ &= \vartheta + \operatorname{arctg}\left(\frac{1}{\gamma_\mathbf{v}}\frac{s\sin(\varphi-\vartheta)}{r + s\cos(\varphi-\vartheta)}\right). \end{aligned} \tag{B.0.12}$$

The explicit formula for the angle Θ, that we were looking for, is the following:

$$\Theta(r,s,\varphi-\vartheta) = \vartheta + \operatorname{arctg}\left(\frac{1}{\gamma_\mathbf{v}}\frac{s\sin(\varphi-\vartheta)}{r + s\cos(\varphi-\vartheta)}\right). \tag{B.0.13}$$

Simple cases

We conclude some simple cases of the explicit formula for Θ, which are more used in special relativity theory than the general case of Equation (B.0.13). In particular the case where $\varphi = \vartheta$ will be used in Appendix C.

- The first easy situation is when $\vartheta = 0$. In this case $B(\mathbf{v}) = B_r$ and we obtain

$$\Theta = \operatorname{arctg}\left(\frac{1}{\gamma_{\mathbf{v}}}\frac{s\sin\varphi}{r + s\cos\varphi}\right) = \operatorname{arctg}\left(\frac{1}{\gamma_{\mathbf{v}}}\frac{u_y}{r + u_x}\right). \tag{B.0.14}$$

- When $\varphi = \vartheta$, then $\mathbf{u}$ and $\mathbf{v}$ are collinear, hence we expect $\mathbf{v} \oplus \mathbf{u}$ to be collinear as well, $\Theta = \vartheta = \varphi$. Indeed

$$\Theta = \vartheta + \operatorname{arctg}(0) = \vartheta. \tag{B.0.15}$$

- In the case $r = 1$ we obtain

$$\Theta = \vartheta + \operatorname{arctg}\left(\sqrt{1 - r^2}s\sin(\varphi - \vartheta)\right) = \vartheta, \tag{B.0.16}$$

  which is related to the property (5.2.23) of the relativistic addition law.

- When $\vartheta = \frac{\pi}{2}$, the expression for Θ is given by:

$$\Theta = \operatorname{arctg}\left(\gamma_{\mathbf{v}}\frac{r + s\cos\varphi}{s\sin\varphi}\right). \tag{B.0.17}$$

  There are different ways to obtain the previous formula. One can use a boost along the y-direction instead of B_r, or equivalently exchange x' and y' in Equation (B.0.14). Another way is to start from formula (B.0.13) and use the following relations:

$$\operatorname{arctg}\alpha \pm \operatorname{arctg}\beta = \operatorname{arctg}\left(\frac{\alpha \pm \beta}{1 \mp \alpha\beta}\right), \tag{B.0.18}$$

$$-\operatorname{arctg}\alpha = \operatorname{arctg}(-\alpha). \tag{B.0.19}$$

  Indeed we can perform the following computations:

$$\begin{aligned}
\Theta &= \frac{\pi}{2} + \operatorname{arctg}\left(\frac{1}{\gamma_{\mathbf{v}}}\frac{s\sin(\varphi - \pi/2)}{r + s\cos(\varphi - \pi/2))}\right) \\
&= \lim_{x\mapsto+\infty}\operatorname{arctg}x + \operatorname{arctg}\left(\frac{1}{\gamma_{\mathbf{v}}}\frac{-s\cos\varphi}{r + s\sin\varphi}\right) \\
&\overset{(B.0.19)}{=} \lim_{x\mapsto+\infty}\operatorname{arctg}x - \operatorname{arctg}\left(\frac{1}{\gamma_{\mathbf{v}}}\frac{s\sin\varphi}{r + s\cos\varphi}\right) \\
&\overset{(B.0.18)}{=} \lim_{x\mapsto+\infty}\operatorname{arctg}\left(\frac{x - \frac{1}{\gamma_{\mathbf{v}}}\frac{s\sin\varphi}{r+s\cos\varphi}}{1 + x\frac{1}{\gamma_{\mathbf{v}}}\frac{s\sin\varphi}{r+s\cos\varphi}}\right) \\
&= \operatorname{arctg}\left(\gamma_{\mathbf{v}}\frac{r + s\cos\varphi}{s\sin\varphi}\right).
\end{aligned} \tag{B.0.20}$$

Appendix C

Monotonicity of the symmetrized relative entropy

In Chapter 5 we have introduced the concept of relative entropy, which played an important role in the definitions of chromatic attributes in Chapter 6.
Relative entropy between two states, see Definition 5.4 in Chapter 5, is clearly not symmetric. If symmetry is needed, e.g. to use it as a metric for color discernability as mentioned in Chapter 9, it is natural to define its symmetrized version.

Definition C.0.1 (Symmetrized relative entropy)**.** Let $\mathbf{s}, \mathbf{t}$ be two quantum states and $\rho_{\mathbf{s}}, \rho_{\mathbf{t}}$ be their associated density matrices. Their symmetrized relative entropy is given by

$$R_S(\rho_{\mathbf{s}}, \rho_{\mathbf{t}}) = \frac{R(\rho_{\mathbf{s}}||\rho_{\mathbf{t}}) + R(\rho_{\mathbf{t}}||\rho_{\mathbf{s}})}{2}. \tag{C.0.1}$$

In the following we will make a small abuse of notation using symbols of the corresponding state symbols $\mathbf{s}, \mathbf{t}$ or the chromatic vector ones $\mathbf{v_s}, \mathbf{v_t}$ instead of $\rho_{\mathbf{s}}, \rho_{\mathbf{t}}$, i.e. $R_S(\mathbf{v_s}, \mathbf{v_t}) = R_S(\rho_{\mathbf{s}}, \rho_{\mathbf{t}})$. Let $\rho_{\mathbf{s}}, \rho_{\mathbf{t}}$ have the following expressions:

$$\rho_{\mathbf{s}} = \frac{1}{2}\begin{pmatrix} 1 + s\cos\varphi & s\sin\varphi \\ s\sin\varphi & 1 - s\cos\varphi \end{pmatrix}, \qquad \rho_{\mathbf{t}} = \frac{1}{2}\begin{pmatrix} 1 + t\cos\psi & t\sin\psi \\ t\sin\psi & 1 - t\cos\psi \end{pmatrix}, \tag{C.0.2}$$

then, starting from Equation (5.4.4), straightforward computations lead to the following, more explicit, expression for R_S:

$$R_S(\mathbf{s}, \mathbf{t}) = \frac{1}{2}\left[\frac{s - t\cos(\varphi - \psi)}{2}\log_2\left(\frac{1+s}{1-s}\right) + \frac{t - s\cos(\varphi - \psi)}{2}\log_2\left(\frac{1+t}{1-t}\right)\right]. \tag{C.0.3}$$

The interest of proving the following proposition is explained in detail in Chapter 9.

Proposition C.0.2 (Monotonicity of the symmetrized relative entropy)**.** *Let $\mathbf{s}, \mathbf{t}$ be two quantum states, $\mathbf{v_s}, \mathbf{v_t}$ being their associated chromatic vectors. Let $\mathbf{e}$ be an effect, with effect vector $\mathbf{v_e}$, then the symmetrized relative entropy between $\mathbf{v_s}$ and $\mathbf{v_t}$ is not-increasing after applying Einstein-Poincaré's addition law w.r.t. $\mathbf{v_e}$ on the left as follows:*

$$R_S(\mathbf{v_s}||\mathbf{v_t}) \geq R_S(\mathbf{v_e} \oplus \mathbf{v_s}||\mathbf{v_e} \oplus \mathbf{v_t}). \tag{C.0.4}$$

Proof of the collinear case. Let us start by calling $\mathbf{s}'$ and $\mathbf{t}'$ the states whose chromatic vectors are $\mathbf{v_e} \oplus \mathbf{v_s}$ and $\mathbf{v_e} \oplus \mathbf{v_t}$, respectively. Let $(s, \vartheta), (t, \psi), (r, \vartheta), (s', \varphi'), (t', \psi')$ be the polar coordinates of the vectors $\mathbf{v_s}, \mathbf{v_t}, \mathbf{v_e}, \mathbf{v_e} \oplus \mathbf{v_s}, \mathbf{v_e} \oplus \mathbf{v_t}$, respectively. Using Equation (C.0.3), the thesis is equivalent to prove that the following expression

$$R_S(\mathbf{s}, \mathbf{t}) = \frac{1}{2}\left[\frac{s - t\cos(\varphi - \psi)}{2}\log_2\left(\frac{1+s}{1-s}\right) + \frac{t - s\cos(\varphi - \psi)}{2}\log_2\left(\frac{1+t}{1-t}\right)\right], \tag{C.0.5}$$

is greater or equal to the following one

$$R_S(\mathbf{s}', \mathbf{t}') = \frac{1}{2}\left[\frac{s' - t'\cos(\varphi' - \psi')}{2}\log_2\left(\frac{1+s'}{1-s'}\right) + \frac{t' - s'\cos(\varphi' - \psi')}{2}\log_2\left(\frac{1+t'}{1-t'}\right)\right]. \tag{C.0.6}$$

We are considering only the case of collinear vectors, hence $\varphi = \psi = \vartheta$. Since $\cos(\varphi - \psi) = 1$, Equation (C.0.5) has the following expression:

$$R_S(\mathbf{s}, \mathbf{t}) = \frac{s - t}{4}\log_2\left(\frac{(1+s)(1-t)}{(1-s)(1+t)}\right). \tag{C.0.7}$$

By formula (B.0.13) also $\varphi' = \psi' = \vartheta$, so $\cos(\varphi' - \psi') = 1$. Moreover $s' = \frac{r+s}{1+rs}$ and $t' = \frac{r+t}{1+rt}$, thus Equation (C.0.6) can be simplified as follows:

$$R_S(\mathbf{s}', \mathbf{t}') = \frac{s' - t'}{4}\log_2\left(\frac{(1+s')(1-t')}{(1-s')(1+t')}\right). \tag{C.0.8}$$

Notice that

$$\frac{(1+s')(1-t')}{(1-s')(1+t')} = \frac{1 + \frac{r+s}{1+rs}}{1 - \frac{r+s}{1+rs}}\frac{1 - \frac{r+t}{1+rt}}{1 + \frac{r+t}{1+rt}} = \frac{(1+r)(1+s)}{(1-r)(1-s)}\frac{(1-r)(1-t)}{(1+r)(1+t)} = \frac{(1+s)(1-t)}{(1-s)(1+t)}. \tag{C.0.9}$$

Furthermore

$$s' - t' = \frac{s+r}{1+rs} - \frac{t+r}{1+rt} = \frac{1-r^2}{(1+rs)(1+rt)}(s-t). \tag{C.0.10}$$

Hence Equation (C.0.8) becomes

$$R_S(\mathbf{s}', \mathbf{t}') = (s-t)\frac{1-r^2}{4(1+rs)(1+rt)}\log_2\left(\frac{(1+s)(1-t)}{(1-s)(1+t)}\right). \tag{C.0.11}$$

The inequality that we want to prove, $R_S(\mathbf{s}', \mathbf{t}') \leq R_S(\mathbf{s}, \mathbf{t})$, in this particular case, has the following expression:

$$\frac{(1-r^2)(s-t)}{4(1+rs)(1+rt)}\log_2\left(\frac{(1+s)(1-t)}{(1-s)(1+t)}\right) \leq \frac{s-t}{4}\log_2\left(\frac{(1+s)(1-t)}{(1-s)(1+t)}\right). \tag{C.0.12}$$

Notice that

$$\log_2\left(\frac{(1+s)(1-t)}{(1-s)(1+t)}\right) \geq 0 \iff \frac{(1+s)(1-t)}{(1-s)(1+t)} \geq 1 \iff s - t \geq 0. \tag{C.0.13}$$

This means that for all s, t, we have that

$$(s-t)\log_2\left(\frac{(1+s)(1-t)}{(1-s)(1+t)}\right) \geq 0, \tag{C.0.14}$$

so Equation (C.0.12) is equivalent to prove that

$$\frac{1-r^2}{(1+rs)(1+rt)} \leq 1. \tag{C.0.15}$$

Straightforward computations show that this is true for all $r, s, t \in [0, 1]$. □

Bibliography

[1] Cie 160-2004, A review of chromatic adaptation transforms. ISBN:9783901906305, 2004.

[2] A. Artusi, T. Pouli, F. Banterle, and A.O. Akyüz. Automatic saturation correction for dynamic range management algorithms. *Signal Processing: Image Communication*, 63:100–112, 2018.

[3] A. Ashtekar, A. Corichi, and M. Pierri. Geometry in color perception. *Black Holes, Gravitational Radiation and the Universe*, pages 535–550, 1999.

[4] D ASTM. 2244–07 e1, standard practice for calculation of color tolerances and color differences from instrumentally measured color coordinates, american society for testing and materials. *American Society for Testing and Materials, West Conshohocken, PA*, pages 3134–97, 2007.

[5] S. Aston and A. Hurlbert. What# thedress reveals about the role of illumination priors in color perception and color constancy. *Journal of vision*, 17(9):4–4, 2017.

[6] K.M.R. Audenaert and J. Eisert. Continuity bounds on the quantum relative entropy—ii. *Journal of Mathematical Physics*, 52(11):112201, 2011.

[7] G. Auletta, M. Fortunato, and G. Parisi. *Quantum Mechanics*. Cambridge University Press, 2009.

[8] J.C. Baez. Division algebras and quantum theory. *Foundations of Physics*, 42(7):819–855, 2012.

[9] N. Banic and S. Loncaric. Flash and storm: Fast and highly practical tone mapping based on naka-rushton equation. In *VISIGRAPP (4: VISAPP)*, pages 47–53, 2018.

[10] A.F. Beardon. The klein, hilbert and poincaré metrics of a domain. *Journal of computational and applied mathematics*, 105(1-2):155–162, 1999.

[11] I. Bengtsson and K. Zyczkowski. *Geometry of Quantum States, an introduction to quantum entanglement*. Cambridge University Press, 2017.

[12] M. Berthier. Geometry of color perception. Part 2: perceived colors from real quantum states and Hering's rebit. *The Journal of Mathematical Neuroscience*, 10(1):1–25, 2020.

[13] M. Berthier, V. Garcin, N. Prencipe, and E. Provenzi. The relativity of color perception. *Journal of Mathematical Psychology*, 103:102562, 2021.

[14] M. Berthier, N. Prencipe, and E. Provenzi. A quantum information-based refoundation of color perception concepts. *SIAM Journal on Imaging Sciences*, 15(4):1944–1976, 2022.

[15] M. Berthier and E. Provenzi. When geometry meets psycho-physics and quantum mechanics: Modern perspectives on the space of perceived colors. In *International Conference on Geometric Science of Information 2019*, volume 11712 of *Lecture Notes in Computer Science*, pages 621–630. Springer Berlin-Heidelberg, 2019.

[16] M. Berthier and E. Provenzi. From Riemannian trichromacy to quantum color opponency via hyperbolicity. *Journal of Mathematical Imaging and Vision*, 63(6):681–688, 2021.

[17] M. Berthier and E. Provenzi. Hunt's colorimetric effect from a quantum measurement viewpoint. In *International Conference on Geometric Science of Information*, volume 12829 of *Lecture Notes in Computer Science*, pages 172–180. Springer Berlin-Heidelberg, 2021.

[18] M. Berthier and E. Provenzi. The quantum nature of color perception: Uncertainty relations for chromatic opposition. *Journal of Imaging*, 7(2):40, 2021.

[19] M. Berthier and E. Provenzi. Quantum measurement and colour perception: theory and applications. *Proceedings of the Royal Society A*, 478(2258):20210508, 2022.

[20] S. Bianco and R. Schettini. Two new von kries based chromatic adaptation transforms found by numerical optimization. *Color Research & Application: Endorsed by Inter-Society Color Council, The Colour Group (Great Britain), Canadian Society for Color, Color Science Association of Japan, Dutch Society for the Study of Color, The Swedish Colour Centre Foundation, Colour Society of Australia, Centre Français de la Couleur*, 35(3):184–192, 2010.

[21] E.J. Breneman. Corresponding chromaticities for different states of adaptation to complex visual fields. *JOSA A*, 4(6):1115–1129, 1987.

[22] M.H. Brill. Minimal von kries illuminant invariance. *Color Research & Application: Endorsed by Inter-Society Color Council, The Colour Group (Great Britain), Canadian Society for Color, Color Science Association of Japan, Dutch Society for the Study of Color, The Swedish Colour Centre Foundation, Colour Society of Australia, Centre Français de la Couleur*, 33(4):320–323, 2008.

[23] M.H. Brill and G. West. Group theory of chromatic adaptation. *Die Farbe*, 31(1-3):4–22, 1983.

[24] G. Buchsbaum. A spatial processor model for object colour perception. *Journal of the Franklin Institute*, 310:337–350, 1980.

[25] G. Buchsbaum and A. Gottschalk. Trichromacy, opponent colours coding and optimum colour information transmission in the retina. *Proc. Royal Society of London B*, 220:89–113, 1983.

[26] R.W. Burnham, R.M. Evans, and S.M. Newhall. Prediction of color appearance with different adaptation illuminations. *JOSA*, 47(1):35–42, 1957.

[27] P. Busch, M. Grabowski, and P.J. Lahti. *Operational quantum physics*, volume 31. Springer Science & Business Media, 1997.

[28] A. Cayley. On the colouring of maps. *Proceedings of the London Mathematical Society*, 9:148, 1878.

[29] J. Chen and A.A. Ungar. The bloch gyrovector. *Foundations of Physics*, 32(4):531–565, 2002.

[30] D. Cheng, B. Price, S. Cohen, and M.S. Brown. Beyond white: Ground truth colors for color constancy correction. In *Proceedings of the IEEE International Conference on Computer Vision*, pages 298–306, 2015.

[31] B. Colbois and C. Vernicos. Les géométries de Hilbert sont à géométrie locale bornée. In *Annales de l'institut Fourier*, volume 57, pages 1359–1375, 2007.

[32] J. Cortese. Relative entropy and single qubit Holevo-Schumacher-Westmoreland channel capacity. *arXiv: Quantum Physics*, 2002.

[33] C.P. Crocetti and W.P. Bethke. *Scientific and Technical Aerospace Reports*, 1.

[34] W.J. Culver. On the existence and uniqueness of the real logarithm of a matrix. *Proceedings of the American Mathematical Society*, 17(5):1146–1151, 1966.

[35] D.M. Dacey and B.B. Lee. The'blue-on'opponent pathway in primate retina originates from a distinct bistratified ganglion cell type. *Nature*, 367(6465):731–735, 1994.

[36] D.M. Dacey and B.B. Lee. Functional architecture of cone signal pathways. *Color vision: From genes to perception*, page 181, 2001.

[37] K.K. de Valois. *Seeing*. Academic Press, 2000.

[38] R.L. de Valois and K.D. de Valois. Neural coding of color. 1997.

[39] P. Debevec and J. Malik. Recovering high dynamic range radiance maps from photographs. In *Proc. of the 24th annual conf. on Computer graphics*, pages 369–378, 1997.

[40] P.A.M. Dirac. *The Principles of Quantum Mechanics*. Number 27 in International Series of Monographs on Physics. Oxford University Press, Oxford, 4th edition, 1982.

[41] M.P. do Carmo. *Differential geometry of curves and surfaces*. Prentice Hall, 1976.

[42] J. Drösler. Color similarity represented as a metric of color space. In *Contributions to mathematical psychology, psychometrics, and methodology*, pages 19–37. Springer, 1994.

[43] J. Drösler. The invariances of weber's and other laws as determinants of psychophysical structures. *Geometric representations of perceptual phenomena*, 1995.

[44] E. Dubois. The structure and properties of color spaces and the representation of color images. *Synthesis lectures on image, video, and multimedia processing*, 4(1):1–129, 2009.

[45] M. Ebner. Color constancy. Wiley. 2007.

[46] G.G. Emch. *Algebraic methods in statistical mechanics and quantum field theory*. Courier Corporation, 2009.

[47] R.J. Ennis and Q. Zaidi. Geometrical structure of perceptual color space: mental representations and adaptation invariance. *Journal of vision*, 19(12):1–1, 2019.

[48] M.D. Fairchild. The hdr photographic survey. In *Color and imaging conference*, volume 2007, pages 233–238. Society for Imaging Science and Technology, 2007.

[49] M.D. Fairchild. *Color appearance models*. Wiley, 2013.

[50] J. Faraut and A. Koranyi. *Analysis on Symmetric Cones*. Clarendon Press, Oxford, 1994.

[51] I. Farup. Hyperbolic geometry for colour metrics. *Optics Express*, 22(10):12369–12378, 2014.

[52] S. Ferradans, M. Bertalmío, E. Provenzi, and V. Caselles. An analysis of visual adaptation and contrast perception for tone mapping. *IEEE Transactions on Pattern Analysis and Machine Intelligence*, 33(10):2002–2012, 2011.

[53] S. Ferradans, M. Bertalmío, E. Provenzi, and V. Caselles. Generation of hdr images in non-static conditions based on gradient fusion. In *Proceedings of the VISAPP Conference, February 24-26, Rome, Italy*, pages 31–37. SciTePress, 2012.

[54] S. Ferradans, R. Palma-Amestoy, and E. Provenzi. An algorithmic analysis of variational models for perceptual local contrast enhancement. *Image Processing On Line*, 5(10):219–233, 2015.

[55] G. Finlayson, H. Gong, and R.B. Fisher. Color homography: theory and applications. *IEEE transactions on pattern analysis and machine intelligence*, 41(1):20–33, 2017.

[56] G.D. Finlayson, M.S. Drew, and B.V. Funt. Color constancy: generalized diagonal transforms suffice. *JOSA A*, 11(11):3011–3019, 1994.

[57] V. Fock. *The theory of space, time and gravitation*. Elsevier, 2015.

[58] B.V. Funt and B.C. Lewis. Diagonal versus affine transformations for color correction. *JOSA A*, 17(11):2108–2112, 2000.

[59] P.V. Gehler, C. Rother, A. Blake, T. Minka, and T. Sharp. Bayesian color constancy revisited. In *2008 IEEE Conference on Computer Vision and Pattern Recognition*, pages 1–8. IEEE, 2008.

[60] T. Gevers, A. Gijsenij, J. van de Weijer, and J-M. Geusebroek. *Color in Computer Vision, Fundamentals and Applications*. Wiley, 2012.

[61] A. Gijsenij, T. Gevers, and J. van de Weijer. Computational color constancy: Survey and experiments. *IEEE transactions on image processing*, 20(9):2475–2489, 2011.

[62] A. Gilchrist. Lightness and brightness. *Current Biology*, 17(8):R267–R269, 2007.

[63] A. Gilchrist, C. Kossyfidis, F. Bonato, T. Agostini, J. Cataliotti, X. Li, B. Spehar, V. Annan, and E. Economou. An anchoring theory of lightness perception. *Psychological review*, 106(4):795, 1999.

[64] M. Gogberashvili. Split quaternions and particles in (2+1)-space. *The European Physical Journal C*, 74(12):1–9, 2014.

[65] B.E. Goldstein. *Sensation and Perception, 9th Edition*. Cengage Learning, 2013.

[66] R.C. Gonzalez and R.E. Woods. Digital image processing. Prentice Hall. 2002.

[67] H. Grassmann. Zur Theorie der Farbenmischung. *Annalen der Physik*, 165(5):69–84, 1853.

[68] A. Guennec, N. Prencipe, and E. Provenzi. Color correction with lorentz boosts. In *2021 The 4th International Conference on Image and Graphics Processing*, ICIGP 2021, page 162–168, New York, NY, USA, 2021. Association for Computing Machinery.

[69] B.C. Hall. *Lie groups, Lie algebras, and representations: an elementary introduction*, volume 222 (2nd ed.). Springer, 2015.

[70] C.L. Hardin. A new look at color. *American Philosophical Quarterly*, 21(2):125–133, 1984.

[71] T. Heinosaari and M. Ziman. *The mathematical language of quantum theory: from uncertainty to entanglement*. Cambridge University Press, 2011.

[72] E. Hering. *Zur Lehre vom Lichtsinne: sechs Mittheilungen an die Kaiserl. Akademie der Wissenschaften in Wien*. C. Gerold's Sohn, 1878.

[73] D.H. Hubel. *Eye, Brain, and Vision*. Scientific American Library, 1995.

[74] L.M. Hurvich and D. Jameson. Some quantitative aspects of an opponent-colors theory. i. chromatic responses and spectral saturation. *JOSA*, 45(7):546–552, 1955.

[75] L.M. Hurvich and D. Jameson. Some quantitative aspects of an opponent-colors theory. ii. brightness, saturation, and hue in normal and dichromatic vision. *JOSA*, 45(8):602–616, 1955.

[76] L.M. Hurvich and D. Jameson. Some quantitative aspects of an opponent-colors theory. iii. changes in brightness, saturation, and hue with chromatic adaptation. *JOSA*, 46(6):405–415, 1956.

[77] L.M. Hurvich and D. Jameson. Some quantitative aspects of an opponent-colors theory. iv. a psychological color specification system. *JOSA*, 46(6):416–421, 1956.

[78] M. Jafari and Y. Yayli. Matrix theory over the split quaternions. *International journal of geometry*, 3(2):57–69, 2014.

[79] P. Jordan, J. von Neumann, and E. Wigner. On an algebraic generalization of the quantum mechanical formalism. *Annals of Math.*, 35:29–64, 1934.

[80] D.B. Judd. Ideal color space. *Color Eng*, 8(44):2405, 1970.

[81] J. Keener and J. Sneyd. *Mathematical Physiology*. Springer, 2008.

[82] D. Kim, J. Kim, S. Nam, D. Lee, Y. Lee, N. Kang, H-E. Lee, B. Yoo, J-J. Han, and S.J. Kim. Large scale multi-illuminant (lsmi) dataset for developing white balance algorithm under mixed illumination. In *Proceedings of the IEEE/CVF International Conference on Computer Vision*, pages 2410–2419, 2021.

[83] F.A.A. Kingdom. Lightness, brightness and transparency: A quarter century of new ideas, captivating demonstrations and unrelenting controversy. *Vision research*, 51(7):652–673, 2011.

[84] M. Koecher. Jordan algebras and differential geometry. In *Actes, Congrès Intern. Math.*, volume 1, pages 279–283, 1970.

[85] J.J. Koenderink. *Color for the Sciences*. The MIT Press, 2010.

[86] J.J. Koenderink and M.A. van de Grind, W.A .and Bouman. Opponent color coding: A mechanistic model and a new metric for color space. *Kybernetik*, 10(2):78–98, 1972.

[87] J.J. Koenderink and A.J. van Doorn. The structure of colorimetry. In *International Workshop on Algebraic Frames for the Perception-Action Cycle*, pages 69–77. Springer, 2000.

[88] J.J. Koenderink and A.J. van Doorn. *Perspectives on colour space*. Oxford University, 2003.

[89] K. Koščević, V. Stipetić, E. Provenzi, N. Banić, M. Subašić, and S. Lončarić. Hd-race: Spray-based local tone mapping operator. In *2021 12th International Symposium on Image and Signal Processing and Analysis (ISPA)*, pages 264–269, 2021.

[90] D.H. Krantz. Color measurement and color theory: I. representation theorem for grassmann structures. *Journal of Mathematical Psychology*, 12(3):283–303, 1975.

[91] D.H. Krantz. Color measurement and color theory: Ii. opponent-colors theory. *Journal of Mathematical Psychology*, 12(3):304–327, 1975.

[92] J.H. Krantz and B. L. Schwartz. Interactive sensation laboratory exercises (isle), 2015.

[93] K. Kraus, A. Böhm, J.D. Dollard, and W.H. Wootters. States, effects, and operations: fundamental notions of quantum theory. lectures in mathematical physics at the university of texas at austin. *Lecture notes in physics*, 190, 1983.

[94] R. Lafer-Sousa, K.L. Hermann, and B.R. Conway. Striking individual differences in color perception uncovered by 'the dress' photograph. *Current Biology*, 25(13):R545–R546, 2015.

[95] E.H. Land and J.J. McCann. Lightness and Retinex theory. *Journal of the Optical Society of America*, 61(1):1–11, January 1971.

[96] L.D. Landau and E.M. Lifshitz. *The classical theory of fields*. Pergamon, 1971.

[97] K. Lechner. *Classical Electrodynamics*. Springer, 2018.

[98] H-C. Lee. *Introduction to Color Imaging Science*. Cambridge University Press, 2005.

[99] R. Lenz, T.H. Bui, and J. Hernández-Andrés. Group theoretical structure of spectral spaces. *Journal of Mathematical Imaging and Vision*, 23(3):297–313, 2005.

[100] R. Lenz, P. L. Carmona, and P. Meer. The hyperbolic geometry of illumination-induced chromaticity changes. In *2007 IEEE Conference on Computer Vision and Pattern Recognition*, pages 1–6. IEEE, 2007.

[101] C. Li, Z. Li, Z. Wang, Y. Xu, M.R. Luo, G. Cui, M. Melgosa, M.H. Brill, and M. Pointer. Comprehensive color solutions: Cam16, cat16, and cam16-ucs. *Color Research & Application*, 42(6):703–718, 2017.

[102] B. Lindbloom. Delta e (cie 2000), http://brucelindbloom.com/Eqn_DeltaE_CIE2000.html. 2009.

[103] B. Lindbloom. Delta e (cie 1994), http://brucelindbloom.com/Eqn_DeltaE_CIE94.html. 2011.

[104] A. Lou, I. Katsman, Q. Jiang, S. Belongie, S-N. Lim, and C. De Sa. Differentiating through the fréchet mean. In Hal Daumé III and Aarti Singh, editors, *Proceedings of the 37th International Conference on Machine Learning*, volume 119, pages 6393–6403. PMLR, 13–18 Jul 2020.

[105] M.R. Luo, G. Cui, and C. Li. Uniform colour spaces based on ciecam02 colour appearance model. *Color Research & Application: Endorsed by Inter-Society Color Council, The Colour Group (Great Britain), Canadian Society for Color, Color Science Association of Japan, Dutch Society for the Study of Color, The Swedish Colour Centre Foundation, Colour Society of Australia, Centre Français de la Couleur*, 31(4):320–330, 2006.

[106] D.L. MacAdam. Visual sensitivities to colour differences in daylight. *Journal of the Optical Society of America A*, 32(5):247–274, 1942.

[107] R. Mantiuk, R. Mantiuk, A. Tomaszewska, and W. Heidrich. Color correction for tone mapping. *Computer Graphics Forum (Proc. EUROGRAPHICS)*, 28(3):193–202, 2009.

[108] J.C. Maxwell. Experiments on colour as perceived by the eye, with remarks on colour-blindness. *Proceedings of the Royal Society of Edinburgh*, 3:299–301, 1857.

[109] K. McCrimmon. Jordan algebras and their applications. *Bulletin of the American Mathematical Society*, 84:612–627, 1978.

[110] K. McCrimmon. *A taste of Jordan Algebras*. Springer-Verlag, New York, 2004.

[111] M. Melgosa. Cie / iso new standard: Ciede2000. 2013.

[112] N.D. Mermin. Relativity without light. *American Journal of Physics*, 52(2):119–124, 1984.

[113] V. Moretti. *Spectral theory and quantum mechanics: mathematical foundations of quantum theories, symmetries and introduction to the algebraic formulation*. Springer, 2017.

[114] K.I. Naka and W.A.H. Rushton. S-potentials from luminosity units in the retina of fish (cyprinidae). *Journal of Physiology*, 185:587–599, 1966.

[115] Y. Nayatani. A colorimetric explanation of the helmholtz–kohlrausch effect. *Color Research & Application: Endorsed by Inter-Society Color Council, The Colour Group (Great Britain), Canadian Society for Color, Color Science Association of Japan, Dutch Society for the Study of Color, The Swedish Colour Centre Foundation, Colour Society of Australia, Centre Français de la Couleur*, 23(6):374–378, 1998.

[116] I. Newton. Opticks, or, a treatise of the reflections, refractions, inflections & colours of light. Courier Corporation. 1952.

[117] I. Newton. A new theory about light and colors. *American journal of physics*, 61(2):108–112, 1993.

[118] M. Nölle, M. Suda, and W. Boxleitner. H2si-a new perceptual colour space. In *2013 18th International Conference on Digital Signal Processing (DSP)*, pages 1–6. IEEE, 2013.

[119] M. Ohya and D. Petz. *Quantum entropy and its use*. Springer Science & Business Media, 2004.

[120] C. Oleari. *Misurare il colore: spettrofotometria, fotometria e colorimetria: fisiologia e percezione*. Hoepli, 1998.

[121] B. Ottosson. *A perceptual color space for image processing. Available at https://bottosson.github.io/posts/oklab/*, 2020.

[122] A. Papoulis. *The Fourier integral and its applications*. 1962.

[123] D. Petz. *Quantum information theory and quantum statistics*. Springer Science & Business Media, 2007.

[124] N. Prencipe, V. Garcin, and E. Provenzi. Origins of hyperbolicity in color perception. *Journal of Imaging*, 42(6):1–19, 2020.

[125] N. Prencipe and E. Provenzi. Embedding naka-rushton's equation in the geometric setting of möbius transformations. In *2021 12th International Symposium on Image and Signal Processing and Analysis (ISPA)*, pages 259–263, 2021.

[126] N. Prencipe and E. Provenzi. Geometric models for color perception. *Cultura e Scienza del Colore-Color Culture and Science*, 13(02):50–56, 2021.

[127] E. Provenzi. A differential geometry model for the perceived colors space. *International Journal of Geometric Methods in Modern Physics*, 13(08):1630008, 2016.

[128] E. Provenzi. *Computational Color Science: Variational Retinex-like Methods*. John Wiley & Sons, 2017.

[129] E. Provenzi. Geometry of color perception. Part 1: Structures and metrics of a homogeneous color space. *The Journal of Mathematical Neuroscience*, 10(1):1–19, 2020.

[130] D. Purves, B. Lotto, and T. Polger. Color vision and the four-color-map problem. *Journal of Cognitive Neuroscience*, 12(2):233–237, 2000.

[131] J.G. Ratcliffe. *Foundations of hyperbolic manifolds*, volume 149. Springer.

[132] M. Reed, B. Simon, B. Simon, and B. Simon. *Methods of modern mathematical physics*, volume 1. Elsevier, 1972.

[133] E. Reinhard, E.A. Khan, A.O. Akyuz, and G. Johnson. *Color imaging: fundamentals and applications*. CRC Press, 2008.

[134] E. Reinhard, G. Ward, S. Pattanaik, and P. Debevec. *High Dynamic Range Imaging, Acquisition, Display, And Image-Based Lighting*. Morgan Kaufmann Ed., 2005.

[135] H.L. Resnikoff. Differential geometry and color perception. *Journal of Mathematical Biology*, 1:97–131, 1974.

[136] B. Russell. *The problems of philosophy*. OUP Oxford, 2001.

[137] J. Schanda. *Colorimetry: understanding the CIE system*. John Wiley & Sons, 2007.

[138] E. Schrödinger. Grundlinien einer theorie der farbenmetrik im tagessehen (Outline of a theory of colour measurement for daylight vision). Available in English in Sources of Colour Science, Ed. David L. Macadam, The MIT Press (1970), 134-82. *Annalen der Physik*, 63(4):397–456; 481–520, 1920.

[139] S.A. Shafer. Using color to separate reflection components. *Color Research & Application*, 10(4):210–218, 1985.

[140] R. Shapley and C. Enroth-Cugell. *Visual adaptation and retinal gain controls*, volume 3, chapter 9, pages 263–346. Progress in Retinal Research, 1984.

[141] S.K. Shevell and P.R. Martin. Color opponency: tutorial. *JOSA A*, 34(7):1099–1108, 2017.

[142] L. Shi. Re-processed version of the gehler color constancy dataset of 568 images. *http://www. cs. sfu. ca/˜ color/data/*, 2000.

[143] L. Silberstein. Investigations on the intrinsic properties of the color domain. *JOSA*, 28(3):63–85, 1938.

[144] L. Silberstein. Investigations on the intrinsic properties of the color domain. ii. *JOSA*, 33(1):1–10, 1943.

[145] A.R. Smith. Color gamut transform pairs. *ACM Siggraph Computer Graphics*, 12(3):12–19, 1978.

[146] F. Strocchi. *An introduction to the mathematical structure of quantum mechanics: a short course for mathematicians*, volume 28. World Scientific, 2008.

[147] P.K. Townsend. The jordan formulation of quantum mechanics: A review., supersymmetry, supergravity, and related topics, f. del alguila, ja de azcárraga and le ibanes, 1985.

[148] A.A. Ungar. Einstein's special relativity: Unleashing the power of its hyperbolic geometry. *Computers & Mathematics with Applications*, 49(2-3):187–221, 2005.

[149] A.A. Ungar. *Analytic hyperbolic geometry and Albert Einstein's special theory of relativity*. World scientific, 2008.

[150] J. Vazquez-Corral, A. Galdran, P. Cyriac, and M. Bertalmío. A fast image dehazing method that does not introduce color artifacts. *Journal of Real-Time Image Processing*, 17(3):607–622, 2020.

[151] Vlatko Vedral. The role of relative entropy in quantum information theory. *Reviews of Modern Physics*, 74(1):197, 2002.

[152] H. von Helmholtz. Kürzeste Linien im Farbensystem (shortest lines in the color system). *Sitzungsberichte der Preussischen Akademie der Wissenschaften zu Berlin*, 17:1071–1083, 1891.

[153] H. von Helmholtz. *Treatise on physiological optics. Courier Corporation*, volume 3. Courier Corporation, 2005.

[154] J. von Kries. Chromatic adaptation. *Festschrift der Albrecht-Ludwigs-Universität*, pages 145–158, 1902.

[155] J. von Neumann and R. Kurzweil. *The computer and the brain*. Yale University Press, 2012.

[156] H. von Schelling. Concept of distance in affine geometry and its applications in theories of vision. *JOSA*, 46(5):309–315, 1956.

[157] G. Ward, H. Rushmeier, and C. Piatko. A visibility matching tone reproduction operator for high dynamic range scenes. *IEEE Transactions on Visualization and Computer Graphics*, 3:291–306, 1997.

[158] J.W. Weinberg. The geometry of colors. *General Relativity and Gravitation*, 7(1):135–169, 1976.

[159] G. West and M.H. Brill. Necessary and sufficient conditions for von kries chromatic adaptation to give color constancy. *Journal of Mathematical Biology*, 15(2):249–258, 1982.

[160] L. Wittgenstein, G.E.M. Anscombe, L.L. McAlister, and M. Schättle. *Remarks on colour*. Blackwell Oxford, 1977.

[161] W.K. Wootters. The rebit three-tangle and its relation to two-qubit entanglement. *Journal of Physics A: Mathematical and Theoretical*, 47(42):424037, 2014.

[162] J.A. Worthey and M.H. Brill. Heuristic analysis of von kries color constancy. *JOSA A*, 3(10):1708–1712, 1986.

[163] G. Wyszecky and W. S. Stiles. *Color science: Concepts and methods, quantitative data and formulas. John Wiley & Sons*. John Wiley & Sons, 1982.

[164] Zhiyong Yang and Dale Purves. A statistical explanation of visual space. *Nature neuroscience*, 6(6):632–640, 2003.

[165] H. Yilmaz. Color vision and a new approach to general perception. In *Biological prototypes and synthetic systems*, pages 126–141. Springer, 1962.

[166] H. Yilmaz. On color perception. *Bulletin of Mathematical Biophysics*, 24:5–29, 1962.

[167] S.W. Zamir, J. Vazquez-Corral, and M. Bertalmío. Vision models for wide color gamut imaging in cinema. *IEEE Transactions on Pattern Analysis and Machine Intelligence*, 43(5):1777–1790, 2019.